




8-2013

From Loop to Strand: Characterization of the Conformation and Dynamics of the Human Plasminogen Activator Inhibitor-1 Reactive Center

Tihami Qureshi
tqureshi@utk.edu

Follow this and additional works at: https://trace.tennessee.edu/utk_graddiss

 Part of the [Biochemistry, Biophysics, and Structural Biology Commons](#)

Recommended Citation

Qureshi, Tihami, "From Loop to Strand: Characterization of the Conformation and Dynamics of the Human Plasminogen Activator Inhibitor-1 Reactive Center. " PhD diss., University of Tennessee, 2013.
https://trace.tennessee.edu/utk_graddiss/2470

This Dissertation is brought to you for free and open access by the Graduate School at TRACE: Tennessee Research and Creative Exchange. It has been accepted for inclusion in Doctoral Dissertations by an authorized administrator of TRACE: Tennessee Research and Creative Exchange. For more information, please contact trace@utk.edu.

To the Graduate Council:

I am submitting herewith a dissertation written by Tihami Qureshi entitled "From Loop to Strand: Characterization of the Conformation and Dynamics of the Human Plasminogen Activator Inhibitor-1 Reactive Center." I have examined the final electronic copy of this dissertation for form and content and recommend that it be accepted in partial fulfillment of the requirements for the degree of Doctor of Philosophy, with a major in Biochemistry and Cellular and Molecular Biology.

Cynthia B. Peterson, Major Professor

We have read this dissertation and recommend its acceptance:

Elizabeth Howell, Nitin Jain, Daniel M. Roberts, Engin Serpersu, Chunlei Su

Accepted for the Council:

Carolyn R. Hodges

Vice Provost and Dean of the Graduate School

(Original signatures are on file with official student records.)

From Loop to Strand: Characterization of the Conformation and
Dynamics of the Human Plasminogen Activator Inhibitor-1
Reactive Center

A Dissertation Presented for the
Doctor of Philosophy
Degree
The University of Tennessee, Knoxville

Tihami Qureshi
August 2013

Dedication

This work is dedicated to

my amma & papa

Drs. Mohammad Humayun Aziz & Halima Akhtar Qureshi

Acknowledgements

Growing up, my father would encourage us by quoting Thomas Edison's, "genius is 1% inspiration and 99% perspiration." Although I do not even begin to approach this status, I, nevertheless, must acknowledge the individuals that have been the Muses to my inspiration and supplied the fuel for the perspiration I needed to complete this work. To my mentor, Cynthia B. Peterson, thank you so much for providing your guidance, support, and encouragement when I needed it, and especially for knowing exactly when I needed it.

To my parents, Drs. Mohammad Humayun Aziz and Halima Akhtar Qureshi, you have always believed in me and loved me, and I appreciate and love you both more than I can express. A special thanks to my amma for ensuring that I was properly nourished during my writing period by cooking curry chicken (a.k.a. "soul food") for me. To my four lovely sisters, in order of age, Hasina Akhtar Mohyuddin, Tamanna Qureshi, Taaseen Qureshi, and Maahin Qureshi, thank you for always being there for me. You have been instrumental to my success, especially during my preliminary exam when you the guys (you know which ones) drove to Knoxville to drill me until my presentation was in passing condition, and you other two for listening to my endless ranting. To my nephews and niece, Ibrahim, Mohammed, Isa, and Rania, your smiles have lightened my days and lessened the burden of this journey. I will always hold you all close to my heart. To my best friend, Paul Willard, thank you sincerely for your continued support and companionship. Without these people, I couldn't have done it (literally, the birthday money kindly gifted to me was used, judiciously, I think, to pay my graduation fees ☺). Thanks, guys!!! I love you!

Much thanks to my committee members, in alphabetical order, Drs. Liz Howell, Nitin Jain, Dan Roberts, Engin Serpersu, and Chunlei Su. Your expertise, insight, and direction have been invaluable to me. Many thanks to previous and current lab members, especially Larry Thompson and Sumit Goswami for helping me get acquainted with different theories/techniques during my first year in the lab, Carlee McClintock for purifying protein indispensable to my experiments, and Nancy Horn for her guidance and help troubleshooting various problems. Also, thanks to the many undergrads and rotation students who I have worked with over the years, in particular Matthew Ramsey for facilitating MTSL labeling and Kyle McWilliams for his work on homology modeling.

Abstract

Plasminogen activator inhibitor-1 (PAI-1), with its cofactor vitronectin (VN), controls the rate of plasmin-mediated fibrin breakdown in blood clots by inhibiting tissue-plasminogen activator (tPA) and urokinase-plasminogen activator (uPA). The activity of PAI-1 is attributed to its reactive center loop (RCL), which is solvent-exposed in an active conformation, but inserts as an additional strand into its central β [beta]-sheet during transition to a latent state and during inhibition. VN slows the latency transition, and the rate at which PAI-1 inhibits the plasminogen activators (PAs) also differs. However, the steps during the latency transition, mechanism of VN stabilization, and basis for inhibitory rate differences are unclear, and all involve the RCL. To address these issues, this study combines computational methods with cysteine-scanning mutagenesis of the RCL for fluorescence and electron paramagnetic resonance (EPR) spectroscopy to investigate changes in the RCL due to interactions with these ligands. Homology modeling of the RCL indicates sampling of a limited energy-conformation landscape for this region. Fluorescence investigation of the latency transition suggest that RCL detachment to assume the latent conformation occurs within the first 10 minutes of the process, which typically has a half-life of about 1 hour. Equilibrium-binding studies indicate that VN, its N-terminal somatomedin B (SMB) domain, and a longer truncation involving an intrinsically disordered domain (SMB-IDD) increase the solvent exposure of the RCL in stabilizing PAI-1. Studies with active site-blocked PAs reveal that both dock at the RCL, but rest differently on its top, employing distinct exosite interactions and mobility constraints on the RCL that likely effect the kinetics of its interaction with PAI-1. Thereby, this study provides detailed structural information on

the PAI-1 RCL, and new insights into the latency process and interaction with PAs. Such information is valuable in the development of inhibitors specific for the interaction of PAI-1 with either PA, and in targeting this biomarker in diseases states caused by the dysregulation of PAI-1. Overall, the results from this work reveal that ligand interactions fine-tune the activity of PAI-1 by affecting the conformation and dynamics of the RCL from its position as a solvent-exposed loop to an inserted β [beta]-strand.

Table of Contents

Chapter 1	Life of PAI-1: Physiological Roles, Regulation & Paradoxes	1
1.1.	Introduction	1
1.1.a.	PAI-1 in Human Physiology	1
1.1.b.	PAI-1 Genetics & Signal Transduction	4
1.1.c.	Thermodynamics & Mechanisms: How Serine Proteases & Serpins Work	6
1.1.d.	Conformational Flexibility in PAI-1 Function	15
1.1.e.	Roles of the RCL	25
1.1.f.	Glycosylation, Mutation, and Cofactor Effects on PAI-1 Stability	27
1.2.	Rationale for Study	32
Chapter 2	The Metastable RCL Occupies Limited Conformations That Change During Latency Transition	35
2.1.	Introduction	35
2.1.a.	Fluorescence Detects Changes in Solvent Accessibility	35
2.1.b.	EPR Spectroscopy Provides Information on Protein Dynamics	37
2.1.c.	Objective of Study	39
2.2.	Methods & Materials	39
2.2.a.	Homology Modeling of PAI-1 RCL	39
2.2.b.	Prediction of Solvent Accessibility for PAI-1 RCL Homology Models	39
2.2.c.	Protein Contacts Analysis	40
2.2.d.	PAI-1 Cloning & RCL Mutagenesis	40

2.2.e.	Restriction Digestion Screening of PAI-1 RCL Mutants	42
2.2.f.	PAI-1 RCL Mutant Growth, Expression, & Purification	42
2.2.g.	Labeling of PAI-1 RCL Cys Mutants	45
2.2.h.	Assessment of PAI-1 RCL Cys Mutant Activity	46
2.2.i.	Aggregation & Dimerization Tests of PAI-1 RCL Mutants	47
2.2.j.	Desalting & Molecular Mass Determination	47
2.2.k.	PAI-1 RCL Cys Mutant Stability	48
2.2.l.	Unlabeled & Labeled PAI-1 Stability By Gel Electrophoresis	49
2.2.m.	PEG-Coating Cuvettes for Fluorescence Experiments	50
2.2.n.	Titration of NBD-PAI-1 with VN	50
2.2.o.	Single-Point Relative Quantum Yield Determination	50
2.2.p.	PAI-1 Latency Transition via Steady-state Fluorescence	51
2.2.q.	PAI-1 RCL Mobility via Electron Paramagnetic Resonance (EPR)	52
2.3.	Results	53
2.3.a.	Homology Modeling Investigates RCL Conformations	53
2.3.b.	Purification of PAI-1 RCL Mutants Yields Sufficient Quantities for Conformation & Dynamics Studies	56
2.3.c.	Mutations & Labeling Modestly Affect the Activity & Stability of PAI-1	58
2.3.d.	NBD Reports Unique Micro-environments at the RCL	71
2.3.e.	Transition to the Latent Conformation is Accompanied by Changes in RCL Conformation	76
2.4.	Discussion	86

2.4.a.	How does flexibility of the RCL affect its conformation?	86
2.4.b.	Why does MTSL have distinct effects from NBD on PAI-1 stability?	88
2.4.c	What steady-state changes occur during latency transition?	90
2.5.	Conclusions	93
Chapter 3	Vitronectin Prevents Full Insertion of the PAI-1 RCL	95
3.1.	Introduction	95
3.1.a.	Structural Organization of VN & Oligomerization	95
3.1.b.	VN on PAI-1 Conformational Stability & Specificity	100
3.1.c.	Objective of PAI-1-VN Study	103
3.2.	Methods & Materials	105
3.2.a.	Purification of VN, SMB, & SMB-IDD	105
3.2.b.	Assessment of Full-length VN Oligomeric State	105
3.2.c.	Steady-state Fluorescence of VN & Truncations on PAI-1 RCL Solvent Accessibility	106
3.2.d.	EPR of VN & Truncations on PAI-1 RCL Mobility	107
3.2.e.	Detection of Free Sulfhydryls & Labeling Integrity of MTSL-PAI-1	107
3.3.	Results	107
3.3.a.	VN & its Truncations Exert Similar Conformational Changes in the RCL	107
3.3.b.	The Dynamics of the RCL Are Unaffected By VN & Truncations	112
3.4.	Discussion	116

3.4.a.	How does VN binding affect the conformation of the RCL?	116
3.5.	Conclusions	119
Chapter 4	PAI-1 Forms Distinct Michaelis Complexes with Plasminogen Activators	120
4.1.	Introduction	120
4.1.a.	Structural Basis for PA Function	120
4.1.b.	PAs as Proteases & Signaling Molecules	125
4.1.c.	Regulation & Clearance of PAs	131
4.1.d.	Objective of PAI-1-PA Study	131
4.2.	Methods & Materials	132
4.2.a.	Materials	132
4.2.b.	Equilibrium Binding of PAs by Steady-State Fluorescence	132
4.2.c.	PA Binding on PAI-1 RCL Mobility via EPR	132
4.2.d.	Modeling of PAI-1-tPA Michaelis Complex	133
4.3.	Results	133
4.3.a.	Active Site-Blocked PAs Utilize Different PAI-1 Exosites in the Michaelis Complex	134
4.3.b.	RCL Dynamics in the Michaelis Complex are Affected by uPA Binding	136
4.3.c.	Model of PAI-1-tPA Michaelis Complex	140
4.4.	Discussion	143
4.4.a.	How does noncovalent Michaelis complex formation affect serpin inhibition rates?	143
4.4.b.	How do exosites affect PAI-1 reactions with PAs?	145

4.4.c.	Why inhibit tPA v. uPA interaction with PAI-1?	149
4.4.d.	How does interaction with VN affect PAI-1 interaction with PAs?	150
4.5.	Conclusion	151
	Future Directions	152
	References	155
	Vita	177

List of Tables

Chapter 1

Table 1.1	Conformational State & Presence of Cofactor on PAI-1 Inhibition of Plasminogen Activators	14
Table 1.2	Effects & Epitopes of PAI-1 Conformation-Sensing Antibodies	18
Table 1.3	Global Conformational Changes Accompanying Transition of Active PAI-1 to Latent & Cleaved States By Functional Region	20
Table 1.4	Comparisons of RCL Interactions in the Active & Latent States of PAI-1	24
Table 1.5	Residues Scanned by Cysteine Mutagenesis to Probe the Conformation & Dynamics of PAI-1 RCL	34

Chapter 2

Table 2.1	Primer Design & Engineering of Unique Restriction Sites to Facilitate Screening of Single-Cysteine RCL Mutants of PAI-1	41
Table 2.2	Comparison of RCL Interactions in Homology Models & Crystal Structures of Different Conformations of PAI-1	55
Table 2.3	Expected Digestion Patterns in Screening of PAI-1 RCL Mutants	57
Table 2.4	Activity & Conformational Distribution PAI-1 RCL Cys Mutants	64
Table 2.5	Labeling Stoichiometry of NBD-PAI-1	66
Table 2.6	MALDI-MS of Unlabeled & Labeled PAI-1 RCL Cys Mutants	67
Table 2.7	Relative Quantum Yields of NBD-Labeled RCL Mutants of PAI-1	73
Table 2.8	Comparison of Half-lives Obtained for NBD-labeled PAI-1 via tPA inhibition & Steady-state Fluorescence	82

Chapter 4

Table 4.1	Potential Energy & Root-Mean-Squared Deviation of Docked & Restrained PAI-1-tPA Michaelis Complex Models	143
Table 4.2	Interactions in PAI-1-PA Michaelis Complexes	144
Table 4.3	Common Serpin-Serine Protease Exosite Interactions	144
Table 4.4	Serpin-Serine Protease Exosite Contribution & Inhibition Rates	146

List of Figures

Chapter 1

Figure 1.1	PAI-1 Regulates Hemostasis by Inhibiting Plasminogen Activators	2
Figure 1.2	Multiple Signaling Pathways Are Involved in PAI-1 Expression	5
Figure 1.3	Serine Proteases Catalyze the Hydrolysis of Peptide Bonds	7
Figure 1.4	Metastable Structure of PAI-1 with Important Functional Regions Highlighted	9
Figure 1.5	PAI-1 Primary Sequence & Secondary Structure	10
Figure 1.6	Branched Pathway of the Serpin Inhibitory Mechanism	13
Figure 1.7	Structural Flexibility Enables PAI-1 to Adopt Many Global Conformations	16
Figure 1.8	Monoclonal Antibodies Provide Information on PAI-1 Conformation	17
Figure 1.9	The RCL is Solvent-Exposed in the Active State & Tightly Associated With the Protein Core in the Latent Conformation of PAI-1	21
Figure 1.10	α -Helix F Covers The Shutter Region in Metastable Conformations of PAI-1	23
Figure 1.11	The Mobile Gate Region of PAI-1 Widens to Allow RCL Insertion In The Latent Conformation	23
Figure 1.12	Serpins Are Highly Specific Inhibitors Despite Similarities in RCL Sequence	26
Figure 1.13	Glycosylation of PAI-1 Slows Latency Conversion	28
Figure 1.14	The Active Conformation is Stabilized by Mutation of The Gate & Shutter Regions in 14-1B Variant of PAI-1	28

Figure 1.15	Vitronectin Binds At The Flexible Joint Region & Stabilizes PAI-1 in The Active Conformation	31
-------------	--	----

Chapter 2

Figure 2.1	Fluorescence Using The NBD Probe	36
Figure 2.2	Electron Paramagnetic Resonance Using The MTSL-Probe	38
Figure 2.3	Purification Scheme for PAI-1 RCL Cys Mutants	44
Figure 2.4	Representative Absorption Spectra to Determine Labeling Stoichiometry	46
Figure 2.5	The Stability of PAI-1 Determined By The Inhibition of tPA	49
Figure 2.6	Homology Models of PAI-1 RCL	54
Figure 2.7	Restriction Digestion to Screen For PAI-1 RCL Mutants	57
Figure 2.8	Growth & Expression of PAI-1 RCL Cys Mutants	59
Figure 2.9	Analysis of PAI-1 RCL Cys Mutant Purification	59
Figure 2.10	Assessment of PAI-1 RCL Cys Mutant Activity	61
Figure 2.11	Functional Distribution PAI-1 RCL Cys Mutants	62
Figure 2.12	Relative Stoichiometry of Inhibition of PAI-1 RCL Cys Mutants	63
Figure 2.13	PAI-1 RCL Cys Mutants Exist in A Non-Aggregated, Monomeric State	65
Figure 2.14	Confirmation of NBD Labeling of PAI-1 Cys Mutants by Matrix-Assisted Laser Desorption Ionization Mass Spectrometry	67
Figure 2.15	Mutation & NBD-Labeling of The RCL on PAI-1 Stability	69
Figure 2.16	Effect of MTSL-Labeling of The RCL on PAI-1 Stability	70
Figure 2.17	VN Binds with High-Affinity to PAI-1	72

Figure 2.18	Single-Point Measurements For Relative Quantum Yield Determination of NBD-PAI-1	73
Figure 2.19	Effect of Buffers, Temperature, & PEG on NBD-PAI-1 Fluorescence	75
Figure 2.20	Steady-state RCL Insertion During Latency Transition of PAI-1	77
Figure 2.21	Initial Decrease in Fluorescence During Latency Transition	79
Figure 2.22	Half-life of RCL Insertion	81
Figure 2.23	Mobility at Different Positions of The RCL (s4A) in Active & Latent Conformations of PAI-1	84
Figure 2.24	Changes in RCL Dynamics From The Active to Latent State of PAI-1	85
Figure 2.25	Effect of Quality Factor on MTSL-PAI-1 EPR Measurements	87
Figure 2.26	Model of PAI-1 Latency Transition	92
Chapter 3		
Figure 3.1	VN Is A Promiscuous, Bi-Lobed, Multi-Domain Glycoprotein	96
Figure 3.2	Complex Formation with VN Stabilizes & Alters the Specificity of PAI-1	98
Figure 3.3	Model of VN Stabilization of PAI-1	102
Figure 3.4	VN & Heparin Make PAI-1 A More Efficient Thrombin Inhibitor	102
Figure 3.5	Heparin Binding Alters the Specificity of PAI-1	104
Figure 3.6	α 1-Acid Glycoprotein Stabilizes The Active Conformation of PAI-1	104
Figure 3.7	VN forms higher-order complexes with PAI-1	108
Figure 3.8	Effect of VN & its Truncations on the Solvent Accessibility of PAI-1 RCL	110

Figure 3.9	VN Binding to PAI-1 on The RCL Solvent Accessibility Is Influenced by Buffer Effects	111
Figure 3.10	Binding of VN & its Truncations on the Dynamics at Different Positions in the RCL	113
Figure 3.11	Change in RCL Dynamics Due to Binding of VN & its Truncations	114
Figure 3.12	MTSL Probe Remains Conjugated to PAI-1 in The Presence of VN & Its Truncations	115
Chapter 4		
Figure 4.1	Serine Protease Domains Consist of Two β -Barrels & Several Surface-Exposed Loops	121
Figure 4.2	The Structure of tPA is Important for Binding Fibrin & Activating Plasminogen	123
Figure 4.3	uPA Structure Supports Plasminogen Activation & Localized Pericellular Proteolysis	124
Figure 4.4	Proteolytic Functions of Plasminogen Activators	126
Figure 4.5	Plasminogen Activators as Signaling Molecules	128
Figure 4.6	Receptor-Mediated Endocytosis in the Clearance of PAI-1 & Plasminogen Activators	130
Figure 4.7	LRP-1 Binds to A Cryptic Site on PAI-1	130
Figure 4.8	PA Binding of PAI-1 RCL in Michaelis Complex	135
Figure 4.9	Binding of Plasminogen Activators Affects the Dynamics at Different Positions in the RCL	137
Figure 4.10	Changes in Mobility of the RCL upon Michaelis Complex Formation	138
Figure 4.11	MTSL Probe Remains Conjugated to PAI-1 in The Presence of Active Site-Blocked Plasminogen Activators	139

Figure 4.12	Michaelis Complex of PAI-1 with PAs	141
Figure 4.13	Close-up of PAI-1-PA Michaelis Complex Interface	142
Figure 4.14	Location of Serine Protease Exosites on Serpin Top	147

List of Abbreviations

14-1B	Stable PAI-1 mutant with N150H, K154T, Q319L, M154I mutations
AUC	Analytical ultracentrifugation
DTNB	5,5'-dithiobis-(2-nitrobenzoic acid (Ellman's reagent)
EDTA	Ethylenediaminetetraacetic acid
EPR	Electron paramagnetic resonance
HB	Hydrogen bond
HM	Homology modeling
HPLC	High-pressure liquid chromatography
HYD	Hydrophobic interaction
IDD	Intrinsically-disordered domain (residues 44-149 of VN)
IMAC	Immobilized metal affinity chromatography
ION	Ionic bond
LRP	Low-density lipoprotein receptor-associated protein
MALDI	Matrix-assisted laser desorption ionization
MMP	Matrix metalloproteinase
MOPS	3-Morpholinopropane-1-sulfonic acid
MS	Mass spectrometry
MTSL	2,5-Dihydro-2,2,5,5-tetramethyl-3-[[[(methylsulfonyl)thio]methyl]-1H-pyrrol-1-yloxy
NBD	<i>N,N'</i> -Dimethyl- <i>N</i> -(iodoacetyl)- <i>N'</i> -(7-nitrobenz-2-oxa-1,3-diazol-4-yl) ethylenediamine
P	Nomenclature for position of RCL residues according to its distance from the scissile bond; C-terminal residues indicated by prime (')
PA	Plasminogen activators (tPA and uPA)

PAI-1	Plasminogen activator inhibitor-1
PEG	Polyethylene glycol
Plg	Plasminogen
Pln	Plasmin
QY	Quantum yield
RCL	Reactive center loop
RMSD	Root-mean-squared deviation
RT	Room temperature
SI	Stoichiometry of inhibition
SMB	Somatomedin B domain (N-terminal residues 1-44 of VN)
SPD	Serine-protease domain (* indicates active site contains S195A mutation)
tPA	Tissue plasminogen activator
uPA	Urokinase plasminogen activator
uPAR	uPA receptor
VN	Vitronectin

Chapter 1 Life of PAI-1: Physiological Roles, Regulation, & Paradoxes

1.1. Introduction

1.1.a. PAI-1 in Human Physiology

Biological systems of serine proteases and serine protease inhibitors (serpins) reach far into each kingdom of life, including Archae, Bacteria, and Eukarya. These systems sustain diverse processes, such as digestion, inflammation, and blood homeostasis (i.e. hemostasis) [1]. The step-wise activation of serine proteases from their zymogen forms creates potentially dangerous proteolytic cascades that must be controlled spatially and temporally by serpins. This ensures their proper function and prevents their escape [2]. Plasminogen activator inhibitor-1 (PAI-1), discovered in the 1970s and found only in vertebrates ranging from the cold-blooded zebrafish to the warm-blooded humans, is one such serpin of great biological importance. Of the 36 human serpins, PAI-1 is a plasma & tissue-associated serpin that is a multi-specific [3] inhibitor of tissue- and urokinase-plasminogen activators (tPA & uPA) with anti-fibrinolytic [4], pro- and anti-adhesive [5, 6], and pro-inflammatory properties [7]. PAI-1 balances hemostasis by regulating blood clot formation (i.e. coagulation) via thrombin cleavage of fibrinogen, and breakdown of fibrin clots (i.e. fibrinolysis) by plasmin [4] (**Fig. 1.1**). Consequently, too much PAI-1 can lead to thrombotic or fibrotic states in which excessive fibrin accumulates, potentially blocking blood vessels and disrupting oxygen supply to tissues, whereas too little PAI-1 can lead to hyperfibrinolytic and mild bleeding states [8, 9]. In the extracellular matrix (ECM), PAI-1 is further involved in regulating cell adhesion and migration, and thereby tissue remodeling, by interacting with its physiological cofactor, vitronectin (VN) [10].

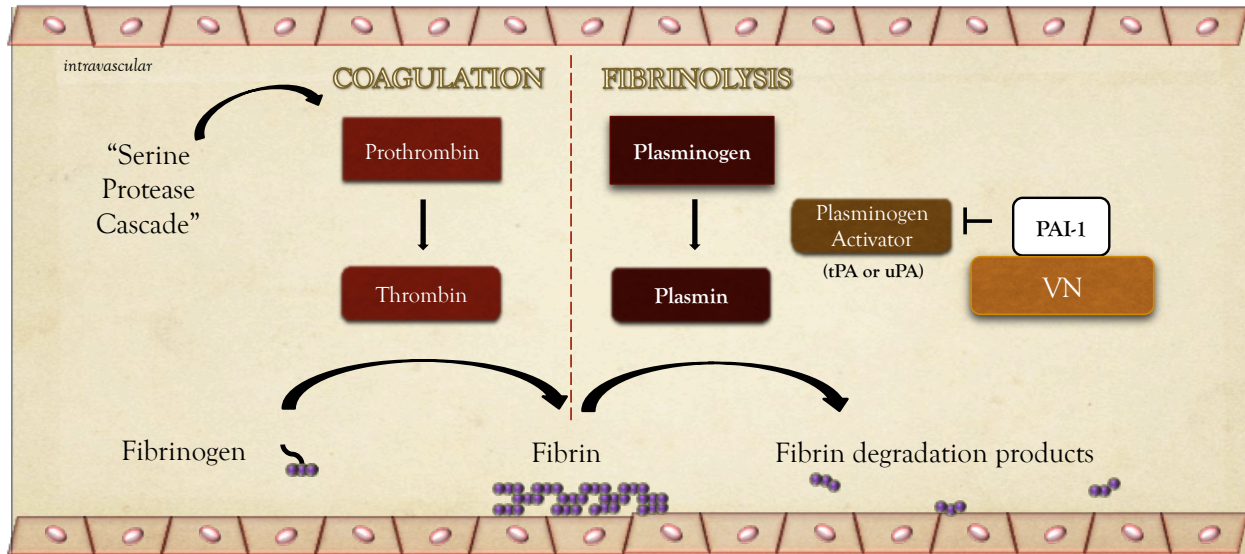


Figure 1.1 PAI-1 Regulates Hemostasis by Inhibiting Plasminogen Activators. In response to injury and/or other intrinsic/extrinsic factors, the coagulation cascade is activated, which involves the activation of inactive zymogen forms of serine proteases by cleavage, and subsequent activation of downstream serine proteases. The reaction culminates in the activation of prothrombin to thrombin, which then cleaves the soluble fibrinogen to insoluble fibrin that deposits at the site of injury. During fibrinolysis, plasmin is activated from plasminogen by plasminogen activators (PAs, i.e. tPA and uPA) to cleave fibrin, forming fibrin degradation products and resolving the clot. PAI-1 slows fibrinolysis by inhibiting PAs. Its cofactor, vitronectin (VN), stabilizes PAI-1 and localizes it to the clot site.

Plasminogen activation plays a significant role in thrombosis [11], ischemic and hemorrhagic stroke [12], and cancer metastasis [13-19] by degradation of basement membranes and invasion into the bloodstream. PAI-1 may appropriately be expected to halt these effects by inhibiting plasminogen activators (PAs), but, paradoxically [20-23], contributes to the severity of cancers, presumably via competing with cell surface receptors (e.g. integrins, uPA receptor) for its cofactor. Thereby, PAI-1 is increasingly being used as a poor prognostic biomarker in these situations and is a desired target by pharmaceutical means.

Additionally, the dysregulation of PAI-1 has multiple physiological consequences. Increased circulating levels of PAI-1 are associated with the greater risk of cardiovascular disease (CVD) [24-28] and the hardening of blood vessels (i.e. atherosclerosis) [29], which is characterized by scarring and inflammation, and exacerbated by cholesterol deposition. PAI-1 is also involved in inflammatory processes, including the systemic inflammatory response syndrome (or sepsis) [30, 31] and the autoimmune rheumatoid arthritis of the joints [32], by inhibiting efferocytosis (i.e. phagocytosis) of apoptotic neutrophils [7]. The increased expression of PAI-1 in the formation of new blood vessels (i.e. angiogenesis) [33] further facilitates metastasis in certain cancers [17, 20, 34]. In adipose tissue, PAI-1 acts as a signaling molecule to affect the metabolic syndrome [35-37], which is characterized by obesity, dyslipidemia, hypertension (high blood pressure), and diabetes mellitus, the latter which is commonly caused by insulin sensitivity or resistance resulting in high blood glucose levels. In the brain, PAI-1, with tPA, regulates the circadian clock [38] responsible for rhythmic biological processes, including sleep and hormone production. PAI-1 is also implicated

in hair loss (i.e. alopecia) [39]. Due to its diverse roles, the tight regulation of PAI-1 expression is required for its proper function in these physiological processes.

1.1.b. PAI-1 Genetics & Signal Transduction

In humans, the PAI-1 gene is located on the q arm of chromosome 7 [40]. Deletion of this gene results in viable individuals that develop normally, but with the hyperfibrinolytic and mild bleeding states previously mentioned [8], while deletion of this arm of chromosome 7 causes a genetic disorder called William's syndrome, which is characterized by elfin features and an unusual trust in strangers [41]. The PAI-1 gene codes for a 402 amino acid protein containing a signal sequence with two possible cleavage sites, resulting in a ~43 kilodalton (kDa) polypeptide with 379 or 381 residues (the residue numbering used this dissertation is based on the shorter polypeptide). Upon removal of the signal sequence, PAI-1 is secreted and circulates in the plasma at concentrations of 5 - 20 ng/ml [30]. PAI-1 is primarily synthesized by the liver hepatocytes [42], but is also produced and secreted by platelets, adipocytes, and during acute-phase responses, by endothelial cells lining blood vessels and smooth muscle cells forming their walls.

A 4G/5G polymorphism in the regulatory region upstream of the PAI-1 promoter (**Fig. 1.2**), in which 4 or 5 guanines provide a binding site for a transcriptional activator or repressor, respectively, results in the increased and decreased expression of PAI-1, respectively [40]. The latter contributes to the role of PAI-1 in CVD [27]. The regulatory region also contains response elements for glucose and the very-low-density lipoprotein (VLDL). Several signaling pathways and molecular transducers further regulate PAI-1 expression. Via the insulin receptor, a receptor tyrosine kinase, insulin signals through

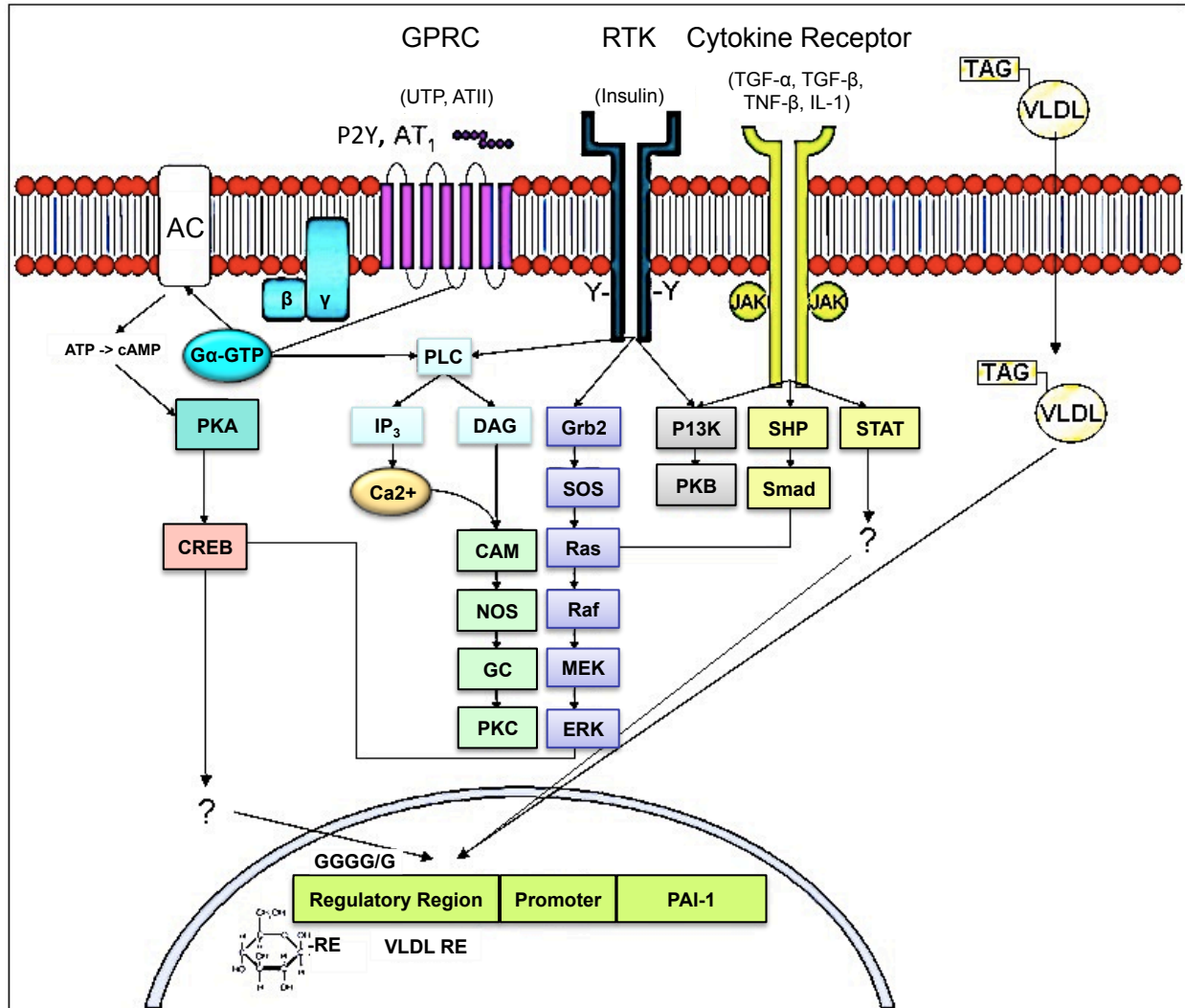


Figure 1.2 Multiple Signaling Pathways Are Involved in PAI-1 Expression. The expression of PAI-1 is regulated by many factors, including cytokines (TGF- β , TGF- α , TNF- β), nucleotides (UTP), peptides (ATII), cholesterol, and glucose homeostasis molecules (insulin, VLDL), via signaling through their respective receptors. Possible downstream signaling molecules and the organization of the PAI-1 gene are also shown. The regulatory region of the PAI-1 gene includes a 4G/5G polymorphic region, and response elements (RE) for glucose and VLDL.

the phosphatidylinoside-3-kinase (PI3K) & Ras/ERK pathways to induce PAI-1 expression [43]. The effects of glucose, VLDL, and insulin on its expression connect PAI-1 to the metabolic syndrome [25, 35, 36, 43-45]. Small molecules and peptides, including the nucleotide uridine triphosphate and angiotensin II, respectively, bind to their G-protein-coupled receptors, the purinergic (P2Y) and AT₁ receptor, initiating the cyclic adenosine monophosphate and phospholipase C signaling pathways to stimulate PAI-1 expression [46-49]. PAI-1 expression is also increased by signaling resulting from the binding of the pro-inflammatory cytokines, transforming growth factor- α and - β (TGF- α , TGF- β) [50, 51], tumor necrosis factor- α (TNF- α) [52], and interleukin-1 (IL-1) to their respective receptors [53]. When present, lipopolysaccharide, a common component of the outer membrane of Gram-negative bacteria, also induces PAI-1 expression [54] and contributes to PAI-1 in sepsis. In addition to its expression by these molecules and signaling pathways, the function of PAI-1 critically depends on its mechanism of action.

1.1.c. Thermodynamics & Mechanisms: How Serine Proteases & Serpins Work

Like other serpin-protease pairs, PAI-1 inhibits PAs by mimicking their natural substrates and allowing initial processing by the protease. Serine proteases catalyze the hydrolysis of peptide bonds (**Fig 1.3**) using an acid-base mechanism [1]. Despite the thermodynamics favoring hydrolysis, the planar and double-bond character of the peptide bond connecting amino acids in proteins renders it kinetically stable [55]. This feature necessitates the use of enzymes (proteases) to break proteins into their constituent parts (and ultimately amino acids) for removal from the body or recycling for future use and incorporation into newly synthesized proteins. The mechanism by which

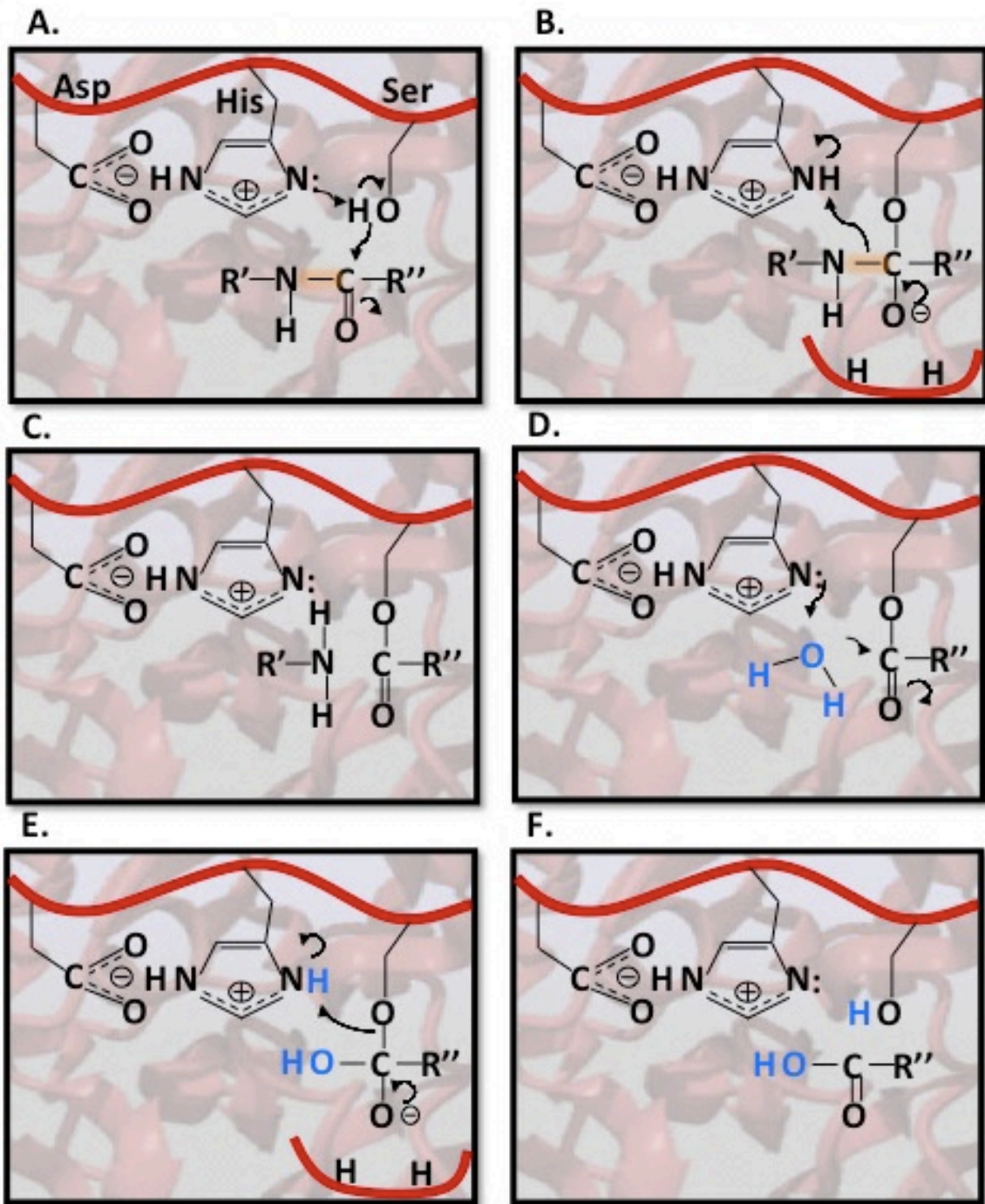


Figure 1.3 Serine Proteases Catalyze the Hydrolysis of Peptide Bonds. Hydrolysis occurs in two steps including acylation (panels A-C) and deacylation (panels D-F). The catalytic triad' serine nucleophile, histidine base, and aspartate residues, as well as peptide bond substrate (orange) and water (blue), are depicted. The oxyanion hole is represented in panels B & E. Arrows indicate the flow of electrons.

serine proteases perform this function involves two steps that include acylation via a covalent intermediate followed by deacylation. Serine proteases employ a catalytic triad consisting of a serine nucleophile, a histidine base, and an aspartate residue to help orient the base in its cleavage of peptide bonds. In this mechanism, the serine nucleophile is activated by deprotonation by the adjacent histidine base (**Fig. 1.3 A**). The resulting alkoxide can then attack an incoming carbonyl carbon, leading to the formation of an unstable tetrahedral intermediate, and transition state formation is stabilized by donation of backbone hydrogen bonds from the oxyanion hole (**Fig. 1.3 B**). The tetrahedral intermediate, bearing a formal negative charge on the carbonyl oxygen collapses, resulting in cleavage of the peptide bond and consequent release an amide product and acylated enzyme (**Fig 1.3 C**). To regenerate the enzyme, deacylation occurs by water entering the active site, where it functions as a nucleophile (as serine does in the first half of the reaction), and is deprotonated, forming a hydroxyl that attacks the carbonyl carbon (**Fig. 1.3 D**). A tetrahedral intermediate stabilized by the oxyanion hole again forms and collapses (**Fig.1.3 E**), releasing a carboxylic acid product and regenerating the enzyme (**Fig 1.3 F**).

PAI-1, like other serpins, employs a conformation-based suicide mechanism [4, 56] to inhibit its target serine proteases. This mechanism incorporates concerted conformational changes [57] involving communication between the three β -sheets (sA, sB, & sC) and nine α -helices (hA-hI) that comprise the folding core of the protein (**Fig. 1.4 - 1.5**). Foremost, the reactive center loop (RCL), containing the pseudo-substrate scissile bond (P1-P1') recognized by cognate serine proteases, stretches over sB and sC, but is tethered close to the serpin body [58] in the inhibitor-active conformation.

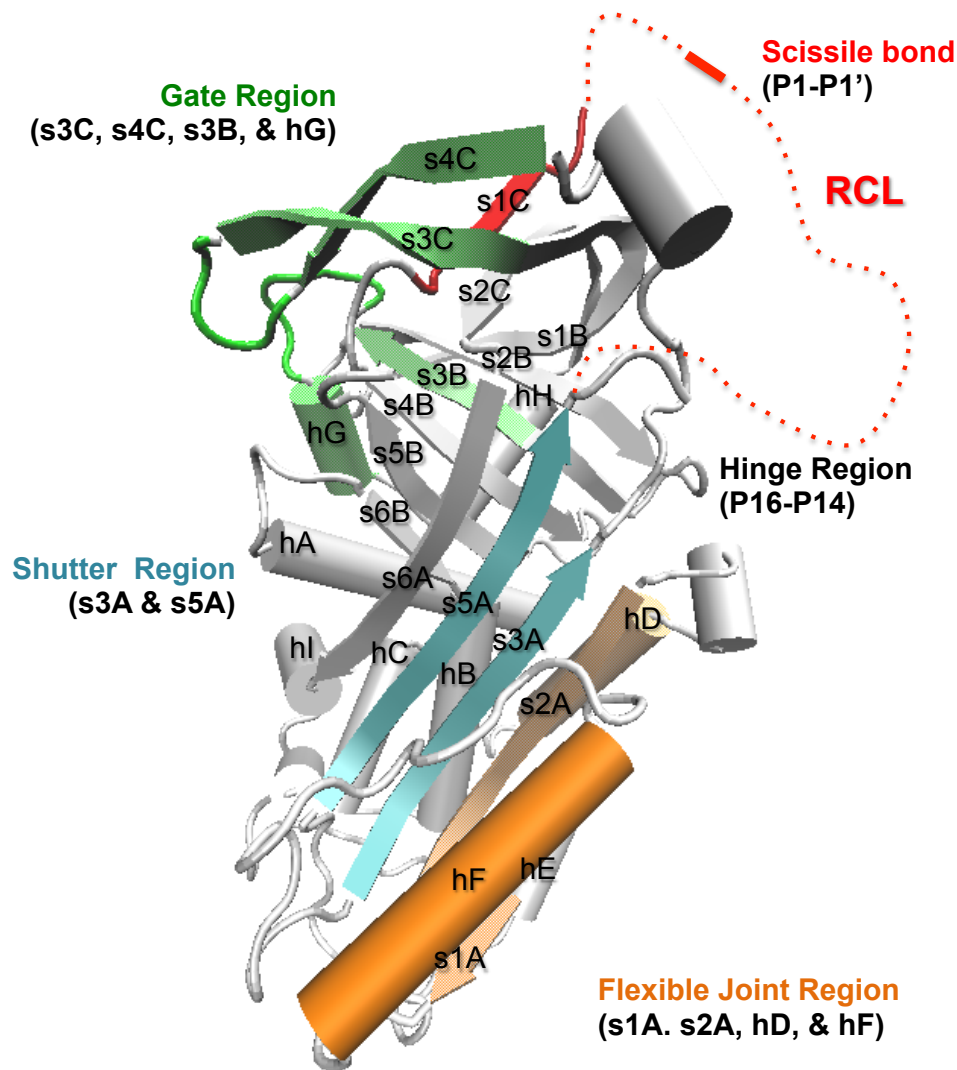


Figure 1.4 Metastable Structure of PAI-1 with Important Functional Regions Highlighted. The active, metastable structure of PAI-1 (Protein data bank, PDB 3Q02;[59]) is shown with secondary structure elements and important functional regions in protease inhibition and self-regulation by latency transition indicated, including the RCL (*red*), the gate (*green*), the shutter (*cyan*), and the flexible joint (*orange*) regions. Residues adjacent to the scissile bond (P1-P1') are specified by their position P and distance from this point, where C-terminal residues are indicated by a prime ('). Rendering constructed using the graphics program Visual Molecular Dynamics (VMD 1.9).

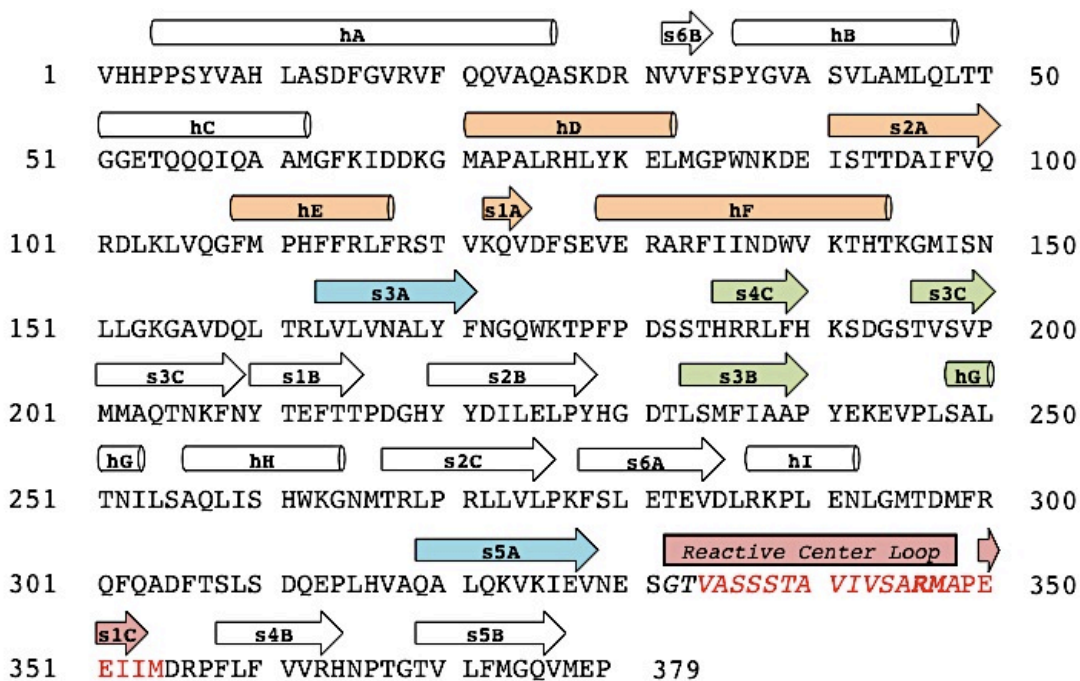


Figure 1.5 PAI-1 Primary Sequence & Secondary Structure. The structure of PAI-1 consists of nine α -helices (hA-hI) and three β -sheets, including a five- to six-stranded sheet A (s1A - s6A; RCL is s4A in latent), a six-stranded sheet B (s1B - s6B), & a four-stranded sheet C (s1C - s4C). Helices are indicated by cylinders and β -strands by arrows. The unresolved residues of the RCL are in italics, and scissile bond residues in bold italics. Functional regions are colored as in Fig. 1.5, and secondary structure assignments are based on the metastable crystal structure of PAI-1 (3Q02).

Residues of the RCL are designated by the position P and distance from the scissile bond, with C-terminal residues indicated by a prime ('). Other important regions for PAI-1 function include the hinge (P17-P14, but defined here as P14-P11), the gate (s3C, s4C, s3B, and hG), the shutter (s3A/s5A), and the flexible joint regions (s1A, s2A, hD, and hF), which are named according to their role in conformational transitions (as described below). Despite the ~25% sequence homology among its family members, serpins share a high degree of conservation in this tertiary fold.

With the RCL exposed, PAI-1, akin to other serpins, is kinetically trapped in a metastable fold that is required for successful inhibition [60]. Unlike most of its family members, the RCL of PAI-1 is on a timed switch and spontaneously ($\Delta G \sim -9$ kcal/mol) [61] inserts as the fourth strand into its central β -sheet A (s4A) without proteolytic cleavage, giving rise to the inactive latent conformation (c.f. Fig. 1.7). This latent transition occurs under physiological conditions (37°C, pH 7.4) with a half-life of ~1-2 hrs and represents the final product of serpin folding [62]. In comparison, only 10% of the serpin, antithrombin III (ATIII), converts to its latent form after 10 hrs at 37°C [58]. Yet, RCL insertion during latency is distinct from its insertion during inhibition, with the former several magnitudes slower than the latter [63] and entropically-driven [64]. Accordingly, PAI-1 rapidly inhibits PAs at rates approaching the diffusion limit (10^6 - 10^7 M⁻¹s⁻¹) [65]. In the latter case, cleavage of the scissile bond is coupled to the enthalpically-driven [64], fast insertion of the RCL as s4A [66, 67], leading to a 70 Å “North to South pole” translocation [68] followed by “crushing” of the enzyme [69] against the serpin scaffold (**Fig. 1.6**). This sequence of events leads to kinetic trapping of the protease at the acyl enzyme stage of its mechanism. If insertion of the RCL is

delayed, e.g. by mutation of PAI-1 to a canonical serpin consensus residue [70-72], lowering temperature [73] and pH [74-76], or by the presence of non-ionic solvents [77], deacylation of the serpin-attached acyl enzyme occurs, releasing the protease. This causes the cleaved PAI-1 to behave as a substrate for the protease instead of an inhibitor [69, 78]. Due to this behavior, the serpin mechanism is generally considered to be branched between inhibitor and substrate pathways that share a common path until the point of insertion [69, 78], in contrast to the initial pathway model in which PAI-1 is predestined to be either an inhibitor or substrate [79].

The rates that define the interaction of PAI-1 and PAs during inhibition (**Fig. 1.6**) include the rates of noncovalent Michaelis complex formation (k_{assoc} , or k_1), cleavage and acylation ($k_{\text{acylation}}$, or k_2), displacement of the P'-side of the serpin RCL from the protease active site, which is required to prevent reversible acylation, and RCL insertion to form of the final covalent complex (k_i) or cleaved serpin hydrolyzed to release the free protease (k_s). Since k_1 is fast, the second-order rate of inhibition (k_{inhib}) is limited by the reversible rates of acylation and loop-displacement, and irreversible rates of RCL insertion [limiting rate of insertion, $k_{\text{lim}} = (k_2 k_3^*) / (k_2 + k_{-1} + k_3^*)$ where $k_3^* = k_3(k_i + k_s) / (k_{-3} + k_i + k_s)$] [80]. These rates differ for PAI-1 with PAs and depend on their conformational state, presence of cofactors (**Table 1.1**), and exosite interactions, defined as interactions outside the serpin P4-P3' residues and the protease active-site (S4-S3' specificity pockets) [81]. In general, native PAI-1 inhibits the two-chain form of tPA (tc-tPA) faster than uPA and the single-chain form of tPA (sc-tPA) (i.e. $k_{\text{inhib}} \text{ tc-tPA} > \text{uPA} > \text{sc-tPA}$), whereas uPA is inhibited faster by denatured and refolded PAI-1 ($k_{\text{inhib}} \text{ uPA} > \text{tc-tPA} > \text{sc-tPA}$). Also, while VN increases k_{inhib} of refolded PAI-1 with both PAs, it

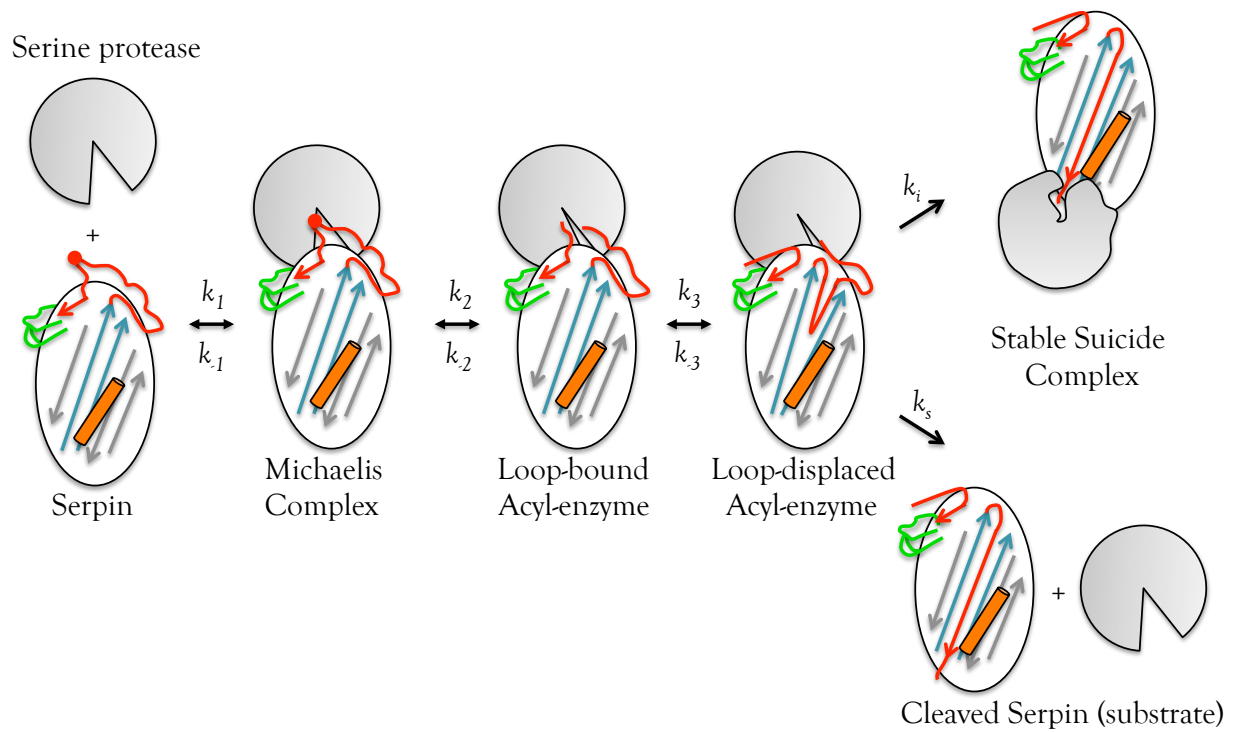


Figure 1.6 Branched Pathway of the Serpin Inhibitory Mechanism. Serpins (coloring scheme for functional regions conserved from Fig.1.5; scissile bond as red dot) use a suicide mechanism to inhibit serine proteases (grey) via the formation of a noncovalent Michaelis complex, the covalent acyl-enzyme, the loop-displaced enzyme, and the final, stable complex, which, if deacylates, forms a cleaved, inactive serpin that has then behaved as a substrate. Kinetics of individual interactions are defined by the indicated rate constants (k).

Table 1.1 Effects of Conformational State & Presence of Cofactor on PAI-1 Inhibition of Plasminogen Activators

Conformation PAI-1	PA	VN Cofactor	$k_{inh} (M^{-1}s^{-1})$	$k_{resoc} (M^{-1}s^{-1})$	$k_{lim} (s^{-1})^*$	$K_m (\mu M)^*$	$k_{lim}/K_m (\mu M^{-1}s^{-1})$	
Refolded	sc-tPA	-		$(1.34 \pm 0.02) \times 10^7$ ^a				
		-	$(2.6 \pm 0.5) \times 10^7$ ^b $(9.2 \pm 3.1) \times 10^6$ ^c	$(3.7 \pm 1.0) \times 10^7$ ^a				
	uPA	+	$(3.1 \pm 0.6) \times 10^7$ ^b					
		-	$(4.8 \pm 0.4) \times 10^6$ ^b $(11.7 \pm 0.8) \times 10^6$ ^c $(3.7 \pm 0.2) \times 10^7$ ^b	$(1.6 \pm 0.5) \times 10^8$ ^a				
Native	sc-tPA	-	$(6.8 \pm 1.1) \times 10^6$ ^d	$(36.3 \pm 5.3) \times 10^6$ ^e	3.4 ± 0.1 ^{e,h}	0.29 ± 0.03 ^{e,h}	11.7 ^e	
		-	$(2.3 \pm 0.4) \times 10^7$ ^d $(12.8 \pm 0.6) \times 10^6$ ^e $(15.4 \pm 1.4) \times 10^6$ ^g $(1.0 \pm 0.1) \times 10^7$ ^h	$(4.45 \pm 0.12) \times 10^7$ ^h	2.4 ± 0.2 ^f 2.26 ± 0.01 ⁱ	0.06 ± 0.02 ^f 0.06 ± 0.01 ⁱ	12 ^h 37.67 ⁱ	
	uPA	+			1.7 ± 0.1 ^f 2.25 ± 0.03 ⁱ	0.09 ± 0.02 ^f 0.12 ± 0.01 ⁱ	18.75 ⁱ	
		-	$(1.1 \pm 0.2) \times 10^7$ ^d $(5.5 \pm 0.4) \times 10^6$ ^e $(8.1 \pm 0.7) \times 10^6$ ^g $(5.0 \pm 0.4) \times 10^6$ ^h	$(5.9 \pm 0.1) \times 10^6$ ^e $(1.34 \pm 0.02) \times 10^7$ ^h	22.8 ± 0.2 ^{e,h} 26.0 ± 1.8 ^f 14.49 ± 0.53 ⁱ	2.6 ± 0.1 ^{e,h} 3.0 ± 0.6 ^f 1.19 ± 0.13 ⁱ	8.8 ^{e,h} 12.18 ⁱ	
	14-1B	tc-tPA	-			3.9 ± 0.1 ^f 5.45 ± 0.13 ⁱ	3.55 ± 0.04 ^f 0.86 ± 0.05 ⁱ	6.34 ⁱ
			+			0.20 ± 0.01 ⁱ 0.60 ± 0.01 ⁱ	0.06 ± 0.01 ⁱ 0.10 ± 0.01 ⁱ	3.2 ⁱ 6.1 ⁱ
		uPA	-			5.66 ± 0.15 ⁱ 6.55 ± 0.22 ⁱ	0.46 ± 0.04 ⁱ 1.28 ± 0.09 ⁱ	12.3 ⁱ 5.1 ⁱ
			+					

^a Ref. [82]

35°C, pH 7.2, PBS

^b Ref. [11]

37°C, pH 7.8, Tris

^c Ref. [83]

PBS

^d Ref. [84]

23°C, pH 7.8, Tris

^e Ref. [85]

25°C, pH 7.4, HEPES

^f Ref. [86]

25°C, pH 7.4, PO4

^g Ref. [57]

25°C, pH 7.4, HEPES

^h Ref. [87]

25°C, pH 7.4, HEPES

ⁱ Ref. [80]

25°C, pH 7.4, HEPES

* NBDP9 background

reduces the efficiency of inhibition (k_{lim}/K_m) of native and a stable mutant of PAI-1, 14-1B, with both PAs.

The conformational changes that occur during inhibition and latency transition require the flexibility of the serpin scaffold, which is also exploited by non-inhibitory serpins. However, in contrast to inhibitory serpins, non-inhibitory serpins do not require RCL insertion for its function. For instance, the hydrophobic pocket formed by hH, s3B-4B, and the s4/5B loop on its “back” (c.f. Fig. 1.4) is used by non-inhibitory hormone-binding serpins to bind their ligands. In the latter case, the hormone binds with high affinity to one state, is transported, and then released from the serpin upon conformational change to another state for which it has low affinity. The conformations of inhibitory and non-inhibitory serpins also differ considerably in thermodynamic stability, with RCL-inserted forms significantly more stable than RCL-exposed forms. Consequently, the protease-complexed state ($T_m >100^\circ\text{C}$) [88] of PAI-1 is more stable than its latent state ($T_m \sim 68-70^\circ\text{C}$), while its active state is the least stable ($T_m \sim 45-55^\circ\text{C}$) [59, 70].

1.1.d. Conformational Flexibility in PAI-1 Function

In addition to thermodynamic stability, the conformations of PAI-1 differ at important functional regions. Due to its inherent flexibility [89-91], PAI-1 can adopt six main conformations, which, in order of increasing stability, include the inhibitor-active, pre-latent (not shown) and noncovalent complex, inhibitor-inactive latent, final protease-complexed, and cleaved-substrate conformations (**Fig. 1.7**). Each requires dramatic structural changes and repositioning of the RCL via distinct conformational routes. Thus

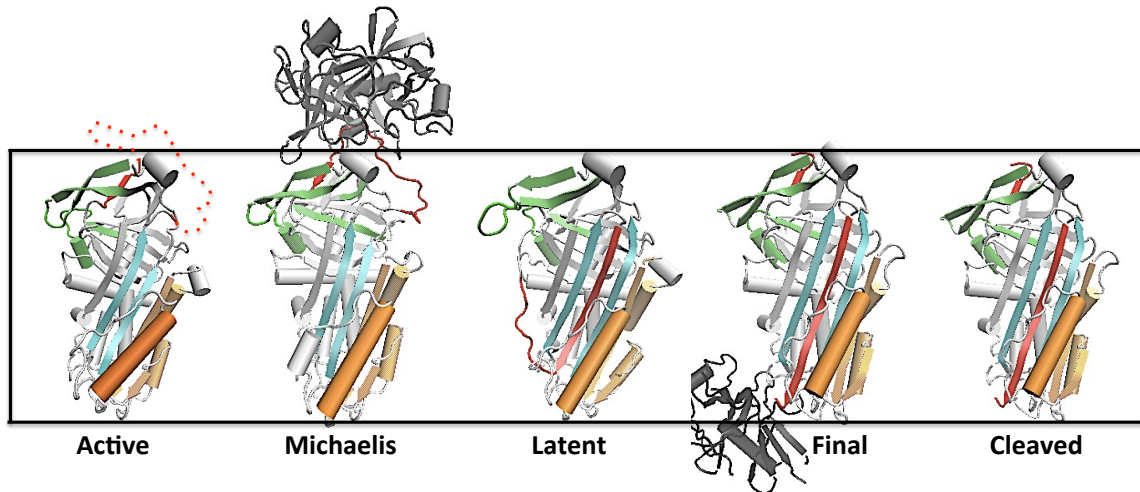


Figure 1.7 Structural Flexibility Enables PAI-1 to Adopt Many Global Conformations. PAI-1 can assume multiple conformations, which include the active metastable conformation (3Q02), the noncovalent Michaelis complex (3PB1), the inactive latent conformation (1C5G), the final complex (1TB6), and the cleaved substrate conformation (3EOX). Functional regions of the serpin are colored as indicated in Fig. 1.5. Serine proteases are shown in **black**. Graphics were constructed using VMD 1.9. The final complex is based on the structure of the thrombin-antithrombin complex and the pre-latent structure of PAI-1 is currently unresolved.

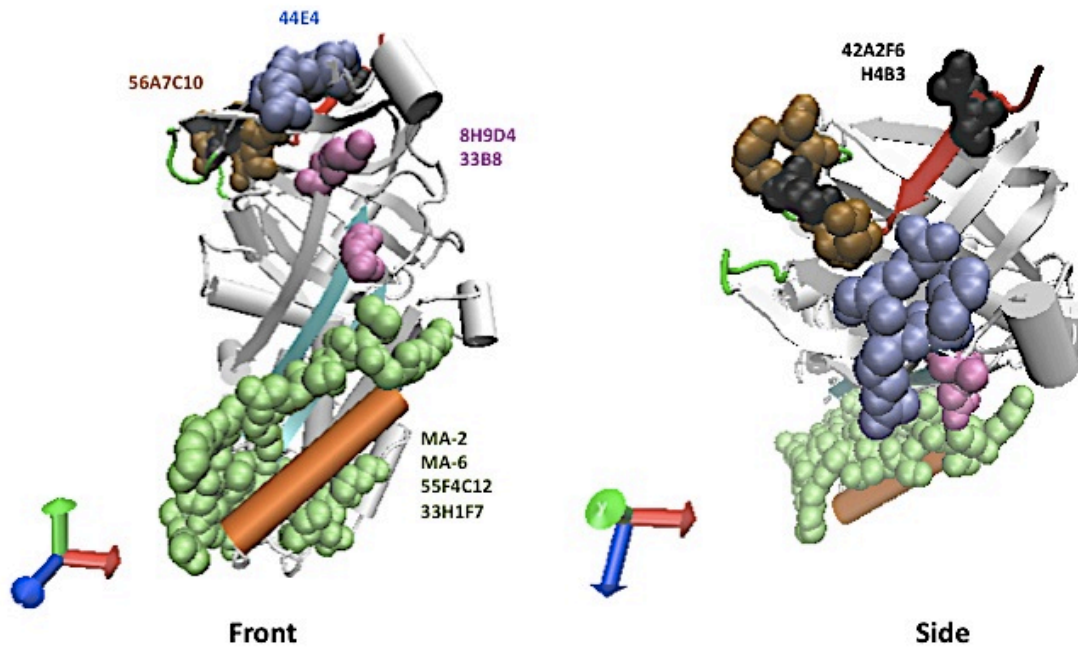


Figure 1.8 Monoclonal Antibodies Provide Information on PAI-1 Conformation. The location of the indicated PAI-1 mAb epitopes are shown in space-filling rendering and colored accordingly (44E4, 42A2F6, H4B3, 56A7C10, 8H9D4, 33B8, MA-2, MA-6, 55F4C12, & 33H1F7). PAI-1 secondary structural elements are also highlighted (s1C, gate loops, shutter, and hF). Representations constructed using VMD 1.9.

Table 1.2 Effects & Epitopes of PAI-1 Conformation-Sensing Antibodies

<i>mAb</i>	<i>Epitope</i>	<i>Mechanism of PAI-1 Neutralization</i>
2	s1A, hF, hF/s3A loop	Converts to substrate
6	s1A, hF, hF/s3A loop	Converts to substrate
55F4C12	hF opposite SMB BS	Converts to substrate by decreasing fast insertion (k_{lim})
33H1F7	hF opposite SMB BS	Converts to substrate by decreasing fast insertion (k_{lim})
H4B3	Cleft when s1C detaches	Accelerates latency
33B8	Pre-inserted hinge/hD	Accelerates latency
8H9D4	277 (s6A), 327 (s5A)	Converts to substrate by preventing disordering of protease active site
44E4	H185, R186, R187 (s4C)	Blocks Michaelis formation
42A2F6	K243 (s3B/hG loop), E350	Blocks Michaelis formation
56A7C10	E242, K243, E244 (s3B/hG loop), E350, D355 (P9'). R356 (P10')	Blocks Michaelis formation

it is likely that the RCL directs the conformational and functional changes between these forms. However, due to meta-stability of PAI-1, crystallization of native form has been elusive. Therefore, the use of conformation-specific monoclonal antibodies (mAbs) has been utilized to provide details on PAI-1 (**Fig. 1.8, Table 1.2**) [65, 67, 68, 85, 92-97]. Diverse methods, including fluorescence [98-105], hydrogen-deuterium exchange (HDX) coupled to mass spectrometry (MS) [90, 91], digestion by non-target proteinases [73, 89, 106], and mutagenesis analyses [70-72, 107-109], have also provided significant insight into the folding enigma of this protein and have mapped out important regions in its various transitions (**Table 1.3**).

In the active conformation, the RCL of PAI-1 projects from the serpin scaffold and is solvent-exposed (**Fig. 1.9**). By measuring the distance between P1' and P3 to E313 at its opposite pole using donor-donor energy migration (DDEM) [58], the RCL was determined to be tethered close to the protein core. Also, in this conformation, hF and hF/s3A loop cover and interact extensively with the parallel-stranded shutter, of which sA contains mostly hydrophobic and s5A half polar and nonpolar residues (**Fig. 1.10**). Since its hydrogen bonds are longer and weaker, the parallel organization of the shutter is less stable than its antiparallel organization in the RCL-inserted states. Also, the C-terminus of PAI-1 occupies a hydrophobic pocket formed by s2C, s6A, s4B, and s5B (involving residues P276, F278, L280, F358, and P379; c.f. Fig. 1.4) [66, 110], which in other serpins is occupied by its gate region. The latter position of the C-terminus is hypothesized to mobilize the gate region of PAI-1 and contribute to its more labile nature in comparison to other serpins [66]. Mutagenesis of this region indicates that the gate modulates the height of the energy barrier from active to latent forms [116].

Table 1.3 Global Conformational Changes Accompanying Transition of Active PAI-1 to Latent & Cleaved States By Functional Region

<i>Functional Region</i>	<i>Active</i> ★★	<i>Pre-latent</i>	<i>Latent</i> ★	<i>Final Complex</i> ⌘	<i>Cleaved (Substrate)</i> ¶¶¶
RCL (P14-P8')	Exposed	Partially Inserted ¶¶	Inserted	Inserted	Inserted
Hinge (P14-P11)	Exposed	Inserted	Inserted	Inserted	Inserted
s1C (P4'-P8')	Attached	Partially detached ¶	Detached	Attached	Attached
Shutter (s3A, s5A)§	Closed - partially open (parallel)	Partially open (parallel, pigeon-toe conformation) ❖	Open (occupied by s4A making β -sheet A antiparallel)	Open (occupied by s4A making β -sheet A antiparallel)	Open (occupied by s4A making β -sheet A antiparallel)
α -Helix F ★★★	Over shutter (not displaced)	Over shutter (not displaced)	Over shutter (returned after displacement)	Over shutter (returned after displacement)	Over shutter (returned after displacement)
Gate (s3Cs, 4C, s3B, hG)	Mobile (width~7Å)	Not Determined	More mobile (width~14Å)	Not Determined (~7 Å in α_1 AT-T complex) ○	Mobile (width~7Å)
Flexible Joint (s1A, s2A, hD, hE)	High affinity for VN +	Not Determined	Low affinity for VN +	Low affinity for VN ◆	Low affinity for VN ◆
Change in Covalent Structure	No	No	No	Yes	Yes

- ★★★ Ref. [111]
- ★★ Ref. [59]
- ★ Ref. [112]
- + Ref. [113]
- ¶¶¶ Ref. [114]
- ¶¶ Ref. [58, 65]
- ¶ Ref. [94]
- ⌘ Ref. [81]
- ❖ Ref. [92]
- ◆ Ref. [10]
- Ref. [115]

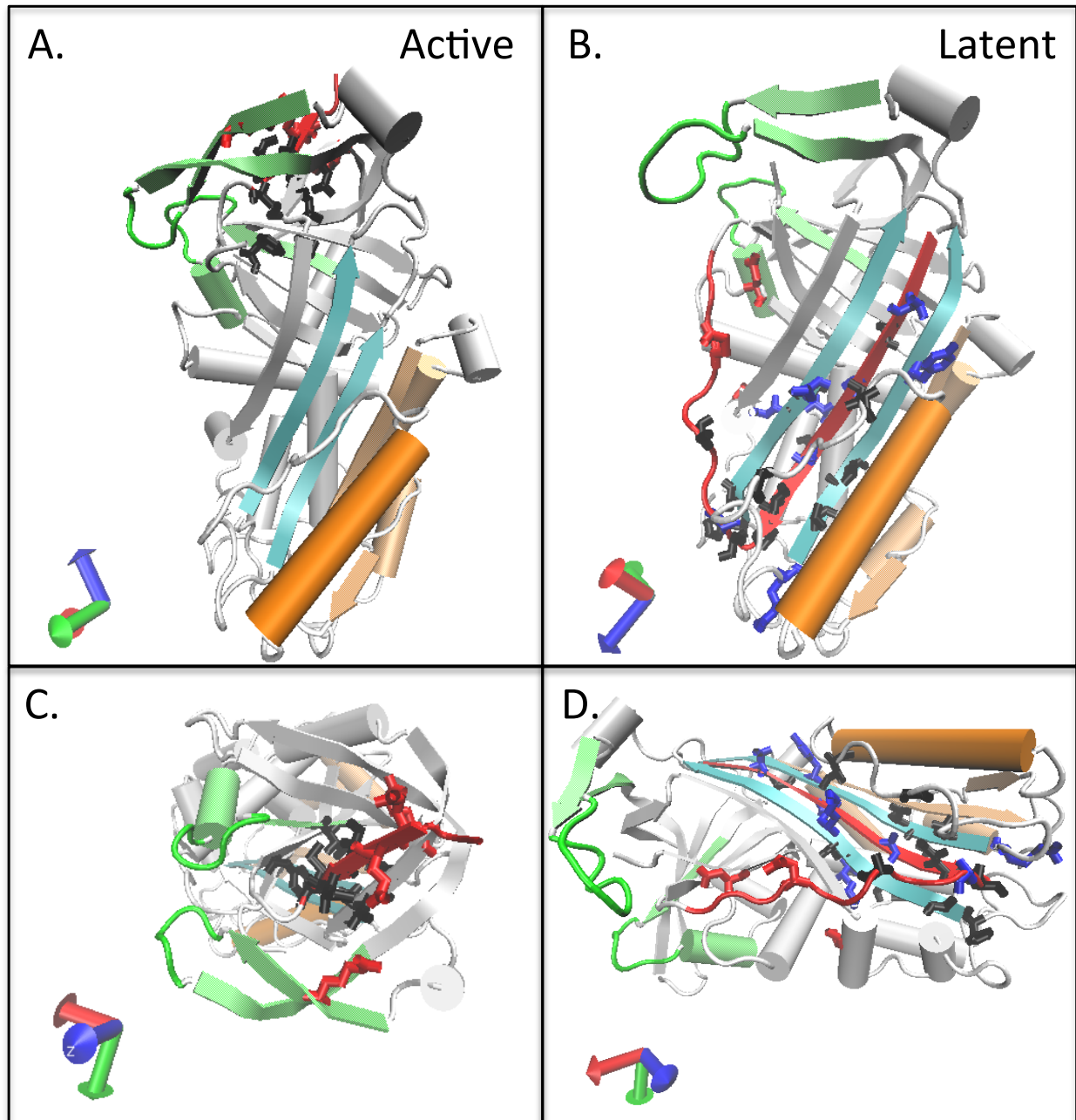


Figure 1.9 The RCL is Solvent-Exposed in the Active State & Tightly Associated With the Protein Core in the Latent State of PAI-1. PAI-1 in the active conformation is shown from two views (**A** & **C**), in which the RCL is mostly unresolved. In the latent conformation (**B** & **D**), the RCL is inserted as the fourth strand in the central β -sheet A (s4A). The secondary structure of functional regions is colored as in previous figures. Side-chains of the RCL and interacting residues are shown as lines and colored according to its participating interaction (hydrophobic - **black**, hydrogen-bond - **blue**, and ionic **red**). Representations were constructed in VMD 1.9 using the crystal structures of active (3Q02)[59] and latent (1C5G)[66] PAI-1.

During inhibition, the solvent-exposed RCL of PAI-1 forms a noncovalent Michaelis docking complex and is cleaved at the scissile bond by PAs. To form the final complex, the C-terminal RCL (including s1C) must be displaced from the protease active, and exosites released upon insertion of its N-terminal portion into sA. RCL insertion is limited by its access to the parallel-stranded shutter and hindered by the placement of hF. Furthermore, the opening of the shutter is restricted by interactions of s3A and s5A [73, 107] with hF “on top” and hB “on bottom” [108]. Upon displacement of hF and opening of the shutter, the RCL inserts, resulting in the reorganization of sA into a six-stranded antiparallel β -sheet. Following insertion, hF returns to its previous position over the shutter and newly inserted s4A [69]. Since most of the favorable enthalpy from RCL cleavage [61] is expended upon its insertion, the return of hF is hypothesized to provide the potential to “lock” the protease in the final complex [111]. Successive insertion of the RCL residues also is hypothesized to provide the energy for hF displacement [111]. Interestingly, s5A is connected in primary sequence to the RCL, and s3A is connected N-terminally to s4C of the gate and C-terminally to hF, thereby offering a possible route of communication between these structural elements.

While the structural changes during inhibition have been investigated thoroughly [68, 87, 117], much less is known about the conformational steps from the metastable to latent state of PAI-1 [4, 88, 92]. Despite this limitation, the structural requirements for latency transition that are known involve global conformation changes, including full detachment of s1C from its participating β -sheet to allow RCL insertion without cleavage, widening of the gate loops from 7 Å to 14 Å (**Fig. 1.11**) to allow s1C through and elongation of P2-P10' alongside the protein surface, opening of the shutter,

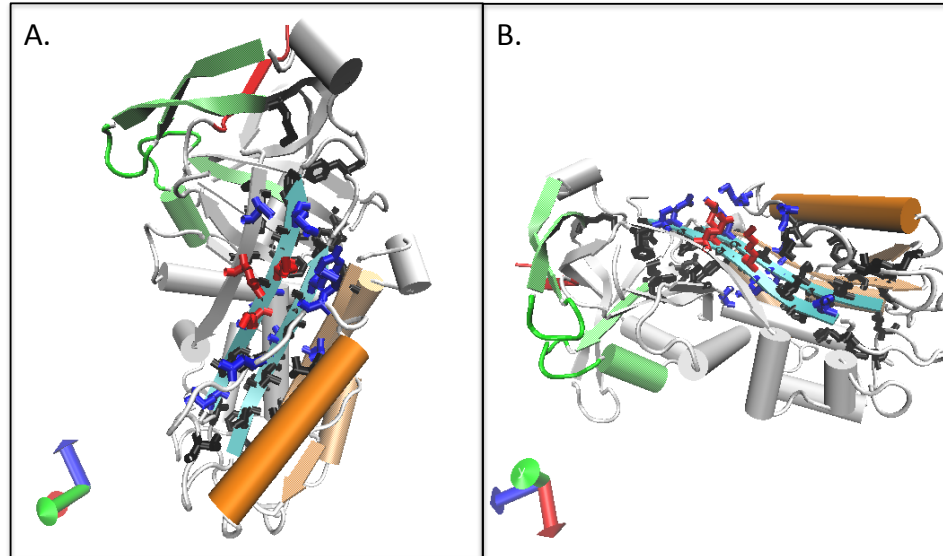


Figure 1.10 α -Helix F Covers The Shutter Region in Metastable Conformations of PAI-1. Active PAI-1 is shown from two views (A-B) with secondary structure of functional regions colored as in previous figures. Side-chains of the shutter and interacting residues are shown as lines and colored according to its participating interaction (hydrophobic - **black**, hydrogen-bond - **blue**, and ionic **red**). Representations were constructed in VMD 1.9 using the crystal structures of active (3Q02) and latent (1C5G) PAI-1.

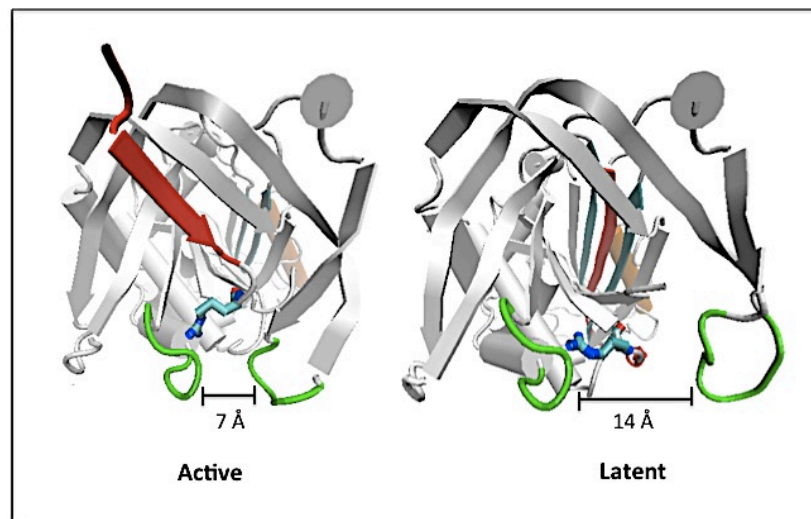


Figure 1.11 The Mobile Gate Region of PAI-1 Widens to Allow RCL Insertion In The Latent Conformation. The gate region of PAI-1 in the active (3Q02) and latent (1C5G) conformations is shown from the 'top' view. The distance between the gate loops (**green**) is indicated and other functional regions colored as previously. The side chain of Arg356 (P10') is shown as lines. Distances were calculated using MOE and structures rendered in VMD 1.9.

Table 1.4 Comparisons of RCL Interactions in the Active & Latent States of PAI-1

<i>Metastable</i>						
<i>Type*</i>	<i>Residue</i>	<i>First Contact</i>		<i>Residue</i>	<i>Second Contact</i>	
		<i>Number</i>	<i>RCL Position</i>		<i>Number</i>	<i>Location in 2^o Structure</i>
ION	GLU	350	P4'	ARG	271	s2C
ION	GLU	351	P5'	ARG	187	s4C
HYD	ILE	352	P6'	LEU	273	s2C
HYD	ILE	353	P7'	VAL	274	s2C
HYD	MET	354	P8'	ILE	237	s3B
HYD	MET	354	P8'	LEU	275	s2C
HYD	PHE	358	P12'	ILE	237	s3B
HYD	PHE	358	P12'	LEU	275	s2C
HYD	PHE	358	P12'	PHE	278	s2C/s6A loop
HYD	PHE	358	P12'	MET	354	s1C/RCL/P8'

<i>Latent</i>						
<i>Type*</i>	<i>Residue</i>	<i>First Contact</i>		<i>Residue</i>	<i>Second Contact</i>	
		<i>Position</i>	<i>RCL Position</i>		<i>Number</i>	<i>Location in 2^o Structure</i>
HB	THR	333	P14	TYR	228	s2B/s3B loop
HYD	VAL	334	P13	MET	147	hF/s3A loop
HB	SER	336	P11	LEU	169	s2B
HB	THR	339	P8	GLY	38	hB
HB	THR	339	P8	GLN	322	s5A
HYD	VAL	341	P6	VAL	42	hB
HYD	VAL	341	P6	LEU	43	hB
HYD	VAL	341	P6	LEU	46	hB
HYD	VAL	341	P6	LEU	165	s3A
HYD	VAL	341	P6	VAL	317	hI/s5A loop
HYD	ILE	342	P5	LEU	152	s3A/hF loop
HYD	ILE	342	P5	VAL	164	s3A
HYD	ILE	342	P5	LEU	321	s5A
HYD	VAL	343	P4	LEU	163	hF/s3A loop
HYD	VAL	343	P4	LEU	315	hI/s5A loop
HB	SER	344	P3	THR	161	hF/s3A loop
HYD	MET	347	P1'	LEU	321	s5A
HB	GLU	350	P4'	ARG	30	hA/hB loop
HB	GLU	350	P4'	ASP	285	s6A
ION	GLU	350	P4'	ARG	30	hA/hB loop
ION	GLU	350	P4'	LYS	288	hI

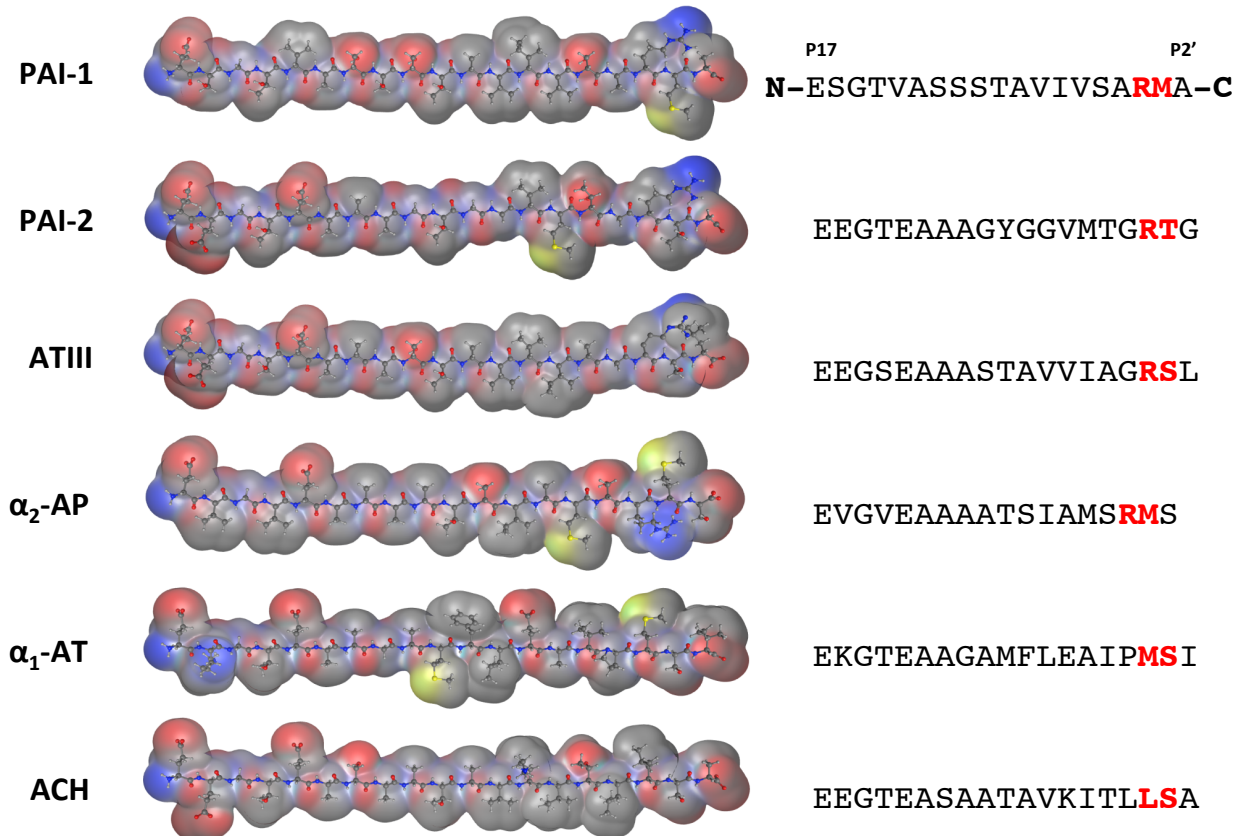
* HB = hydrogen bond, HYD = hydrophobic interaction, ION = ionic bond

insertion of P14-P11 before displacing hF to fully insert up to P4 with P-even residues buried and P-odd exposed, and return of helix F over sA [112]. Upon its insertion, the RCL is tightly associated with its core by participating in many hydrophobic and hydrogen-bonding interactions with the shutter and hF/s3A loop (**Table 1.4**).

Prior to full insertion, PAI-1 may also adopt a pre-latent conformation in which the RCL is reversibly and partially inserted up to P11 [58] and the s1C is partially detached [94]. Pre-insertion of the RCL in this low populated conformation (from crystallization and NMR studies) [66, 94, 118] is not required for recognition [60] by PAs. Also, cleavage by PAs, but not Michaelis complex formation, triggers insertion of the RCL [57, 69, 117] and may shift the equilibrium of PAI-1 towards to the pre-latent conformer. Since s1C detachment occurs in this state, the rate-limiting step for the latency process is hypothesized to be opening of or RCL passage through the gate.

1.1.e. Roles of the RCL

Serpins are specific inhibitors of their target serine protease. However, a comparison of the RCL composition of various serpins, including the intracellular PAI-2, antithrombin III (ATIII), α_2 -antiplasmin (α_2 -AP), α_1 -antitrypsin (α_1 -AT), and antichymotrypsin (ACH), shows that these serpins share a high degree of homology [56, 84] (**Fig. 1.12**). Overall, the consensus of the RCL is for small, nonpolar residues, with acidic residues at the hinge (P16-P17), a small, uncharged residue at P14, and basic residues at the scissile bond. Accordingly, the replacement of P14 in PAI-1 with a basic residue such as arginine (PAI-1_R) results in its complete substrate behavior, which has been manipulated to provide mechanistic details (e.g. k_{assoc} , $k_{\text{acylation}}$) of the inhibitory process [60, 78], and conformational information about the central β -sheet of PAI-1



CONSENSUS RCL: Glu-E/D-Gly-Thr-Glu-Ala-Ala-Ala-Ala-Thr-p/n-non-non-non-p/n-non-Arg-Ser-non

Figure 1.12 Serpins Are Highly Specific Inhibitors Despite Similarities in RCL Sequence. The RCL of PAI-1 is shown in comparison to that of other inhibitory serpins, including PAI-2, antithrombin III (ATIII), α_2 -antiplasmin, α_1 -antitrypsin (α_1 -AT), and antichymotrypsin (ACH). RCL peptides (*left*) were constructed using Molecular Operating Environment (MOE2010), and atoms displayed in the ball-and-stick model inside the molecular surface (*red* - acidic, *blue* - basic, *yellow* - sulfur, *gray* = nonpolar). The P1-P1' scissile bond residues in the RCL sequences (*right*) are also shown in *red*, with the P-designations at the top, and the RCL consensus sequence at the bottom.

variants in the presence of RCL-mimicking peptides (e.g. rigidity of 14-1B sA) [92]. Also, N-terminal RCL chimeras, in which P17-P2 are replaced by the corresponding residues in PAI-2, ATIII, and the serpin consensus sequence, show a minor impact on the specificity of the serpin [84]. Similarly, the activity of PAI-1 is largely unaffected by alanine-scanning, charge reversal, and homology mutagenesis of P4'-P10' [116]. In contrast, replacement to proline at most positions in RCL, including P14 and P12 [119-121], decreases the k_{lim} of PAI-1 with PAs and increases its substrate behavior, while PAI-1 with proline at the P1 position is not an inhibitor. Also, the substitution of P-even residues in the N-terminal portion of the RCL, which point inwards towards the hydrophobic core, with the negatively charged glutamate slows the latency transition of PAI-1 [66].

Saturation mutagenesis of P1-P1' [122] and combinatorial mutagenesis of the P3-P1 (Ser-Ala-Arg) [83] residues demonstrates the necessity for a basic residue at the P1 position and the strict positional requirement of Arg-Met at the scissile bond for successful inhibition, respectively (i.e. R-M at P3-P2 or P2-P1 are not inhibitors). Appropriately, the length of the RCL, in addition to the identity of its residues, is highly conserved among serpins [123]. Consequently, additions and deletions within the N-terminal P4-P3 region of the RCL result in increased substrate behavior, indicating the prerequisite for tight tethering in distorting protease upon complex formation [123]. Also, additions and deletions within the C-terminal P3'-P5' residues of PAI-1 result in the accelerated and lengthier latency transition, respectively [124].

1.1.f. Glycosylation, Mutation, and Cofactor Effects on PAI-1 Stability

Native human PAI-1 is glycosylated, resulting in its greater stability than

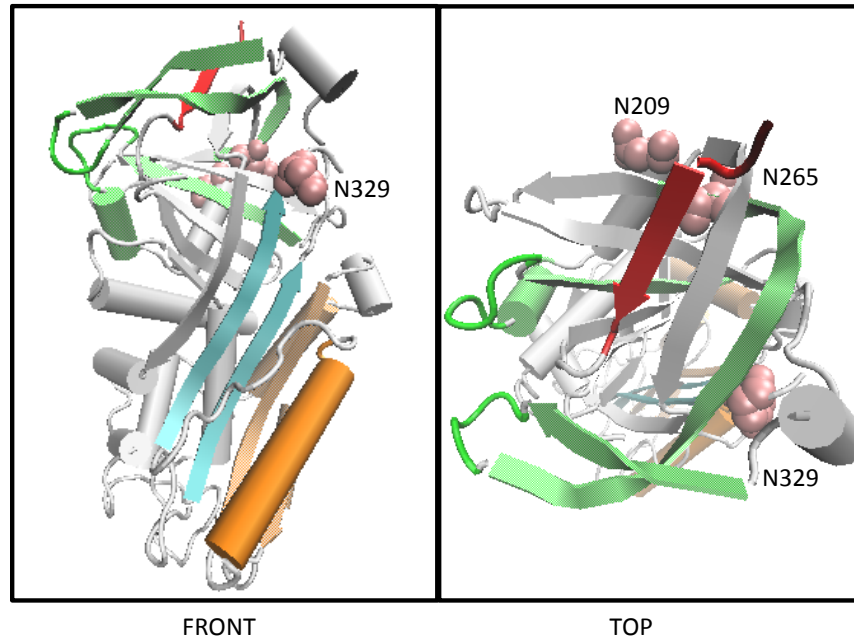


Figure 1.13 Glycosylation of PAI-1 Slows Latency Conversion. PAI-1 contains three possible N-linked glycosylation sites, which residues are shown as space-filling representation (*pink*). Functional regions are colored as previously described and structures were rendered using VMD 1.9.

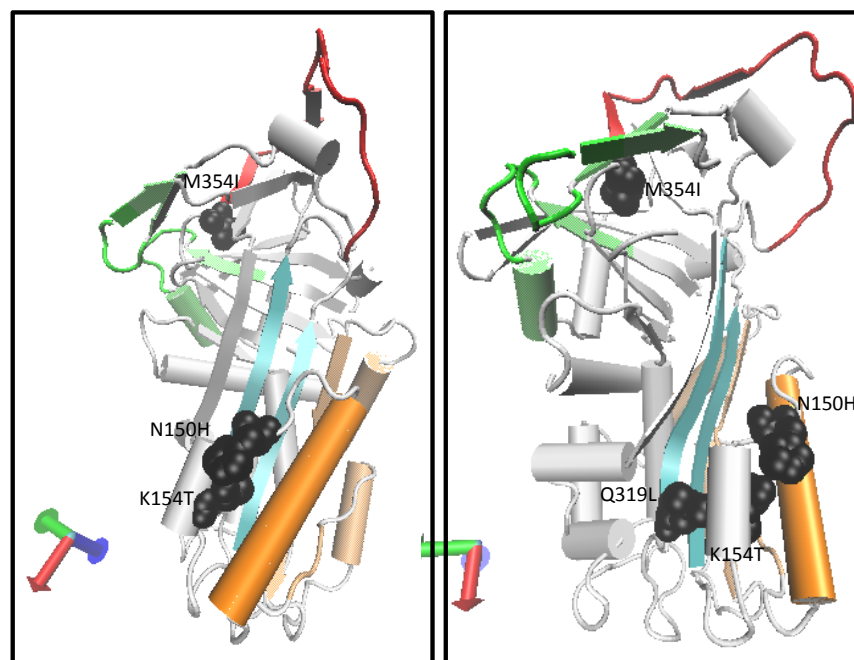


Figure 1.14 The Active Conformation is Stabilized by Mutation of The Gate & Shutter Regions in 14-1B Variant of PAI-1. The quadruple 14-1B mutant of PAI-1 has an active half-life of ~145 hrs. Residues mutated are indicated and shown as space-filling representation (*black*). Functional regions are colored as previously described and structures based on PDB 1B3K were rendered using VMD 1.9.

than unglycosylated recombinant PAI-1 [4]. Glycosylated PAI-1 present *in vivo* has a half-life in plasma longer than the latter *in vitro* (i.e. ~6 hrs versus ~1-2 hrs at physiological temperature and pH), but is still much more labile than other plasma components (e.g. the half-life of serum albumin is ~19 days). Three potential glycosylation sites at N209, N265, and N329 exist on PAI-1 (**Fig. 1.13**), but only the former two are modified [4]. The N-linked glycosylation at position 265 particularly affects the latency transition of PAI-1 by binding in the hydrophobic cleft covered by s1C in the gate region, which slows the latency transition of PAI-1. Since latent PAI-1 in this glycosylated form has been recovered from plasma, tissues [92], and platelets [10], the latency transition as a mechanism of self-regulation of PAI-1 is physiologically relevant. Other biochemical properties of PAI-1 are unaffected by absence of this post-translational modification [4].

In addition to glycosylation, the stability of PAI-1 is particularly affected by mutations in functional regions that are important in the conformational changes from the metastable to RCL-inserted forms of PAI-1 (i.e. during latency transition and inhibition). The quadruple 14-1B mutant of PAI-1 exemplifies the latter (**Fig. 1.14**). Via molecular evolution using phase-display methods, the N150H (hF/s3A loop), K154T (hF/s3A loop), Q319L (s5A), and M354I (s1C) mutations in 14-1B result in PAI-1 with an inhibitory half-life of ~145 hrs and denaturation temperature ~10°C higher than its native form [70]. In contrast, the single mutations only modestly increase the stability of PAI-1. These mutations result in the formation of a unique hydrogen-bond network created over the shutter region where the RCL inserts [108].

Conformational differences between native and 14-1B PAI-1 make conclusions

regarding mechanism based on the former debatable [4]. A 3_{10} helix present in the loop connecting hF (covering the shutter) to s3A of the shutter in 14-1B is absent in the metastable W175F structure of PAI-1 [59]. [The W175F mutation, located at the region where the RCL hinge inserts (i.e. breach region), is kinetically more stable ($t_{1/2} \sim 7$ hrs), but shares the same thermodynamic stability as native PAI-1.] Also, while 14-1B binds to VN and is stabilized in a fashion similar to wt-PAI-1, the 338B mAb and RCL-mimicking peptides indicate that the RCL and shutter in the mutant differ from that of the wild-type protein [92]. Thereby, the decreased mobility and greater extension of the RCL, resulting in less extensive pre-insertion, and a shutter closed near the flexible hinge region, possibly due to the proposed hydrogen-bonded network, is hypothesized to explain the increased stability of 14-1B relative to native PAI-1.

Importantly, VN also influences the stability of PAI-1 in its RCL-exposed active conformation. VN binds with high affinity ($K_d \sim 0.1-1$ nM) [62] via its 44-residue N-terminal SMB domain to Q125, R103, and M112 of flexible joint region of PAI-1 (**Fig. 1.15**). Binding at this site is responsible for the stabilizing effect of VN on PAI-1 [91, 92, 113, 125], modestly increasing its inhibitory lifetime by $\sim 1.5-2$ -fold [80]. The interaction of VN and PAI-1 extends beyond this region to an additional site mapped to a region outside the SMB domain of VN and hE (R115 and R118) in PAI-1 near its heparin-binding site [80]. Binding at this lower affinity site ($K_d \sim 100$ nM), like heparin, does not stabilize PAI-1 [113, 126]. VN also affects the interaction of PAI-1 with divalent transition metals by reversing the destabilization of PAI-1 caused by these metals [62, 127]. However, the mechanism by which VN stabilizes PAI-1 and affects the metal-PAI-1 interaction is not clear, and hypotheses range from a purely steric one, involving closure

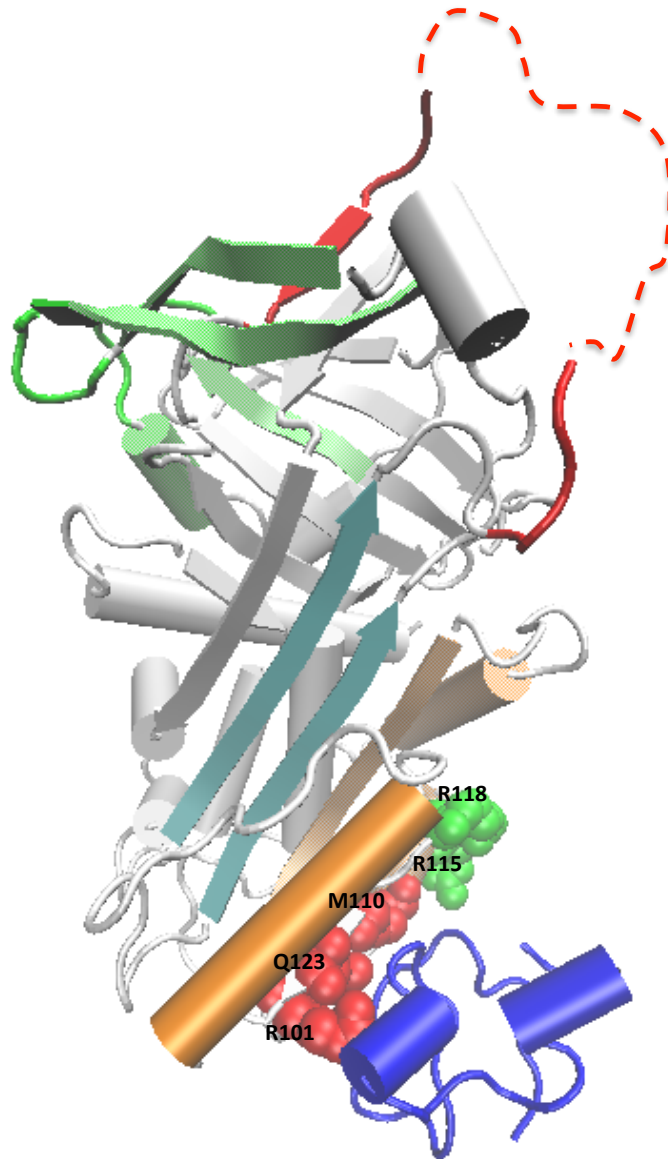


Figure 1.15 Vitronectin Binds At The Flexible Joint Region & Stabilizes PAI-1 in The Active Conformation. The N-terminal somatomedin B domain (SMB, **blue**) is shown in complex with PAI-1 (1OC0). Residues that comprise the primary high-affinity (**red**) and secondary low-affinity (**green**) VN binding sites on PAI-1 are displayed as spaced-filled spheres. The representation was generated in VMD 1.9.

of the bottom of the shutter via binding the flexible joint region [92, 125], to changing the RCL conformation, making it more solvent exposed upon complex formation [4, 92, 104].

1.2. Rationale for Study

The RCL of PAI-1 directs its conformational transitions during latency and protease inhibition, but its native structure has been elusive by crystallographic methods. Structural information gathered by additional means can be beneficial in the development of its use as a druggable target. In Chapter 2, homology modeling is performed to understand the flexible nature of the RCL, not readily apparent or artifactual (i.e. resolved due to crystal packing) in available structures, and to gain possible insights into the metastable folding of loop regions in serpin structures. Also, although its mechanism of inhibition has been investigated in great detail, much less is known about the steps from the metastable to the latent state of PAI-1, including the limiting step. To investigate this transition as reported from the RCL, single-cysteine mutants were engineered along its length to covalently attach the environmentally sensitive fluorescent NBD (N,N' - dimethyl - N - (iodoacetyl) - N' - (7 - nitrobenz - 2 - oxa - 1,3 - diazol - 4 - yl) ethylene diamine) or paramagnetic spin MTSL (2,5 - dihydro - 2,2,5,5 - tetramethyl - 3 - [[[(methylsulfonyl) thio] methyl] - 1H - pyrrol - 1 - yloxy) probes. Of the 22 residues, 17 were selected based on the contacts formed in the latent conformation (**Table 1.5**) and functional importance, including hinge residues involved in pre-insertion, and gate residues involved in s1C detachment.

VN stabilizes PAI-1 and slows its latency rate by a yet unclear mechanism. As its cofactor, the outcome of physiological processes that involve PAI-1 also involves VN. A

better understanding of this mechanism can provide valuable information on the PAI-1-VN interaction. In Chapter 3, the models of PAI-1 stabilization by VN are discussed and involvement on the RCL hypothesized. Using PAI-1 labeled at the RCL, the effect of VN and its truncations, SMB and SMB-IDD, binding at the distal flexible joints site on RCL solvent-accessibility, and thus conformation, and dynamics are investigated to provide information on the mechanism of VN-mediated PAI-1 stabilization.

In Chapter 4, the interaction of PAI-1 and PAs in the Michaelis complex is investigated. For native PAI-1, k_{lim} and K_m for tc-tPA is ~9X slower and ~16X smaller, respectively, than that of uPA [80, 85-87] (**Table 1.1**). Since the stoichiometry of inhibition (SI ratio = $1 + k_s/k_i$), describing the propensity of PAI-1 to partition between the inhibitory and substrate branches during RCL insertion, is the same for PAI-1 with both PAs [57, 85, 87], the noted differences in k_{lim} are due to differences in exosite interactions [68]. Utilization of exosites increases serpin specificity and inhibition rates via effects on scissile bond orientation and overall binding affinities [128]. The main exosite exploited by PAI-1 and PAs is between the acidic P4'-P5' residues in PAI-1 contacting the surface-exposed 37-loop of PAs [129]. This interaction has been demonstrated to effect k_{lim} via loop-displacement (k_3), and is stronger for tPA than uPA [68, 85, 87]. Furthermore, the resolved crystal structure of the Michaelis complex between 14-1B PAI-1 and active site-blocked uPA shows the utilization of additional surface-exposed loops of uPA in exosite interactions with PAI-1 [81].

Although the P4'P5'-37-loop exosite interaction on k_{lim} has been studied, the contribution of other exosites, as identified by PAI-1-uPA Michaelis structure, is unclear. In an effort to investigate the latter and explain the noted differences in inhibition rates,

the binding of active site-blocked sc-tPA (tPA-SPD*) and uPA (uPA-SPD*) in the Michaelis complex with PAI-1 was investigated using the RCL-labeled single mutants. Based on these results, a model of the Michaelis complex between PAI-1 and tPA constructed, providing new information on exosite interactions to explain differences in rates of PA inhibition by PAI-1. Together, these studies provide a comprehensive look at the RCL of PAI-1.

Table 1.5 Residues Scanned by Cysteine Mutagenesis to Probe the Conformation & Dynamics of PAI-1 RCL

	<i>Residue</i>	<i>Number</i>	<i>RCL Position</i>
1	THR	333	P14
2	VAL	334	P13
3	ALA	335	P12
4	SER	336	P11
5	SER	338	P9
6	THR	339	P8
7	VAL	341	P6
8	ILE	342	P5
9	SER	344	P3
10	MET	347	P1'
11	ALA	348	P2'
12	PRO	349	P3'
13	GLU	350	P4'
14	GLU	351	P5'
15	ILE	352	P6'
16	ILE	353	P7'
17	MET	354	P8'

Chapter 2 The Metastable RCL Occupies Limited Conformations That Change During Latency Transition

2.1. Introduction

2.1.a. Fluorescence Detects Changes in Solvent Accessibility

Fluorescence (**Fig. 2.1 A**), frequently employed for structural investigation, localization studies, and investigation of protein-protein interactions, occurs when an excited electron emits light of a lower energy and longer wavelength than it absorbs [130]. This radiative process includes three main steps, including absorption and excitation, a transient fluorescence lifetime, and emission. During fluorescence, a ground state electron is excited to a higher energy state upon absorption of light of a wavelength that is equal in energy to the difference between its two energetic states. The excited electron remains in the higher energy state for a time that defines its fluorescence lifetime, which typically ranges from femtoseconds (10^{-15} s) to nanoseconds (10^{-9} s). During this excited lifetime, the electron can lose energy as heat due to thermal motions, molecular vibrations, or by radiationless processes, including distance-dependent resonance energy transfers, before entering the lowest energy excited state. From this state, the electron returns to ground state by releasing energy and emitting light of a longer wavelength.

To probe conformational changes that occur in RCL by its solvent accessibility, the NBD fluorophore (**Fig. 2.1 B**) was employed due to its prior use, frequently at the P9 position to provide mechanistic details of the inhibitory process [4, 5, 12, 13, 25, 26, 33, 35-39]. The utility of this probe is also in its high extinction coefficient, quantum yield, and sensitivity to local environmental changes. Specifically, then environmental impact on its spectral properties includes a reduced, red-shifted or enhanced, blue-shifted

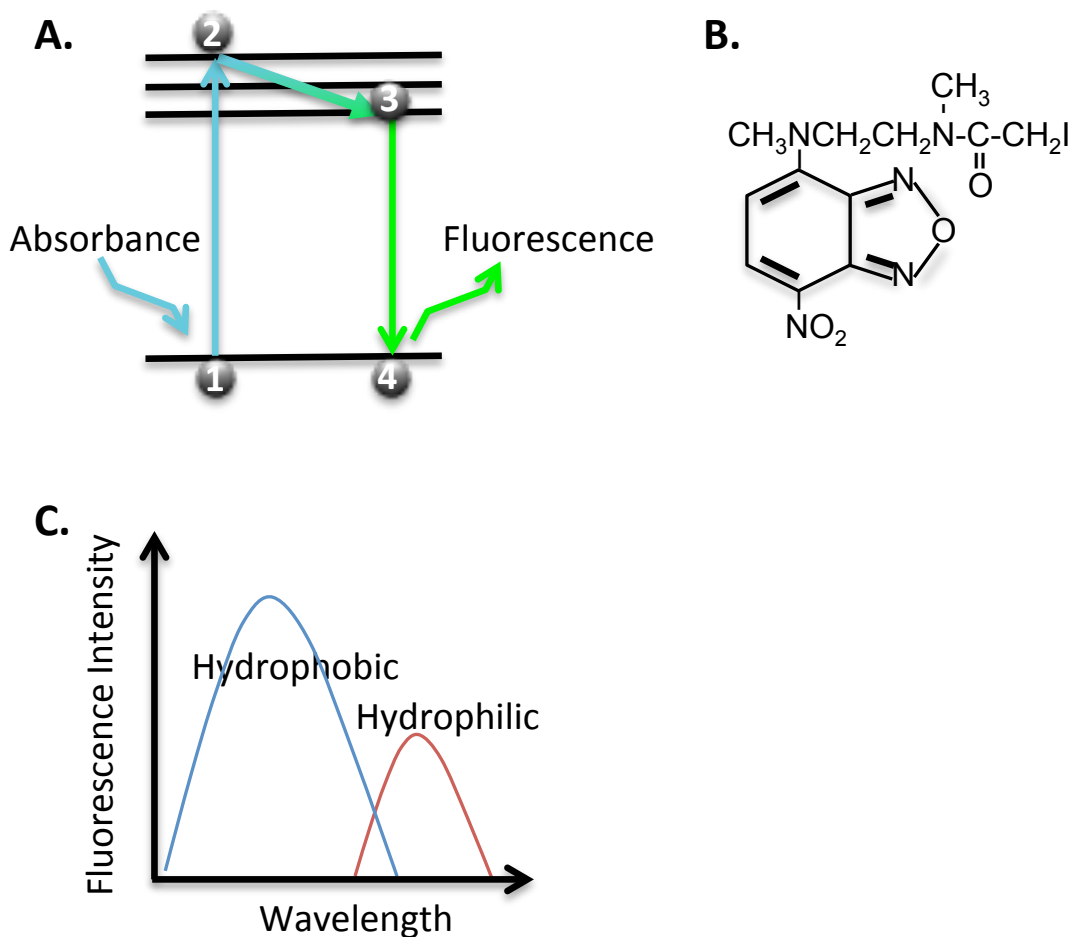


Figure 2.1 Fluorescence Using The NBD Probe. **A.** Fluorescence is the process by which a ground state electron (1) absorbs light of the wavelength that is equal in energy to the difference between two energetic states and is excited to a high energy state (2), where it can lose energy (3), and upon returning to ground state (4), emits light of a longer wavelength and lower energy than absorbed. **B.** The structure of the thiol-reactive fluorescent NBD probe chosen for this study. The spectral properties of NBD (**C.**) include an enhanced, blue-shifted and reduced, red-shifted fluorescence in hydrophobic and hydrophilic environments, respectively.

fluorescence in hydrophilic and hydrophobic environments, respectively (**Fig. 2.1 C**), and thereby can be used for conformational investigation.

2.1.b. EPR Spectroscopy Provides Information on Protein Dynamics

To complement structural investigation by fluorescence, electron paramagnetic resonance (EPR) spectroscopy is used to investigate PAI-1 RCL dynamics. (**Fig. 2.2**) The resonance of an unpaired electron harboring paramagnetic properties occurs when it absorbs radiation of a frequency (ν) that is equal in energy to the energy difference (ΔE) between its two states (h is Planck's constant) (**Fig. 2.2 A**). Typical EPR experiments involve sweeping the magnetic field at a constant frequency, usually in the microwave range (9-10 GHz, i.e. X-band). The resulting absorption spectra are converted to the first derivative. The line-widths (H_0) in these derivative spectra provide information on nanosecond dynamics (~ 1 -100 ns) that depend on the rotational correlation time, τ_c , i.e. the time it takes the spin-label side chain to rotate 1 radian. Sharper and broader line-widths, corresponding to larger and smaller inverse line-widths (H_0^{-1}), thereby indicate greater or more restricted motion, respectively

The paramagnetic MTSL probe (**Fig. 2.2 B**) was chosen for investigation of RCL dynamics due to its extensive use and thorough characterization [131-134]. The MTSL signal is split into three peaks due to the interaction of its paramagnetic electron with the nearby nitrogen nucleus (i.e. a hyperfine interaction) (**Fig. 2.2 C**). EPR using the MTSL probe can be used to provide specific information about the location (e.g. α -helix, β -strand) and environment (e.g. polar, hydrophobic) of an individual residue, the proximity of individual residues, and changes in local structure due to intramolecular conformational changes or dynamic interactions [135]. Advantages of EPR include the

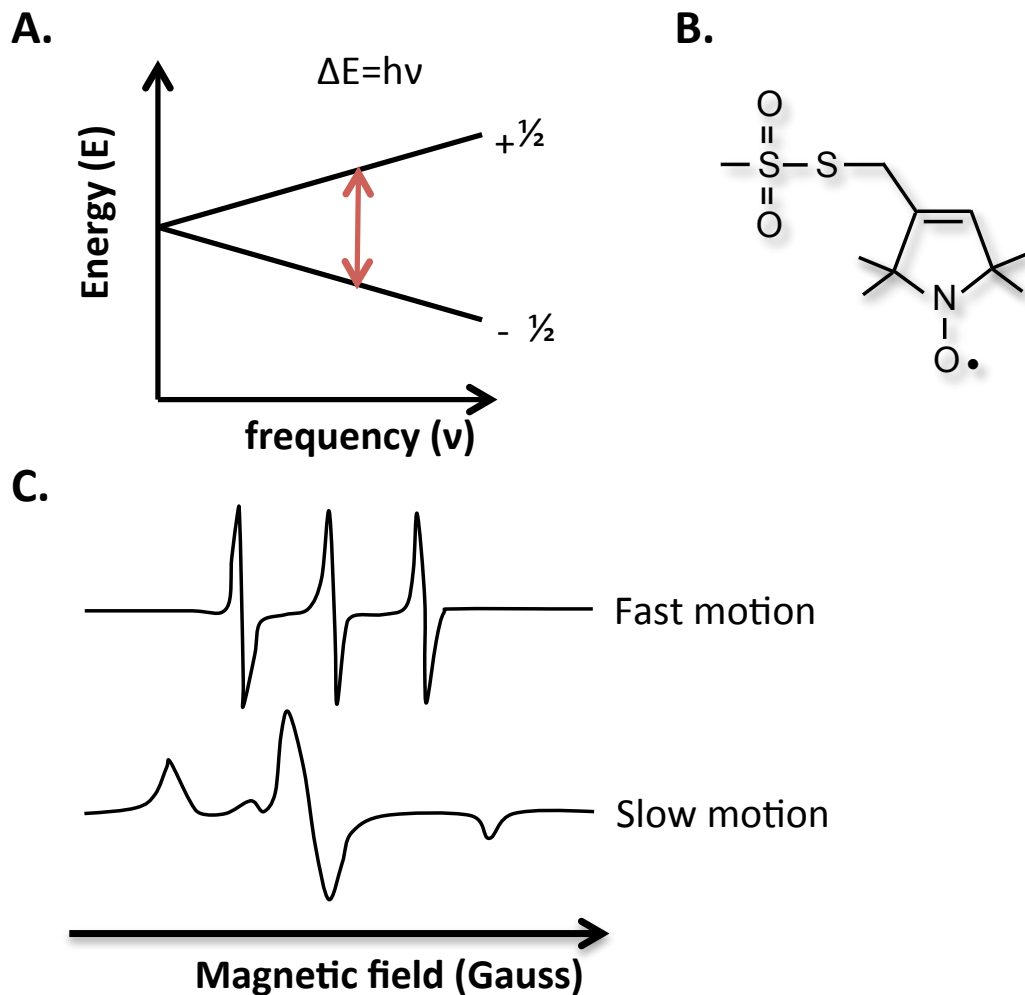


Figure 2.2 Electron Paramagnetic Resonance Using The MTSL-Probe. **A.** Electron paramagnetic resonance occurs when a molecule with an unpaired electron (i.e. paramagnetic) absorbs radiation of a frequency (ν) that is equal in energy to the energy difference (ΔE) between the two states (h is Planck's constant). Typical EPR experiments involve sweeping the magnetic field at a constant frequency. **B.** Structure of the MTSL probe chosen for investigation of RCL dynamics. **C.** The characteristic MTSL signal is split into three peaks due to the interaction of the paramagnetic electron with the nitrogen nucleus. Sharp line-widths in EPR spectra of MTSL indicate fast motion, while broad line-widths indicate slow motion.

use of relatively small sample size, lack of molecular weight or size restrictions, and insignificant interference of non-paramagnetic contaminants on the resulting signal [135, 136].

2.1.c. Objective of Study

The RCL plays a central role in PAI-1 function, but structural details are missing. A better understanding of its conformation, dynamics, and latency transition can provide useful information for the development of inhibitors to PAI-1 in the treatment of CVD and certain cancers. Using homology modeling, fluorescence, and EPR spectroscopy, the conformation and dynamics of the RCL are investigated to provide this lacking information.

2.2. Methods and Materials

2.2.a. Homology Modeling of PAI-1 RCL

The RCL of PAI-1 was modeled in Molecular Operating Environment (MOE, 2010) using the metastable structure of PAI-1 (PDB ID: 3Q02) as a template. Initially, the signal sequence was removed from the target sequence (NP_000593.1) and subsequently aligned (using MOE align) against the PDB template sequence in which the RCL is unresolved. Following the alignment, the core structure of PAI-1 was refined by energy minimization using the CHARMM27 force field parameters and fixed partial charges. The RCL was modeled with all other parameters default. Three low energy structures resulted from homology modeling of the RCL (HM1-3).

2.2.b. Prediction of Solvent Accessibility for PAI-1 RCL Homology Models

The solvent accessibility of a residue in the RCL homology models was predicted in MOE2010 based on an independent probability accounting for its structural class and

a conditional probability, for which the residue in a window of residues is compared to a reference GLY-X-GLY tripeptide, where X is the residue in question. The residue was classified as buried, partially-exposed, or exposed if the probability of the residue is < 9%, < 36%, or > 36% of its reference value, respectively. Probabilities of the buried class are plotted.

2.2.c. Protein Contacts Analysis

Inter- and intrachain contacts within crystal structures or homology models were reported in MOE2010-2012 using a cut-off distance for hydrophobic and ionic interactions of 4.5 Å, and treating histidine and methionine as basic and hydrophobic, respectively. Side-chain to main-chain hydrogen bonds are also included.

2.2.d. PAI-1 Cloning & RCL Mutagenesis

The human PAI-1 gene, cloned without a His-tag into the pET24d(+) vector within HindIII & NcoI restriction sites for inducible expression and selection via kanamycin resistance, was a kind gift from Grant Blouse (Novo Nordisk A/S, Clayton, NC). Oligonucleotide primers (Invitrogen Custom DNA Oligos) were designed to contain a single cysteine mutation at the desired RCL position along with a unique restriction site to facilitate screening (**Table 2.1**), and mutations were introduced by PCR according to manufacturer's instructions using the Stratagene Quik Change® II XL Site-directed Mutagenesis kit. The resulting *Dpn1*-treated products were also accordingly transformed into β-mercaptoethanol-treated XL-10 Gold ultracompetent cells via a 30 min incubation on ice followed by a 30 sec heat-shock at 42°C, return to ice for 2 min, addition of 0.5 ml warm SOC media (Invitrogen™), incubation at 37°C and 250 rpm for 1-2 hrs, and inoculation onto LB-agar plates supplemented with 50 µg/ml kanamycin for

Table 2.1 Primer Design & Engineering of Unique Restriction Sites to Facilitate Screening of Single-Cysteine RCL Mutants of PAI-1

Primer	Length	G+C	%GC	N	%N	T _m	Mutation	Sequence	Restriction Site Introduced	Recognition Sequence
P14FWD	38	23	61	4	11	78	T333C	5'-GAGGTGAACGAGAGIG GGTGT GTGGCCTCCTCATCCAC-3'	TaqII'	CACCCA
P14REV	38	23	61	4	11	78	T333C	5'-GTGGATGAGGAGGCCAC ACACCCA CTCTCGTTACCTC-3'		
P13FWD	35	22	63	3	9	79	V334C	5'-GTGAACGAGAGTGGC ACGTGCG CCTCCTCATCCAC-3'	PmlI	CACGTG
P13REV	35	22	63	3	9	79	V334C	5'-GTGGATGAGGAGGCC GCA CGTGCACCTCTCGTTAC-3'		
P12FWD	35	21	60	3	9	78	A335C	5'-CGAGAGTGGCAGGGT TGCTCTTC ATCCACAGCTG-3'	SapI	GCTCTTC
P12REV	35	21	60	3	9	78	A335C	5'-CAGCTGTGGAT GAAGAGCA CACCGTGCCACTCTCG-3'		
P11FWD	28	19	68	2	7	78	S336C	5'-GGCACGGTGGCC TGCTCTTC CACAGCTG-3'	SapI	GCTCTTC
P11REV	28	19	68	2	7	78	S336C	5'-CAGCTGTG GAAGAGCA GGCCACCGTGCC-3'		
P8FWD	38	24	63	4	11	79	T339C	5'-CGGTGGCCTCCTCATCC TGGCA AGTCATAGTCTCAGCC-3'	FspI	TGCGCA
P8REV	38	24	63	4	11	79	T339C	5'-GGCTGAGACTATGAC TGGCA GGATGAGGAGGCCACCG-3'		
P6FWD	36	21	58	3	8	78	V341C	5'-CCTCATCCACAGC ATGCA TAGTCTCAGCCCGCATGG-3'	NsiI	ATGCAT
P6REV	36	21	58	3	8	78	V341C	5'-CCATGCGGGCTGAGACT ATGCA TGCTGTGGATGAGG-3'		
P5FWD	35	22	63	3	9	79	I342C	5'-CTCATCCACAGCTGT TGCG TCAGCCCGCATGG-3'	BsmBI	CGTCTC
P5REV	35	22	63	3	9	79	I342C	5'-CCATGCGGGCT GAGACGCA GACAGCTGTGGATGAG-3'		
P3FWD	34	22	65	3	9	79	S344C	5'-CACAGCTGTATAGTCT TGGCA CGCATGGCCCC-3'	FspI	TGCGCA
P3REV	34	22	65	3	9	79	S344C	5'-GGGGGCCATGCG TGGCA GACTATGACAGCTGTG-3'		
P1' FWD	41	24	59	4	10	79	M347C	5'-CATAGTCTCAGCCCG TGTGCA CCGAGGAGATCATCATGG-3'	ApaLI	GTGCAC
P1'REV	41	24	59	4	10	79	M347C	5'-CCATGATGATCTCCTCGGG TGCA AGCGGGCTGAGACTATG-3'		
P2'FWD	41	23	56	4	10	78	A348C	5'-CATAGTCTCAGCCCGCAT TGTCCG GAGGAGATCATCATGG-3'	BspEI	TCCGGA
P2'REV	41	23	56	4	10	78	A348C	5'-CCATGATGATCTCCT TCCG ACACATGCGGGCTGAGACTATG-3'		
P3'FWD	35	21	60	3	9	78	P349C	5'-CTCAGCCCGCAT GGCATGC GAGGAGATCATCATGG-3'	SphI	GCATGC
P3'REV	35	21	60	3	9	78	P349C	5'-CCATGATGATCTCTC GATGC ATGCGGGCTGAG-3'		
P4'FWD	33	22	67	3	9	79	E350C	5'-GCCCGCATGGCCCC TGC GAGATCATCATGGAC-3'	(none)	n/a
P4'REV	33	22	67	3	9	79	E350C	5'-GTCCATGATGATCTC GCA AGGGGGCCATGCGGGC-3'		
P5'FWD	37	23	62	4	11	78	E351C	5'-GCCCGCATGGCCCCGA ATGCA TCATCATGGACAGAC-3'	NsiI	ATGCAT
P5'REV	37	23	62	4	11	78	E351C	5'-GTCTGTCCATGAT ATGCA TCGGGGCCATGCGGGC-3'		
P6'FWD	35	22	63	3	9	79	I352C	5'-CGCATGGCCCCGAGGA ATGCA TCATGGACAGACC-3'	NsiI	ATGCAT
P6'REV	35	22	63	3	9	79	I352C	5'-GGTCTGTCCAT ATGCA TCCTCGGGGGCCATGCG-3'		
P7'FWD	34	21	62	3	9	78	I353C	5'-GGCCCCGAGGAGAT ATGCA TGGACAGACCCCTTC-3'	NsiI	ATGCAT
P7'REV	34	21	62	3	9	78	I353C	5'-GAAGGTCTGTCC ATGCA TATCTCCTCGGGGGCC-3'		
P8'FWD	41	24	59	4	10	79	M354C	5'-GGCCCCGAGGAGAT CATATGC AGACACCCCTTCCTTTG-3'	NdeI	CATATG
P8'REV	41	24	59	4	10	79	M354C	5'-CAAAGAGGAAGGTCTGTC GCATATG ATCTCCTCGGGGGCC-3'		

Base-pair substitutions to incorporate cysteine mutations and restriction sites are bolded in **black** and **blue**, respectively.

overnight growth and selection.

2.2.e. Restriction Digestion Screening of PAI-1 RCL Mutants

For screening, at least five transformed colonies were inoculated into 10-25 ml fresh Terrific Broth (TB) + 50 µg/ml kanamycin and grown overnight at 37°C and 250 rpm. Cultures were harvested by centrifugation (Beckman Coulter Avanti™ Centrifuge J-25) for 10 min at 10,000 x *g* and 4°C. Plasmids were purified using the Promega Wizard® *Plus* SV Minipreps DNA Purification System. To detect the incorporation of mutations via the presence of engineered restriction sites, purified plasmids (~50-100 ng in 1-3 µl) were treated with 1-2 µl and 2.5 µl (10%) of their corresponding restriction endonuclease and NEB buffer (**Table 2.3**), respectively, and dH₂O added up to 25 µl for the total reaction mixture. Reactions were incubated for at least 1 hr at the specified temperatures, and subsequently analyzed by electrophoresis in a 0.8% agarose gel at 100 V for 1 hr. Digested plasmids were visualized by ethidium bromide fluorescence under UV radiation, and documented using the Bio-Rad Quantity One software and ChemiDoc XRS photodocumentation system. Samples with the correct digestion pattern were sequenced, and plasmids with the correct mutations were transformed into *Escherichia coli* Rosetta 2 DE3 pLysS cells (Invitrogen), which codes for rare eukaryotic codons for optimal expression without posttranslational modification in this prokaryotic system.

2.2.f. PAI-1 RCL Mutant Growth, Expression, & Purification

Plasmids with the correct RCL mutation were transformed into *E. coli* Rosetta 2 DE3 pLysS cells for growth, expression, and large-scale cell harvest. Typical conditions for growth were 30-37°C in TB (supplemented with 50 µg/ml kanamycin and 34 µg/ml

chloramphenicol) with shaking at 250-300 rpm. At mid- to late log phase, cells were cooled to 15°C and protein expression induced with 1 mM isopropyl β-D-1-thiogalactopyranoside (IPTG). After overnight induction, cultures were harvested by centrifugation for 30 min at 10,000 x *g* and 4°C. Harvested cells were prepared for purification by resuspension in buffer [50 mM NaH₂PO₄, 1 mM EDTA, 1 mM DTT, 1 mg/100 mg protease inhibitor cocktail for use with bacterial cell extracts (Sigma-Aldrich Corp., St. Louis, MO), 20 mg lysozyme, pH 6.5], lysed on ice by sonication at an amplitude of 7 with 30 seconds 'on' and 1 minute 'off' for 15 pulses (Fisher Scientific 550 Sonicator Dismembrator), and cell debris removed by centrifugation for 30 min at 10,000 x *g* and 4°C. All subsequent steps were performed in the presence of the reducing agent, dithiothreitol (DTT), and at 15°C to prevent dimerization and latency transition, respectively. Recombinant single-cysteine RCL mutants of PAI-1 were purified in three chromatographic steps (**Fig. 2.3**), including **1.**) cation exchange (SP-Sepharose FF), which separates based on charge, with the negatively-charged matrix binding positively-charged proteins, while similarly charged molecules flow through [the isoelectric point (pI), under which proteins are positively-charged, of wild-type (wt) PAI-1 and all RCL mutants is 7.146 and 7.144, respectively, except for P4' and P5' mutants, which have a pI of 7.491]; **2.**) immobilized metal affinity chromatography (IMAC; chelating-Sepharose FF charged with nickel), which is commonly used for His₆-tagged proteins, but employed here due to the ability of PAI-1 to bind metals [137]; and **3.**) gel filtration (Sephacryl S-100 HR)(GE Healthcare, Piscataway, NJ), which separates based on size, with larger molecules eluting earlier than smaller molecules that travel through the pores of the matrix. Samples taken throughout the purification were analyzed by

1. Cation Exchange

2. IMAC

3. Gel Filtration

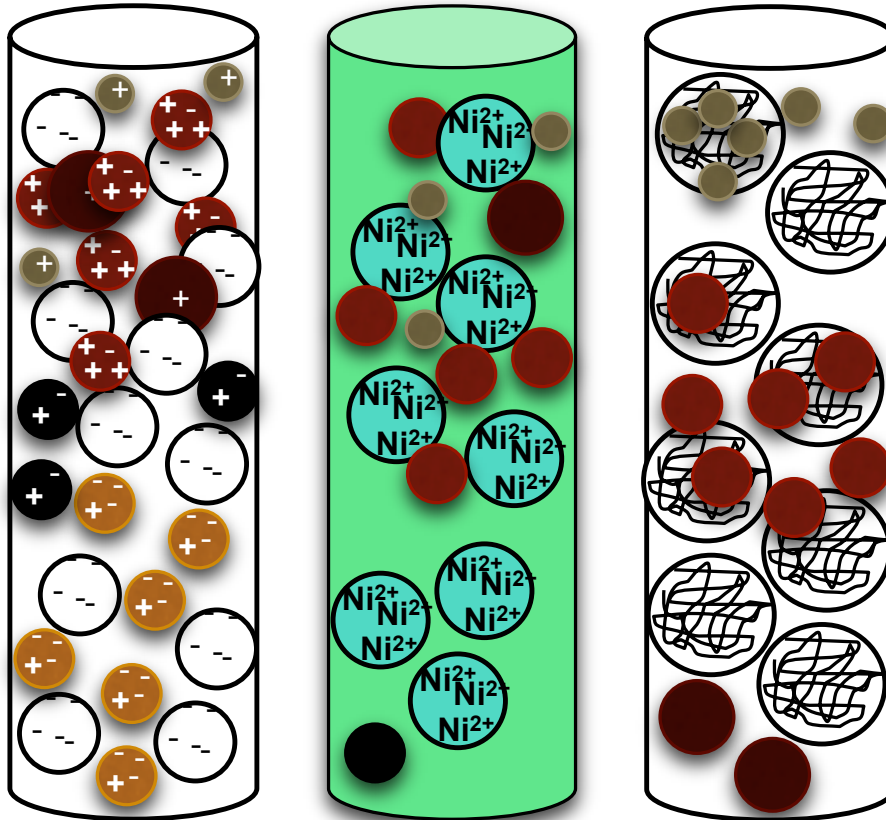


Figure 2.3 Purification Scheme for PAI-1 RCL Cys Mutants. PAI-1 RCL cys mutants were purified from lysed *E. coli* in three consecutive steps – 1.) cation exchange separates based on charge; 2.) immobilized metal affinity chromatography (IMAC) separates based on affinity for metals; and 3.) gel filtration separates based on size.

SDS-PAGE (10% polyacrylamide, reducing) at 150 V for ~ 2 hrs, followed by Western blotting (rabbit anti-human PAI-1, Molecular Innovations Inc, Novi, MI) and matrix-assisted laser desorption ionization time-of-flight mass spectrometry (MALDI-TOF-MS) (as described below) to confirm identity and purity of the protein yielded.

2.2.g. Labeling of PAI-1 RCL Cys Mutants

DTT was removed from the purified single-cysteine mutant protein for labeling purposes via a disposable PD-10 desalting column (GE Healthcare Life Sciences) equilibrated with PBS at 4°C according to manufacturer's protocol. The fluorescent and spin probes, NBD [N,N'-dimethyl-N-(iodoacetyl)-N'-(7-nitrobenz-2-oxa-1,3-diazol-4-yl) ethylenediamine; D-2004, Invitrogen Molecular Probes] and MTSL [2,5-dihydro-2,2,5,5-tetramethyl-3-[[[(methylsulfonyl)thio]methyl]-1H-pyrrol-1-yl]oxy; Cat. No. 087500, Toronto Research Chemicals], were added at 10-20X molar excess at 10% of the total reaction volume and incubated (covered) to label on ice at 4°C overnight and ≥ 4 hrs, respectively. After incubation, free probe was removed by an additional PD-10 step. An absorbance spectrum of the yielded protein was collected (**Fig. 2.4**), from which the degree of NBD labeling was determined using the following equation:

$$(A_{NBD} / \epsilon_{NBD}) * (MW_{PAI-1} / mg_{PAI-1} ml^{-1}) = mole\ NBD / mole\ PAI-1$$

where the A_{NBD} is the absorbance at 492 nm, ϵ_{NBD} , is the extinction coefficient for NBD (25,000 M⁻¹cm⁻¹), and the MW of recombinant unglycosylated human PAI-1 used for the calculation is 43,000 mg/mmol ($\epsilon_{PAI-1} = 0.83\ mg\ ml^{-1}\ cm^{-1}$). MTSL-labeling was confirmed using a Bruker EMX EPR spectrometer (see Ch. 2.2.q.).

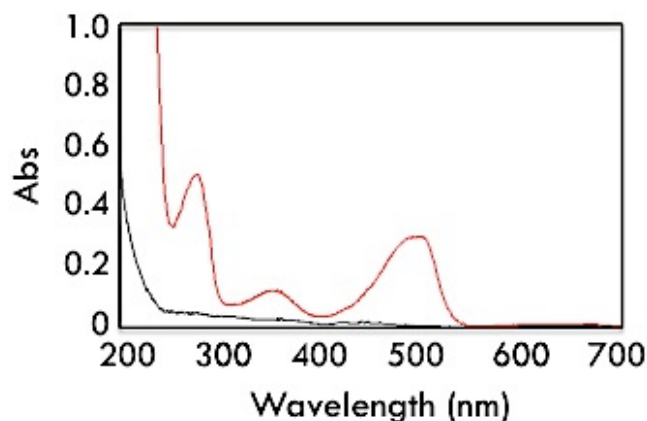


Figure 2.4 Representative Absorption Spectra to Determine Labeling Stoichiometry. The *red* trace is the spectrum of the labeled protein, while the *black* trace is that of the buffer.

2.2.h. Assessment of PAI-1 RCL Cys Mutant Activity

Single-chain and two-chain tPA (sc-tPA, tc-tPA; Molecular Innovations, Novi, MI) were titrated with increasing equivalents of PAI-1, from sub-stoichiometric to excess concentrations, and incubated for 30 min at ambient temperature in PBS, pH 7.4. Reactions were analyzed by SDS-PAGE under reducing and non-reducing conditions. Experiments were performed in duplicate or triplicate, and a digital image of the gels created using the Bio-Rad Quantity One™ software on the Bio-Rad Photo Documentation System (ChemiDocXRS scanner). To quantify the amount of active, dimeric, latent, and cleaved PAI-1 that is observed for these mutant constructs, densitometry of each band in the lane corresponding to 1:1 PAI-1:tPA in a single representative gel was performed using Bio-Rad Image Lab Software (Molecular Imager® Systems). The results were normalized as percent of total intensity after background subtraction. From the latter results, the relative stoichiometry of inhibition (SI ratio) was estimated from the ratio of the normalized percentage of cleaved (substrate) to active (inhibitor) PAI-1 present for each construct. PAI-1 activity was also

determined indirectly by titrating tc-tPA with PAI-1 as described above, incubating at room temperature, and then adding 1 mM of the chromogenic tPA substrate, Spectrozyme tPA (American Diagnostics Inc., Stamford, CT) in 100 mM Tris, 1% BSA, 1 mM EDTA, pH 7.4 at 37°C. The absorbance of the *p*-nitroaniline product at 405 nm (BioTek Synergy4 plate reader, Gen5 Software, Costar 96-well half area plate) was recorded and equivalent to fully inhibit tPA determined to assess PAI-1 activity. Plate activity assays were performed in triplicate.

2.2.i. Aggregation & Dimerization Tests of PAI-1 RCL Mutants

Unlabeled PAI-1 RCL mutants were incubated at room temperature in PBS (pH 7.4), an aliquot removed periodically, and quenched with equimolar tc-tPA. Samples were analyzed by non-reducing SDS-PAGE on a 10% polyacrylamide gel at 150 V for ~ 2hrs and visualized by Coomassie stain. Mutants were also dialyzed (Slide-A-Lyzer, MWCO 10K, Thermo Scientific) in PBS (pH 7.4) at 4°C for at least 4 hours for assessment by analytical ultracentrifugation (AUC). 400 μ l of 4 μ M dialyzed protein and dialysate were loaded into the sample and reference centerpiece sectors, respectively, of an assembled ultracentrifuge cell, sealed with torque pressure, and analyzed by sedimentation velocity (Beckman-Coulter Analytical Ultracentrifuge XL-A) under vacuum at 50,000 rpm (25°C). The absorbance traces collected over time were plotted against the cell radius and fit to a *c*(*s*) distribution model using SEDFIT [138], along with residuals of the fits and the distribution plot of distinct sedimenting species.

2.2.j. Desalting & Molecular Mass Determination

Samples were desalted by high performance liquid chromatography (HPLC) prior to analysis by MALDI-TOF-MS to obtain molecular mass information. Salts were

removed from PAI-1 via a hydrophobic C18 column (Phenomenex, Jupiter 4u, Proteo 90 Å, 250 x 4.60 mm, 4 micron) connected to a HPLC pump (Agilent Technologies 1200 Series), with Solvent A (default) and B containing H₂O/0.1% trifluoroacetic acid (TFA) and acetonitrile (ACN)/0.085% TFA (w/v), respectively. Under temperature control at 28°C, samples were separated using the following linear gradient:

<i>Time (min)</i>	<i>%B</i>	<i>Flow (ml/min)</i>	<i>Max. Pressure (bar)</i>
0	5	1	300
5	5	1	300
20	95	1	300
23	95	1	300
26	5	1	300
30	5	1	300

Typical retention times were ~15 min for PAI-1. The desalted samples collected were subsequently dissolved in 10 mg/ml sinapic acid matrix (Fluka Analytical) and spotted on a Bruker Anchor Chip target plate containing hydrophobic surfaces surrounding a hydrophilic patch at each spot. After drying, target plates were placed in the chamber of a Bruker Daltonics Microflex mass spectrometer and gas-phase ions separated in the positive-polarity mode in a vacuum without reflection. Using the Flex Control software, the instrument was calibrated (quadratic) with the Bruker Protein Calibration Standard II for MS that covers the 20,000-70,000 Da mass range. Masses were derived from the resulting spectra using the Flex Analysis software.

2.2.k. PAI-1 RCL Cys Mutant Stability

PAI-1 was incubated at 37°C in buffer [50 mM MOPS, 100 mM (NH₄)₂SO₄, 0.1 mM EDTA, pH7.4] and quenched with tc-tPA at various time points. Initial rates were measured by adding Spectrozyme tPA to the reactions and recording the absorbance of

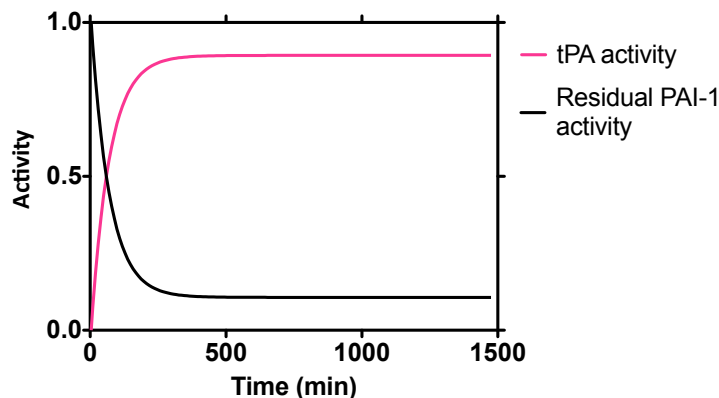


Figure 2.5 The Stability of PAI-1 Determined By The Inhibition of tPA. PAI-1 was incubated at 37°C in MOPS (pH 7.4), quenched with tPA, and its residual activity assayed indirectly by tPA cleavage of its chromogenic substrate, Spectrozyme tPA, and measuring the rate of evolution of the *p*-nitroaniline product at 405 nm. Initial rates of tPA activity were plotted over time. The residual PAI-1 activity was determined from the negative slope of tPA activity.

p-nitroaniline at 405 nm for 5 min. The slope obtained from the latter was plotted against each time point as tPA activity (**Fig. 2.5**). Data were collected for ≥ 10 half-lives. The residual PAI-1 activity was taken as the negative slope of tPA activity, and fit (using the nonlinear least squares method in GraphPad Prism Version 5.0b) to a one-phase exponential curve corresponding to the transition of PAI-1 to the latent state from which the active half-life was determined.

2.2.1. Unlabeled & Labeled PAI-1 Activity By Gel Electrophoresis

Unlabeled, NBD-labeled, and MTSL-labeled PAI-1 constructs (4 μ M) were incubated in the absence or presence of equimolar sc-tPA in PBS (pH 7.4) at ambient temperature for 30 minutes. Samples were resolved under non-reducing conditions by

SDS-PAGE on a 10% polyacrylamide at 150 V for ~2 hrs and visualized by Coomassie stain.

2.2.m. PEG-Coating Cuvettes for Fluorescence Experiments

To prevent adsorption of protein, cuvettes (Starsted, four optical-sided acrylic) were coated as previously described. Briefly, 10 mg/ml PEG 20000 was added to cuvettes and incubated overnight. After incubation, cuvettes were decanted, rinsed with dH₂O, and centrifuged briefly bottom up in a tabletop centrifuge. Cuvettes were then dried at 60°C for at least 2 hrs.

2.2.n. Titration of NBD-PAI-1 with VN

Native monomeric VN, purified from plasma (c.f. Ch. 3.2.a.), was resuspended from an ammonium sulfate precipitate, dialyzed overnight in PBS (pH 7.4) at 4°C, and its concentration determined spectrophotometrically (Cary 50 Series UV-Vis Spectrophotometer) according to Beer-Lambert's law [$c = A/(l\epsilon)$, where c is the concentration, A is the absorbance at 280 nm, l is the path length (1 cm), and ϵ is the extinction coefficient (1 mg ml⁻¹ cm⁻¹ for VN)]. 0.5 μM NBD-PAI-1 in 2 ml MOPS buffer [50 mM MOPS, 100 mM (NH₄)₂SO₄, 1 mM EDTA, pH 7.4] was added to a PEG-coated cuvette and placed in a Perkin Elmer LS 50B Luminescence spectrometer at ambient temperature. NBD-PAI-1 was titrated with increasing concentrations of VN, excited at 480 nm, and the emission spectra from 500-600 nm collected. Samples were corrected for dilution by multiplying the resulting intensity by the ratio of the final to initial volumes. After correcting for dilution, the maximum intensity from the resulting spectra was plotted against VN concentration, fit to a one-site binding curve by nonlinear regression (GraphPad Prism), and the dissociation constant (K_d) determined.

2.2.o. Single-Point Relative Quantum Yield Determination

To determine the contribution of the efficiency of NBD fluorescence to the magnitude of fluorescence changes observed, single-point measurements were taken to estimate the relative quantum yield (QY) for NBD-PAI-1. Based on labeling stoichiometry, NBD-PAI-1 concentration was adjusted to 0.25 μM NBD in 2 ml buffer containing 50 mM NaH_2PO_4 , 300 mM NaCl , 1 mM EDTA, 0.1% PEG 8000 (w/v), pH 7.4. Samples were added to a PEG-coated cuvette and placed in a Perkin Elmer LS 50B Luminescence spectrometer connected to circulating water bath (Lauda-Brinkmann RM6) set such that the temperature in the chamber was 37°C. Using FL Winlab software, absorbance scans from 400-520 nm and emission scans from 500-600 nm were collected. Emission scans were collected after excitation at 480 nm. The absorbance at the theoretical wavelength maximum of 480 nm for NBD and area of fluorescence of the emission can were used to calculate the relative quantum yield using the following equation:

$$Q_{\text{prot}} = Q_{\text{ref}} (\int_{\text{ref}} / \int_{\text{prot}}) (A_{\text{prot}} / A_{\text{ref}})$$

where Q_{prot} and Q_{ref} is the relative quantum yield of NBD-PAI-1 and NBD_{free}, respectively, A is the absorbance at 480 nm, and \int is integral of the intensity of the fluorescence emission (i.e. area of fluorescence). \int was calculated using GraphPad Prism software. Q_{ref} was arbitrarily set to 0.5, assuming 50% efficiency for NBD_{free}.

2.2.p. PAI-1 Latency Transition via Steady-state Fluorescence

NBD-labeled RCL constructs were added to a PEG-coated cuvette at a concentration of 300-500 nM PAI-1 in 2 ml buffer containing 50 mM NaH_2PO_4 , 300 mM

NaCl, 1 mM EDTA, 0.1% PEG 8000, pH 7.4 and sealed with mylar plate sealer. The cuvette was then placed in a Perkin Elmer LS 50B Luminescence spectrometer at 37°C. Samples were excited at 480 nm and fluorescence emission spectra from 500-600 nm were collected every 5 minutes (for 5-7 hrs followed by 3 overnight time points) until saturation occurred. Results are plotted as the normalized intensity at the average wavelength maximum of 530 nm for NBD-labeled PAI-1 according to the following equation:

$$[(F-F_0)/F_0]*100$$

where F is the fluorescence intensity at 530 nm at a given time point, and $F_0 = F_{\min}$, which is the lowest fluorescence intensity at 530 nm measured over time. The plots of the normalized fluorescence over time were analyzed in GraphPad Prism using the nonlinear least squares fitting criteria to a single, one-phase exponential curve from which the half-life of insertion was determined. All experiments performed in triplicate.

2.2.q. PAI-1 RCL Mobility via Electron Paramagnetic Resonance (EPR)

MTSL-labeled PAI-1 was dialyzed in 4 L buffer (PBS, pH 7.4) at 4°C and diluted to a final concentration of 2 μ M. Reactions were added to a 100 mm high-precision quartz capillary (Wilmad Glass, inner diameter 1.012 ± 0.013 mm), sealed with Teflon plugs, and placed in the cavity of a Bruker EMX EPR Spectrometer at ambient temperature. The frequency was held constant at ~ 9.5 GHz and center field was set at 3360 G with a sweep width of 100 G. The time constant and conversion time were set to 655.29 ms and 20.48 ms, respectively, with a resolution in X of 2048 for 5 scans. Spectra were collected at an attenuation of 10 dB, receiver gain of $2.00E+05$, amplitude

modulation of 4 G, and frequency modulation of 100 kHz. All other parameters were kept at default. From the resulting spectra, the scaled mobility (M_s) was determined using the following equation:

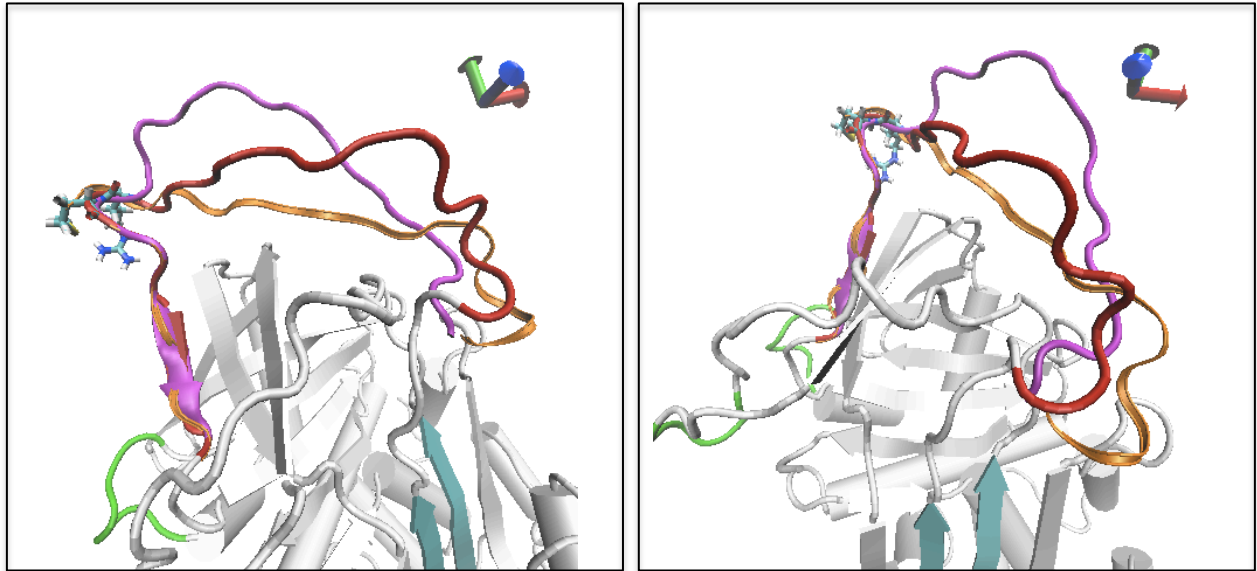
$$M_s = (\bar{\delta}^{-1} - \bar{\delta}_i^{-1}) / (\bar{\delta}_i^{-1} - \bar{\delta}_m^{-1})$$

where $\bar{\delta}$ is the width of central resonance line of MTSL-PAI-1 labeled at a residue of the RCL and $\bar{\delta}^{-1}$ is its inverse, $\bar{\delta}_i$ is the line-width of most immobilized RCL residue, and $\bar{\delta}_m$ is the line-width of most mobile RCL residue. The change in mobility (ΔH_0^{-1}) was determined from the central field MTSL peak by subtracting the average inverse line-width of active MTSL-PAI-1 to that of latent MTSL-PAI-1. All experiments were performed in triplicate. Latent MTSL-PAI-1 was prepared by incubation at 37°C for ≥ 1 week.

2.3. Results

2.3.a. Homology Modeling Investigates RCL Conformations

The RCL of PAI-1 is defined elsewhere as P16-P10' [112] or P14-P10' [66], but here as the 22 residues from P14-P8' based on mutants generated for this study. These residues were homology modeled using the metastable W175 structure as a template due its thermodynamic similarity to wild-type PAI-1 (**Fig. 2.6 A**) [59]. Although the body of the serpin was constrained and partial charges fixed, the results surprisingly yield only three low energy conformations for the RCL, indicating sampling of a small energy-conformational landscape for this region [139, 140]. Molecular dynamics of the three structures within 0.8 kcal/mol also reveal only small populations of loop conformers (data not shown). The modeled structures differ in extension and probability of solvent



B.

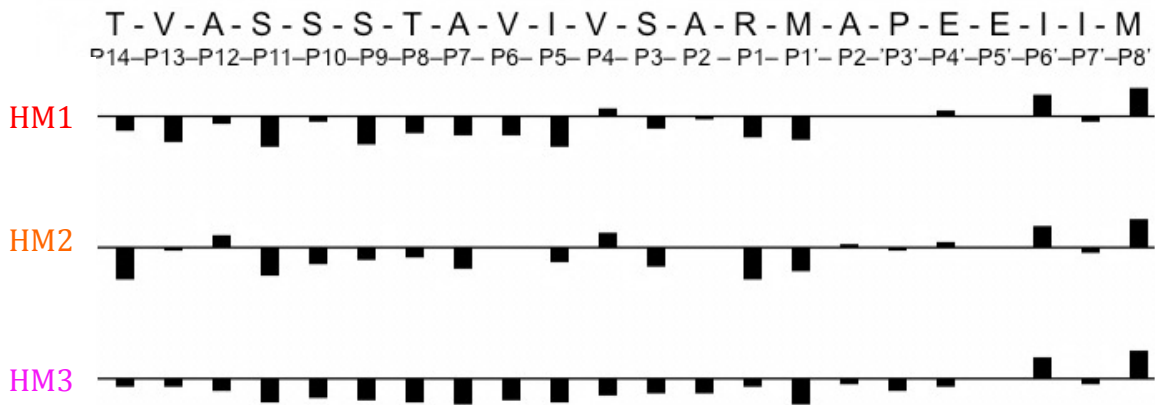


Figure 2.6 Homology Models of PAI-1 RCL. The RCL was homology modeled in MOE using the energy-minimized metastable structure of PAI-1 as a template (3Q02). **A.** Close up of the three low-energy loop conformations resulting from modeling: HM1 (*red*), HM2 (*orange*), and HM3 (*magenta*). **B.** Probabilities of solvent exposed surface in the RCL homology models were predicted by MOE2010. Decreases and increases represent greater and lesser solvent exposure, respectively. RCL residues are identified by their P-designation with respect its distance from the P1-P1' scissile bond, with residues C-terminal indicated with a prime (').

Table 2.2 Comparison of RCL Interactions in Homology Models & Crystal Structures of Different Conformations of PAI-1

Homology Models							LATENT (1C5G)							
First Contact				Second Contact			First Contact				Second Contact			
Model Type	Residue	Position	Location	Residue	Number	2 ^o Structure	Type	Residue	Position	Location	Residue	Number	2 ^o Structure	
1	ION	GLU	350	P4'	ARG	346	P1	THR	333	P14	TYR	228	s2B/s3B loop	
2	HB	ILE	342	P5	LYS	207	s3C	HYD	VAL	334	P13	MET	147	hF/s3A loop
1,2,3	HB	GLU	351	P5'	ARG	187	s4C	HB	SER	336	P11	LEU	169	s2B
1,2,3	ION	GLU	351	P5'	ARG	187	s4C	HB	THR	339	P8	GLY	38	hB
1,2,3	HYD	ILE	352	P6'	LEU	224	s2B	HB	THR	339	P8	GLN	322	s5A
1,2,3	HYD	ILE	352	P6'	LEU	273	s2C	HYD	VAL	341	P6	VAL	42	hB
1,2,3	HYD	MET	354	P8'	LEU	224	s2B	HYD	VAL	341	P6	LEU	43	hB
1,2,3	HYD	MET	354	P8'	ILE	237	s3B	HYD	VAL	341	P6	LEU	46	hB
1,2,3	HYD	MET	354	P8'	LEU	273	s2C	HYD	VAL	341	P6	LEU	165	s3A
1,2,3	HYD	MET	354	P8'	LEU	275	s2C	HYD	VAL	341	P6	VAL	317	hl/s5A loop
1,2,3	HYD	PHE	358	P12'	MET	354	a1C	HYD	ILE	342	P5	LEU	152	s3A/hF loop
METASTABLE (3QO2)														
First Contact				Second Contact			First Contact				Second Contact			
Type	Residue	Number	Position	Residue	Number	2 ^o Structure	Type	Residue	Position	Location	Residue	Number	2 ^o Structure	
ION	GLU	350	P4'	ARG	271	s2C	HYD	VAL	343	P4	LEU	163	hF/s3A loop	
ION	GLU	351	P5'	ARG	187	s4C	HB	SER	344	P3	THR	161	hF/s3A loop	
HYD	ILE	352	P6'	LEU	273	s2C	HYD	MET	347	P1'	LEU	321	s5A	
HYD	ILE	353	P7'	VAL	274	s2C	HB	GLU	350	P4'	ARG	30	hA/hB loop	
HYD	MET	354	P8'	ILE	237	s3B	HB	GLU	350	P4'	ASP	285	s6A	
HYD	MET	354	P8'	LEU	275	s2C	ION	GLU	350	P4'	ARG	30	hA/hB loop	
HYD	PHE	358	P12'	ILE	237	s3B	ION	GLU	350	P4'	LYS	288	hl	
HYD	PHE	358	P12'	LEU	275	s2C								
HYD	PHE	358	P12'	PHE	278	s2C/s6A loop								
HYD	PHE	358	P12'	MET	354	s1C/RCL/P8'								

HB = hydrogen bond
HYD = hydrophobic interaction
ION = ionic bond

exposure of the RCL (**Fig. 2.6 B**), but overlap considerably at s1C and, interestingly, the scissile bond. Overlap of s1C residues P4-P8' in the models is expected, as these residues are resolved in the template structure. However, the scissile bond overlap, forming a small protrusion in the models, is absent in crystal structures of the thermodynamically stable active 14-1B PAI-1 conformer, in which the RCL is resolved due to crystal packing and interaction with edge-strands of sA or sC [112, 141, 142].

In terms of protein contacts (**Table 2.2**), all of the models are predicted to participate in the same noncovalent interactions, with the exception of an ionic interaction bridging P4' (E350) to P1 (R364) and a hydrogen bond between P5 (I342) to K207 (s3C) in the gate region in model 1 (*red*) and model 2 (*orange*), respectively. Most

of these contacts involve s1C interactions with the gate, as in the metastable structure, and thereby indicate strand attachment. In contrast, these interactions are mostly absent in the latent structure in which s1C is detached. Furthermore, the distance between P3 and P1' to position 313 on the opposite pole of PAI-1, estimated to be ~ 55 Å and ~ 68 Å – 69 Å from solution [58] and crystal methods [112], respectively, was measured to be an average of ~63 – 64 Å in the models. The latter indicates that the modeling parameters favor an RCL that is close to the body of the serpin.

2.3.b. Purification of PAI-1 RCL Mutants Yields Sufficient Quantities for Conformation & Dynamics Studies

In addition to homology modeling, cysteine-scanning mutagenesis of the RCL was performed in order to investigate the steps in the latency process by steady-state methods. Mutagenesis was facilitated by the fact that PAI-1 does not contain intrinsic cysteine residues and, due to the large number of mutants generated, by the creation of unique restriction sites for screening purposes. By comparing the band pattern upon restriction digestion (**Fig. 2.7**) to the expected result if the correct mutation was incorporated (**Table 2.3**), PAI-1 RCL cysteine mutants were screened relatively quickly. For instance, of the five colonies per construct screened for the P1', P2', P5', and P6' mutations, only 2, 0, 4, and 2, respectively, of the plasmids purified from these colonies show the correct digestion pattern with the restriction enzyme for which sites were engineered, and thus were the ones confirmed by sequencing.

All mutants were expressed as recombinant proteins in *E. coli* (as described under Methods 2.2.f.). To maximize yields, cells were grown to high density in the logarithmic phase (**Fig. 2.8 A**) before induction of protein expression by the addition of

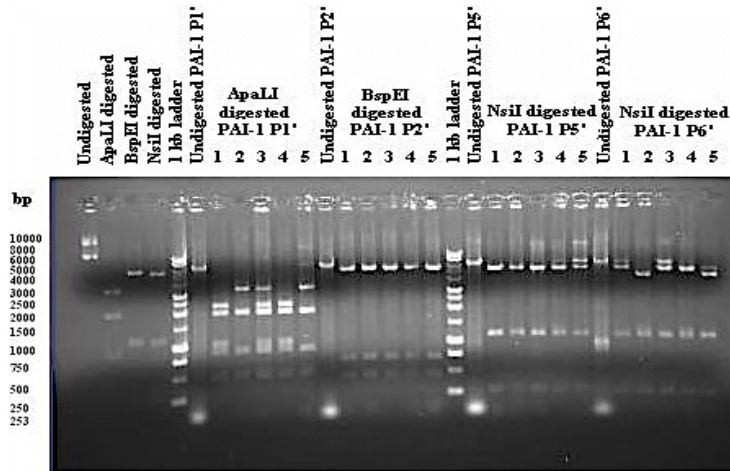


Figure 2.7 Restriction Digestion to Screen For PAI-1 RCL Mutants. Mutations to the human PAI-1 gene in the pET24(d+) vector were introduced by PCR, the resulting plasmids transformed into *Escherichia coli* cells, and plasmids purified. A representative agarose gel (0.8%) displaying the digestion pattern of five transformed colonies per construct with their respective restriction enzymes to screen for the presence of mutated plasmids is shown (c.f. Table 2.3). Controls for wild-type (wt) plasmids are contained in the first four lanes.

Table 2.3 Expected Digestion Patterns in Screening of PAI-1 RCL Mutants

pET24d(+)	5236 bp					
PAI-1	1140 bp					
pET24d(+)- wt PAI-1	6639 bp					
Restriction Enzyme	Sites on pET Vector	Sites on PAI-1	Cys Mutant	Sites on PAI-1 w/ Δ	# Expected Bands	Fragment Size (bp)
ApaLI	1042, 2977, 3477 (2446, 4381, 4881)	2	P1' (M347C)	2, 1039	5	500, 1037, 1403, 1935, 1760
BspEI	3, 2352 (1407, 5756)	351	P2' (A348C)	351, 1042	4	348, 691, 886, 4714
FspI	2144 (3548)	n/a	P3 (S344C) P8 (T339C)	1030 1015	2	2518, 4121 2533, 4106
NdeI	n/a	n/a	P8' (M354C)	1060	1	6639
NsiI	4215, 4481 (5619, 5885)	n/a	P6 (V341C) P5' (E351C) P6' (I352C) P7' (I353C)	1021 1051 1054 1057	3	266, 4598, 1775 266, 4568, 1805 266, 4565, 1808 266, 4562, 1811
SphI	537 (1941)	n/a	P3' (P349C)	1045	2	896, 5743
PmlI	n/a	n/a	P13 (V334C)	1000	1	6639
SapI	3047 (4451)	n/a	P12 (A335C) P11 (S336C)	1003 1006	2	3448, 3191 3445, 3194
TaqII	970, 1188 (2374, 2592)	406, 566	P14 (T333C)	406, 566, 997	5	160, 218, 431, 1377, 4453
BsmBI	1677, 2804, 4381	n/a	P5 (I342C)	1024	4	1127, 1577, 1878, 2057

IPTG, upon which linear growth was established (**Fig. 2.8 B**) by lowering incubation temperatures to minimize latency transition of translated PAI-1 and entrance into the stationary or death phase for the cells, as evidenced by the lack of a plateau or decrease in optical density (OD) at 600 nm, respectively. PAI-1 expression was confirmed by Western blot (**Fig. 2.8 C**). Typical cell harvests and protein yields ranged from ~27.4 - 72.4 grams and ~21.6 - 87.7 milligrams, respectively. The purity of the PAI-1 RCL mutant protein obtained from these cells was analyzed by SDS-PAGE (**Fig. 2.9 A**) and Western blot (**Fig. 2.9 B**). Most of the *E. coli* proteins were removed by cation exchange, leaving few lower molecular weight proteins for removal by IMAC and gel filtration. Moreover, RCL mutant purity and identification by molecular mass were assessed by HPLC (data not shown) and MALDI-TOF-MS (c.f. Fig. 2.14 A, Table 2.6), respectively.

2.3.c. Mutations & Labeling Modestly Affect the Activity & Stability of PAI-1

Because serpins employ a conformation-based inhibitory mechanism, which can be affected at multiple levels, including its metastable fold or RCL insertion, the consequence of mutations on serpin function necessitates evaluation by more than one method [56, 143]. Thus, the activity and stability of the RCL mutants were assessed by its ability to inhibit one of its targets, tPA, and characterize its effect on PAI-1. Theoretically, PAI-1 forms stoichiometric (1:1) final serpin-protease suicide complexes with PAs. However, due to the labile nature of PAI-1, preparations generally contain some degree of latent protein, which can be separated by hydrophobic interaction chromatography (e.g. phenyl Sepharose) [85, 144] based on the additional β -strand character of latent PAI-1 upon RCL insertion, or by affinity chromatography using active

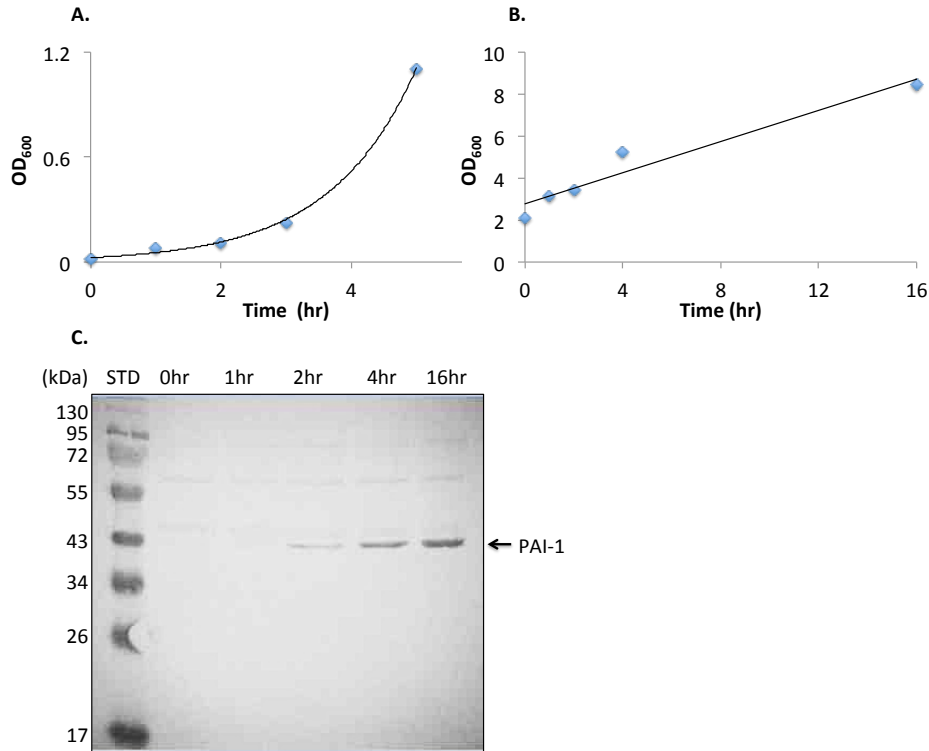


Figure 2.8 Growth & Expression of PAI-1 RCL Cys Mutants. Sequenced plasmids containing the correct RCL mutation in the PAI-1 gene were transformed into *E. coli* Rosetta 2 DE3 pLysS cells for growth and expression. Representative curves (for the PAI-1 P9 S338C mutant) of the optical density at 600 nm over time to observe cell growth (A) at 30°C before induction and (B) at 15°C after induction with 1 mM IPTG are shown. (C) Western blot verifies the induction of PAI-1 expression.

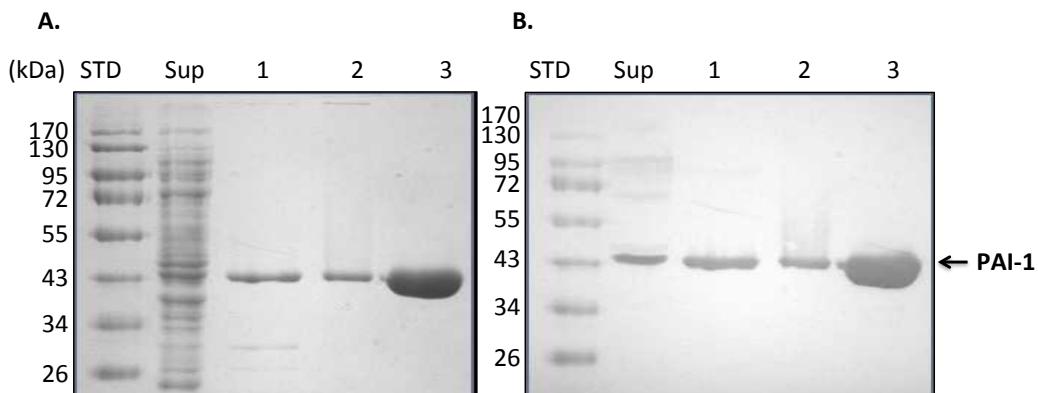
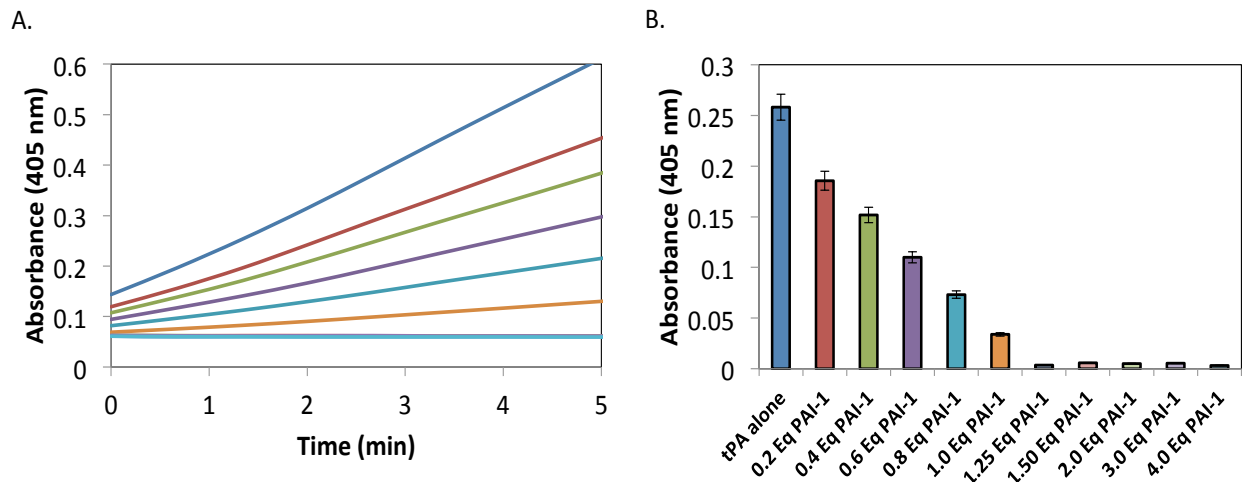


Figure 2.9 Analysis of PAI-1 RCL Cys Mutant Purification. A representative (A) SDS-PAGE and (B) Western blot are shown for the purification of PAI-1 (P6 V341C) via (1) cation exchange, (2) immobilized metal affinity chromatography, and (3) gel filtration. Molecular weight standards (STD) are shown to the left of the supernatant (Sup) from which PAI-1 was purified.

site-blocked (S195A) serine proteases [145], which bind only the active serpins. Since reversal to the active conformation is non-spontaneous and therefore generally adds to the background in these experiments, the latter step was omitted in the purification of PAI-1. Therefore, to determine the amount of active RCL mutant present in these preparations, varying equivalents of PAI-1 were added to tPA, and the amount of *p*-nitroalanine produced from the cleavage of Spectrozyme tPA by tPA was measured using the absorbance of the product at 405 nm (**Fig. 2.10**). Since only active PAI-1 inhibits tPA, the decrease in the tPA activity indicates the increased presence of active PAI-1, and the plateau represents the equivalent required to fully inhibit tPA. For instance, in the representative assay, full inhibition occurs at 1.25 equivalents, which indicates that 80% of the PAI-1 RCL mutant present is active. However, this method does not detect the cleaved forms that arise from substrate behavior of PAI-1, which may be increased due to mutation of the RCL. Thus, an additional activity assay was performed by titrating tPA with the RCL mutant and analyzing by SDS-PAGE (**Fig. 2.11**). Again, the decrease in tPA and increase in complex formation was used to estimate the percent active PAI-1 mutant present. Cleavage in substrate PAI-1 results in its slightly faster migration than unmodified PAI-1 under electrophoresis, and can thereby be detected as the lower band in the PAI-1 doublet that appears in the gel at ~43 kDa. At sub-stoichiometric concentrations (i.e. 0.50 - 0.75 equivalents PAI-1 to tPA), the PAI-1 present in the top band of the doublet is the latent form, while at higher stoichiometries, is unreacted due to saturation of tPA. The equivalent at the saturation point indicates the amount of active PAI-1 present. In this analysis, reducing conditions (**Fig. 2.11 B**) were generally used for clarity, but non-reducing (**Fig. 2.11 A**) also used to



2.10 Assessment of PAI-1 RCL Cys Mutant Activity. tPA was titrated with increasing concentrations of PAI-1 to determine the equivalent required to fully inhibit tPA. **(A)** Spectrozyme tPA is added to PAI-1-tPA mixtures and the absorbance at 405 nm recorded. **(B)** The absorbance at 405 nm after two minutes is plotted against PAI-1 equivalent. A representative assay (for PAI-1 P9 S338C) is shown. Error bars are plotted as standard deviations.

detect the formation of PAI-1 dimers (~86 kDa) due to presence of cysteine in the RCL. In the representative assay under both conditions, the excess occurs at 1.25 to 1.5 equivalents of one PAI-1 RCL mutant to tPA, indicating that 67% - 80% of the preparation contains active PAI-1 RCL mutant protein.

To determine if the mutations affect insertion of the RCL, the SI ratio, describing the partition between inhibitory and substrate branches of the serpin pathway, was estimated by SDS-PAGE of 1:1 PAI-1:tPA mixtures and densitometry of the resulting products of electrophoresis (**Fig. 2.12**). From this analysis, the P13 mutant near the hinge and P3 to P5' mutants about the scissile bond show increased substrate PAI-1, and thus, have greater relative SI ratios, while the P4' and P6' RCL mutants show the

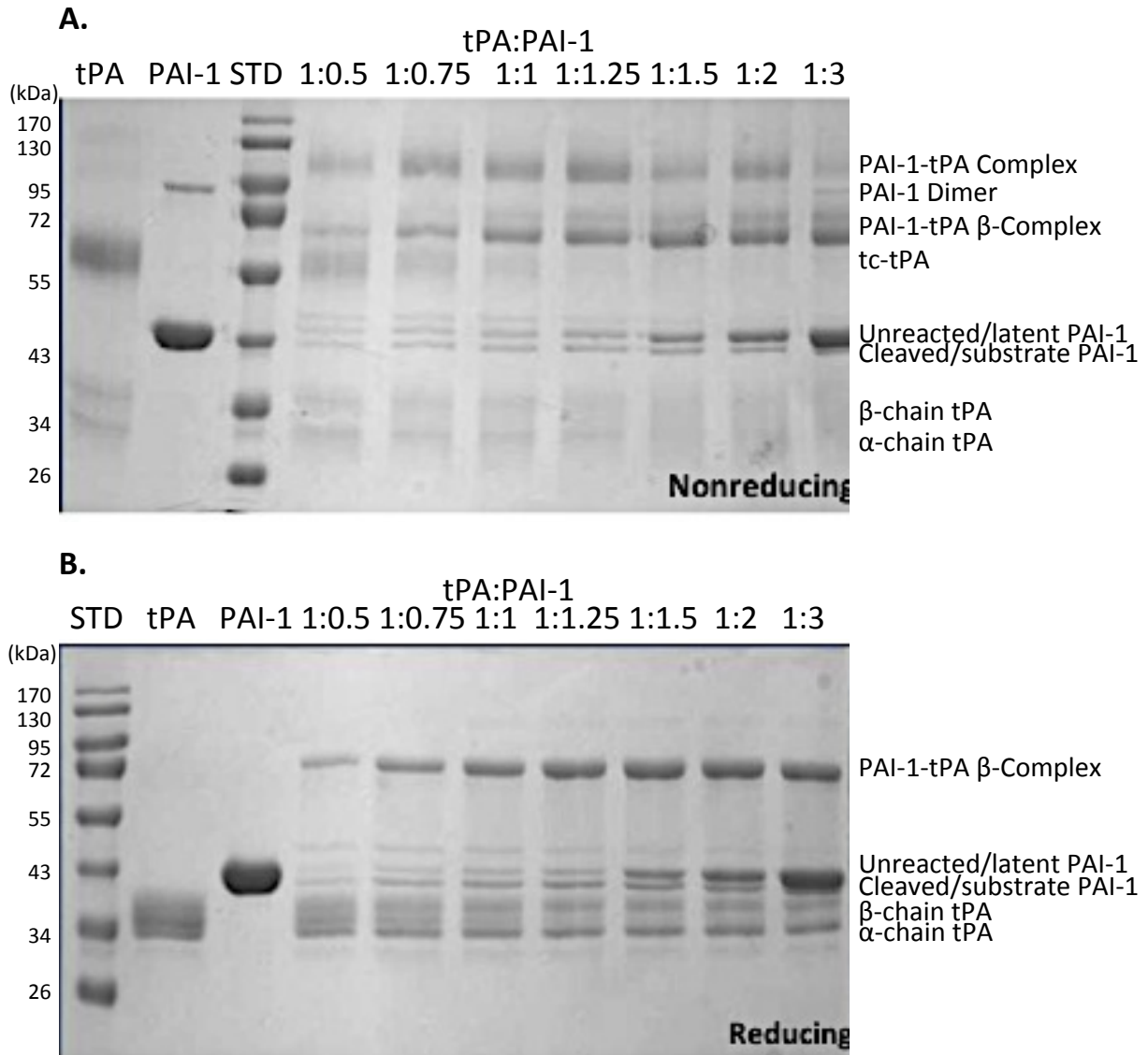


Figure 2.11 Functional Distribution PAI-1 RCL Cys Mutants. tc-tPA was titrated with increasing concentrations of PAI-1 and its complexes separated under **(A)** nonreducing and **(B)** reducing conditions to resolve different functional species of PAI-1 (i.e. active, latent, substrate) and determine the equivalent of PAI-1 required to fully inhibit tPA. Ratios represent the concentration of tPA:PAI-1. A representative assay (for PAI-1 P9 S338C) is shown.

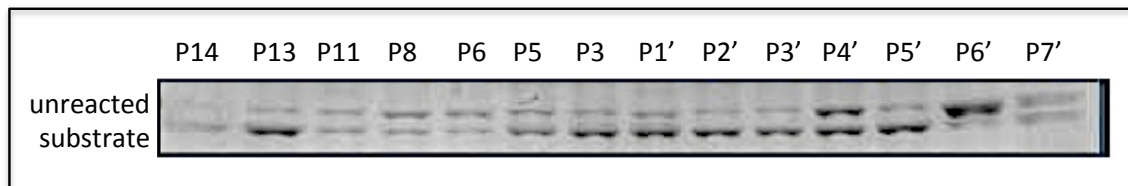


Figure 2.12 Relative Stoichiometry of Inhibition of PAI-1 RCL Cys Mutants. PAI-1 was added 1:1 to tPA and analyzed by SDS-PAGE. The relative stoichiometry of inhibition (SI ratio), relating the tendency of PAI-1 to partition into the inhibitory and substrate branches of the serpin pathway is indirectly estimated by the amount of substrate PAI-1 formed upon reacting with tPA. (Active PAI-1 in complex with tPA is not shown.)

significant presence of latent protein, perhaps due to complications during purification. The low SI ratio due to cysteine mutation of the P14 residue has been previously reported [60]. Densitometry was also used to estimate the conformational distribution of active, dimer, and latent RCL mutant, which are tabulated (**Table 2.4**) next to the results obtained from the chromogenic and electrophoretic activity assays. The results of the activity assays are similar and indicate high activity ($\geq 80\%$) for most constructs by both methods, which is comparable to wt-PAI-1 (data not shown). However, the activity assessed by the two methods differ for the P14, P2', P4', and P7' constructs, a result which may be due to detection of substrate behavior in the electrophoretic versus chromogenic assay, or variations in experimental conditions between the two assays. Most constructs have a low latent protein content (average of $\sim 14.5\%$), except P6, as previously mentioned. Also, RCL mutants, maintained in the presence of DTT prior to labeling, have a low tendency to dimerize by disulfide formation, as supported by an insignificant amount of dimer detected over time (**Fig. 2.13**), with dimer appearing only at high concentrations (**Fig. 2.11**). Also, sedimentation velocity experiments

Table 2.4 Activity & Conformational Distribution PAI-1 RCL Cys Mutants

<i>Unlabeled Construct</i>	<i>Equivalent PAI-1 per tPA for Full Inhibition (% Active PAI-1) †</i>	<i>% Active PAI-1 ★</i>	<i>% PAI-1 Dimer ★</i>	<i>% Latent PAI-1 ★</i>	<i>% Substrate PAI-1 ★</i>
P14	1.5 (67%)	80	1	9	10
P13	1.5 (67%)	67	1	3	29
P12	2 (50%)	63	4	28	5
P11	1.25 (80%)	94	0	4	2
P9	1.25 (80%)	93	0	3	4
P8	1.25-1.5 (67-80%)	75	0	15	10
P6	1.25 (80%)	82	0	9	9
P5	1.5 (67%)	78	1	14	7
P3	1.25-1.5 (67-80%)	70	1	11	18
P1'	2 (50%)	64	1	9	26
P2'	2 (50%)	75	1	8	16
P3'	2 (50%)	51	2	33	14
P4'	1.25 (80%)	67	1	18	14
P5'	1.25 (80%)	85	1	6	8
P6'	>4 (<25%)	30	1	61	8
P7'	2 (50%)	73	0	23	4
P8'	3 (33%)	38	2	39	21

† Based on plate assay as described under Methods

★ Based on densitometry of gel assays as described under Methods

indicated that PAI-1 RCL mutants exist as a single, un-aggregated monomeric species (Fig. 2.13).

DTT was removed from PAI-1 RCL mutant protein prior to labeling with the NBD and MTSL probes. Typical labeling stoichiometries for NBD labeling ranged from 0.75 to 1 mol NBD/mol PAI-1, but were lower (0.1-0.4 mol NBD/mol PAI-1) for P6'-P8', likely due to limited accessibility of residues in these positions in s1C (Table 2.5). Labeling was also confirmed by MALDI-MS (Fig. 2.14, Table 2.6), which measures the mass-to-charge ratio of gas phase ions to accurately determine molecular masses. Labeling with NBD (MW 419.18 Da, including the 126.9 Da iodine atom) results in the addition of

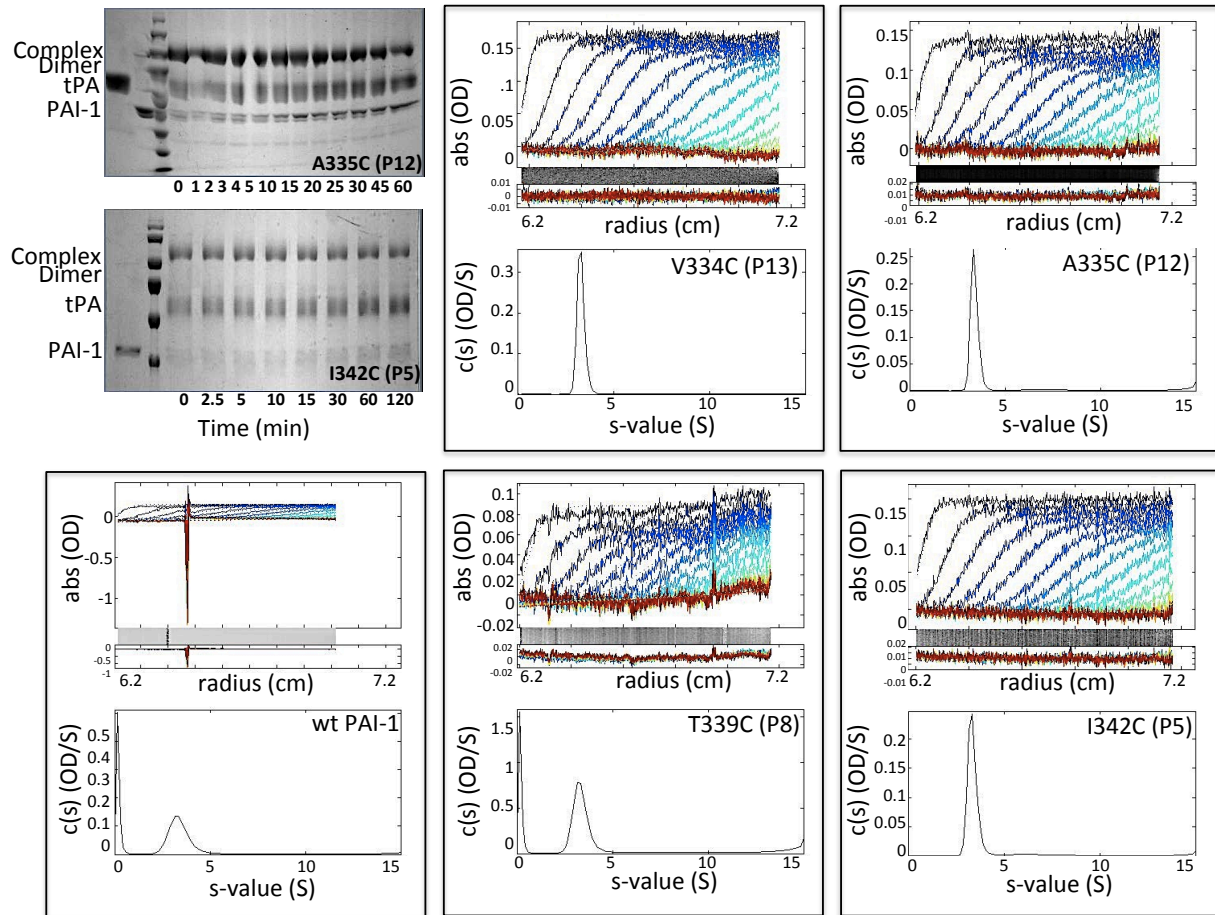


Figure 2.13 PAI-1 RCL Cys Mutants Exist in A Non-Aggregated, Monomeric State. In the *top left* panel, the indicated unlabeled PAI-1 RCL mutants were analyzed by non-reducing SDS-PAGE to determine if dimeric PAI-1 forms over time. In the remaining panels, 4 μ M of the indicated unlabeled PAI-1 RCL mutants were analyzed by sedimentation velocity. The absorbance traces are shown at the *top*, the residuals at the *middle*, and the distribution plot of sedimenting species at the *bottom* of each panel.

Table 2.5 Labeling Stoichiometry of NBD-PAI-1

<i>RCL Position</i>	<i>mol NBD/mol PAI-1*</i>
P14	0.83
P13	0.70
P12	1.09
P11	1.07
P9	0.78
P8	1.09
P6	0.66
P5	1.23
P3	1.09
P1'	1.29
P2'	0.79
P3'	1.02
P4'	1.11
P5'	1.00
P6'	0.40
P7'	0.45
P8'	0.12

*Based on single measurement of A_{280} and $\epsilon = 0.93$ mg/ml/cm for PAI-1, and A_{492} and $\epsilon = 25,000$ M⁻¹cm⁻¹ for NBD.

292.28 Da to PAI-1. Small variances up to 30 Da are observed in the experimentally determined masses compared to their theoretical values, and may be due to the instrument calibration and/or analysis in linear mode without the use of a reflectron, which refocuses ions avert to spatial, temporal, or kinetic effects on the separation. The masses of a few constructs (P11, P8, P5, P4', and P6'-8') were not determined since the labeling success of the previously tested constructs strongly suggested that similar results would be obtained.

To determine if the introduction of the mutations or labeling with a molecular probe affects the function and stability of PAI-1, several stability assays were performed

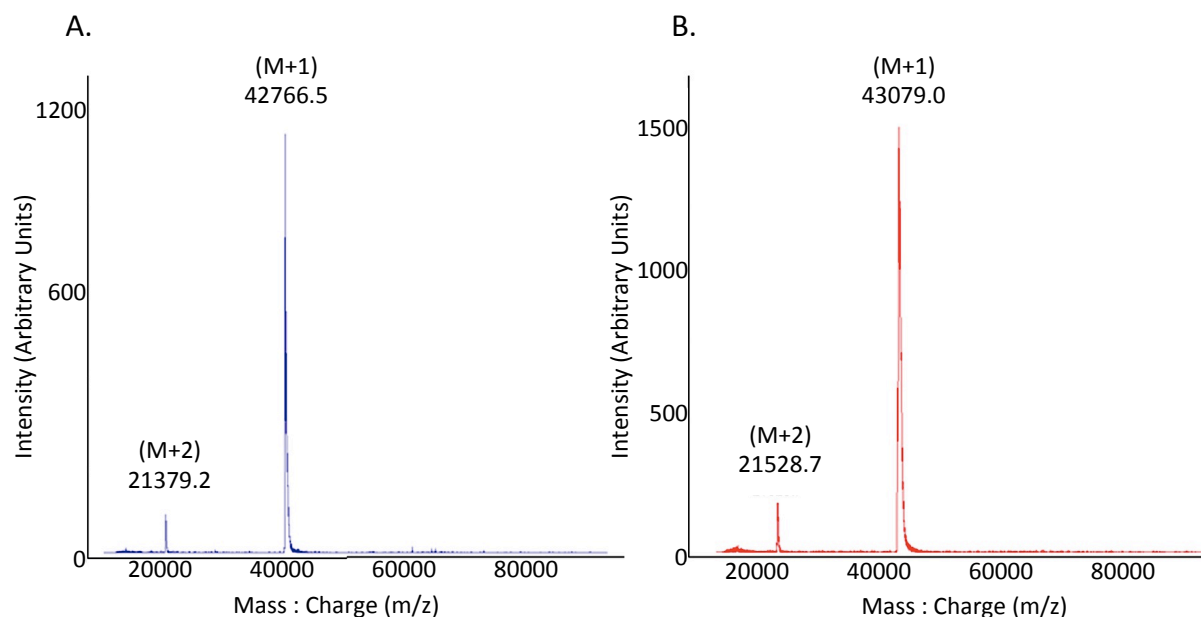


Figure 2.14 Confirmation of NBD Labeling of PAI-1 Cys Mutants by Matrix-Assisted Laser Desorption Ionization Mass Spectrometry. Purified PAI-1 RCL cys mutants were HPLC-purified and analyzed by MALDI-TOF-MS. Representative spectra for an (A) unlabeled and (B) labeled RCL mutant are shown (c.f. Table 2.6).

Table 2.6 MALDI-MS of Unlabeled & Labeled PAI-1 RCL Cys Mutants

RCL Position	Unlabeled PAI-1			NBD-labeled PAI-1		
	Theoretical Mass (Da)	Experimental Mass (Da)	Theoretical - Experimental (Da)	Theoretical Mass (Da)	Experimental Mass (Da)	Theoretical - Experimental (Da)
P14	42771.42	42764.50	6.92	43063.70	43080.70	17.00
P13	42773.39	42767.00	6.39	43065.67	43041.90	23.77
P12	42801.45	42789.90	11.55	43093.73	43075.30	18.43
P11	42785.45	42784.60	0.85	43077.73	n.d.	n/a
P9	42785.45	42789.60	4.15	43077.73	43078.50	0.77
P8	42771.42	42767.10	4.32	43063.70	n.d.	n/a
P6	42773.39	42786.50	13.11	43065.67	43079.00	13.33
P5	42759.39	42755.90	3.49	43051.67	n.d.	n/a
P3	42785.45	42782.90	2.55	43077.73	43071.70	6.03
P1'	42741.33	42736.50	4.83	43033.61	43031.20	2.41
P2'	42801.45	42799.40	2.05	43093.73	43063.00	30.73
P3'	42775.41	42752.40	23.01	43067.69	43047.50	20.19
P4'	42743.41	42748.50	5.09	43035.69	n.d.	n/a
P5'	42743.41	42741.00	2.41	43035.69	43021.50	14.19
P6'	42759.37	42746.70	12.67	43051.65	n.d.	n.d.
P7'	42759.37	42757.50	1.87	43051.65	n.d.	n.d.
P8'	42741.33	42744.70	3.37	43033.61	n.d.	n.d.

n.d. = not determined

Theoretical masses calculated in SEDENTERP.

(**Fig 2.15**) as described under Methods (2.2.k). Most mutations confer similar stability to or exhibit slightly increased stability compared to wt-PAI-1, even upon labeling, consistent with previous data [58, 78]. In particular, mutation in the hinge (P14, P12, P11) and adjacent to the scissile bond (P6, P3) stabilized PAI-1, whereas mutation of P6'-P7' in s1C rendered PAI-1 less stable. However, these changes are minor in comparison to the effect of the single W175F and quadruple 14-1B mutations on PAI-1, which exhibit inhibitory half-lives of ~7 to 145 hrs, respectively [59, 70]. In terms of labeling, conjugation of the NBD probe N-terminal (P14, P9-P8, P6, and P5) and C-terminal (P1', and P3'-P5') to the scissile bond resulted in the marginally greater stability of PAI-1, whereas labeling of P12 reversed the stabilizing effect of the mutation. Except for P14, the half-lives of labeled-PAI-1 increase towards P8 and decreased towards s1C, similar to the trend observed when P-even positions of the RCL were mutated to glutamate in an effort to reduce the latency rate of PAI-1 [66].

Since NBD-labeling shows small effects on the stability of PAI-1, the effect of the MTSL probe on the activity of PAI-1 was tested at representative positions, P9 & P1', in the RCL. The activity of MTSL-PAI-1 in the absence and presence of tPA was also compared to the activity of its unlabeled and NBD-labeled counterparts (NBD-P2' was used in place of NBD-P1', which was not available at the time of the experiment) (**Fig. 2.16**). In the absence of tPA, unlabeled, NBD-labeled, and MTSL-labeled P9 (**Fig. 2.16 A**) and P1' (**Fig. 2.16 B**) show similar results and electrophoretic mobility. Also, for both constructs, the NBD-labeled and MTSL-labeled protein samples contain a small amount of dimer and unlabeled or degraded protein, respectively. In the presence of tPA, MTSL-P1' forms slightly more substrate than unlabeled P1' or NBD- P2'. These results

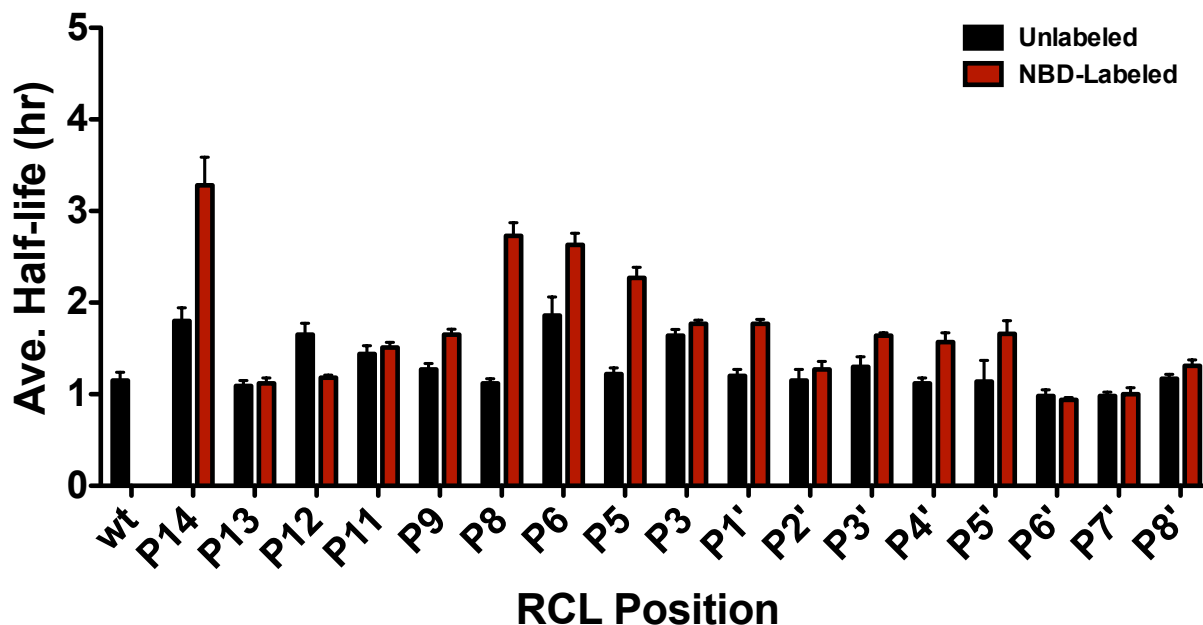


Figure 2.15 Mutation & NBD-Labeling of The RCL on PAI-1 Stability. Unlabeled (*black*) and labeled (*red*) PAI-1 cys mutants were incubated at 37°C in MOPS buffer (pH 7.4) and its residual activity assayed indirectly by the addition of 50 nM tPA. 1 mM Spectrozyme tPA, a chromogenic substrate for tPA, was added to the reaction and the absorbance of its *p*-nitroaniline product measured at 405 nm. Initial rates were plotted over time and the inhibitory half-life determined. Residues are ordered from N-terminal to C-terminal in the RCL according to its P designation relative to the P1-P1' scissile bond.

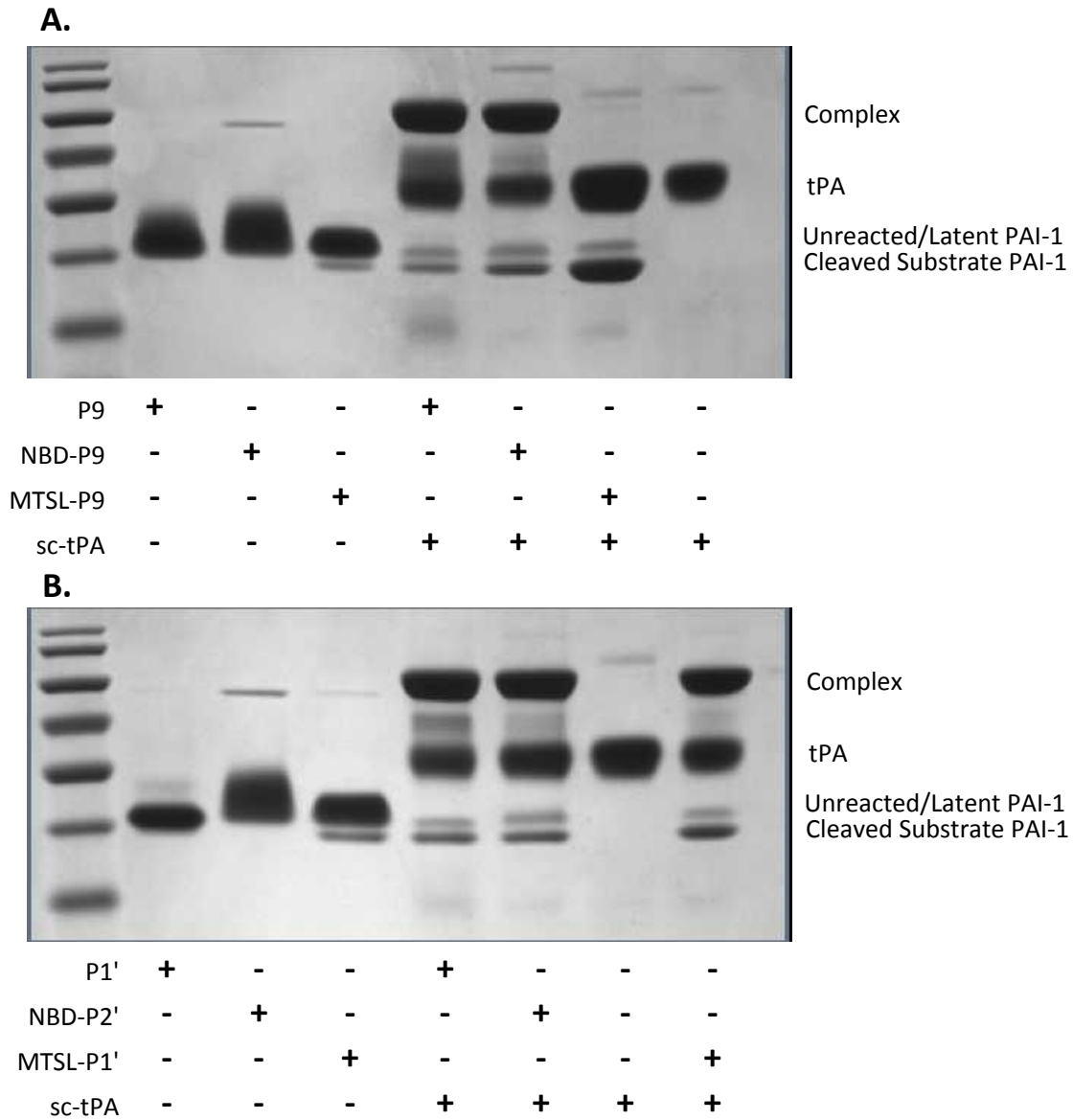


Figure 2.16 Effect of MTSL-Labeling of The RCL on PAI-1 Stability. Representative unlabeled, NBD-labeled, and MTSL-labeled PAI-1 constructs were incubated in the absence or presence of equimolar single-chain tPA (sc-tPA) in PBS (pH 7.4) at ambient temperature for 30 minutes. Samples were resolved under non-reducing conditions by SDS-PAGE on a 10% polyacrylamide gel. Results for the (A) PAI-1 P1' RCL mutant (M347C) and (B) PAI-1 P9 RCL mutant (S338C) are shown. Molecular weight standards are contained in the left-most lane, and components present (+) in succeeding lanes are indicated below the lane.

indicate that MTSL-labeling has similar effects as NBD-labeling at the P1' position. In striking contrast, MTSL-P9 is completely converted into substrate in the presence of tPA, while unlabeled and NBD-labeled P9 show similar formation of complexes with tPA. The latter indicates that MTSL-P9 assumes an RCL-exposed active conformation and interacts with tPA, but upon cleavage, releases the protease.

2.3.d. NBD Reports Unique Micro-environments at the RCL

To test the ability of NBD fluorescence to provide specific information on PAI-1, the affinity for VN (**Fig. 2.17**) and relative quantum yield (QY) (**Fig. 2.18, Table 2.7**) of RCL-labeled mutants were determined. A K_d of ~ 10 nM for the PAI-1-VN interaction, comparable to published values [10, 62], indicates this method is reliable in determining characteristics of PAI-1. Also, the absorbance (**Fig. 2.18 A**) and fluorescence spectra (**Fig. 2.18 B**), with excitation and emission maxima of ~ 480 nm and ~ 530 nm, respectively, were used to estimate the relative QY of NBD-PAI-1 (**Table 2.7**). The QY, defined as the amount of photons emitted per photons absorbed, is used as a measure of efficiency of the fluorescence process. Accurate QY measurements require the use of sophisticated photon-counting equipment, which was unavailable for these experiments.

An alternative method is to calculate the QY with respect to a reference at multiple concentrations, or by single point measurements. Due to the lack of a NBD QY reference value in the literature under the conditions employed in these experiments, the relative QY of NBD_{free} was arbitrarily set to 0.5 to assume 50% efficiency of its fluorescence. The results of the relative QY measurements indicate that the relative QY of NBD-PAI-1 are all similarly high, with a slightly decreasing trend towards the C-terminal position of the RCL.

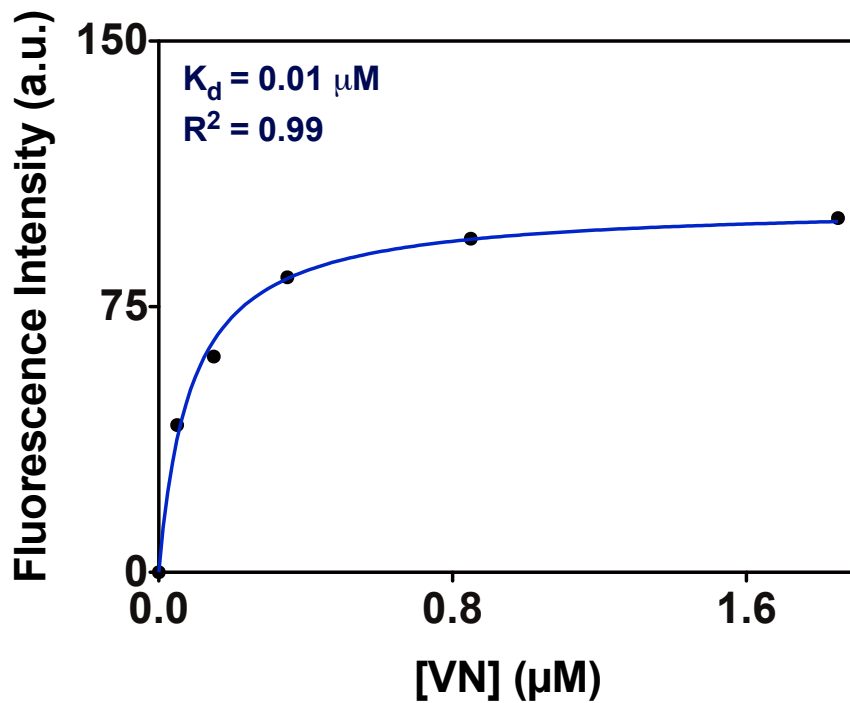


Figure 2.17 VN Binds with High-Affinity to PAI-1. 0.5 μM NBD-PAI-1 was titrated with increasing concentrations of VN, excited at 480 nm, and the emission spectra from 500-600 nm collected. The maximum intensity from the resulting spectra is plotted against VN concentration, fit to a one-site binding curve by nonlinear regression (GraphPad Prism), and the dissociation constant (K_d) determined. Spectra were collected in MOPS (pH 7.4) at ambient temperature. A representative curve is shown (for PAI-1 labeled at the P14 position). Results based on single experiment.

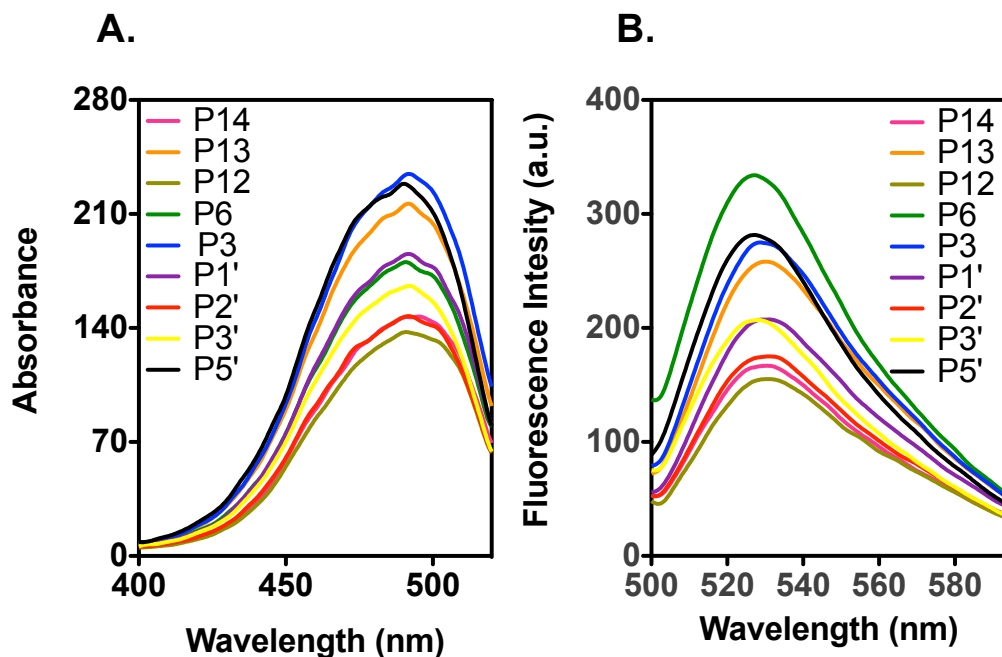


Figure 2.18 Single-Point Measurements For Relative Quantum Yield Determination of NBD-PAI-1. (A) Absorption and (B) emission spectra for NBD-PAI-1 normalized to a concentration of 0.25 μ M NBD were obtained to approximate fluorescence quantum yields (c.f. Table 2.7). Emission spectra were collected after excitation at 480 nm. NBD-labeled RCL residues tested are indicated.

Table 2.7 Relative Quantum Yields of NBD-Labeled RCL Mutants of PAI-1

<i>NBD_{free}</i> & <i>NBD-Labeled PAI-1</i>	<i>Labeling Stoichiometry</i>	<i>Area of Fluorescence (a.u.)</i>	<i>Absorbance (a.u.)*</i>	<i>Relative Q Yield</i>
NBD	n/a	16725	257	0.5**
P14	0.83	8531	135	0.49
P13	0.7	12617	201	0.47
P12	0.7	7938	126	0.45
P6	0.59	10923	168	0.45
P3	0.97	13545	218	0.43
P1'	1.14	10838	171	0.42
P2'	0.79	8657	135	0.41
P3'	1.02	10091	155	0.41
P5'	1	14067	217	0.41

*Absorbance at the theoretical excitation wavelength maximum (480 nm) for NBD.

**Assuming 50% efficiency, the quantum yield of *NBD_{free}* was arbitrarily set to 0.5.

Because buffers and temperature affect its stability [73, 77], the effect of the latter on PAI-1 was tested for NBD at the P9 position of the RCL to detect if perturbations in fluorescence occur (**Fig. 2.19**). To ensure that the results obtained for NBD-PAI-1 fluorescence are not due to non-specific adsorption of the protein to the cuvette used in these experiments, the half-lives of loop insertion were determined as described under Methods (2.2.b) in non- and PEG-coated cuvettes (**Fig. 2.19 A**). Whereas the half-life obtained at the specified temperature and pH in the PEG-coated cuvette are similar to that previously reported (i.e. $t_{1/2} \sim 19$ v. 23 hrs [105]), the result for NBD-PAI-1 in a non PEG-coated cuvette is very fast, indicating adsorption to the cuvette surface. Thereby, all cuvettes were coated prior to latency experiments by fluorescence (2.2.1.). Also, as expected, increasing the temperature at a constant pH (**Fig. 2.19 B**) resulted in a faster half-life comparable to that obtained under physiological temperatures [73] than at room temperature. Furthermore, the half-lives measured in different buffers (**Fig. 2.19 C**), are similar, but slightly longer in phosphate-containing buffers due to the known stabilizing effect of the latter on PAI-1 [146]. However, in measuring the half-lives of PAI-1 in MOPS, inconsistent results with large standard deviations were obtained (**Fig. 2.19 D**) that were not observed in phosphate buffers. To determine if components in the MOPS buffer are responsible for the observed discrepancies, the half-life of NBD-PAI-1 was tested in buffers in which the concentration was lowered to 0.1 M (data not shown) and PEG was removed. The removal of PEG, but not lowering EDTA concentrations, from MOPS buffer resulted in a half-life consistent with the expected value, indicating that PEG interacts with or affects the solvation of the protein in the presence of MOPS. Upon removal of PEG in the latter,

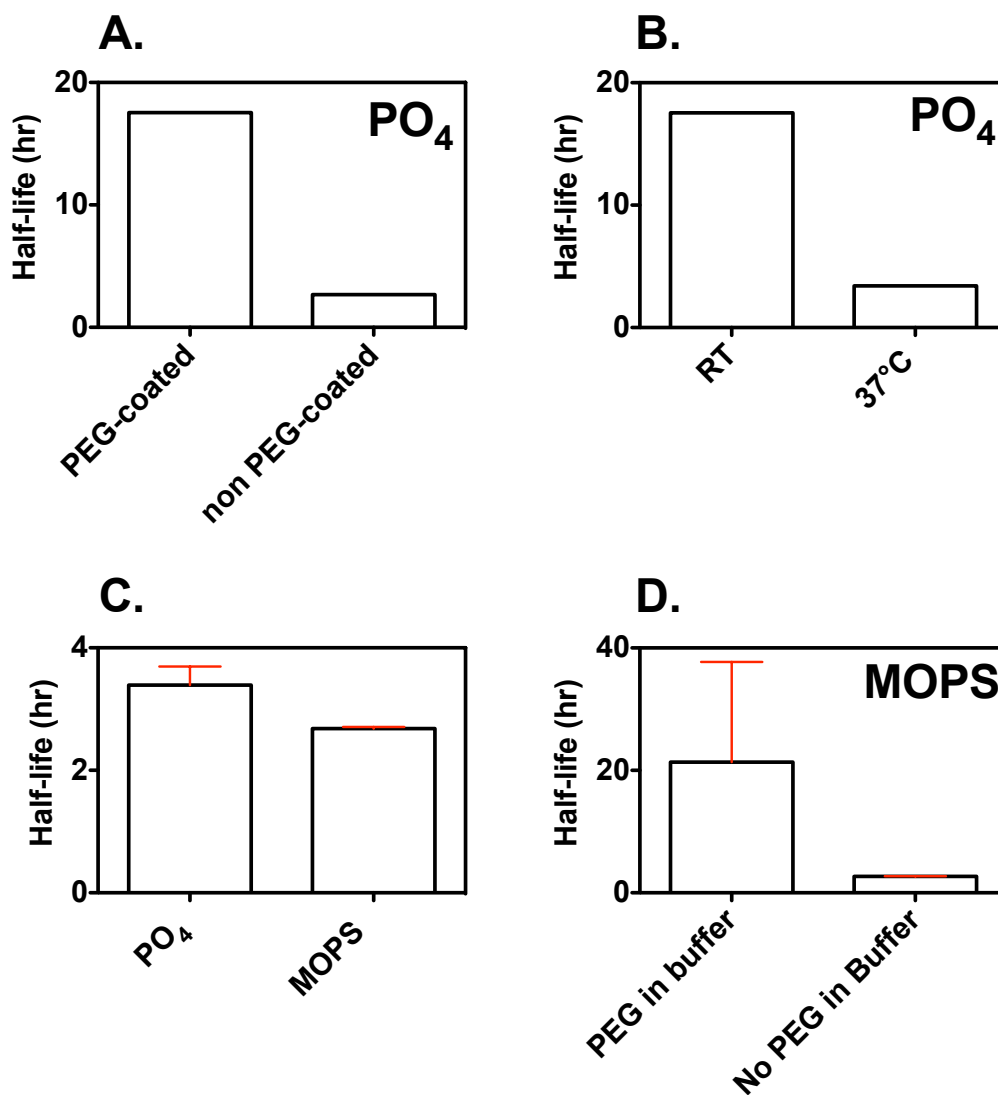


Figure 2.19 Effect of Buffers, Temperature, & PEG on NBD-PAI-1 Fluorescence. 0.5 μ M NBD-PAI-1 was excited at 480 nm and emission spectra from 500-600 nm collected over time. The normalized fluorescence change at 530 nm was plotted against time, fit to a single exponential corresponding to the latency transition, and half-lives determined for NBD-PAI-1 in **(A)** phosphate buffer at room temperature and pH 7.4, **(B)** in phosphate buffer at different temperatures and pH 7.4, **(C)** in different buffers at 37°C and pH 7.4, and **(D)** in MOPS buffer with and without PEG at 37°C and pH 7.4. [PO₄ = 50 mM NaH₂PO₄, 300 mM NaCl, 1 mM EDTA, 0.1% PEG 8000; MOPS = 50 mM MOPS, 100 mM (NH₄)₂SO₄, 1 mM EDTA]. Representative data are for NBD-P9 PAI-1.

the results in both buffers are comparable and reproducible (**Fig. 2.19 C**). Overall, these results reveal that NBD-fluorescence can provide specific information about PAI-1 conformation, but that care must be taken to account for effects of buffer or other additives to the experimental mixture

2.3.e. Transition to the Latent Conformation is Accompanied by Changes in RCL Conformation

The transition to the latent state of PAI-1 is spontaneous and irreversible, with the N-terminal residues of the RCL from P16-P4 inserted as s4A, and P2-P10' extended along the surface of the protein [112]. In this state, the P-even residues point inwards toward the hydrophobic core of the protein, while the scissile bond is tucked near the core and inaccessible for target proteases. To investigate the changes that occur during transition from the active state to this conformation, multiple positions in the RCL were labeled with a fluorescent reporter, and its insertion over time was monitored. Due to the sensitivity of NBD to its local environment, the conformational changes associated with the translocation of the RCL and hinge to the shutter, and s1C through the gate to the surface, of PAI-1 can be observed via its fluorescence. **Figure 2.20** shows a representative graph for the normalized change in fluorescence over time for NBD at various positions in the RCL during the latency process. Except for P5', which shows a consistent decrease over time, each position in the RCL exhibits an increase in fluorescence, indicating burial of the NBD probe in or near the hydrophobic core of the serpin. This increase in fluorescence has been shown previously to correlate with a loss of inhibitory activity, and is attributed to latency transition of PAI-1 [105]. Also, an initial decrease, indicating greater solvent exposure, was observed for all constructs, except

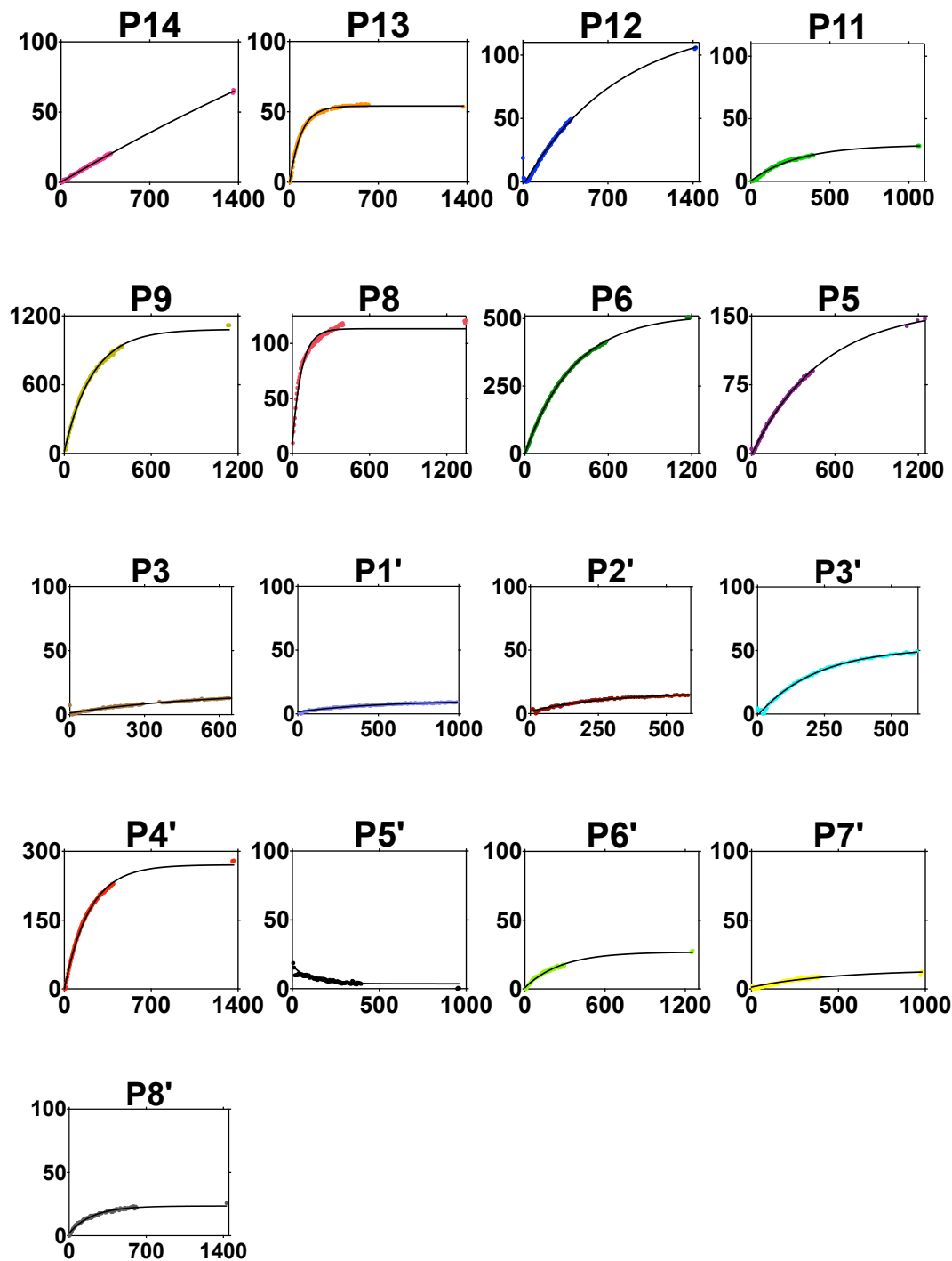


Figure 2.20 Steady-state RCL Insertion During Latency Transition of PAI-1. NBD-labeled PAI-1 was added at 0.3-0.5 μM in 50 mM NaH_2PO_4 , 300 mM NaCl, 1 mM EDTA, 0.1% PEG 8000, pH 7.4 at 37°C. Samples were excited at 480 nm and normalized fluorescence change at 530 nm plotted against time. Data were fit to a single exponential corresponding to the latency transition. All experiments were performed in triplicate, but only one plot is shown above its residuals. Plots are ordered from N-terminal to C-terminal of the RCL.

for P9-P6 (**Fig. 2.21 A**). The decrease was slowed at room temperature and lowering buffer pH (**Fig. 2.21 B**). It should be noted that re-purification, relabeling, extensive dialysis (**Fig. 2.21 C**), changing the buffer (**Fig. 2.21 D**), and elimination of PEG from the buffers (data not shown) did not alter the outcome, indicating that these initial changes report a bona fide structural change in PAI-1. Also, the coated cuvettes were rinsed prior to drying to prevent the possible presence of excess PEG from leaching into the solution, and thus are unlikely to be responsible for the observed decrease. The process detected by this decrease ends within ~10 min for most constructs before increasing exponentially to saturation.

The magnitude of the fluorescence changes at various positions are not correlated with either the labeling stoichiometries (**Table 2.5**) (both of which are similar to reported results [105, 117]), contacts formed in the latent state (c.f. Table 1.4), relative quantum yield (**Table 2.7**), or polymerization (data not shown). For example, P1', which had the highest labeling stoichiometry, exhibits an overall fluorescence change that is similar in magnitude to that of P6'-P8', which have some of the lowest degrees of labeling, likely due to limited access of the latter residues during the labeling reaction. Similarly, P9, which does not make significant contacts in the latent crystal structure, has the highest fluorescence change, followed by P6 and P5, which, unlike the former, participate in several hydrophobic contacts in the latent conformation. Also, P14, while having one of the highest relative QY, shows an intermediate magnitude for the fluorescence change. These results emphasize that the unique microenvironment for various residues positioned in the RCL can be detected by the sensitive NBD probe.

The half-life for insertion of RCL residues was obtained from fitting the data in

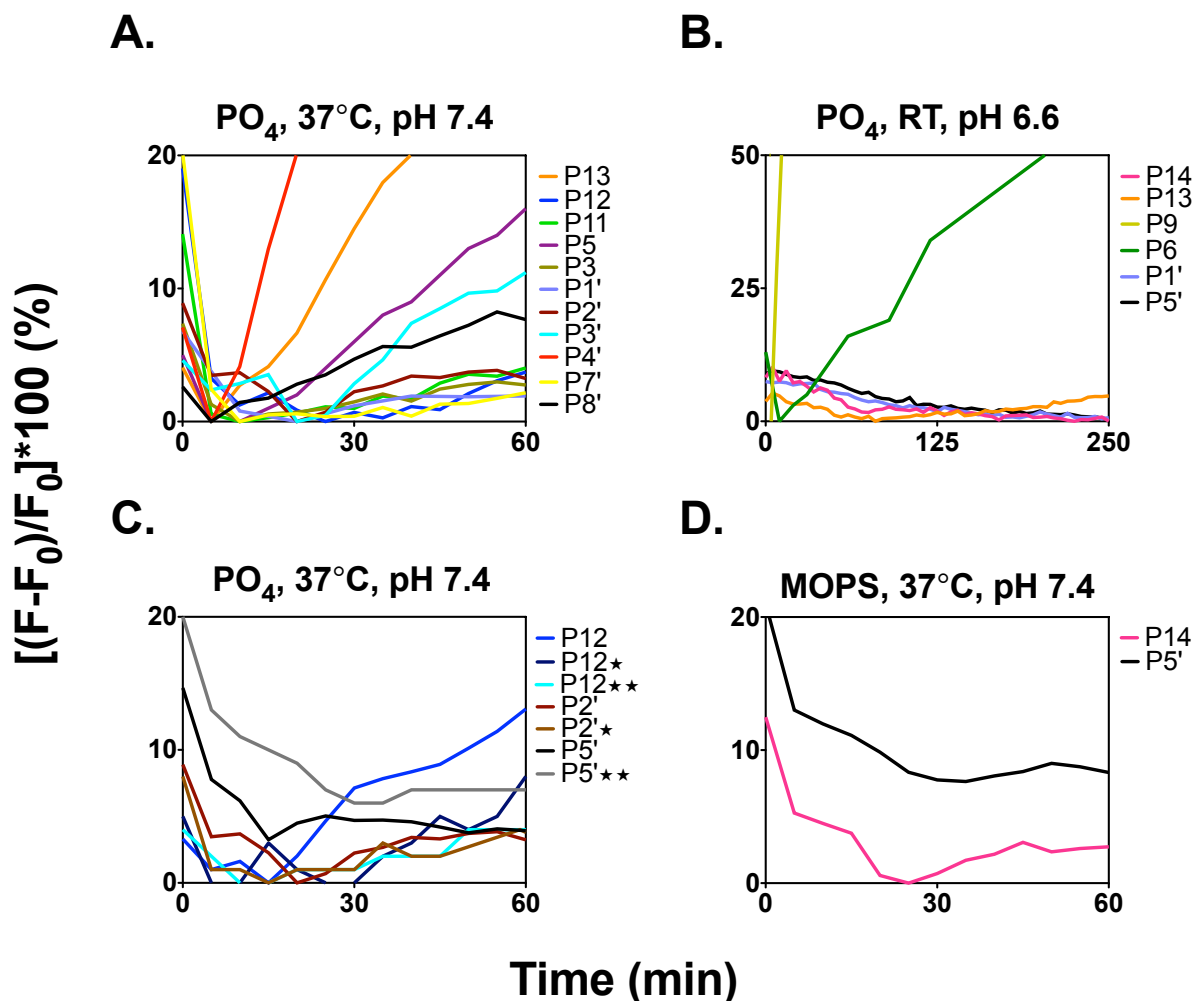


Figure 2.21 Initial Decrease in Fluorescence During Latency Transition. 0.5 μ M NBD-PAI-1 was excited at 480 nm and emission spectra from 500-600 nm collected over time (A) in phosphate buffer at 37°C and pH 7.4, (B) in phosphate buffer at room temperature and pH 6.6, (C) after dialysis (*) and relabeling (**) in phosphate buffer, and (D) in MOPS buffer at 37°C and pH 7.4. Results are plotted as the normalized fluorescence change at 530 nm against time represented as a continuous line without points. Representative data for NBD-labeled RCL mutants tested are indicated. [PO₄ = 50 mM NaH₂PO₄, 300 mM NaCl, 1 mM EDTA, 0.1% PEG 8000 buffer; MOPS = 50 mM MOPS, 100 mM (NH₄)₂SO₄, 1 mM EDTA, 0.1% PEG 8000 buffer]

Figure 2.20 to an exponential one-phase decay model (**Fig. 2.22, red bars**). Except for P14, P12, and P8, the half-life of NBD-PAI-1 generally increases towards P8, as previously observed (c.f. Fig. 2.15). Due to their position at the hinge, the long half-lives observed for P14 & P12 may be due to probe interference in hindering burial of the residues into sA in the latent conformation. Also, the residuals and goodness of fit (**Table 2.8**) indicate that P8 and P5' would fit better to an alternative two-phase decay model (**Fig. 2.22, black bars**). An additional trend of a longer half-life of insertion within error for s1C residues P5'-P8' is also observed. The half-lives of loop-insertion are also considerably longer than the half-lives measured indirectly from the residual PAI-1 activity towards tPA. A noteworthy difference between the two measurements is that the latter only detects inhibitor PAI-1, while the former detects both inhibitor and substrate PAI-1. Insertion of the RCL in PAI-1 that behaves as a substrate has previously been shown to be slower [78], and thereby, the half-lives measured directly by fluorescence can be accordingly longer than that measured by kinetics of substrate inhibition alone.

In addition to conformational effects, the dynamics of the RCL in the active and latent conformations was measured by EPR. The RCL was labeled at the various positions with the paramagnetic MTSL probe, which carries an unpaired electron that, when placed in a magnetic field, resonates by absorption of microwave energy equal in energy to the difference between its electronic states [136]. The magnetic field was swept at a constant frequency, and EPR spectra collected. Individual representative spectra of MTSL-PAI-1 indicate that the dynamics at different positions in the RCL are distinct in the active and latent conformations (**Fig. 2.23**). The change in the dynamics of the RCL was obtained from the difference in the line-width between the active and

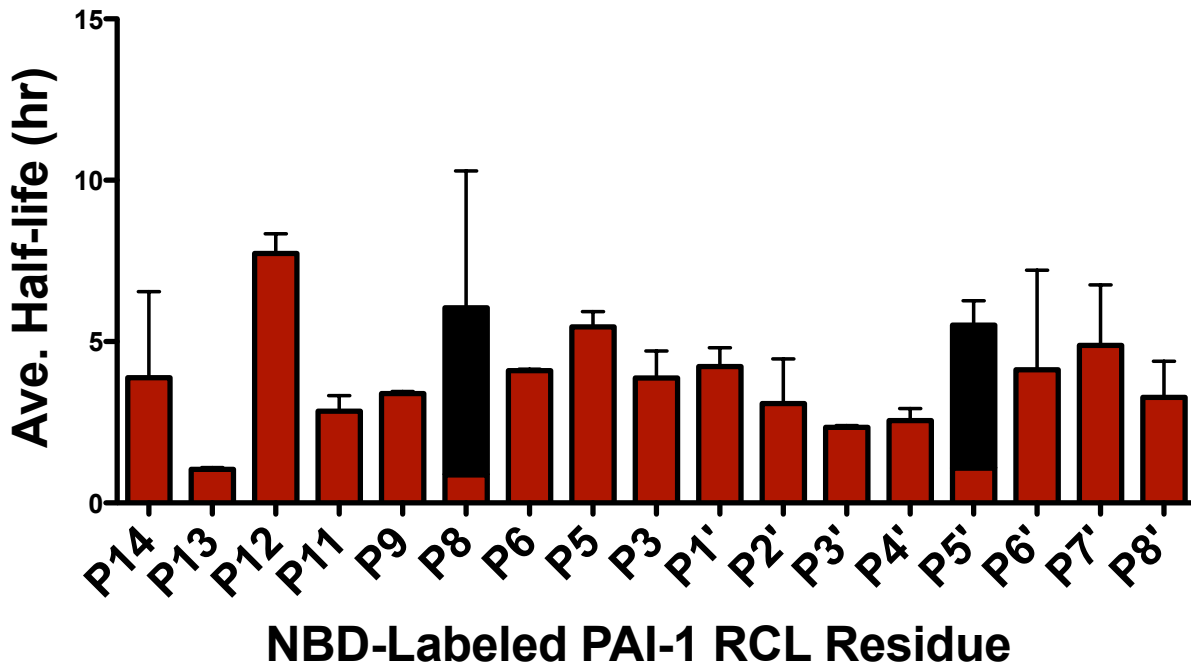


Figure 2.22 Half-life of RCL Insertion. NBD-labeled PAI-1 was added at 0.3-0.5 μM in 50 mM NaH_2PO_4 , 300 mM NaCl, 1 mM EDTA, 0.1% PEG 8000, pH 7.4 at 37°C. Samples were excited at 480 nm and fluorescence emission at 530 nm over time recorded. Data were fit to a single exponential (*red bars*) from which the half-life for insertion of the NBD probe at each RCL position during latency transition was obtained. Initial decreases were excluded before calculating half-lives from a one-phase decay model. A two-phase decay model without exclusion of initial values was used to evaluate certain constructs, for which the slow half-life (*black bars*) is shown. All experiments were performed in triplicate from which an average was plotted with standard deviation error bars.

Table 2.8 Comparison of Half-lives Obtained for NBD-labeled PAI-1 via tPA Inhibition & Steady-state Fluorescence

RCL Position	Half-life (hrs)*	k_{lat} ($\times 10^{-3}$) (min^{-1})*	Half-life (hrs)‡	R^2‡	Half-life (Fast) (hrs)§	Half-life (Slow) (hrs)§	R^2§
P14	3.28 ± 0.31	3.54 ± 0.32	3.88 ± 2.67	0.98			
P13	1.12 ± 0.06	10.33 ± 0.55	1.04 ± 0.05	0.99			
P12	1.18 ± 0.03	9.83 ± 0.25	8.07 ± 0.21	0.99			
P11	1.51 ± 0.06	7.65 ± 0.29	3.12 ± 0.12	0.99			
P9	1.65 ± 0.06	7.01 ± 0.25	3.39 ± 0.03	0.99			
P8	2.73 ± 0.14	4.24 ± 0.21	0.87 ± 0.01	0.95	0.46 ± 0.07	5.18 ± 4.24	0.99
P6	2.63 ± 0.13	4.67 ± 0.18	4.1 ± 0.05	0.99			
P5	2.27 ± 0.12	5.11 ± 0.26	5.46 ± 0.47	0.98			
P3	1.77 ± 0.04	6.54 ± 0.15	4.34 ± 0.36	0.98			
P1'	1.78 ± 0.05	6.55 ± 0.17	4.56 ± 0.07	0.98			
P2'	1.27 ± 0.09	9.13 ± 0.62	2.28 ± 0.01	0.95			
P3'	1.64 ± 0.03	7.04 ± 0.13	2.34 ± 0.06	0.97			
P4'	1.57 ± 0.10	7.38 ± 0.47	2.33 ± 0.04	0.99			
P5'	1.66 ± 0.14	6.98 ± 0.48	1.08 ± 0.08	0.79	0.11 ± 0.01	4.43 ± 0.76	0.97
P6'	0.94 ± 0.02	12.26 ± 0.31	2.4 ± 1.07	0.97			
P7'	1 ± 0.07	11.64 ± 0.82	3.83 ± 0.64	0.97			
P8'	1.31 ± 0.07	8.82 ± 0.46	2.62 ± 0.18	0.95			

* Based on inhibition assays with tPA & fit to single exponential (see Methods)

‡ Based on steady state fluorescence measurements and fit to one phase decay model (see Methods)

§ Based on steady state fluorescence measurements and fit to two-phase decay model

latent conformations of PAI-1 (**Fig. 2.24**). From these results, a periodicity of two is observed from P14 to P3, which indicates a β -strand structure, as expected upon RCL insertion as s4A. Except for P11, the P1'-P8' positions exhibit slightly greater mobility when latent, as expected from this stretch of sequence that is extended along the surface of PAI-1 in the latent conformation. Also, the lack of periodicity in this segment of the RCL indicates the absence of regular secondary structure (i.e. α -helical, indicated by periodicity of 3.6, and β -strands). The greater orientational freedom of probes [e.g. *N*-(4,4-difluoro-5,7-dimethyl-4-bora-3a,4a-diaza-s-indacenyl-3-propionyl)-*N*-(iodoacetyl) ethylenediamine, BYDIA) at the RCL has been previously reported for latent PAI-1, and is due to its more relaxed conformation in this state [99]. Thus, the result with another probe support the EPR results obtained here.

For MTSL-PAI-1, the intensity of the MTSL resonance signal is proportional to the concentration of EPR active species. Therefore, the correlation in signal intensity could result from several phenomena, including probe dimerization, reduction, or removal of the MTSL label. MTSL reduction or removal may occur by the presence of DTT, which is unlikely in this case as MTSL-PAI-1 was passed through two gel-filtration columns during the labeling procedure. A more likely alternative explanation is the resulting signal is due to an equilibrium between the active and latent conformations of PAI-1. A correlation between signal intensity and the amount of active versus latent protein would also better explain the increase in MTSL intensity observed at some RCL positions in the latent state (e.g. P14, P12, P9-P5 in **Fig. 2.23**), for which a gain in EPR active species is improbable. Although the presence of free MTSL can also result in spectra with greater intensities and sharper line-widths, its intensity typically dominates

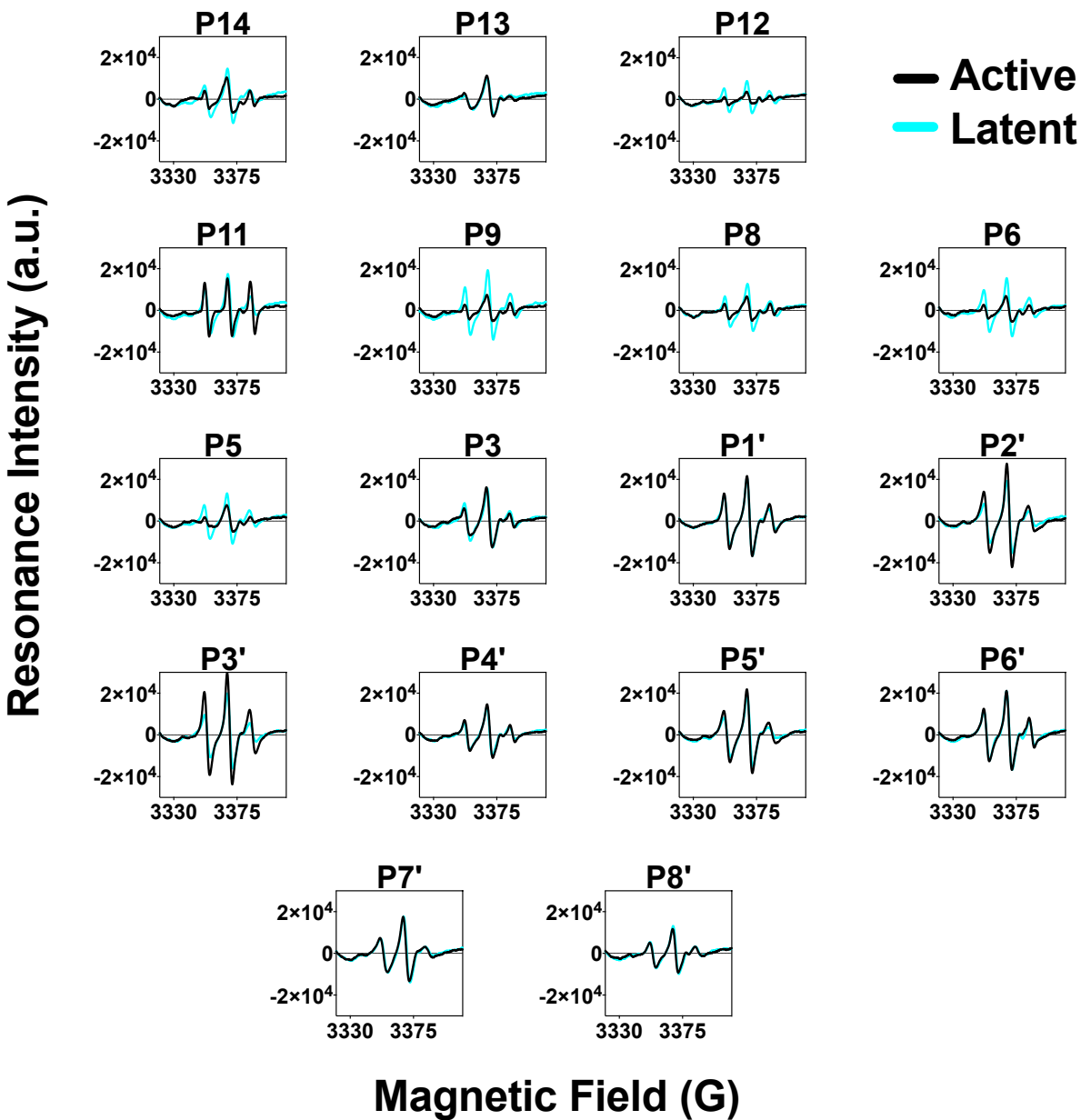


Figure 2.23 Mobility at Different Positions of The RCL (s4A) in Active & Latent Conformations of PAI-1. Latent MTSL-PAI-1 was prepared by incubation at 37°C for 1 week (PBS, pH 7.4). EPR spectra of 2 μ M active (freshly thawed) and 2 μ M latent MTSL-PAI-1 in PBS (pH 7.4) were collected at by sweeping the magnetic field (3310-3410 gauss) at a constant frequency (\sim 9.45 GHz). Representative spectra of active (*black traces*) and latent (*cyan traces*) MTSL-PAI-1 for each RCL position are shown.

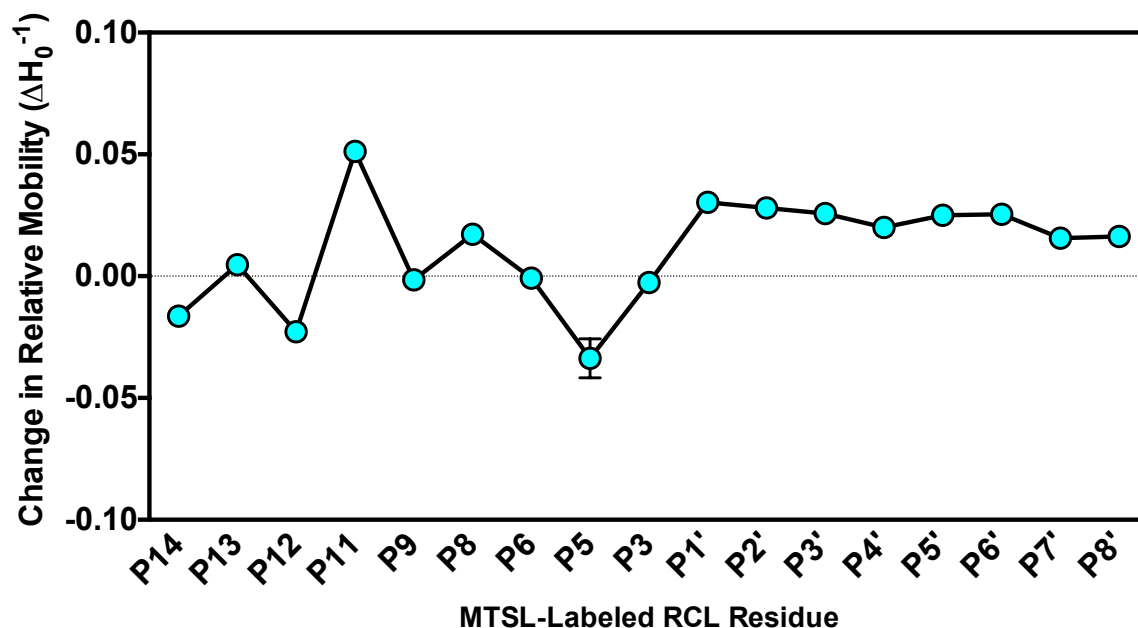


Figure 2.24 Changes in RCL Dynamics From The Active to Latent State of PAI-1. EPR spectra of 2 μM active or latent MTSL-PAI-1 in PBS (pH 7.4) were collected at ambient temperature. The inverse line-widths from the resulting spectra were obtained, and the change in the relative mobility ($1/H_0$) determined by subtracting the average inverse line-width of active MTSL-PAI-1 from the average inverse line-width of latent MTSL-PAI-1. All experiments were performed in triplicate. Standard deviation error bars for most positions are small and not visible in the plot. Residues are ordered from N- to C-terminus of the RCL.

and obscures protein signals, and its peaks (high, center, and low field) are equal and symmetric. In addition, variances in the EPR spectra of MTSL-PAI-1 alone were observed (**Fig. 2.25**). The quality factor, Q , which indicates how efficiently the EPR cavity stores microwave energy ($Q = 2\pi/\text{energy dissipated per cycle} = \nu_{\text{res}}/H_{1/2}$, where ν_{res} is the resonance frequency of the cavity and $H_{1/2}$ is the line-width at $1/2$ height resonance), also varied from 200 to 2200 with day-to-day usage. Smaller variations in Q were observed within shorter time frames. Changes in the Q factor, which is sensitive to electromagnetic interference (EMI), can be minimized, but not controlled. Since the other EPR parameters can be set, the observed variations observed for MTSL-PAI-1 are likely due to fluctuations in the Q factor. Thereby, despite tight standard deviations, small differences in mobility between separate positions are insignificant.

2.4. Discussion

2.4.a. How does flexibility of the RCL affect its conformation?

Homology modeling of the RCL was performed to search for potential conformations that may provide information regarding where the RCL 'starts' in the latency process. Only three low energy structures resulted (**Fig. 2.6**), and molecular dynamics within 0.8 kcal/mol (to allow for thermal motions) also agree with such results. The body of the protein was fixed during modeling, which precludes partially inserted pre-latent forms. However, since this approach typically produces many conformational possibilities, the few models obtained for the RCL is a striking result. While relaxation of this constraint is expected to give rise to more loop conformers, the restricted conformational mobility revealed by homology modeling is likely a consequence of the metastable folding of the RCL to fit its function. Access to few conformations also likely

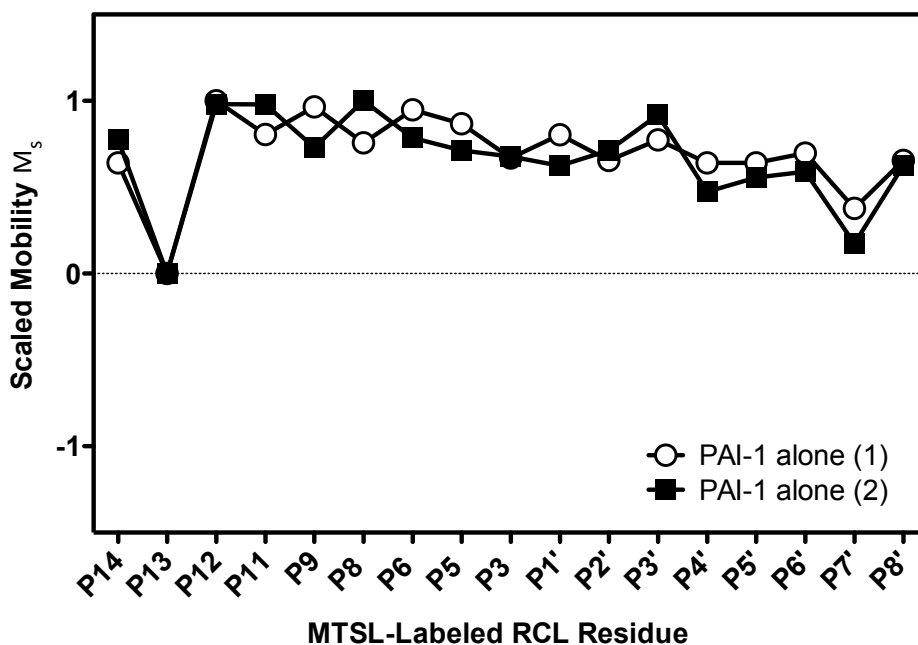


Figure 2.25 Effect of Quality Factor on MTSL-PAI-1 EPR Measurements. EPR spectra of 2 μ M active MTSL-PAI-1 in PBS (pH 7.4) were collected at different times and Q values (\sim 200-2000). The magnetic field (3310-3410 gauss) was swept at a constant frequency (\sim 9.45 GHz). The scaled mobility (M_s) was determined from the inverse line-width of the resulting spectra with respect to the inverse line-widths of the most mobilized and immobilized residue. Residues are ordered from N- to C-terminus of the RCL. All experiments were performed in triplicate.

limits the search for the conformation recognized by target proteases, thereby priming or pre-organizing the serpin to make favorable interactions with target serine proteases. Also, these limited conformations presumably indicate that the metastable kinetic trap is close to and facilitates funneling towards the latent state.

2.4.b. Why does MTSL have distinct effects from NBD on PAI-1 stability?

Despite extensive mutagenesis [66, 94, 107-110, 116, 121, 124, 147], thermodynamic characterization [61, 64], and conformational studies using crystallization [112], limited proteolysis [77, 89], hydrogen-deuterium exchange (HDX) [90], RCL-mimicking peptides [148], and monoclonal antibodies [65], the sequence of events during the transition from active to latent conformation are still not well defined. Single-cysteine mutants of the RCL were thus generated to label with the fluorescent NBD reporter and observe changes that occur during this process. Significant effects on the stability or fold of PAI-1 were not expected for these mutants, as previous studies have shown that the lability is not in the sequence of the RCL [84] and its mutation is tolerated as long as the P1 position is occupied by a basic residue, preferably arginine, and not proline at the P1' position [83, 122]. Indeed, many studies have employed mutation and labeling of the P9 position to elucidate events during inhibition, interaction with target proteases, and mechanism of inactivation by neutralizing monoclonal antibodies [65, 68, 78, 80, 86, 104, 105, 117]. Mutation and labeling of P14, P13 [101], P3, & P1' [58, 99, 100, 104, 117] has been used to a lesser degree to provide information about RCL tethering and nanosecond dynamics. Similar to these studies [58, 100, 105], the results here indicate that the NBD-labeled RCL mutants are folded and

function properly (**Fig. 2.15**), although the SI ratios vary, indicating different degrees of substrate behavior for these mutants (**Fig. 2.12**).

In contrast to NBD-labeling, MTSL-labeling of the P9 position of the RCL results in the curious and complete substrate behavior of PAI-1 (**Fig. 2.16 A**). Upon loop insertion, this residue resides in a mostly hydrophobic environment near the center of s4A in RCL-inserted conformations of PAI-1 (c.f. Fig. 1.10 B & D, Table 1.4). Since the side-chains of P-odd residues point out upon insertion, interference with the close packing of the hydrophobic core is not expected. Also, MTSL, which adds 185.9 Da to PAI-1, is smaller than the NBD probe, which adds 292.28 Da upon labeling, discounting possible steric explanations for the difference. One possibility to account for this peculiar behavior is that the MTSL, but not NBD, probe prevents fast insertion of the RCL during inhibition due to different exosite interactions with tPA in the Michaelis complex. Another possibility is that the MTSL-probe at the P9 position affects the final crushing of the enzyme against the serpin scaffold upon insertion. In this scenario, the nitroxide at the P9 position, but not at P1', may be oriented such that it may react with the ester bond of the acyl enzyme by nucleophilic radical substitution. Since the length of the RCL is important in the close tethering and crushing of the protease [123, 124], substitution at the P9 position could thus result in deacylation of the serpin-protease complex. Though not tested, results for MTSL-labeling of residues around the scissile bond (P5-P3') may be similar to P1', and residues further N-terminal to the target bond may be similar to P9. Alternatively, the effect may only occur at the P9 position. Whether greater exosite interactions or deacylation occurs during (i.e. in following the substrate branch of the inhibitory process) or after insertion remains to be determined.

However, this study employs MTSL for dynamics investigation of the RCL prior to or following latency transition, which is distinct from RCL insertion during inhibition. Thereby, this substrate behavior should not affect the interpretation of the EPR results obtained here.

2.4.c. What steady-state changes occur during latency transition?

Except for P9-P6, an initial decrease was observed within 10 minutes, followed by an exponential increase in fluorescence for a much longer time frame for all RCL residues tested (**Fig. 2.21 A**). Excluding the decrease, this behavior can be adequately described by the single exponential latency process for most mutants, although the changes for P8 and P5' are better explained using a two-step model. The observed initial decrease in fluorescence may be attributed to the partial or full detachment of s1C in preparation to assume the latent conformation, leading to the exposure of P4'-P8' and a change in RCL conformation that is experienced by other RCL residues except for P9-P6. The ensuing increase then describes the insertion of P14-P4 into sA and P2-P8' near the hydrophobic core. The dynamics of the RCL in the latent conformation (**Fig. 2.24**) are also consistent with the insertion of P14-P3 as s4A and P1'-P8' as an extended loop.

Due to their distinct positions, the early-phase changes exhibited by P8 and P5' may not report the same process, in spite of the fact that the second change that occurs at longer times is consistent with RCL insertion. For the P8 residue, which resides under the apex of hF in the latent conformation, an early process occurs with a half-life of ~27 min, which is consistent with the expected displacement of hF prior to full insertion of the RCL in the latent conformation. The hurdle in displacing hF may also explain the

trend of an increasing half-life towards the P8 position. Once hF is displaced, consecutive residues can insert with ease. For the P5' residue, which is located at s1C in the active conformation, but stretched along sA in the latent conformation, an early process occurs with a half-life of ~ 6.6 min, which is close to the 10 min decrease observed at adjacent residues, likely representing s1C detachment. The decrease in fluorescence indicating greater solvent exposure observed at the P5' position is puzzling, but may be due to an interaction with a water molecule in its vicinity during its transition to the latent state. Following detachment, the longer half-lives for insertion of P5'-P8' s1C residues may be due to its slow passage through the gate. Whether hF displacement or passage through the gate is the rate-limiting step of the latency process is not clear, and requires further investigation.

To unify these results here with the currently accepted paradigm for the latency transition, the following model is proposed (**Fig. 2.26**). Starting from the native, metastable state (**Fig. 2.26 A**), crystallization and DDEM studies reveal that the RCL is extended, but close to the protein core, limiting its possible conformations according to homology modeling. Within the first ~10 minutes of the latency process during which a decrease in fluorescence, or greater solvent exposure, of the RCL is observed, the central β -sheet partially opens (**Fig. 2.26 B**). This opening allows the reversible and partial insertion of the N-terminal portion of the RCL (as detected by the 33B8 mAb and DDEM studies) concomitant with the partial detachment of s1C from its host β -sheet (as detected by the H4B3 mAb) (**Fig. 2.26 C**; c.f. Table 1.2). A detached s1C and partially inserted RCL results in the pre-latent conformation of PAI-1. For further RCL insertion, the gate must widen (**Fig. 2.26 D**) and hF must be displaced (**Fig. 2.26 H**). The two

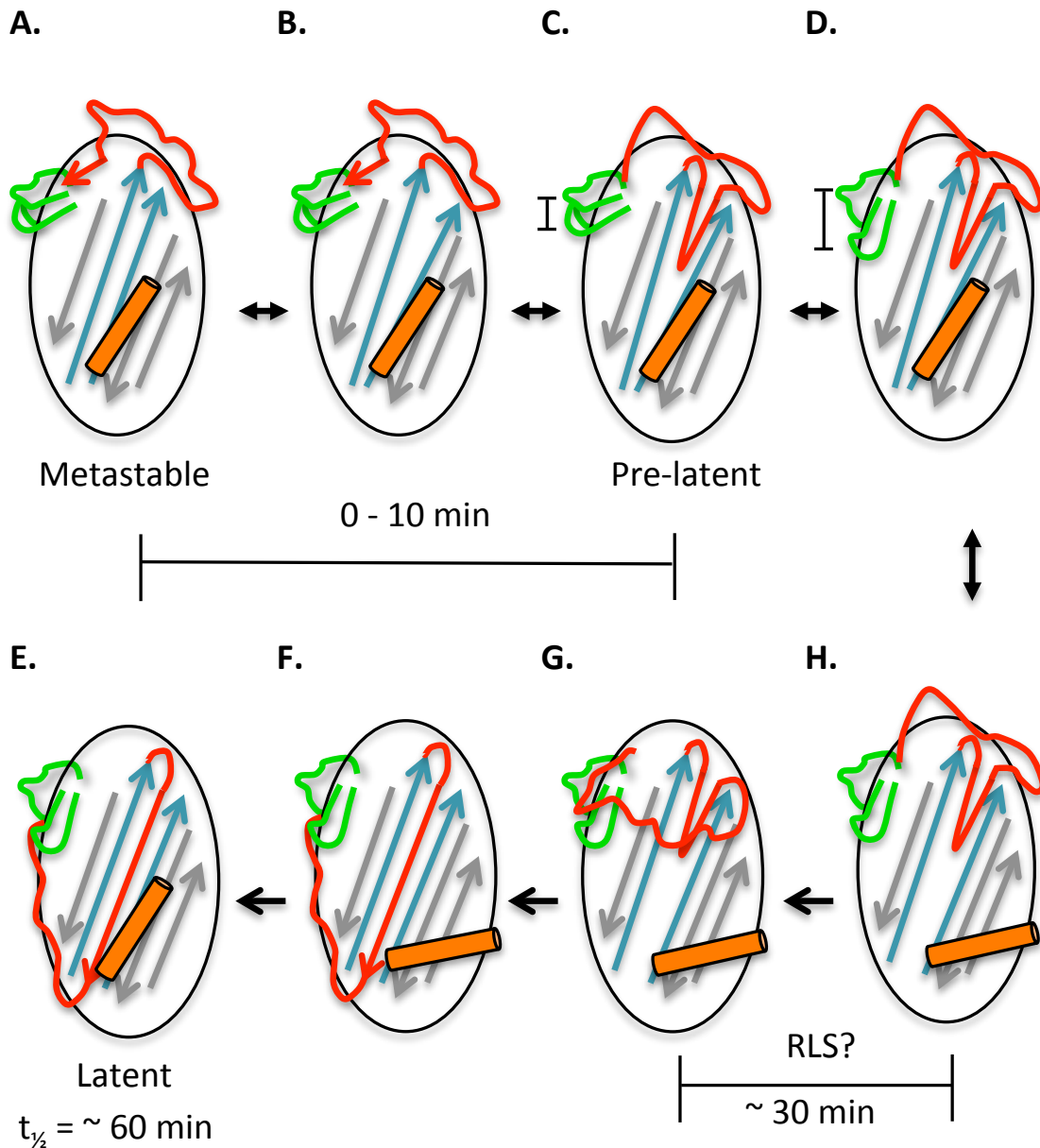


Figure 2.26 Model of PAI-1 Latency Transition. The RCL is shown in **red**, with s1C depicted as a red arrow, the gate loops in **green**, the shutter β -strands as **blue** arrows, and hF as an **orange** cylinder. Additional strands of the central β -sheet A are shown as **gray** arrows. Starting from the native, metastable state (**A**), the RCL is extended, but close to the protein core. In the steps toward the latent conformation, the shutter partially opens (**B**). This allows the RCL to partially insert and s1C to partially detach, reversibly, in the pre-latent conformation (**C**). For further RCL insertion, the gate must widen (**D**) and hF must be displaced (**H**). The C-terminal RCL may then pass through the gate and consecutive N-terminal RCL residues insert as s4A (**G**). When the N-terminal RCL is fully inserted as s4A and C-terminal RCL extended along the surface of the serpin (**F**), hF returns to its position over the shutter and the latency process is completed (**E**).

events are reasoned to occur in concert within the next ~20 min of the latency process based on the first-phase of the transition reported from the P8 position. Also, the C-terminal RCL must pass through the gate region (**Fig. 2.26 G**), which occurs on a longer time-scale, as evidenced from the half-lives reported from the P5' to P8' positions. The rate-limiting step of the latency transition, which may be widening of the gate, passage through the gate, or hF displacement, likely occurs between the conformation changes proposed in **Figures 2.26 G-H**. With hF displaced, consecutive N-terminal RCL residues can insert. Once these residues are fully inserted as s4A, and C-terminal RCL extended along the surface of the serpin (**Fig. 2.26 F**), hF can return to its position over the shutter (**Fig. 2.26 E**). Thus, the latency transition with its many steps is completed with a half-life of ~ 1 hr.

2.5. Conclusions

The tight control of PAI-1 expression and activity is crucial for its proper function and physiological effect. The pre- and post- transcriptional and translational regulation, including by polymorphic regions in the genetic material, glycosylation of the protein, and binding of its cofactor, provide several points that serve as a system to check and balance PAI-1 levels. Importantly, the activity of PAI-1 is curbed by its latent transition, which is a valid mechanism of self-regulation *in vivo*. This transition and the conformation of the RCL were both poorly characterized prior to this study. Using a combined approach of homology modeling, steady-state fluorescence, and EPR, the findings here provide evidence that the structures available to the RCL appear to occupy a circumscribed conformational space, placing the metastable state close to its global free-energy minimum. To get to this state, s1C detachment occurs as an early

event of the latency process. The slower insertion of the RCL, likely limited by its passage through the gate or hF displacement, follows. From this “stressed” to “relaxed” transition, the inserted positions experience a greater degree of orientational freedom. Thereby, the results here reveal that latency transition is not a simple monotonic process, but one that involves sequential steps with independent and concerted conformational changes. This work presents new information on both the conformation of the RCL and latency process of PAI-1, which can be used in the design of more effective inhibitors to this inhibitor under its pathophysiological states.

Chapter 3 Vitronectin Prevents Full Insertion of the PAI-1 RCL

3.1. Introduction

3.1.a. Structural Organization of VN & Oligomerization

As its physiological cofactor, VN assists PAI-1 in regulating fibrinolysis and extracellular proteolysis by several mechanisms, including slowing its latency rate, stabilizing its active conformation, affecting its specificity, and localizing it to the site of action [4, 80]. VN also binds additional structurally distinct molecules, including uPAR, integrins, heparin, the antithrombin-thrombin (AT-T) complex, fibrin, plasminogen, collagen, and platelets. In contrast to PAI-1, whose multi-specificity is built upon a single flexible scaffold, the promiscuity of VN is due to possessing several domains and binding sites for its various ligands (**Fig 3.1**). VN contains three structured domains, including the somatomedin B (SMB), central, and C-terminal domains, and a long, unstructured region, the IDD (intrinsically disordered domain). Small-angle x-ray scattering measurements [149] indicate that these domains fit into the overall bi-lobed fold of VN that is extended in solution. The N-terminal SMB domain, solved by crystallography and NMR [125, 150-152], contains 8 cysteines, which form a disulfide knot, and two short α -helices. At the end of the SMB domain is an RGD (Arg-Gly-Glu) sequence and stretch of negatively charged residues that serve as sites for uPAR and integrins, and thus, cell binding. The adjacent IDD is unresolved, but predicted by the PONDR (Predictors of Naturally Disordered Regions) algorithm to be intrinsically disordered [153], and thereby, may gain structure by coupling binding to folding [154-156], as characteristic of these regions. As with the latter domain, the structures of the central and C-terminal domains have not been solved, but were homology modeled

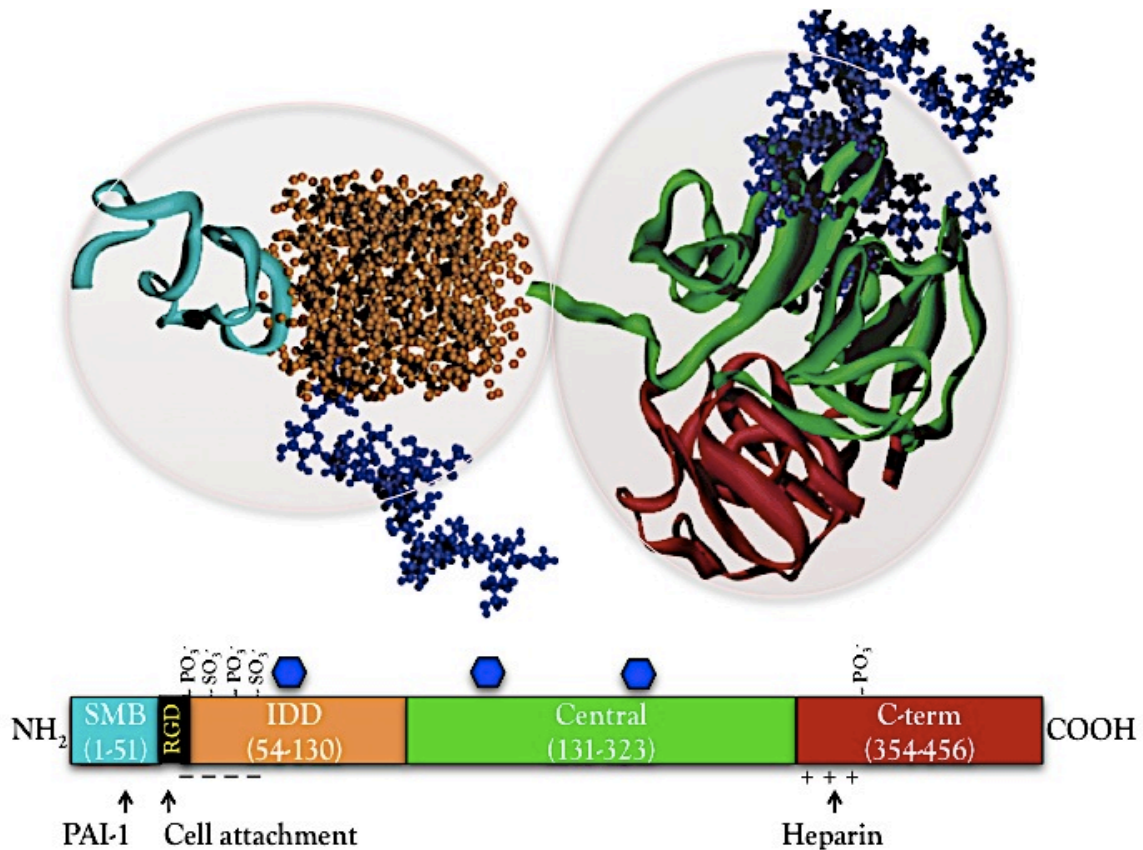


Figure 3.1 VN Is A Promiscuous, Bi-Lobed, Multi-Domain Glycoprotein. VN contains three main domains, which from N- to C- terminus are the somatomedin B domain (SMB, *cyan*), the central domain (*green*), and the C-terminal domain (*red*). The SMB domain is connected to the central domain by an intrinsically disordered domain (IDD, space occupied by *orange* spheres). The global structural model of VN, exhibiting its bi-lobed (*transparent circles*) shape, is displayed over a schematic of its domain organization. Sites for post-translational modifications, including glycosylation (*blue ball-and-sticks in structural model and hexagons in schematic*), phosphorylation (PO_3^-), and sulfation (SO_3^-) sites, are indicated above the domain organization, while clusters of negatively (-) and positively (+) charged residues are shown at its bottom. Adapted from [149].

using the threading method, and thereby predicted as a four-bladed and half β -propeller fold, respectively [153]. The hemopexin-like central domain contains several surface-exposed hydrophobic patches that may be involved in protein-protein interactions and modulating the oligomeric state of VN, while the C-terminal domain contains several positively charged residues for heparin binding. VN also contains multiple sites for post-translational modifications. Glycosylation of VN functions in its multimerization and collagen binding [157], sulfation in its binding of AT-T complexes [158], and phosphorylation in its role in fibrinolysis and extracellular proteolysis by lowering its affinity for PAI-1 [159].

The PAI-1 binding sites on [160] and affinity [10] for VN were controversial before the realization of two binding sites for PAI-1, and its role in the oligomerization of VN. VN is primarily synthesized in the liver and by vascular smooth muscle cells that form the wall of blood vessels, and it circulates at micromolar quantities (0.3-0.6 μ M) in a monomeric form [161, 162]. VN binds to active PAI-1 with subnanomolar affinity ($K_d = 0.1-1$ nM) [4, 62]. This interaction occurs between the SMB domain of VN and the flexible joints region of PAI-1 (**Fig. 3.2**). Specifically, the Asp22 side-chain carboxyl and Phe13 backbone amide groups adjacent to the single turn α -helix in the SMB domain interact electrostatically and via hydrogen bonding with the Arg101 guanidino and the Gln123 side-chain carbonyl groups in the loop connecting s2A to hE of PAI-1, respectively. Because this site overlaps the uPAR and RGD binding sites, PAI-1 competes with these receptors for VN, and thereby modulates cell adhesion and migration.

As with binding sites and affinity, the pro- and anti-migratory (or anti- and pro-

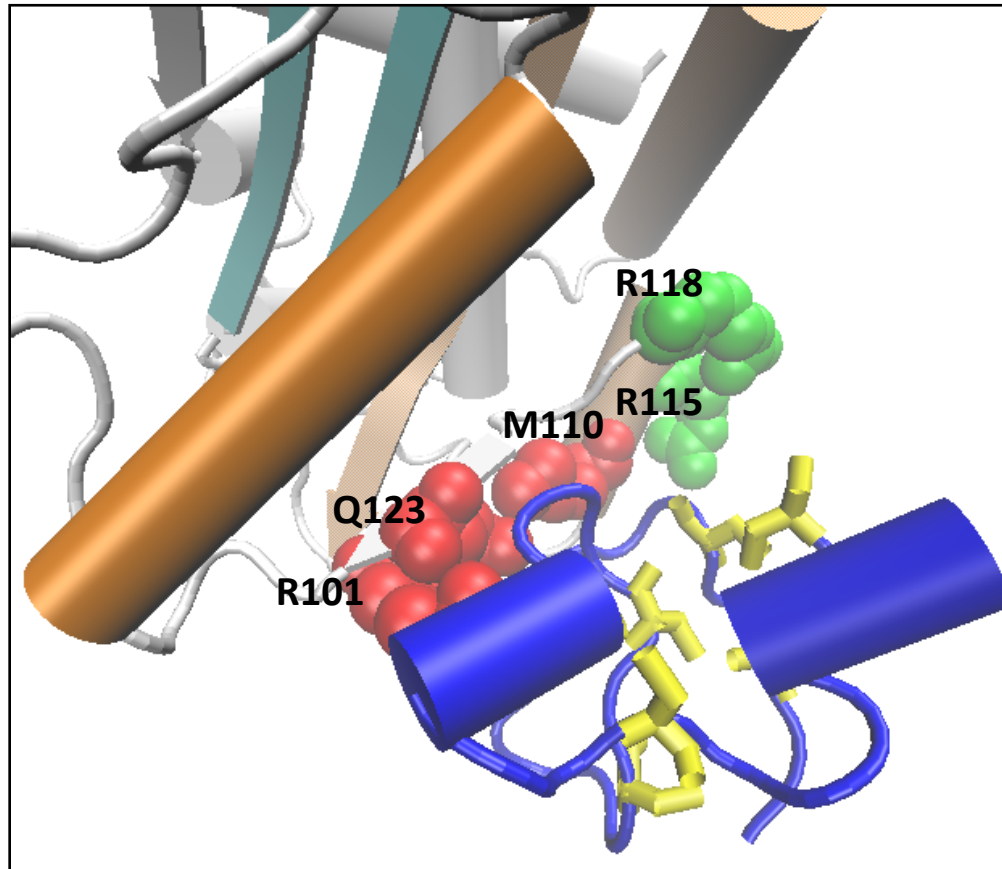


Figure 3.2 Complex Formation with VN Stabilizes & Alters the Specificity of PAI-1. A close-up of the binding interface of PAI-1 (colored as previously described) in complex with the SMB domain of VN (PDB 1OC0)[125] is shown. Binding of the SMB domain (*blue*) of VN to the primary, high-affinity site (*red space-filled spheres*) at the flexible joint region of PAI-1 stabilizes it, while binding of VN at a site outside the SMB domain to the secondary, low-affinity site (*green space-filled spheres*) on PAI-1 may have a role in altering its specificity for target serine proteases. PAI-1 residues involved in binding VN, and the cysteines (*yellow*) forming the disulfide knot in the SMB domain, are indicated. Rendering constructed using VMD 1.9. (c.f. Fig. 1.14)

adhesive, respectively) roles of VN and PAI-1 have also been controversial [6]. Alone, both VN and PAI-1 cause the migration of cells, but via different mechanisms. For its migratory effect, VN binds to uPA-uPAR, where uPA locally activates plasminogen (Plg) to plasmin (Pln), which subsequently activates matrix metalloproteases (MMPs) to degrade the surrounding extracellular matrix (ECM) (c.f. Fig. 4.4), facilitating cell migration. The migratory effect of PAI-1 is due to its interaction with PAs and the low-density lipoprotein receptor-related protein, LRP-1. LRP-1 can bind surface receptors (uPAR, integrins) that attach the cell to the ECM, and to PAI-1-PA complexes, which initiate receptor-mediated endocytosis (c.f. Fig. 4.6), thus leading to internalization of the receptors and cell detachment. Furthermore, at basal PAI-1 levels, PAI-1-VN is anti-migratory, as VN prevents PAI-1 binding to LRP-1, but depending on the microenvironment, can also be pro-migratory, as PAI-1 blocks the binding of cell-surface receptors to VN. Overexpressed PAI-1, in contrast, is pro-migratory via LRP-1. PAI-1 also induces VN to form higher-order oligomers that exhibit pro-adhesive properties and enhanced integrin binding [5].

While monomeric in circulation, VN in the ECM can also exist in a multimeric form for which active PAI-1 has approximately 6-fold higher affinity [10]. The oligomerization of VN into this multimeric form is stimulated *in vitro* by denaturation and refolding [163], but is also induced in a step-wise [164] and concentration-dependent manner by PAI-1 via an intermediate revealed by sedimentation equilibrium to have a stoichiometry of 2:1 PAI-1:VN [165]. Multimeric VN has different adhesive properties from native monomeric VN, although the distinction between the two forms is not always clear from the literature. The observation of 2:1 complexes and the evidence of binding

sites hypothesized in the central and C-terminal domains with affinities ranging from 0.3-190 nM further indicated that VN possesses two binding sites for PAI-1. The presence of a second, lower affinity ($K_d = 50-100$ nM) binding site outside the SMB domain, was confirmed by a recombinant truncation of VN lacking the SMB domain (r Δ SMB) that retains the ability to bind PAI-1 [113, 126]. Similarly, several mutants of PAI-1 mapped a secondary binding site on PAI-1 for VN located on hE and involving residues R115 and R118 (**Fig. 3.2**). Though the two sites on VN can be simultaneously occupied by two PAI-1 molecules upon saturation ([165], rapid kinetic measurements revealing a biphasic binding of PAI-1 to full length monomeric VN, but monophasic binding to the SMB truncation, indicates an extended binding interface exists for the 1:1 PAI-1-VN interaction [80], possibly involving the IDD gaining structure upon binding to hE.

Similar to the previous aspects of their interaction, the ability of VN to bind latent PAI-1 has been debatable [10, 160], as the interaction is undetected by many methods; however, surface plasmon resonance measurements show that VN indeed binds latent PAI-1, albeit with ~100 to 200-fold lower affinity [10, 126] and fast dissociation rates (k_{off}) [126]. Also, VN dissociates from PAI-1 when the sA and flexible joint region are reorganized due to RCL insertion during latency or final complex formation [10, 160, 166]. With respect to these processes, VN stabilizes PAI-1 and alters its specificity.

3.1.b. VN on PAI-1 Conformational Stability & Specificity

By binding to PAI-1, VN increases its thermal stability [125] and slows its latency rate [4]. A mechanism by which VN slows the PAI-1 latency transition was proposed from the crystal structure of the stable 14-1B mutant of PAI-1 in complex with the SMB

domain of VN (**Fig. 3.2**) [125]. This structure suggests that VN binding at the flexible joint of PAI-1 sterically blocks RCL insertion by keeping its shutter in a closed conformation. RCL insertion resulting in the expansion of sA and closing of the hydrophobic gap between s1A/s2A and hD/hE is likewise hindered. Also, whereas the RCL in other 14-1B structures [e.g. active, uncomplexed (1B3K, 1DVM) [141, 142] and in complex with uPA-S195A (3PB1)[81] is resolved, either due to crystal packing effects or binding interactions, the RCL in the 14-1B-SMB complex is unresolved, signifying its greater exposure and/or flexibility in the complex. However, VN binding also results in the increased incorporation of RCL-mimicking peptides of varying lengths (i.e. the P14-P10 pentapeptide and P14-P7 octapeptide) to metastable PAI-1, indicating a 'pigeon-toed' opening of the shutter in the native serpin [92] (**Fig. 3.3**). Since this opening of the shutter suggests more than solely steric effects, VN stabilization of PAI-1 is additionally hypothesized to affect the conformation of the RCL, specifically by shifting the conformational equilibrium of PAI-1 to more solvent-exposed RCL forms [92], which is supported by fluorescent reporters at the P9 and P1' positions of the RCL [104]. Also, the mobile gate that affects the PAI-1 latency transition may be altered by VN binding.

The binding site responsible for the stabilization of PAI-1 by VN is demonstrated by the R101A/Q123K double mutant of PAI-1 [92] and recombinant VN truncation lacking the SMB domain (r Δ SMB) [113, 126]. The R101A/Q123K double mutant in the presence of full length VN and wtPAI-1 in the presence of r Δ SMB fail to result in the stabilization of PAI-1, indicating that PAI-1 stabilization requires SMB binding at its flexible joint. Furthermore, hydrogen-deuterium exchange (HDX) studies of PAI-1 in the presence of the SMB domain indicate this stabilization spreads beyond the binding

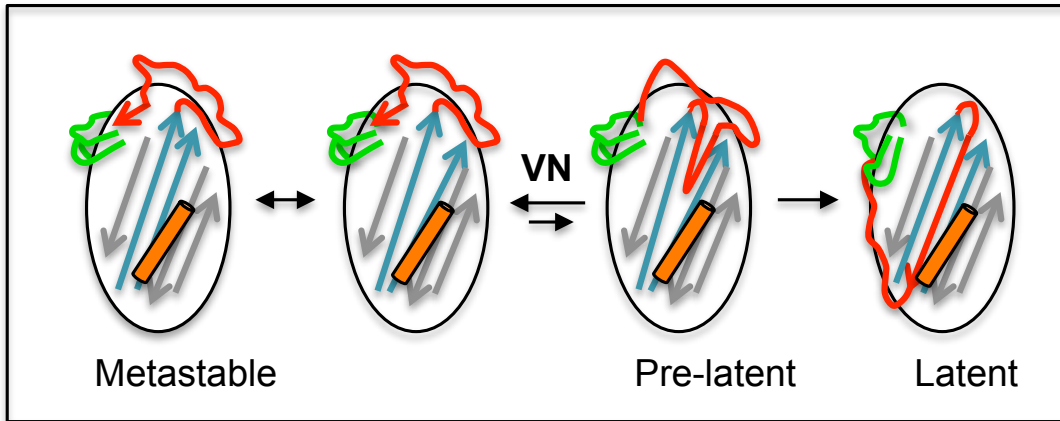


Figure 3.3 Model of VN Stabilization of PAI-1. Global conformations of PAI-1 are represented (as previously described, c.f. Fig. 2.27), including the active-metastable, the pre-latent, and the latent conformations. VN is hypothesized to stabilize PAI-1 by in shifting its conformational equilibrium towards the more active conformation. (Adapted from [92]).

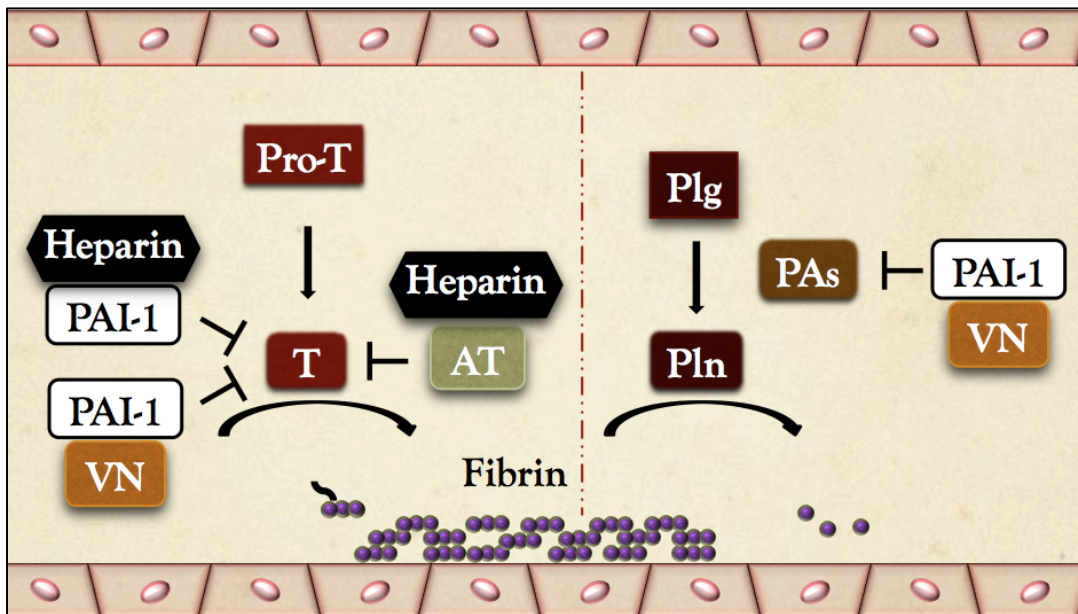


Figure 3.4 VN & Heparin Make PAI-1 A More Efficient Thrombin Inhibitor. PAI-1 primarily inhibits PAs (tPA and uPA) to prevent the activation of plasminogen (Plg) to plasmin (Pln) during fibrinolysis. Thrombin (T), normally activated from its prothrombin (Pro-T) form during coagulation and inhibited by antithrombin (AT), is inhibited also by PAI-1 when the latter is bound to VN or heparin. Heparin also assists AT in the inhibition of thrombin.

interface to hB, hC, and hI underlying the flexible joint [91].

In addition to effects on stability, VN alters the specificity of PAI-1 towards thrombin (**Fig. 3.4**) and increases their association rate (k_{assoc}) by 200- to 270-fold [10, 167]. Though thrombin is mainly responsible for converting fibrinogen to fibrin, its interaction with PAI-1 may function in the clearance of the latter or in regulation of the coagulatory branch in the hemostatic process [168]. However, the role of thrombin inhibition is primarily accomplished by antithrombin, and enhanced by heparin, a glycosylaminoglycan and anticoagulant, which bridges the two. Heparin, like VN, also alters the specificity and makes PAI-1 a more efficient thrombin inhibitor [10, 80, 84, 160, 166, 169]. Residues in PAI-1 that are involved in binding heparin are located in hC, hD, s2A, and its connecting loop (**Fig. 3.5**), which overlaps the secondary binding site on PAI-1 for VN. Unlike VN, heparin does not stabilize PAI-1 [160], and as with the antithrombin-thrombin complex, may serve as a scaffold for the interaction of PAI-1 with thrombin rather than exhibiting effects on the RCL conformation.

Opposite to heparin, α_1 -acid glycoprotein (AGP), an acute-phase anti-inflammatory protein, stabilizes PAI-1, but is not known to alter its specificity [95]. AGP binds to the loop connecting hI to s5A at the flexible joint (**Fig. 3.6**) adjacent to the SMB binding site and “opposite” to the heparin site. Also, AGP only binds to active PAI-1, and thereby is hypothesized to stabilize PAI-1 by restricting the movement of sA.

3.1.c. Objective of PAI-1-VN Study

Although effects on sA and RCL conformation are implicated [4, 92, 104], how this change in conformation stabilizes PAI-1 is unclear. By reporting from the RCL, changes in the solvent accessibility and dynamics that occur in the presence of VN are

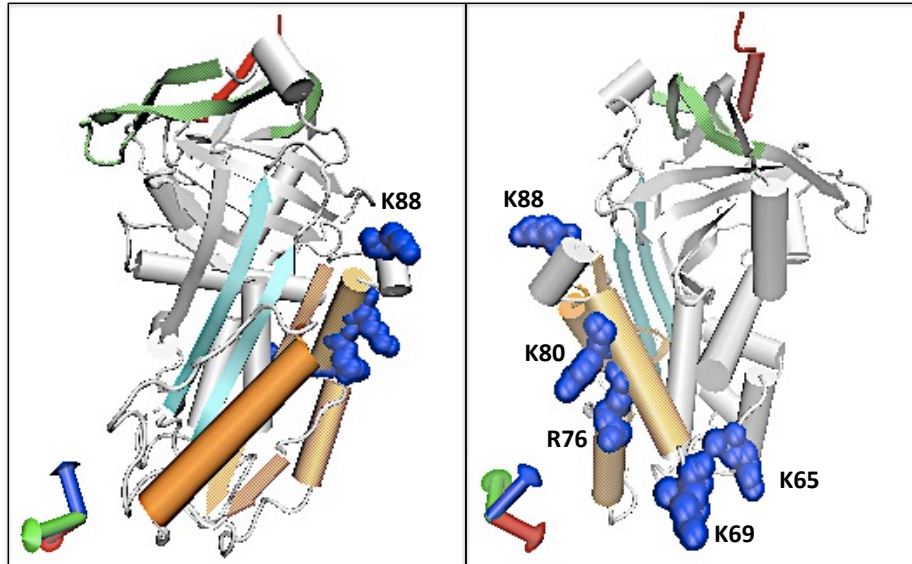


Figure 3.5 Heparin Binding Alters the Specificity of PAI-1. The highly sulfated and negatively charged heparin glycosaminoglycan binds to a site (*blue space-filled spheres*) on PAI-1 (*colored as previously described*) adjacent to the SMB binding site. PAI-1 residues involved in binding heparin are indicated and graphics rendered using VMD 1.9.

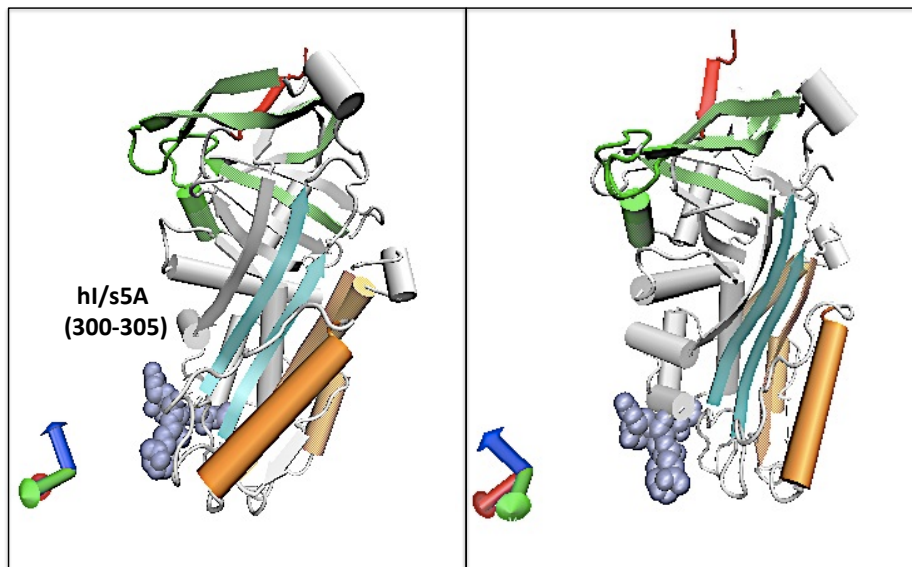


Figure 3.6 α_1 -Acid Glycoprotein Stabilizes The Active Conformation of PAI-1. α_1 -acid glycoprotein (AGP) binds to a site (*iceblue space-filled spheres*) on PAI-1 (*colored as previously described*) adjacent to the SMB binding site. The stretch of residues in PAI-1 that are involved in AGP binding are indicated. Depiction generated using VMD 1.9.

used to provide the lacking information. Also, the proximity of the AGP- and SMB-binding site and of the heparin-binding and secondary VN-binding sites, suggests that these sites may play separate roles in PAI-1 stability and specificity. Binding at these sites may thereby have discrete effects on the RCL. While the secondary binding site on VN for PAI-1 is unknown, it may involve the IDD. To test the latter, the RCL-labeled mutants were investigated by fluorescence and EPR in the presence of the SMB and SMB-IDD truncations of VN.

3.2. Methods & Materials

3.2.a. Purification of VN, SMB, & SMB-IDD

VN was purified from human plasma in several steps, including BaCl₂ precipitation, ammonium sulfate precipitations, treatment with 1mM DTNB and extensive dialyses, anion exchange (DEAE Sephacel), affinity (Blue Sepharose CL-6B and heparin sepharose), and gel filtration (Sephacryl S-200 HR) chromatography, as described previously [62, 127]. Purified VN was confirmed by western blot using a polyclonal anti-VN antibody generated in rabbit. VN, stored as an ammonium sulfate precipitate, was resuspended and dialyzed extensively in buffer before experimentation. Recombinant SMB domain (residues 1-47) was expressed as a thioredoxin-fusion protein from a pET32b vector in Rosetta-gami 2 (DE3) pLysS and purified as described previously [62, 127], including IMAC (nickel-Sepharose FF) followed by thrombin cleavage and gel filtration (S-100).

3.2.b. Assessment of Full-length VN Oligomeric State

VN and wt-PAI-1 were dialyzed in PBS (pH 7.4) at 4°C, diluted to 8 μM and 16 μM, respectively, analyzed by sedimentation velocity at 50,000 rpm and 25°C, and fit to

a c(s) distribution model using SEDFIT as previously described (c.f. Ch. 2.2.j).

3.2.c. Steady-state Fluorescence of VN & Truncations on PAI-1 RCL Solvent

Accessibility

NBD-labeled PAI-1 and its ligands (VN, SMB, & SMB-IDD) were dialyzed in 4 L buffer (PBS, pH 7.4) at 4°C and added to a PEG-coated acrylic cuvette to a final concentration of 0.5 μM and 2 μM, respectively, in 2 ml buffer. Reactions were sealed and incubated at 25°C for 30 min to equilibrate. The cuvette was then placed in a Perkin Elmer LS 50B Luminescence spectrometer at ambient temperature, excited at 480 nm, and the fluorescence emission spectra from 500-600 nm were collected. The intensity at 530 nm was obtained and normalized to determine the percent change in fluorescence due to binding according to the following equation:

$$[(F-F_{PAI})/F_{PAI}]*100$$

where F is the fluorescence intensity of NBD-PAI-1 at 530 nm in the presence of ligand, and F_{PAI} is the average fluorescence intensity of NBD-PAI-1 alone at 530 nm. All experiments were performed in triplicate.

In addition to tests in PBS, initial changes in MOPS (pH 7.4) were measured by adding 1.5 μM human VN (native, monomeric, dialyzed in PBS, pH 7.4) to 0.5 μM NBD-PAI-1 in a PEG-coated cuvette. The emission spectra were collected as described above. Fluorescence values were corrected for dilution by multiplying the resulting intensity at 530 nm by the ratio of the final to initial volumes. The percent change in

fluorescence was determined according to the above equation. Experiments were performed in duplicate.

3.2.d. EPR of VN & Truncations on PAI-1 RCL Mobility

EPR spectra were collected as previously described (c.f. Ch. 2.2.q.), with the exception that dialyzed MTSL-labeled PAI-1 in PBS buffer (pH 7.4) was diluted to a final concentration of 2 μM after the addition of 8 μM ligand (VN, SMB, & SMB-IDD) and incubated at room temperature for 30 min to equilibrate prior to analysis. The change in the mobility (ΔH_0^{-1}) was determined from the central field MTSL peak by subtracting the average inverse line-width of MTSL-PAI-1 alone to that of MTSL-PAI-1 in the presence of ligand. All experiments were performed in triplicate.

3.2.e. Detection of Free Sulfhydryls & Labeling Integrity of MTSL-PAI-1

MTSL-PAI-1 samples were retrieved after EPR experimentation, added to a 96-well plate (Costar, half-area), and 1 mM DTNB added to MTSL-PAI-1 in the absence and presence of ligands. Samples were incubated at ambient temperature for 5 min, and subsequently, the absorbance at 412 nm was measured (BioTek Synergy4 plate reader) to detect the presence of free sulfhydryls. Experiments were performed in duplicate. Samples from EPR/DTNB experiments were HPLC-purified and analyzed by MALDI MS as previously described (c.f. Ch. 2.2.k.) to confirm the presence of the MTSL label on PAI-1.

3.3. Results

3.3.a. VN & its Truncations Exert Similar Conformational Changes in the RCL

As its affinity for PAI-1 depends on its conformation, native VN was purified from human plasma and analyzed by AUC, which confirms its monomeric state (**Fig. 3.7A**)

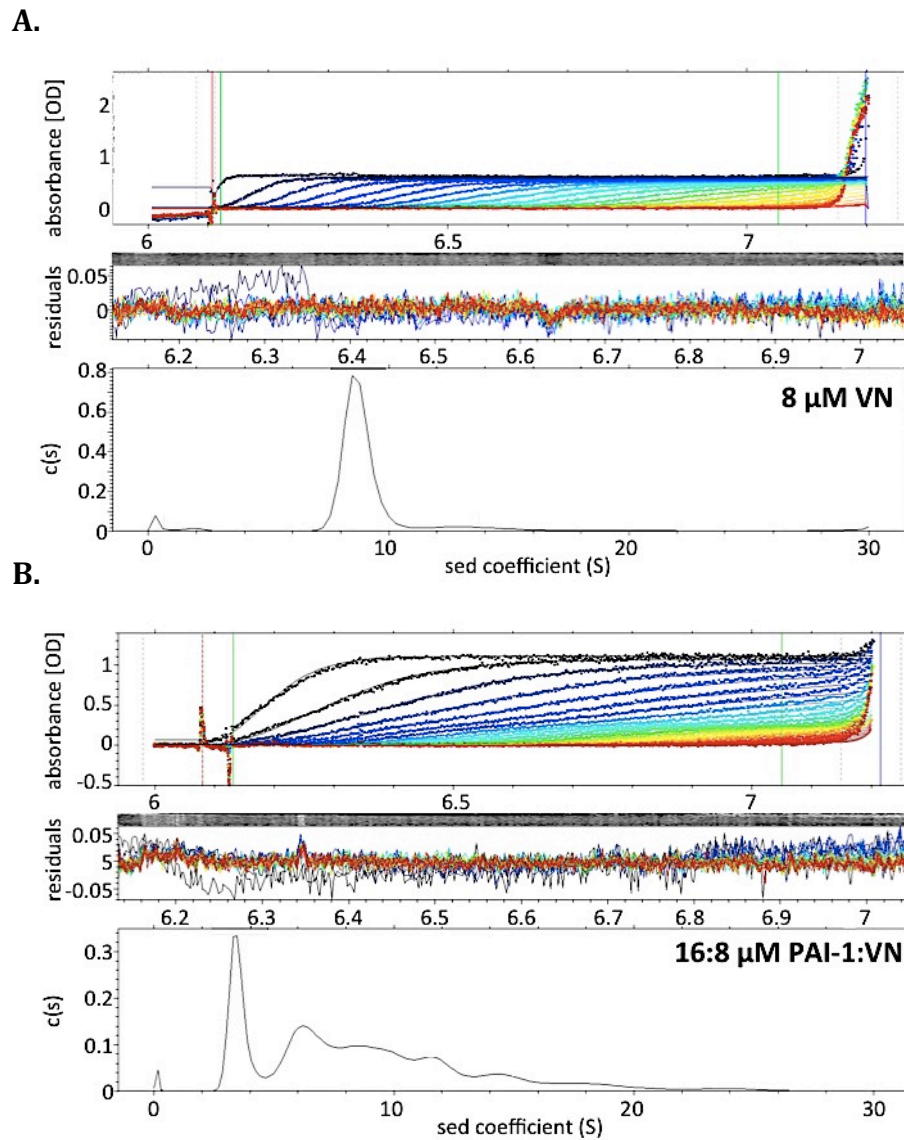


Figure 3.7 VN forms higher-order complexes with PAI-1. Purified VN was added in the absence (**A**) and presence (**B**) of PAI-1 at the indicated concentrations to an ultracentrifuge cell and analyzed by sedimentation velocity. The absorbance traces collected over time and plotted against the cell radius were fit to a $c(s)$ distribution model using SEDFIT in the top panels, the residuals of the fit are shown in the middle panels, and the distribution plot of distinct sedimenting species in the bottom panels.

and ability to form PAI-1-mediated higher-order oligomers (**Fig. 3.7B**). To investigate the conformational effects due to VN binding, the solvent accessibility along the RCL was measured by fluorescence under equilibrium conditions (**Fig. 3.8**). As expected for binding at a distant region, full length VN and its truncations, SMB and SMB-IDD, induce modest changes in the exposure of the RCL that are similar in magnitude at most positions. Hinge residues P14-P13, residues about the scissile bond (P3-P3'), and s1C residues P4'-P5' show less than 10% change in fluorescence due to binding of the three VN constructs. At the P14-P13 positions, the SMB-IDD elicits a slightly greater decrease in fluorescence (~3-6%), representing more solvent exposure, than full length VN or the SMB domain. Also, a ~2-15% increase in fluorescence is observed at P12-P11 in the presence of the VN constructs, indicating a more hydrophobic environment for these near hinge residues. Further along the RCL, the P9-P6 residues show greater solvent exposure (~6-18% fluorescence decrease) due to VN, SMB, and SMB-IDD binding. These residues also do not exhibit an initial decrease during the latency transition of PAI-1 (c.f. Fig. 2.22 A), providing a possible connection between VN binding and PAI-1 stability. At the distal end of the RCL, larger increases of ~17-28% and ~15% are observed for P6' in the presence of VN and SMB-IDD, and P8' in the presence of the SMB domain, respectively, while P7' exhibits less than a ~5% change in solvent accessibility in the presence of these ligands.

In addition to steady-state changes in phosphate buffer, the effect of VN binding on the RCL conformation was tested in MOPS buffer, which was chosen for its low binding of metals in related studies (see Ch. 5). Initial changes at steady state were recorded as described under Methods (c.f. 3.2.c). The results reveal less than 10%

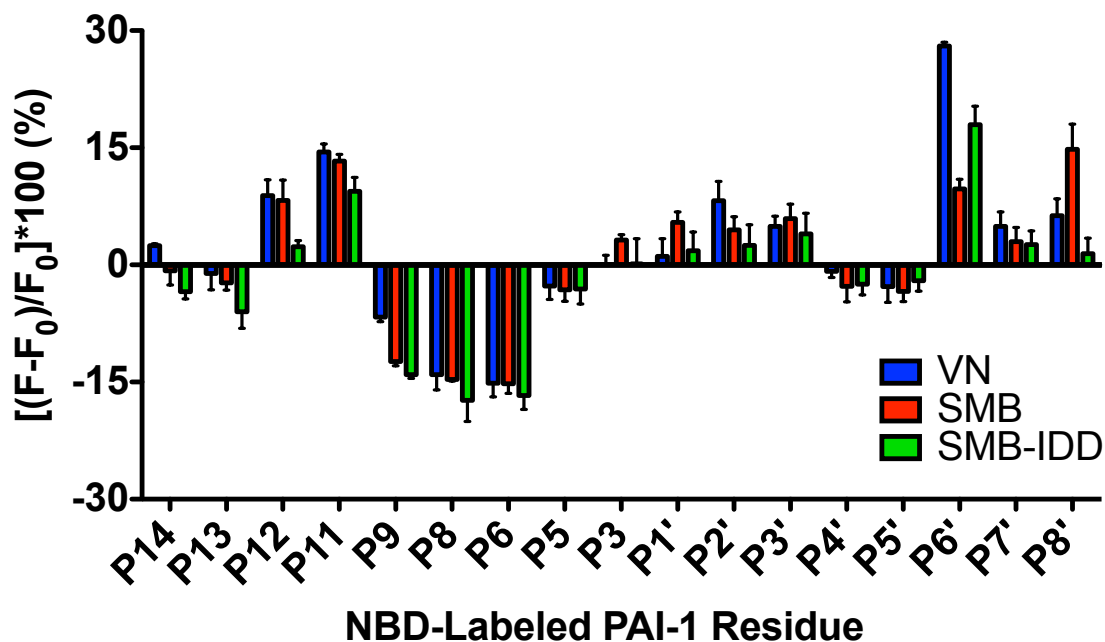


Figure 3.8 Effect of VN & its Truncations on the Solvent Accessibility of PAI-1 RCL. 2 μM VN, SMB and SMB-IDD were added to 0.5 μM NBD-PAI-1 in PBS (pH 7.4), and the fluorescence emission spectra collected at ambient temperature from 500-600 nm with excitation at 480 nm. The emission at 530 nm was taken and normalized to NBD-PAI-1 alone to reveal the percent change in NBD fluorescence at the RCL upon the addition of ligand. Increases and decreases indicate a change in the NBD environment from a more hydrophobic and hydrophilic environment, respectively. Residues are ordered from N- to C-terminus of the RCL and plotted with standard deviation error bars. All experiments were performed in triplicate.

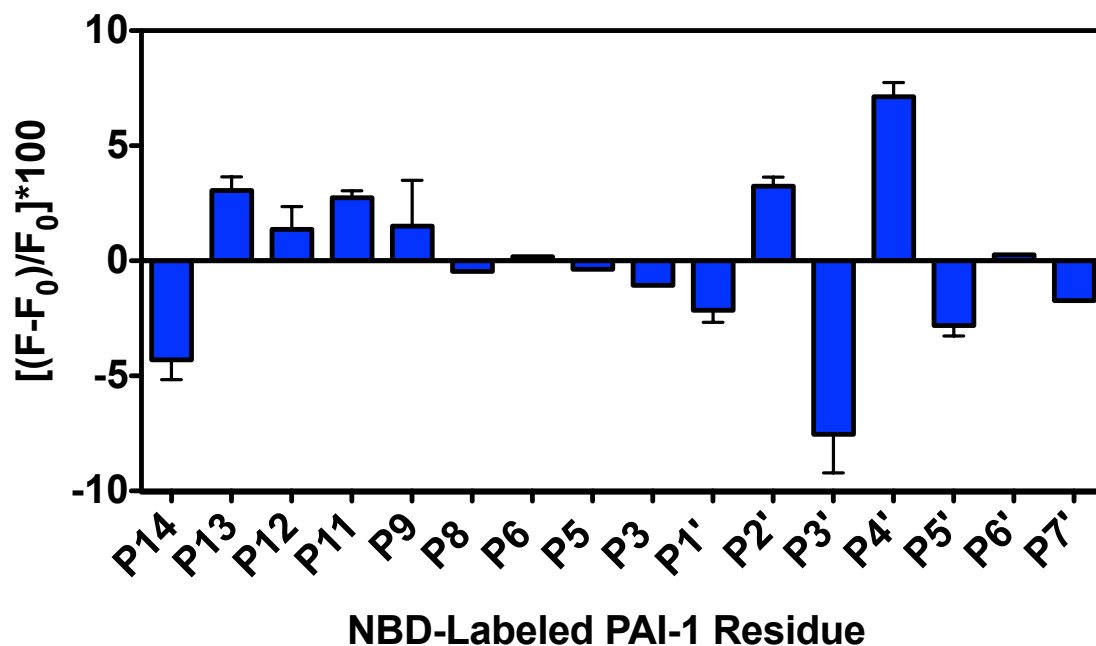


Figure 3.9 VN Binding to PAI-1 on The RCL Solvent Accessibility Is Influenced by Buffer Effects. 1.5 μM VN was added to 0.5 μM NBD-PAI-1 in MOPS (pH 7.4) and the fluorescence emission spectra collected at ambient temperature from 500-600 nm with excitation at 480 nm. The emission at 530 nm was taken and normalized to NBD-PAI-1 alone to reveal the percent change in NBD fluorescence at the RCL upon the addition of ligand (*blue, with standard deviation error bars*). Residues are ordered from N- to C-terminus of the RCL. Experiments were performed as single or duplicate experiments.

changes along the RCL in the presence of full length VN (**Fig. 3.9**). In contrast to results in PBS, the lowest changes are observed at P8-P5 and P6', while the larger changes are observed at P14 and P3'-P4'. A periodicity of two, which is characteristic of β -strand secondary structures, is also observed at P2'-P3' and s1C residues P4'-P7'. These results emphasize the effect of buffers on the solvent accessibility of the PAI-1 RCL.

3.3.b. The Dynamics of the RCL Are Unaffected By VN & Truncations

Resonance spectra of the RCL in the presence of VN and its truncations were collected by EPR to determine if the stabilization of PAI-1 involves changes in its motional dynamics (**Fig. 3.10**). Similar to MTSL-PAI-1 alone (c.f. Fig. 2.25), these spectra indicate that different positions along the RCL are distinct. For instance, the high-field peak at most positions has a sharp shoulder, of which the ratio of the heights differs, while this shoulder at P5' and P7' is smooth. However, an analysis of the line-width of the centerfield peak (**Fig. 3.11**) for MTSL-PAI-1 indicates no significant change in RCL mobility in the presence of these ligands.

As previously discussed (c.f. Ch. 2.3.e.), probe dimerization or loss of the MTSL-label can result in decreases in the resonance signal intensity, although an active-latent signal equilibrium is more likely. Nonetheless, MTSL-PAI-1 was tested for the presence of free sulfhydryls and the spin-label (**Fig. 3.12**). For the former, DTNB was added to MTSL-PAI-1 in the absence and presence of VN, SMB, and SMB-IDD and the absorbance at 412 nm collected (**Fig. 3.12 A**). DTT-free unlabeled P9 containing a single free sulfhydryl, as well as DTNB alone and DTNB in the presence of the ligands only, were used as controls. Based on the results of this assay, the MTSL-PAI-1 samples retrieved from EPR experiments do not possess free sulfhydryls. Also, though

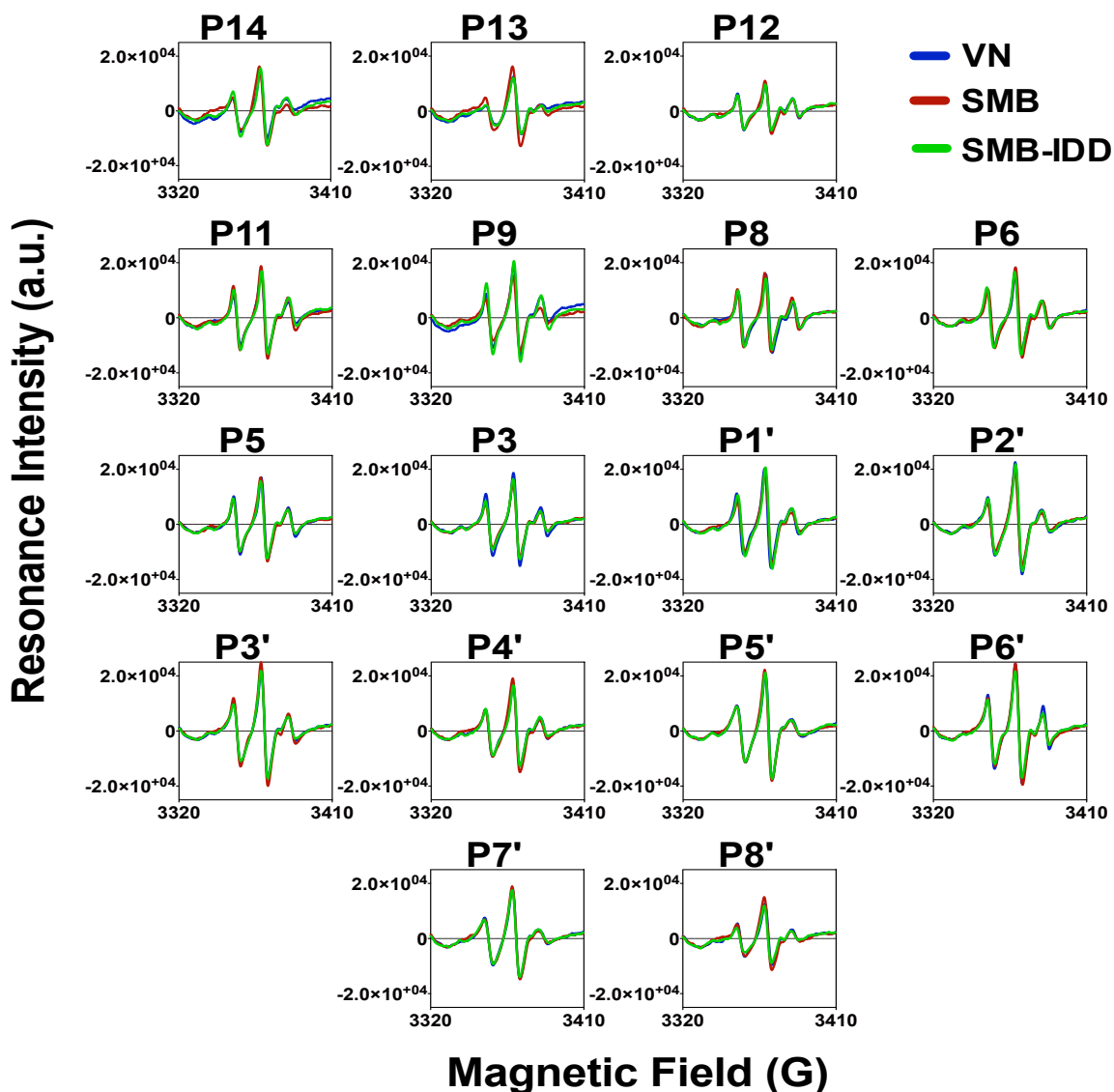


Figure 3.10 Binding of VN & its Truncations on The Dynamics at Different Positions in the RCL. 8 μ M VN, SMB, & SMB-IDD were added to 2 μ M MTSL-PAI-1 in PBS (pH 7.4) and EPR spectra were collected at ambient temperature by sweeping the magnetic field (3310-3410 gauss) at a constant frequency (\sim 9.45 GHz). Representative spectra of MTSL-PAI-1 alone (**black traces**), and in the presence of VN (**blue traces**), SMB (**red traces**), and SMD-IDD (**orange traces**) for each RCL position are shown.

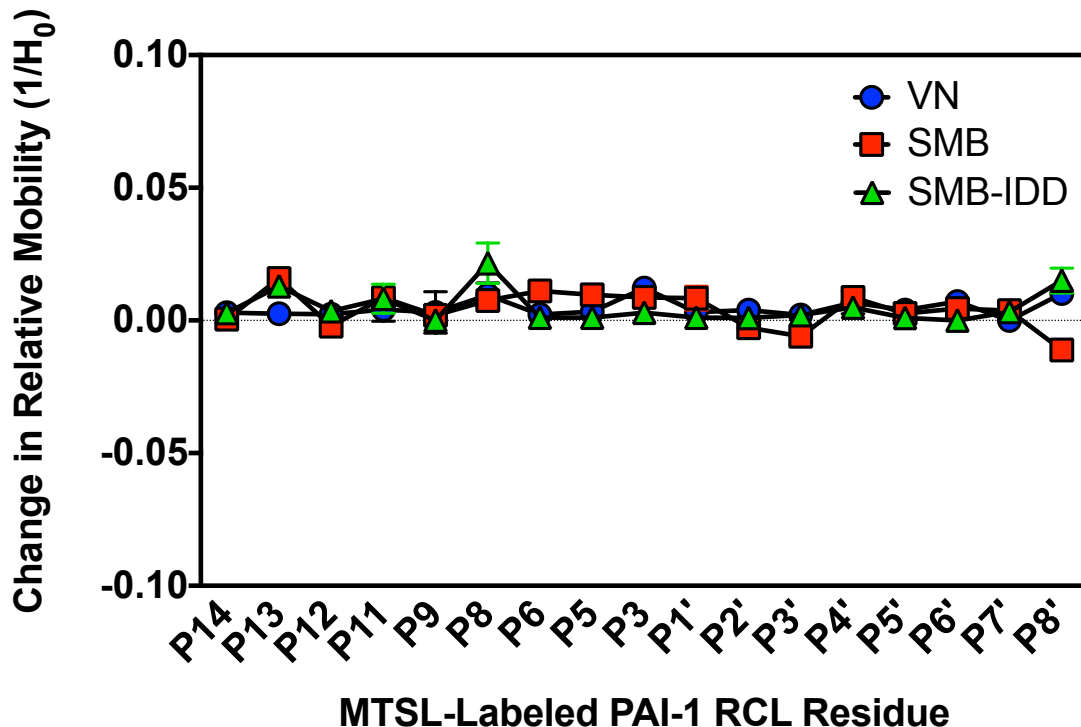


Figure 3.11 Change in RCL Dynamics Due to Binding of VN & its Truncations. 8 μM VN, SMB, & SMB-IDD were added to 2 μM MTSL-PAI-1 in PBS (pH 7.4) and the EPR spectra collected at ambient temperature. The inverse line-width from the resulting spectra was obtained, and the change in the relative mobility ($1/H_0$) determined by subtracting the average inverse line-width of MTSL-PAI-1 alone from the inverse line-width obtained in the presence of ligands. Residues are ordered from N- to C-terminus of the RCL. All experiments were performed in triplicate.

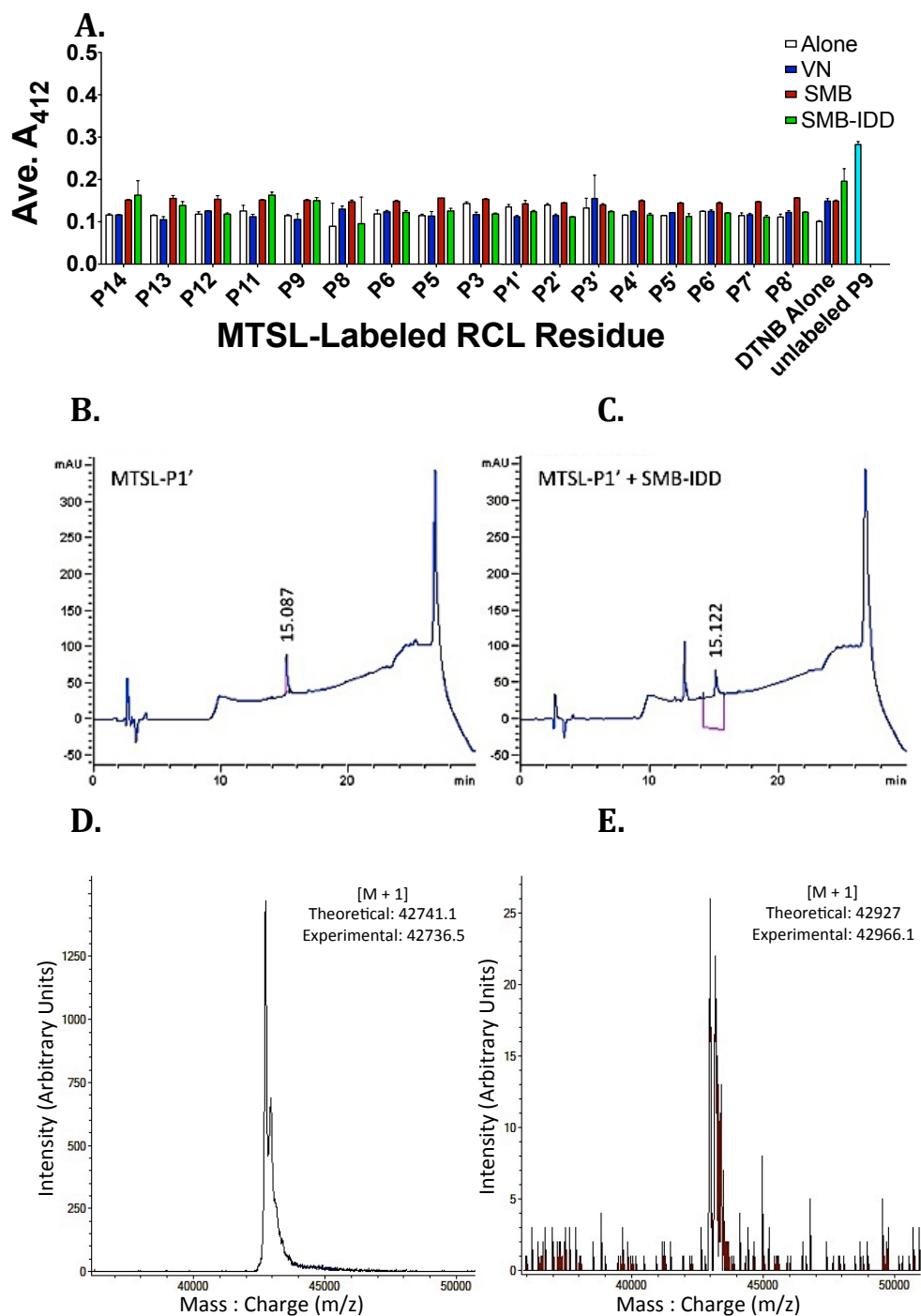


Figure 3.12 MTSL Probe Remains Conjugated to PAI-1 in The Presence of VN & Its Truncations. (A) DTNB was added to MTSL-PAI-1 in the absence and presence of ligands and the absorbance at 412 nm measured to detect the presence of free sulfhydryls. Results are from duplicate experiments. (B-C) Samples from EPR/DTNB experiments were HPLC-purified and analyzed by MALDI MS to confirm presence of MTSL-labeled PAI-1 (E) in comparison to unlabeled PAI-1 (D). Representative chromatograms and spectra are shown.

VN contains 8 cysteines in the SMB domain and 6 in central and C-terminal domain, these residues are disulfide-linked or buried between or within the domains [170, 171]. To determine if PAI-1 was still properly labeled after experimentation and not dimerized, the previous samples were purified by HPLC (**Fig. 3.12 B**) and analyzed by MALDI-MS (**Fig. 3.12 C**). In contrast to unlabeled PAI-1, a control that generates a single peak by HPLC, MTSL-PAI-1 in the presence of VN ligands exhibits two peaks corresponding to two distinct species. MTSL-PAI-1 was collected from the peak at a retention time of ~15 min for molecular mass determination. Despite its low recovery, analyses of the HPLC-purified PAI-1 confirmed the presence of the MTSL-label. These results indicate that the MTSL remains conjugated to the RCL and that the observed signal changes are not due to probe dimerization or loss of the MTSL label.

3.4. Discussion

3.4.a. How does VN binding affect the conformation of the RCL?

Binding of the SMB domain of VN to the flexible joint region stabilizes that active conformation of PAI-1 and slows the latency rate, while binding at the secondary low affinity site on hE may play a role in altering its specificity. Alone in solution, the RCL of PAI-1 is tethered close to the body of the protein. The results from fluorescence experiments (**Fig. 3.8**) show that VN binding to PAI-1 causes changes in the RCL conformation that permit partial insertion of the P14-P11 residues at the hinge, but disfavor full insertion by increasing the solvent exposure of the P9-P6 segment of the RCL. The unusually large pre-insertion of residues P14-P11, beyond which strand insertion is hypothesized to be irreversible, may be one factor contributing to the lability of PAI-1 compared to other serpin [58, 92]. Thereby, by hindering spontaneous RCL

insertion past this point, VN maintains PAI-1 in its active conformation and stabilizes it. Interestingly, the P9-P6 residues exposed upon VN binding do not show an initial decrease during the latency transition, possibly indicating that these are unique positions in regulating RCL insertion. Via conformational effects on these residues of the RCL, VN may also alter the specificity of PAI-1. Furthermore, the possible greater protection of N-terminal RCL residues with no change at the P1-P1' scissile bond observed in the HDX study of the SMB bound to PAI-1 [91] supports the results obtained here. Aside from the changes in its conformation, VN does not affect the dynamics of the RCL in its stabilization of PAI-1, as evidenced by the results obtained by EPR (**Fig. 3.11**). Therefore, effects on the local mobility of individual residues within the loop do not appear to be critical for stabilization of PAI-1

In a previous report [104], the NBD label conjugated to the P9 and P1' positions exhibited no change and a ~10% decrease in fluorescence, respectively, in the presence of full length VN in HEPES buffer [104]. At the same temperature and pH, the P9 and P1' positions exhibit a ~2.5% fluorescence increase and decrease, respectively, in the presence of full length VN in MOPS buffer (**Fig. 3.9**), and a ~7% decrease and ~1% increase (i.e. essentially no change), respectively, in PBS buffer (**Fig. 3.8**). These buffer differences, reminiscent of their unusual effects on PAI-1 stability (c.f. Fig. 2.19), thereby result in differences in the solvent accessibility, and thus conformation, of the RCL. Also, the aforementioned study measured a dissociation constant (K_d) of ~100 nM for full length VN binding to PAI-1, while the K_d measured here is 10 nM (c.f. Fig. 2.16). As affinity measurements are closer to the tight binding characteristic of their interaction and the buffer more physiologically relevant, the results in PBS would seem to more

closely reflect the changes that occur *in vivo* than the results in HEPES or MOPS. Despite these differences, in all three cases, VN affects the conformation of the RCL and increases its solvent exposure.

From the steady-state results (**Figs. 3.8 & 3.11**), the effects of the VN ligands on the RCL conformation and dynamics are comparable, but not the same. Particularly, the results obtained about the P14 hinge and s1C conformation by fluorescence differ notably. Since the SMB represents binding only at the primary high affinity site at the flexible joints region, and full length VN and SMB-IDD represents primary and/or secondary site binding, the unique effects on the RCL conformation reveal that primary and secondary site binding are distinct. However, since the magnitude and changes it produces at most positions of the RCL are similar to VN (**Fig. 3.8**), SMB binding to the flexible joint is primarily responsible for most of the conformational effects on the RCL. Also, full length VN and SMB elicit a more similar conformation on the RCL hinge than SMB-IDD, suggesting that the presence of the central and C-terminal domain affects the IDD interaction with PAI-1. The latter also indicates that the IDD has unique effects on PAI-1 RCL conformation, possibly due to binding at the secondary low affinity-binding site on PAI-1 hE. Binding to this site can explain the effect of VN on PAI-1 specificity by changes in the RCL conformation involving the hinge and gate regions, in addition to changes at the P9-P6 residues previously mentioned. Thereby, the alteration of PAI-1 specificity would require binding at the second site and conformation changes throughout the RCL. Another possibility is the adoption of structure by the disordered domain in the SMB-IDD, which is absent in the SMB truncation. However, since these

differences are small, an alternative hypothesis is that secondary-site binding by VN alters its specificity by affecting another important functional region in PAI-1.

3.5. Conclusions

As PAI-1 utilizes a conformation-based mechanism in its anti-proteolytic functions that may be affected at multiple levels, VN appropriately affects PAI-1 at many levels, including its stability and specificity. As it pertains to PAI-1 stability, evidence from multiple studies indicates that VN binding results in closure of the bottom of the shutter region and extension of the RCL. The results here support a model of VN-mediated stabilization of PAI-1 in which binding increases the solvent exposure of PAI-1 RCL near the hinge region to prevent its full insertion. Thereby, VN slows the latency transition of PAI-1. Furthermore, primary and secondary site binding by VN elicits separate effects on the conformation of the RCL, while the dynamics of the RCL remain largely unchanged. The conformational effects on the hinge, P9-P6 residues, and s1C gate residues likely play a role in altering the specificity of PAI-1. The evidence obtained from these studies also does not refute that IDD may house the secondary binding site on VN for PAI-1.

Chapter 4 PAI-1 Forms Distinct Michaelis Complexes with Plasminogen Activators

4.1. Introduction

4.1.a. Structural Basis of PA Function

In Chapter 1, the mechanism by which serine proteases catalyze the hydrolysis of peptide bonds by sequential acylation and deacylation is presented. This mechanism depends on the structure of the serine protease domain (SPD) responsible for catalysis. The SPD consists of two β -barrels rotated approximately 90° with respect to each other, and several surface-exposed activation and variable loops (**Fig. 4.1**) [172]. A catalytic triad, comprised of a serine nucleophile (Ser195; numbering based on canonical serine protease, chymotrypsin), a histidine base (His57), and an aspartate residue (Asp102) responsible for orienting the catalytic base, are situated at the interface between the two β -barrels. These domains are synthesized as an inactive precursor, or zymogen form, in which the active site is not properly organized for catalysis. Zymogen activation occurs by cleavage of the N-terminus, typically between residues 15-16, followed by insertion of the newly formed N-terminus into a cleft near the active site, forming a salt-bridge that changes the conformation of the SPD to one that is productive for catalysis, and correctly orienting the substrate-binding pockets (S) and oxyanion hole [173]. Several loops, collectively termed the activation loops, are involved in this conformational change, including the L_1 autolysis loop, the L_2 oxyanion hole-stabilizing loop, and the L_3 S_1 entrance-loop. The autolysis and S_1 entrance loops are also termed the 140- (or 147) loop and 217-loop, respectively (based on its location in primary sequence). The zymogen conformation can be readopted by the binding of monoclonal antibodies targeted to the autolysis loop in activated domains [174], shifting the paradigm of

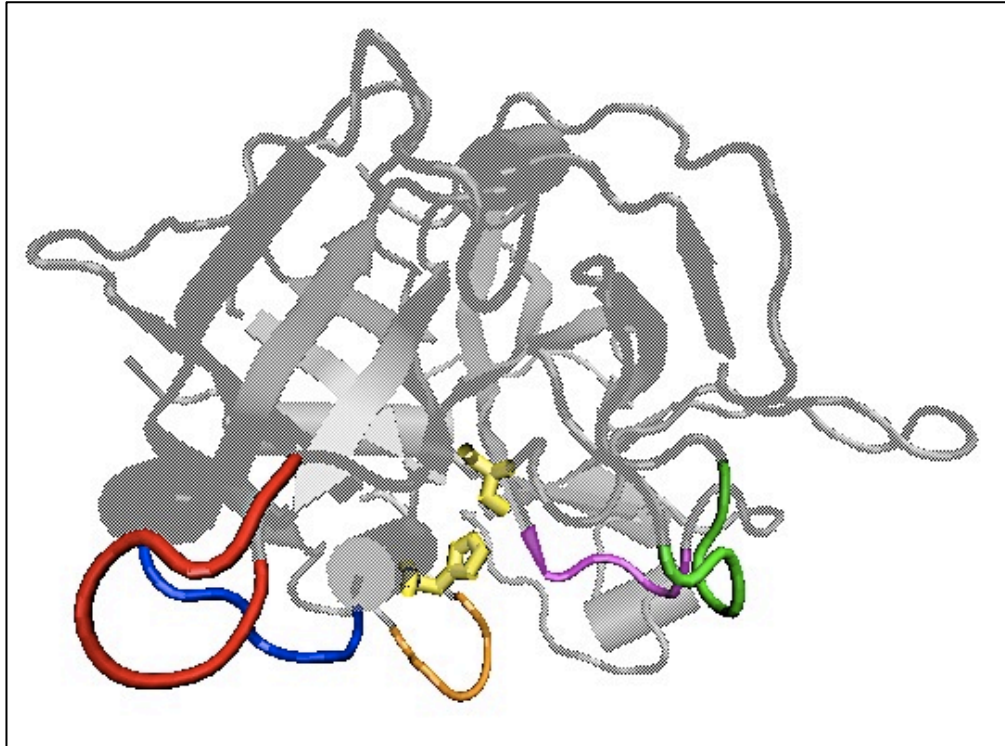


Figure 4.1 Serine Protease Domains Consist of Two β -Barrels & Several Surface-Exposed Loops. The SPD β -barrels are arranged approximately 90° with respect to each other, and the catalytic triad residues, Ser195, His57, and Asp102 (*yellow*), are at the interface (based on PDB 3PB1)[81]. At one pole, the surface-exposed 37-loop (*blue*), 60-loop (*red*), 97-loop (*orange*), 147-autolysis loop (*green*), and the 217-S₁-entrance loop (*magenta*) are clustered. Representations constructed using VMD 1.9.

zymogen activation from irreversible [175-178] to completely reversible. Re-zymogenation using these antibodies has been employed as a mechanism to specifically neutralize serine proteases, as these loops vary to a greater degree than the active sites.

Despite similarities in active site architecture, serine proteases exhibit a great degree of specificity for target substrates due to the presence of variable loops [3, 128], including the 30- (also 37-), 60-, 97-, and 186-loops. These loops frequently participate in exosite interactions outside the active site, which in addition to recognition, are responsible for rate enhancements [128]. For PAs, the variable 37-, 60-, and 97-loops, and the 147- and 217-activation loops, are clustered at one pole of the domain. With the assistance of these loops, the SPD of PAs function in the specific and fast activation of Plg to Pln.

Domains N-terminal to the SPD confer additional functions to PAs. tPA has four domains N-terminal to its SPD (**Fig. 4.2**), including the fibronectin-like finger domain, the epidermal growth factor domain (EGF), and the Kringle 1 and Kringle 2 domains [179]. The finger and Kringle 2 domains afford tPA fibrin-binding specificity, which has been exploited for the use of tPA as a clot-busting thrombolytic. The Kringle domains, formed by three intramolecular disulfide bonds, of tPA contain lysine-binding sites, which provide positively-charged 'knobs' for the negatively-charged 'holes' in soluble fibrin created when the its insoluble fibrinogen form is cleaved by thrombin. The EGF and Kringle 1 domains also are involved in the rapid clearance of tPA by the liver via a process that is facilitated by posttranslational glycosylations. tPA is synthesized as a 70 kDa single chain (sc-tPA) polypeptide, and disulfide-linked via Cys264 in a short linker

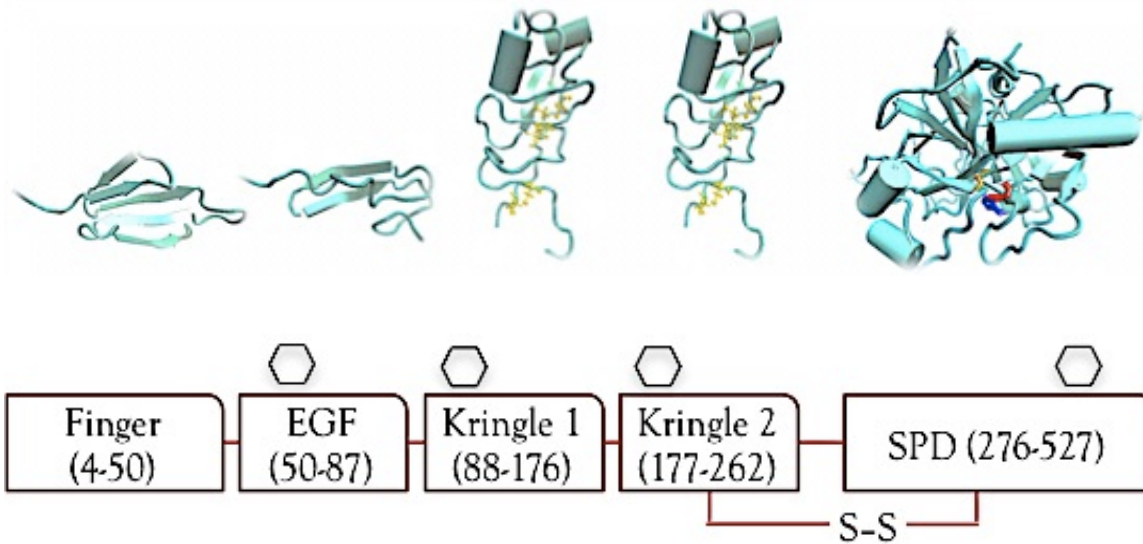


Figure 4.2 The Structure of tPA is Important for Binding Fibrin & Activating Plasminogen. The 70 kDa serine protease consists of five domains, which from N- to C-terminus, include the finger domain, (1TPM)[180], the EGF domain (1EDM)[181], two Kringle domains (1PK2)[182], and the SPD (1BDA)[183]. The domain organization is represented under the corresponding crystal structures. (1EDM is based on the domain from Factor IX, and tPA Kringle 1 on its Kringle 2 structure.) Residues in **yellow** are the cysteines involved in intramolecular disulfides contained in the Kringle domains. Catalytic triad residues, Ser195 (**orange**), His57 (**blue**), & Aspt102 (**red**), are contained in the SPD. Several domains contain glycosylation sites (*hexagons*). Structures were rendered using VMD 1.9.

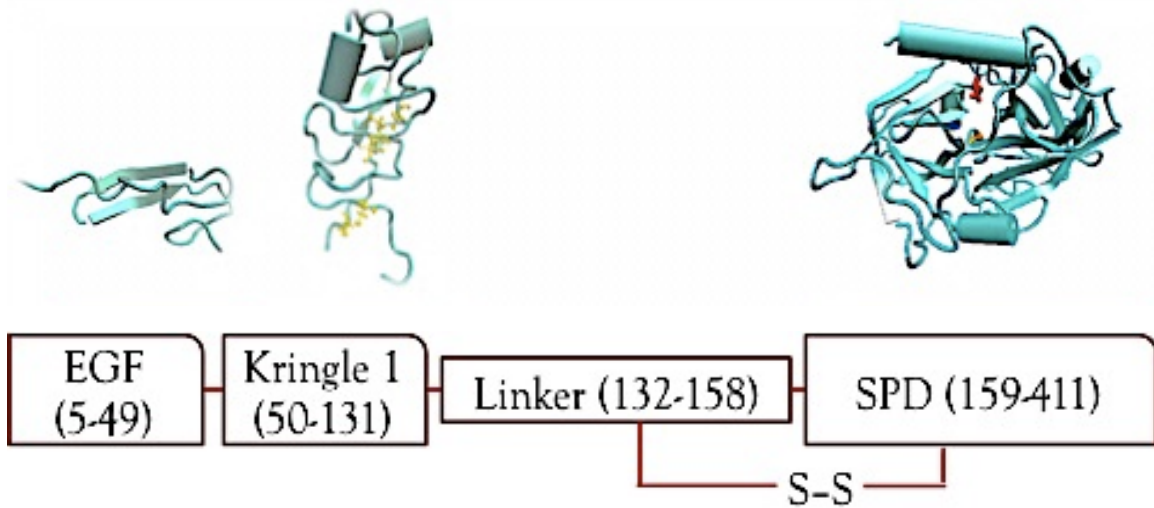


Figure 4.3 uPA Structure Supports Plasminogen Activation & Localized Pericellular Proteolysis. The 54 kDa high molecular weight (HMW) form of uPA consists of three domains arranged schematically from N- to C-terminus under corresponding crystal structures. The EGF (1EDM, based on Factor IX)[181] and Kringle 1 (1PK2, based on tPA Kringle 2)[182] domains are connected by a long linker to the SPD (3PB1)[81]. A 32 kDa lower molecular weight (LMW) form of uPA arises from cleavage of the linker region. Residues involved in disulfides in the Kringle domain are shown in **yellow**. Catalytic Ser195 (**orange**), His57 (**blue**), & Asp102 (**red**) are contained in the SPD. Structures were generated using VMD 1.9.

region and Cys395 in the SPD. In a feedback fashion, PIn processes and cleaves tPA between Arg275-Ile276 in the SPD to give rise to its two-chain form (tc-tPA). tPA is also activated via proteolysis by multiple contact factors (e.g. prekallikrein, kininogen, factor XIIa) [184].

Similarly, uPA, synthesized in a 54 kDa high molecular weight (HMW) form, consists of two domains N-terminal to its SPD (**Fig. 4.3**) [179]. The EFG and Kringle 1 domains of uPA are connected to the SPD by a long linker. Unlike tPA, the Kringle domain of uPA does not contain lysine-binding sites, and therefore, does not possess fibrin-specificity. Also, the EGF domain of uPA, instead of promoting its clearance, is involved in binding the deep hydrophobic pocket formed by the three extracellular finger domains of its cell-surface receptor, uPAR, which activates [185] and localizes uPA to the pericellular region where it participates in extracellular proteolysis. Positive-feedback cleavage by PIn within its long linker region gives rise to a 32 kDa lower molecular weight (LMW) form of uPA. The HMW form is predominantly found in the urine, whereas the LMW form predominates in tissues.

4.1.b. PAs as Proteases & Signaling Molecules

Although sharing the role of Plg activation, its functional domains, expression, and localization establish separate responsibilities for PAs. tPA is mainly expressed and secreted into circulation by endothelial cells lining blood vessels [42, 186], where it primarily activates Plg to PIn during intravascular fibrinolytic events (**Fig. 4.4**). Due to its fibrin-specificity [187], tPA can further assist PIn in fibrin removal. tPA is also abundantly expressed in neural tissue of the brain, where, with PAI-1, it regulates the neurotransmitter, glutamate, and its induction of circadian clock phase shifts [38]. In

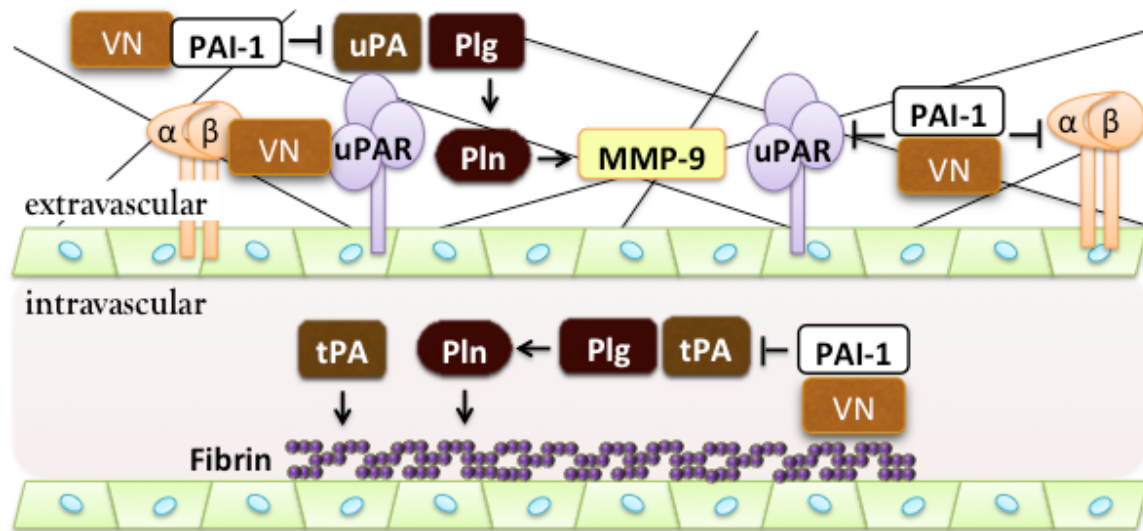


Figure 4.4 Proteolytic Functions of Plasminogen Activators. In intravascular settings, tPA is mainly responsible for plasminogen (Plg) activation, but also can assist plasmin (Pln) in clot dissolution. In the extravascular extracellular matrix (ECM), uPA interacts with its receptor, uPAR, to generate active Pln, which can then activate matrix metalloproteinases (MMP-9, MMP-2) to assist in localized pericellular proteolysis involved in tissue-remodeling. PAI-1 is localized to fibrin clots and the ECM by its VN cofactor to inhibit these PAs. PAI-1 also blocks the interaction of cell-surface receptors (uPAR, integrins) to VN.

contrast, uPA is chiefly expressed and secreted into the extracellular matrix (ECM) by stromal cells [13, 186], where it is localized by uPAR, normally expressed by white blood cells (i.e. monocytes, neutrophils eosinophils, and macrophages), to facilitate Plg activation. Active Pln can subsequently activate the Zn^{2+} -dependent matrix metalloproteinases (MMP-9, MMP-2), which function as collagenases and gelatinases, to assist in degradation of the surrounding ECM. Such pericellular proteolysis is required for tissue remodeling, an important step in normal wound healing [188]. When present, tPA activation of Plg in the ECM similarly results to MMP activation. In both intra- and extravascular locations, PAI-1 is localized by VN to inhibit these PAs. PAI-1 also blocks the interaction of uPAR and cell-surface integrin receptors with VN. Binding of these receptors to VN and other ECM components (collagen, gelatin, etc.) is necessary for the adhesion and migration of cells during tissue remodeling [189].

Due to these protease-dependent roles in fibrinolysis and extracellular proteolysis, PAs have been employed as thrombolytics, but their elevated expression has been implicated in many cancers, including uPA in lung [15], ovarian [17], breast [18], and prostate cancers [190, 191], and tPA in breast, prostate, [16, 192] and pancreatic cancer [193, 194]. Because Plg and subsequent MMP activation results in proteolysis that can provide a metastatic route for malignant cells to invade into the bloodstream, high PA levels serve as poor prognostic biomarkers in these cancers.

PAs also function in processes that do not require its catalytic properties. By interacting with cell-surface receptors, PAs initiate signal transduction pathways that affect its expression, as well as cell survival (**Fig. 4.5**). Binding of tPA to LRP-1 (low-density lipoprotein receptor-associated protein 1) [195], or of the pro-inflammatory

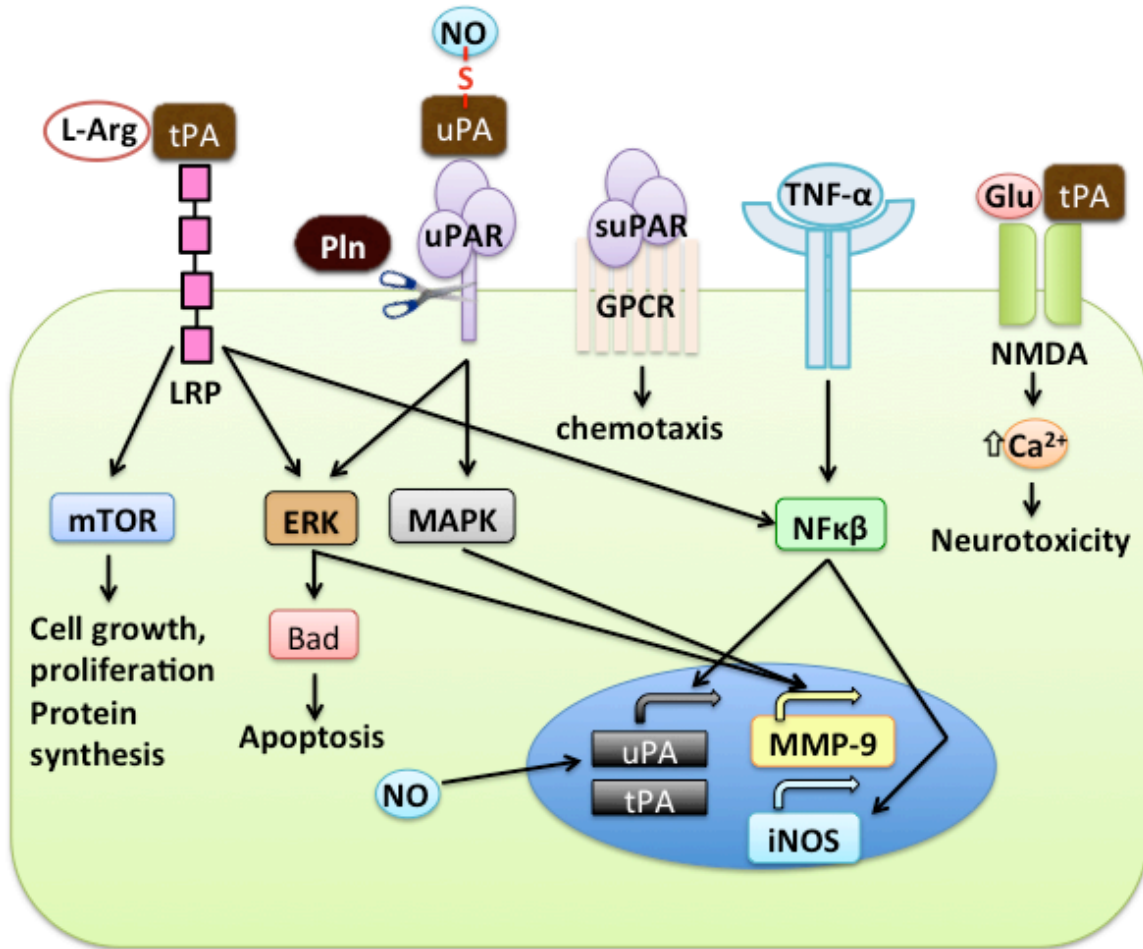


Figure 4.5 Plasminogen Activators as Signaling Molecules. tPA and uPA can interact with cell-surface receptors (LRP, uPAR, NMDA, etc.) and initiate different signal transduction pathways, including the mTOR, ERK, and MAPK signaling pathways, that affect its expression and cellular responses.

cytokine, TNF- α , to its receptor, signals via the transcription factor, NF- κ B (nuclear factor kappa-light-chain-enhancer of activated B cells), to increase PA and iNOS (nitric oxide synthase, inducible form) expression [196]. iNOS uses L-arginine (L-Arg) as a precursor for the synthesis of nitric oxide (NO). L-Arg and S-nitrosylation via NO stabilize tPA and uPA, respectively [197, 198]. NO also increases the expression of the latter.

Both the stabilized and unmodified forms of uPA bind to uPAR, which activates ERK/MAPK (extracellular-signaling regulated kinase/mitogen-activated protein kinase) signaling pathways, including the Ras (GTPase)-ERK and p38-MAPK pathways. These signals result in the increased expression of MMP-9 [199]. In addition to this uPA-uPAR signaling, suPAR signals via the formyl peptide receptor-like G-protein coupled receptor (GPCR) to effect cell movement (chemotaxis) [200]. suPAR is the soluble form of uPAR consisting of its three extracellular finger domains, and arises from cleavage of its GPI (glycosylphosphatidylinositol) -anchor by Pin.

PA signaling moreover effects brain chemistry. As previously mentioned, tPA is expressed in neuronal tissues, where it can bind the glutamate receptor, NMDA (*N*-methyl-D-aspartate) [201]. Increased exogenous tPA, as when injected as a thrombolytic in the treatment of ischemic stroke to relieve O₂ depletion due to vessel blockages, leads to increases in intracellular calcium, an important second-messenger, and can result in neurotoxicity [202-206]. LRP-NF- κ B-mediated increase in NO also contributes to this neurotoxicity. Additionally, tPA-LRP-1 signals via mTOR, a serine/threonine kinase of the PI3K (phosphoinositide-3-kinase) family and mammalian target for rapamycin (a bacterial macrolide used as an immunosuppressant to prevent

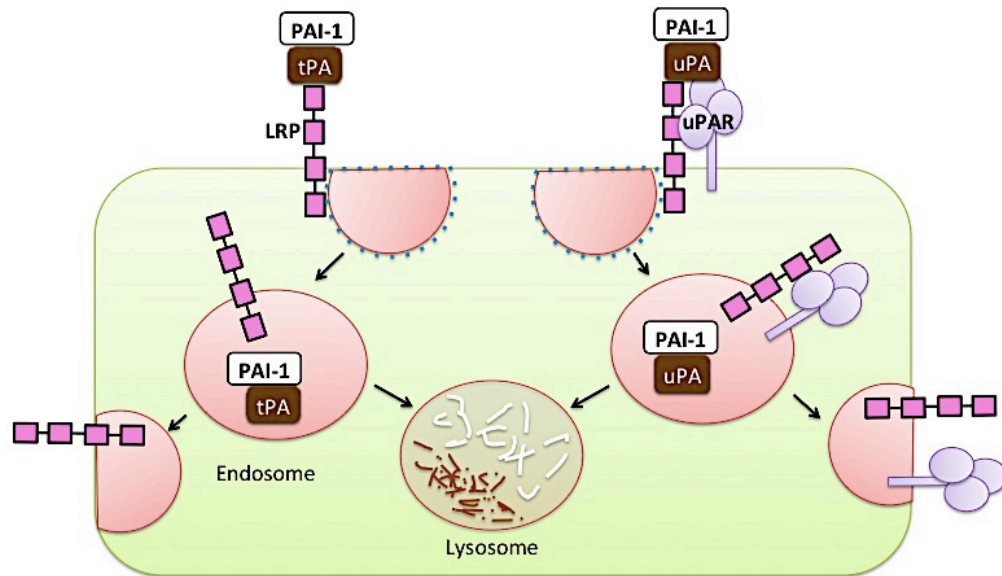


Figure 4.6 Receptor-Mediated Endocytosis in the Clearance of PAI-1 & Plasminogen Activators. LRP-1 binds PAI-1, PAs, and its complexes, which results in endocytosis, followed by degradation inside lysosomes or recycling to the cell surface.

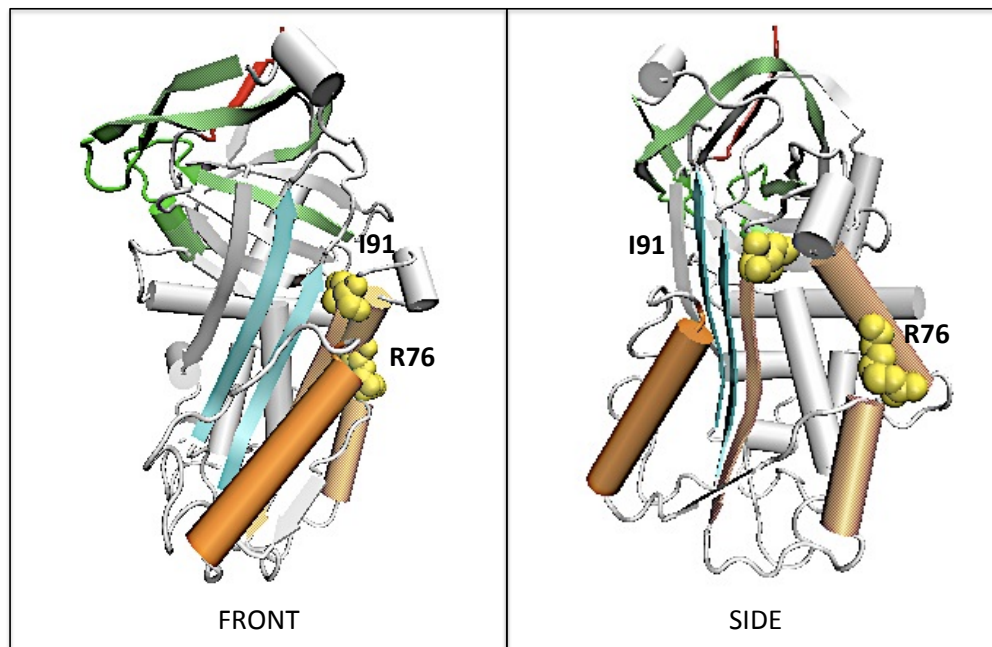


Figure 4.7 LRP-1 Binds to A Cryptic Site on PAI-1. Residues involved in LRP-1 binding are represented as yellow space-filled spheres. The RCL (red), gate (green), shutter (cyan), and flexible joint region (orange) of metastable PAI-1 (3Q02)[59] are also highlighted. Figure generated using VMD 1.9.

organ transplant rejection) to affect cell growth, proliferation, motility, survival, and protein synthesis [207], while its signaling via the ERK/Bad (B-cell lymphoma-2-associated death promoter) pathway culminates in apoptosis of the cell [195].

4.1.c. Regulation & Clearance of PAs

PAs in proteolysis and signaling are mainly regulated by PAI-1, as previously described, and by elimination from circulation. PAs have a circulating half-life of ~6-12 minutes before clearance by the liver [179, 184], and must act on their targets within this timeframe. Also, PAs form complexes with PAI-1 that are stable for years [4], and therefore are cleared locally by receptor-mediated endocytosis via LRP-1 [208] (**Fig. 4.6**). During this process, LRP-1 binds tPA, uPA, PAI-1, and its complexes, prompting endocytosis into clatherin-coated pits, which subsequently fuse with the early endosome. Clatherin dissociates from this vesicle, and ligands dissociate from their receptors. The receptors are then recycled to the cell surface, while the endosome containing the ligands fuses with lysosomes containing hydrolytic enzymes, which degrade the proteins into individual amino acids. Though PA binding to LRP-1 can also initiate signaling pathways, free proteases and free PAI-1 have low affinity for the receptor [4]. Particularly, the low affinity of LRP-1 for PAI-1 is due to its cryptic binding site on the uncomplexed or VN-bound serpin (**Fig. 4.7**). This site is exposed upon cleavage and final complex formation (e.g. with PAs, thrombin), increasing the affinity of and clearance by LRP for the latter [4].

4.1.d. Objective of PAI-1 PA Study

From an understanding of its structure to clearance, a major aim of this work is to determine the structural basis for the differences in PA inhibition by PAI-1 according to

the rationale provided in Ch. 1.2. Specifically, the involvement of exosite interactions in the higher affinity and faster k_{off} of PAI-1 with tc-tPA and uPA, respectively, resulting in the faster inhibition of the former, is investigated here by fluorescence and EPR using the RCL-labeled mutants. Thereby, the contribution of exosite interactions in rate enhancements and specificity can be evaluated.

4.2. Methods & Materials

4.2.a. Materials

Active site-blocked (i.e. S195A) tPA (tPA-SPD*; single-chain, non-enzymatic) was purchased from Molecular Innovations, Inc. (Novi, MI). Active site-blocked uPA (uPA-SPD*) was a kind gift from Mingdong Huang (Fujian Institute of Research on the Structure of Matter, Chinese Academy of Sciences, China).

4.2.b. Equilibrium Binding of PAs by Steady-State Fluorescence

NBD-labeled PAI-1 was dialyzed in 4 L buffer (PBS, pH 7.4) at 4°C and added at a final concentration of 0.5 μM in 60 μl after the addition of 0.5 μM ligand. Reactions were incubated at 25°C for 30 min, 50 μl of the sample was added to a 0.3 cm three-window black-sided quartz cuvette, and placed in a Perkin Elmer LS 50B Luminescence spectrometer at ambient temperature. Spectra were collected and analyzed as previously described (c.f. Ch. 3.2.c).

4.2.c. Effect of PA Binding on PAI-1 RCL Mobility via EPR

EPR spectra were collected as previously described (c.f. Ch. 2.2.q.), with the exception that dialyzed MTSL-labeled PAI-1 in PBS buffer (pH 7.4) was diluted to a final concentration of 2 μM after the addition of 2 μM (due to limited quantity of reagent available) and 8 μM tPA-SPD* and uPA-SPD*, respectively, and incubated at room

temperature for 30 min to equilibrate prior to analysis. The change in the mobility (ΔH_0^{-1}) as previously described (c.f. Ch. 3.2.d). All experiments were performed in triplicate. EPR samples were retrieved, and free sulfhydryls were detected and labeling integrity MTSL-PAI-1 assessed as previously described (c.f. Ch. 3.2.e).

4.2.d. Modeling of PAI-1-tPA Michaelis Complex

The structures of the single-chain tPA serine protease domain (1BDA) and metastable PAI-1 with a homology-modeled RCL (HM1-3; c.f. Fig. 2.6) were individually aligned and superimposed on the ATIII-thrombin Michaelis complex (1TB6) using MOE2012. From the resulting superimposed complexes, tPA was docked to each of the RCL-modeled PAI-1 structures using the automated ZDOCK server [209] according to the lock-and-key model with only a contact between S195 (catalytic) of tPA and Arg346-Met347 (P1-P1') of PAI-1 specified. The top five predictions from the automated docking were obtained and the lowest energy complex with tPA for each RCL-modeled PAI-1 structure chosen for further refinement. Using the CHARMM27 force field in MOE2012, the distances between the carbonyl carbon of PAI-1 Arg346 (P1 Arg C=O) to the hydroxyl oxygen of tPA S195 (S195-OH), and the carbonyl carbon of PAI-1 E351 (P5' Glu) to the guanidino-nitrogen of Arg36 in the tPA 37-loop (37 ArgA), were restrained to a target distance of 3-4 Å, and minimized with weight of 5 kcal mol⁻¹ (Å²)⁻¹. Potential energies of the resulting restrained docked Michaelis complexes were calculated, and contacts between chains reported as previously described (c.f. Ch. 2.2.c.). The model of PAI-tPA complex was then superimposed on the 14-1B-active site-blocked uPA crystal structure (3PB1) and root-mean-squared deviation obtained.

4.3. Results

4.3.a. Active Site-Blocked PAs Utilize Different PAI-1 Exosites in the Michaelis Complex

The NBD-labeled PAI-1 RCL mutants were used to investigate the interactions of PAI-1 and PAs in the Michaelis complex. As the PAs bind PAI-1 at the RCL, increases in NBD fluorescence can provide information about the burial of hydrophobic surfaces that occur due to binding. Equimolar tPA-SPD* and uPA-SPD* were added to NBD-labeled PAI-1, and the consequent changes in fluorescence recorded (**Fig. 4.8 A-B**). The resulting fluorescence changes at the RCL are large for the PAs bound to PAI-1. For residues immediately adjacent to the scissile bond, a decrease in fluorescence is observed at P1'-P2' in the presence of both PAs. A previous report showed that the NBD label at the P1', but not P9, position reduced the affinity of tPA for PAI-1 [117], indicating that the probe at the active site, which requires tight binding, but not at adjacent exosites, which are released upon final complex formation, interferes with PA binding. The decrease at P1'-P2' is thereby consistent with the expulsion of the probe from the active site, leading to its greater solvent exposure. Furthermore, the P4'-P5' positions exhibit a 25% and 1% decrease in fluorescence in the presence of tPA-SPD*. In the presence of uPA-SPD*, a 23% and 110% fluorescence increase is observed. Assuming an interaction with the 37-loop of the PAs, the increase, and thus more hydrophilic nature, would indicate that hydrogen and/or ionic bonding is more important for the interaction of PAI-1 with tPA-SPD*, but not for the PAI-1-uPA-SPD* interaction due to the greater hydrophobic environment of these residues in the presence of the uPA-SPD*. However, such hydrogen and/or ionic interactions can only be implied with respect to the adjacent Glu residue for these positions (i.e. Glu at P5' is present in the

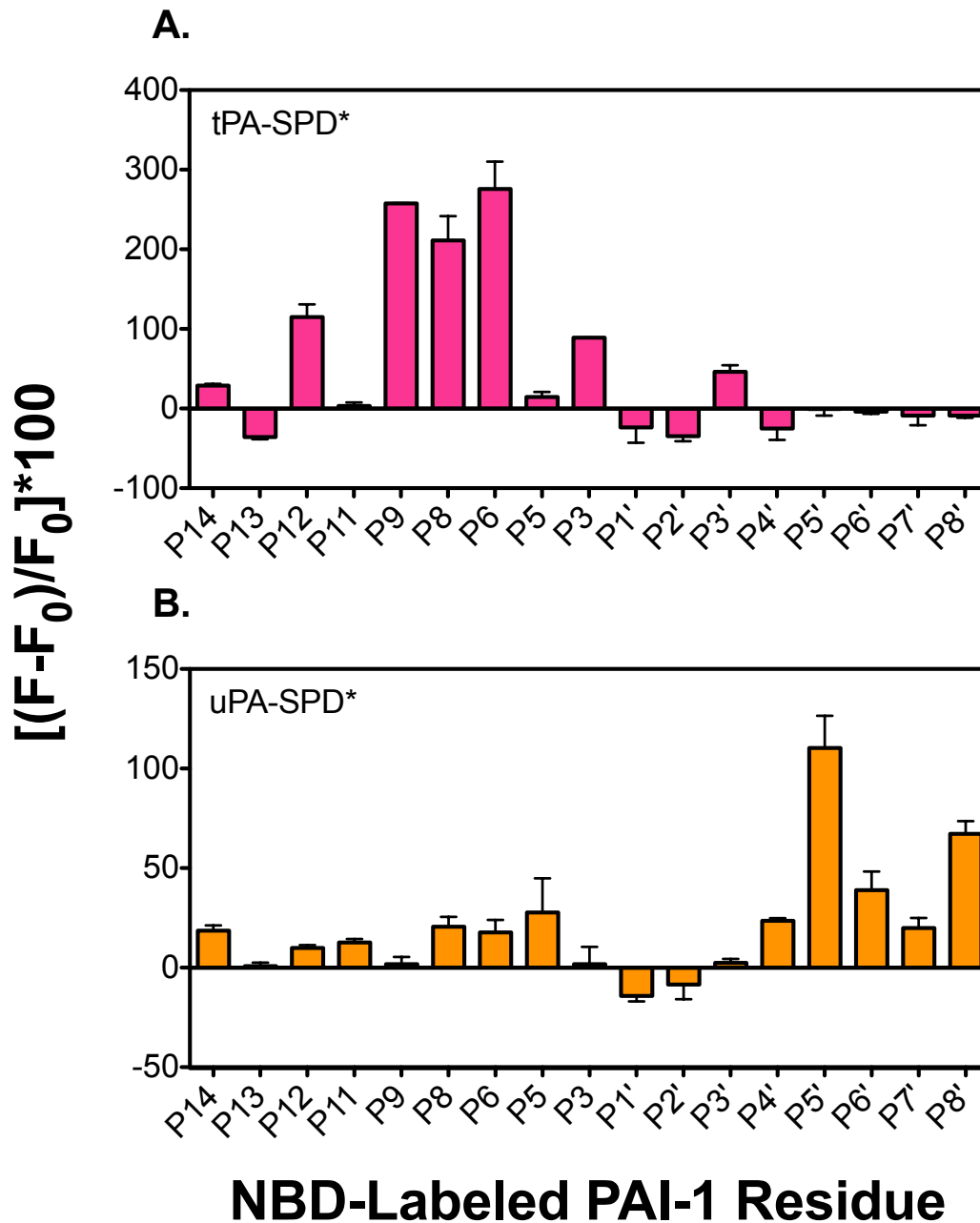


Figure 4.8 PA Binding of PAI-1 RCL in Michaelis Complex. 0.5 μ M NBD-PAI-1 was added to 0.5 μ M tPA-SPD* or uPA-SPD* in PBS, pH 7.4, and its emission at 530 nm collected after excitation at 480 nm. Results are normalized to NBD-PAI-1 alone to obtain the percent change in fluorescence at the RCL upon ligand binding. Residues are ordered N-terminal to C-terminal in the RCL according to its P designation relative to the P1-P1' scissile bond. All experiments were performed in triplicate.

single-cysteine mutant labeled at P4', and vice versa). Most notably, the overall change in fluorescence is greater at the N- and C-terminal RCL for tPA-SPD* and uPA-SPD*, respectively, with the greatest difference between the exosites occurring at positions P9-P6 (~211-275% increase) for tPA-SPD* and P4'-P8' (~19-110% increase) for uPA-SPD*. These results indicate that both PAs rest differently on the serpin top by utilizing distinct exosites in the Michaelis complex.

4.3.b. RCL Dynamics in the Michaelis Complex are Affected by uPA Binding

In addition to fluorescence, the dynamics of the RCL of PAI-1 complexed to PAs were investigated by EPR. Active site-blocked PAs were added to MTSL-labeled PAI-1 and the resonance spectra collected (**Fig. 4.9**). The change in the inverse line-width, or relative mobility (ΔH_0^{-1}), due PA binding is plotted with respect to RCL position (**Fig. 4.10**). The individual spectra indicate that the mobility of the RCL in the absence and presence of the PAs is unique. The inverse line-widths reveal that the relative mobility of the RCL is largely unchanged due to the binding of tPA-SPD*. In contrast, the mobility of the RCL in the presence of uPA-SPD* is considerably restricted, specifically at the N-terminal P14 and P11-P5 positions. In comparison, the average temperature (*B*) factor at this region in the 14-1B PAI-1-uPA-SPD* Michaelis crystal structure [81], which represents the highest populated conformer, indicates these residues are quite mobile, but this difference is likely due to differences between solution and crystal structures. Another factor that may account for the observed results is the difference between the 14-1B compared to metastable structure of PAI-1. Also, a previous report showed that the orientational freedom of a probe conjugated to the P3 position was decreased with respect to the P1' position in the presence of the PAs [100]. The restricted mobility at P3

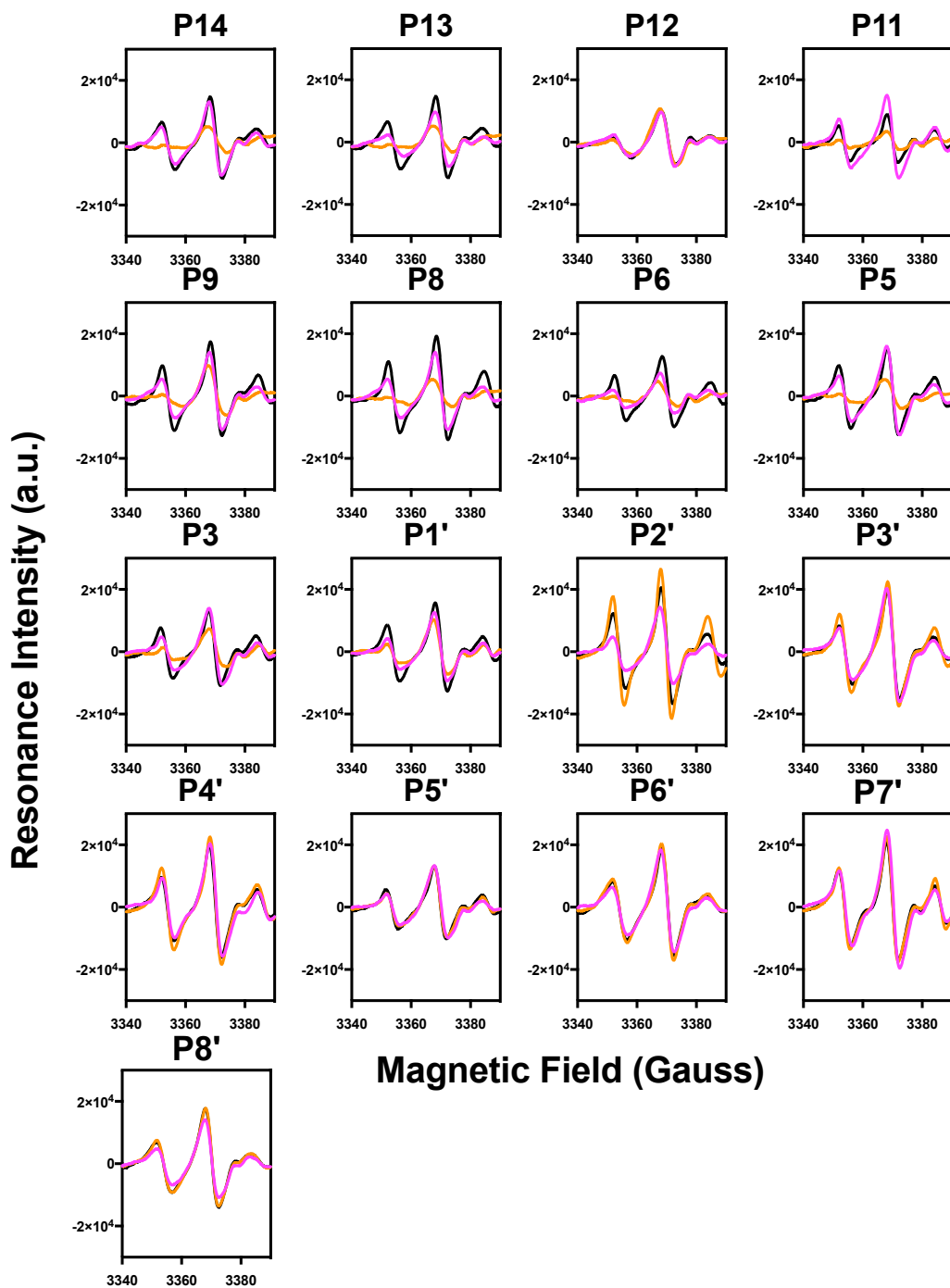


Figure 4.9 Binding of Plasminogen Activators Affects the Dynamics at Different Positions in the RCL. tPA-SPD* and uPA-SPD* were added at 2 μ M and 8 μ M, respectively, to 2 μ M MTSL-PAI-1 in PBS buffer, pH 7.4. EPR spectra were collected at ambient temperature by sweeping the magnetic field (3310-3410 gauss) at a constant frequency (~ 9.45 GHz). Representative spectra of MTSL-PAI-1 alone (**black traces**) and in the presence of tPA-SPD* (**magenta traces**) and uPA-SPD* (**orange traces**) for each RCL position are shown.

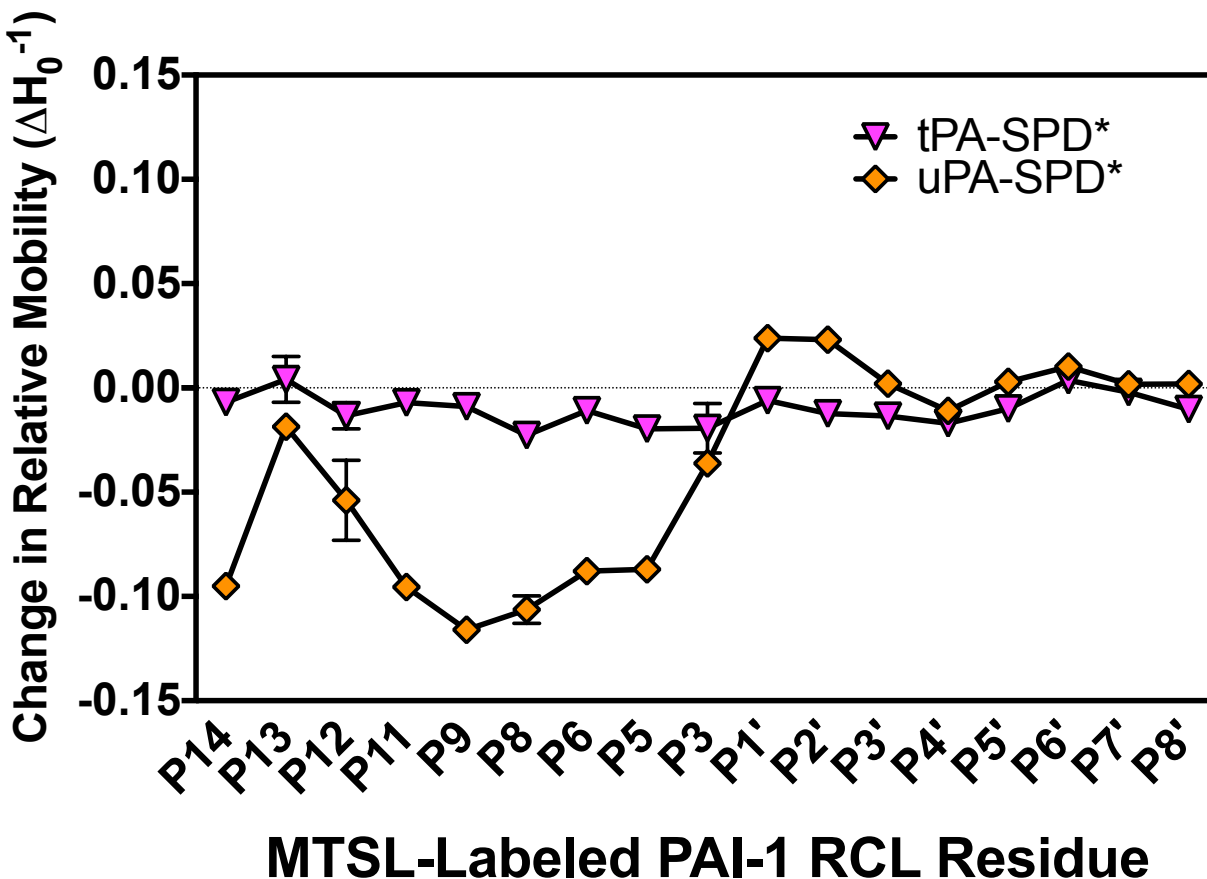


Figure 4.10 Changes in Mobility of the RCL upon Michaelis Complex Formation. 2 μM tPA-SPD* and 8 μM uPA-SPD* was added to 2 μM MTSL-PAI-1 in PBS buffer, pH 7.4 and the EPR spectra collected. The inverse line-width from the resulting spectra was obtained and the change in the relative mobility ($1/H_0$) determined by subtracting the average inverse line-width of MTSL-PAI-1 alone from the inverse line-width obtained in the presence of ligands. Residues are ordered N-terminal to C-terminal in the RCL according to its P designation relative to the P1-P1' scissile bond. All experiments were performed in triplicate.

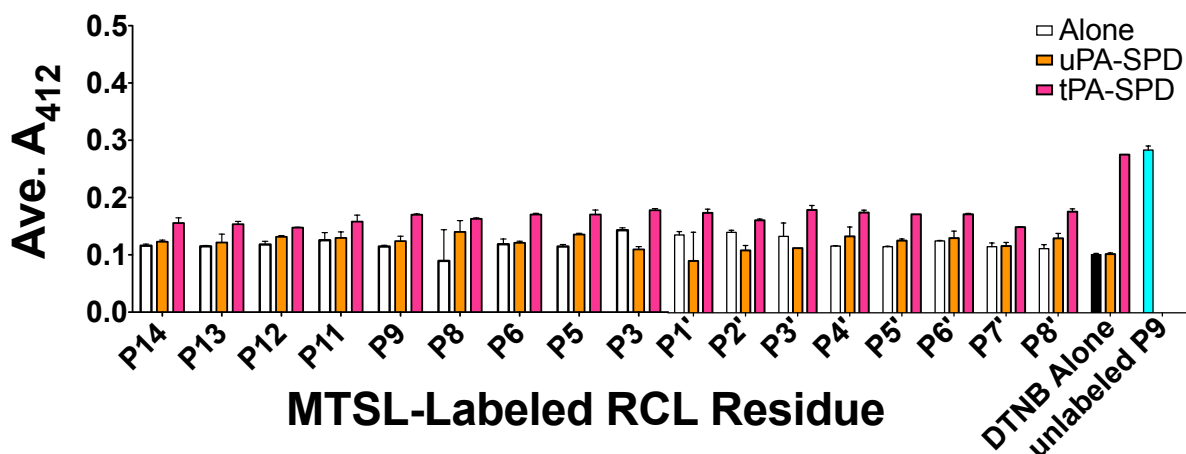


Figure 4.11 MTSL Probe Remains Conjugated to PAI-1 in The Presence of Active Site-Blocked Plasminogen Activators. 1 mM DTNB was added to 2 μ M MTSL-PAI-1 (*white bars*) in the absence and presence of active site-blocked PAs (*as indicated*) and the absorbance at 412 nm recorded. The black bar represents DTNB in the absence of MTSL-PAI-1 and ligands (c.f. Fig. 3.12A).

compared to the P1' position in the presence of both active site-blocked PAs detected by EPR is consistent with the latter study.

As previously explained for MTSL-PAI-1, (c.f. Ch. 2.3.e.), the intensity of the MTSL resonance signal is proportional to the concentration of EPR active species. Though the increases in intensity observed at some RCL positions (e.g. P11 in the presence of tPA-SPD* and P2' in the presence of uPA-SPD*) (**Fig. 4.9**) are unlikely due to an increase in paramagnetic concentration, the decreases in intensities observed (e.g. at P14, P13, etc.) may indicate a loss of the latter. To test this, DTNB was added to MTSL-PAI-1 in the absence and presence of PAs (**Fig. 4.11**) to detect for the presence of free sulfhydryls, which would occur if MTSL was removed and/or dimerized. The resulting low absorbance at 412 nm for MTSL-PAI-1 in complex with PAs, similar to

DNTB alone (*black bar*), indicates the lack of free sulfhydryls. In contrast, the higher absorbance of tPA-SPD* in the absence of MTSL-PAI-1 and unlabeled P9 indicates the presence of a free cysteine, which is expected for the latter. These results also indicate that a free cysteine in tPA-SPD* becomes inaccessible upon complex formation with PAI-1.

4.3.c. Model of PAI-1-tPA Michaelis Complex

The steady-state fluorescence and EPR data presented here reveal clear differences in the Michaelis complex of PAI-1 with tPA-SPD* and uPA-SPD*, with the former and latter resting at the proximal and distal regions of the RCL, respectively. This difference is similar to that of ATIII in the Michaelis complex with thrombin and fXa [3]. Since a structure of its complex with PAI-1 is currently unavailable, a model of the PAI-1-tPA Michaelis complex was constructed based on the latter complex by molecular superimposition and protein-protein docking. Homology modeling of the RCL was required prior to docking in order to use the metastable PAI-1 structure [59], in which the RCL is unresolved, for the Michaelis model. Three low energy RCL-modeled PAI-1 structures resulted (HM1-3) (c.f. Fig. 2.6), to which the serine protease domain of tPA was docked as described under Methods (4.2.d.). After docking, the distances between the scissile bond to the catalytic serine, and P5' to the 37-loop of tPA, were restrained based on distances in the PAI-1-uPA Michaelis crystal structure and biochemical evidence showing a stronger P4'P5'-37-loop interaction for PAI-1 and tPA. Restraining distances as such reveals the path of least resistance to the target distance (3-4 Å), which is in contrast to constraining distances, where the target distance is reached regardless of steric or thermodynamic considerations. The potential energy of the

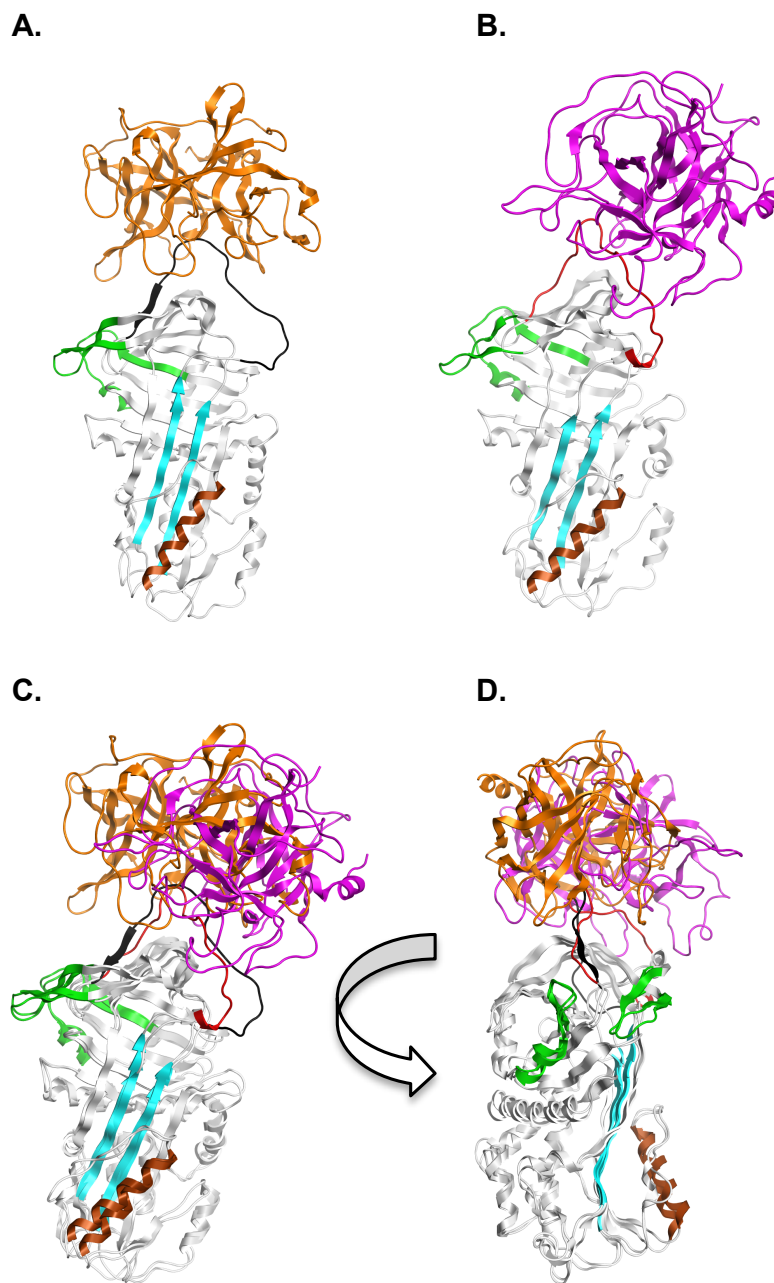


Figure 4.12 Michaelis Complex of PAI-1 with PAs. The (A) crystal structure (3PB1)[81] of the 14-1B variant of PAI-1 (*black RCL*) in the Michaelis complex with the active site-blocked serine protease domain of uPA (*orange*) is shown next to the (B) docked and restrained model of the tPA serine protease domain (1BDA)[183] (*magenta*) in the Michaelis complex with the metastable PAI-1 (3Q02)[59] containing a homology-modeled RCL (*red RCL*). The structures were superimposed about the C_{α} and shown from “front” (C) and “side” (D) views. Secondary structural elements involved in conformational changes of PAI-1, including the gate (*green*), shutter (*cyan*), and helix F (*brown*) of the flexible joint region are highlighted. Rendering created using MOE2012.

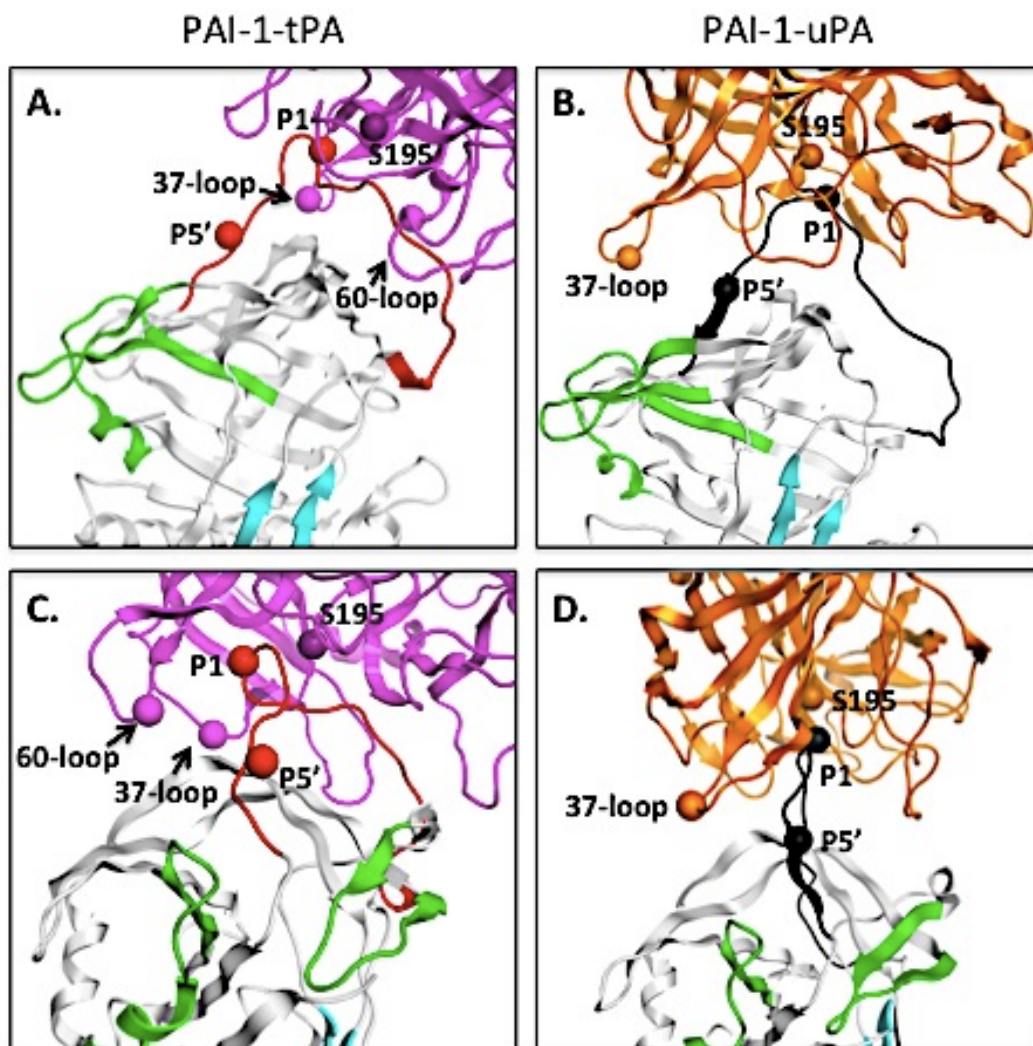


Figure 4.13 Close-up of PAI-1-PA Michaelis Complex Interface. Metastable (*red RCL*) and 14-1B (*black RCL*) PAI-1, in complex with tPA (*magenta*) and uPA (*orange*), respectively, is shown in white with the gate (*green*) and shutter (*cyan*) regions highlighted. Panels A-B show the complexes from the “front.” Panels C-D are “side” views of the binding interface. The C α atom of residues P1 in the RCL, P5' in s1C, Arg-A in the 37-loop of the PAs, and Glu-A of the tPA 60-loop are shown in the space filling rendering and colored according to their participating chain (MOE2012).

Table 4.1 Potential Energy & Root-Mean-Squared Deviation of Docked & Restrained PAI-1-tPA Michaelis Complex Models

Protein 1	Protein 2	Distances (Å)		Distance Restrained (Å)		Potential Energy (kcal/mol)	RMSD (Å)*		# Interface Contacts
		P1-Arg & S195-OH	P5' Glu & 37 ArgA	P1-Arg - S195-OH	P5' Glu - 37 ArgA		PAI-1	tPA	
HM1	tPA	4.02	4.02	11.5	17.15	-3835.61	1.089	1.505	17
HM2	tPA	3.06	3.96	13.08	17.59	-3525.52	1.18	1.551	12
HM3	tPA	3.36	4.02	11.09	17.79	-1628.79	1.501	1.8	16
14-1B	uPA	3.09	9.51	n/a	n/a	-3079.4	n/a	n/a	15

*From C α superimposition of unrestrained structures
n/a not applicable

resulting docked and restrained PAI-1-tPA models were calculated (**Table 4.1**), and the lowest energy model shown superimposed on the 14-1B PAI-1-uPA-SPD* crystal structure (**Fig. 4.12 - 4.13 A-D**), highlighting the different positions occupied by the PAs in the Michaelis complex with PAI-1. The root-mean-squared deviation (RMSD) (**Table 4.1**) of the docked & restrained PAI-1-tPA Michaelis models compared to their unrestrained docked structures is small (<2Å), indicating minimum perturbation of the structures due to the applied distance restraints. Also, two of the three PAI-1-tPA Michaelis models contain more interchain contacts than that of the 14-1B PAI-1-uPA-SPD* Michaelis structure (**Table 4.2**). Interestingly, tPA in the Michaelis model with PAI-1 also possess more contacts with N-terminal RCL residues than does uPA in complex with 14-1B PAI-1, which is consistent with the fluorescence data.

4.4. Discussion

4.4.a. How does noncovalent Michaelis complex formation affect serpin inhibition rates?

Serpin inhibition couples fast RCL insertion to protease translocation, destructing the enzyme active site to varying degrees, including a general deformation to removal of

Table 4.2 Interactions in PAI-1-PA Michaelis Complexes

PAI-1 HM-1				tPA			
Type**	Residue	Number	Location	Residue	Number	SP Numbering*	
1	HB	PRO	270	s2C	ARG	36	37A
2	HB	GLU	350	P4' (s1C)	ARG	36	37A
3	HB	LYS	207	s3C	GLU	64	60A
4	HB	SER	336	P11	ASP	104	97
5	HB	THR	339	P8	THR	105	98
6	HB	ASP	181	helical turn (s4C)	ARG	187	174
7	HB	SER	337	P10	ARG	187	174
8	HB	THR	339	P8	ARG	187	174
9	HB	VAL	343	P4	GLN	213	192
10	HB	SER	344	P3	SER	216	195
11	HB	ARG	346	P1	SER	216	195
12	HYD	MET	347	P1'	PHE	161	150
13	HYD	ILE	342	P5	ILE	234	213
14	HYD	VAL	341	P6	TRP	236	215
15	ION	GLU	350	P4' (s1C)	ARG	36	37A
16	ION	LYS	207	s3C	GLU	64	60A
17	ION	ASP	181	helical turn (s4C)	ARG	187	174

PAI-1 HM-2				tPA			
Type**	Residue	Position	Location	Residue	Number	SP Numbering*	
1	HB	ALA	345	P2	HIS	35	37
2	HB	PRO	270	s2C	ARG	36	37A
3	HB	ARG	346	P1	GLU	41	38
4	HB	LYS	207	s3C	GLU	64	60A
5	HB	THR	339	P8	ASP	103	96
6	HB	SER	337	P10	ASP	104	97
7	HB	SER	338	P9	ASP	104	97
8	HB	ALA	340	P7	TYR	106	99
9	HB	SER	344	P3	LYS	154	143
10	HB	ARG	346	P1	TYR	162	151
11	HB	ARG	346	P1	SER	216	195
12	ION	LYS	207	s3C	GLU	64	60A

PAI-1 HM3				tPA			
Type**	Residue	Position	Location	Residue	Number	SP Numbering*	
1	HB	SER	344	P4	HIS	35	37
2	HB	GLU	350	P4' (s1C)	ARG	36	37A
3	HB	THR	339	P8	HIS	60	57
4	HB	THR	339	P8	GLN	63	60
5	HB	LYS	207	s3C	GLU	64	60A
6	HB	SER	337	P10	ASP	103	96
7	HB	ALA	335	P12	ASP	104	97
8	HB	MET	347	P1'	LYS	154	143
9	HB	ALA	348	P2'	LYS	154	143
10	HB	VAL	343	P4	TYR	162	151
11	HB	ALA	345	P2	TYR	162	151
12	HB	ARG	346	P1	SER	216	195
13	HYD	VAL	341	P6	LEU	44	41
14	HYD	VAL	341	P6	PHE	62	59
15	ION	GLU	350	P4' (s1C)	ARG	36	37A
16	ION	LYS	207	s3C	GLU	64	60A

PAI-1 14-1B				S195A-uPA			
Type**	Residue	Position	Location	Residue	Number	SP Numbering*	
1	HB	SER	183	helical turn (s4C)	THR	146	147
2	HB	ARG	187	s4C	TYR	148	149
3	HB	GLU	212	s1B	ARG	23	37A
4	HB	SER	344	P3	LEU	92	97B
5	HB	ALA	345	P2	GLN	195	192
6	HB	ARG	346	P1	ASP	192	189
7	HB	ARG	346	P1	SER	193	190
8	HB	ARG	346	P1	GLY	221	219
9	HB	GLU	350	P4'	TYR	51	60B
10	HB	GLU	351	P5'	TYR	148	149
11	HYD	ILE	342	P5	LEU	92	97B
12	HYD	MET	347	P8'	VAL	30	41
13	ION	GLU	212	s1B	ARG	23	37A
14	ION	ARG	346	P1	ASP	192	189
15	ION	GLU	350	P4' (s1C)	ARG	20	35

* Serine protease domain numbering based on chymotrypsin

** HB = hydrogen bond, HYD = hydrophobic interaction, ION = ionic bond

the catalytic serine from the histidine base and distortion of oxyanion hole to a conformation incompatible with catalysis [4, 123]. For PAI-1, many structural factors affect RCL insertion, and thus the outcome of the inhibitory process, including: the identity of the RCL residue [60, 122], scissile bond position [83], and length of the RCL required for close tethering of the protease [123, 124]; P'-side loop-displacement from the protease active site and release of exosites interactions upon cleavage, precluding s1C detachment [68] and reversible acylation [117]; accessibility of the RCL to the parallel-stranded shutter, of which opening is limited by interactions of s3A and s5A [73, 107] with hF "on top" and hB "on bottom" [108]; reorganization of sA into a six-stranded antiparallel β -sheet; and displacement and return of hF over s4A upon RCL insertion [69]. Although the RCL hinge (P16-P14) can be pre-inserted [58] prior to formation of the Michaelis complex, and thus formerly hypothesized to facilitate insertion upon cleavage, such a conformation is induced after engaging with proteases and triggered by RCL cleavage [73, 100, 105, 115, 117, 118, 210]. Thereby, the manner in which the RCL is positioned and exosite employed in the Michaelis complex prior to cleavage affects the subsequent rates of acylation, loop-displacement, and insertion [211].

4.4.b. How do exosites affect PAI-1 reactions with PAs?

PAI-1 primarily inhibits PAs ($k_{\text{inhib}} = \sim 10^7$; c.f. Table 1.1), but due to its multi-specificity, can also inhibit other serine proteases, including thrombin ($k_{\text{inhib}} = 1.1 \pm 0.2 \times 10^3 \text{ M}^{-1}\text{s}^{-1}$), plasmin ($k_{\text{inhib}} = 2.7 \pm 0.5 \times 10^4 \text{ M}^{-1}\text{s}^{-1}$) [167], and β -trypsin ($k_{\text{inhib}} = 2.2 \pm 0.1 \times 10^6 \text{ M}^{-1}\text{s}^{-1}$) [85], albeit at slower rates. The basis of this multi-specificity and effect on rates is use of one or more exosites beyond the active site interactions (P4-P3'). Analysis of the Michaelis complex of various serpin-protease pairs suggests that the

Table 4.3 Serpin-Serine Protease Exosite Contribution & Inhibition Rates

<i>Serpin</i>	<i>Protease</i>	$k_i (M^{-1}s^{-1}) \times 10^{7\star}$	% Exosite of Total	
			<i>Contact Surface</i> ⁺	<i>Docking</i> ⁺
a ₁ AT (Pitts)	trypsin	0.18	10.30%	n.a.
ATIII	thrombin	3.7	32.70%	front
	fXa	4.4	29.60%	front
HCII	thrombin	1.1	59.30%	front
PCI	thrombin	0.18 ^{★★}	12.90%	back door
PAI-1	uPA	1.1	~36% ⁺⁺	front
	tPA	2.3	n.d.	front
	trypsin	0.92 ^{★★★}	n.d.	n.a.
	thrombin	0.011	n.d.	n.d.

★ Ref. [211]

★★ Ref. [212], adjusted to values from [211] based on fold-difference

★★★ Ref. [85], adjusted to values from [211] based on fold-difference

+ Ref. [3]

++ Ref. [81]

n.d. not determined

n.a. not applicable

optimal contribution of exosites to the total contact surface is ~30% for favorable rate enhancements, with fewer or more exosites not improving the reaction, but seemly required for better recognition when a more extensive exosites is required (**Table 4.3**) [3]. For instance, the inhibition of thrombin by protein C inhibitor (PCI, 12.9% exosite) and heparin cofactor II (59.3% exosite) is ~20X and ~3X slower, respectively, than its inhibition by ATIII (32.7% exosite) [3, 211]. Accordingly, the rate of β -trypsin inhibition by PAI-1, for which it has no known exosites, is ~2.5X slower than that its inhibition of uPA (36% exosite) [3, 85]. The latter trend also seems to correspond with the manner in which the protease rests on the serpins top (**Fig. 4.14**). Proteases can approach the

Serpin	Protease	k_i ($M^{-1}s^{-1}$) $\times 10^7$
ATIII	fXa	4.4
	thrombin	3.7
HCI	thrombin	1.1
PCI	thrombin	0.18

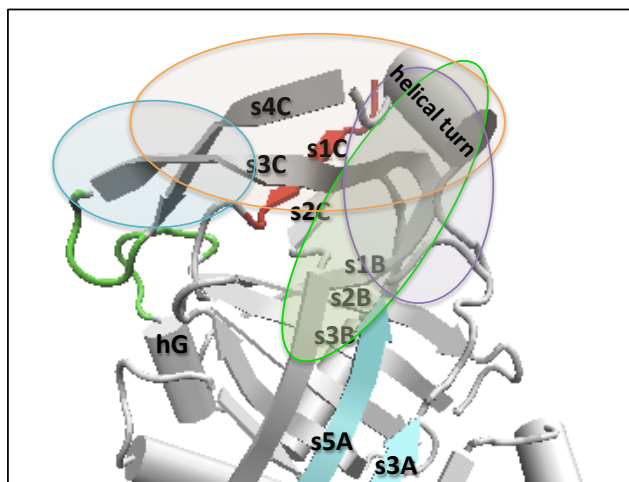


Figure 4.14 Location of Serine Protease Exosites on Serpin Top. The locations of different exosites (*transparent circles*) for representative serpin-serine protease pairs are shown on the PAI-1 scaffold (3Q02 [59], *white* with *red* RCL, *green* gate loops, and *cyan* shutter). Sites (*right*) are colored according to their corresponding pair (*left*).

Table 4.4 Common Serpin-Serine Protease Exosite Interactions

<i>Protease exosite</i>	<i>Serpin exosite</i>
30 loop	s1B
	s3B
60 loop	s2C
	s3C
140 loop	helical turn preceding s4C
	s3C
	s4C

Ref. Whisstock, 2010, *JBC*

Ref. [3]

serpin from two directions: the 'front,' where it encounters the helical turn preceding s4C, followed by sB and sC (e.g. ATIII-thrombin, ATIII-fXa), or the 'back door' (e.g. PCI-thrombin), engaging with s3C [3]. Exosite interactions between the 37-, 60-, and 147-loops (also known as the 30-, 60-, and 140 loops) of the protease with s1-3B, s2-3C, and the helical turn preceding s4C of the serpin, respectively, are frequently employed (**Table 4.4**) [3]. Also, close approach of the protease is required for closely-folded RCLs, as in PAI-1 [58], which limits the range of possible exosites [3, 211].

Certain lines of evidence suggest similar noncovalent Michaelis complexes between PAI-1 and PAs. For instance, the difference in k_{inhib} between the PAs by PAI-1 is small compared to that of thrombin and plasmin by PAI-1 [167]. Also, both PAs share considerable structural similarity (RMSD ~ 1.9 Å) and characteristic features of their serine protease domains [179]. Appropriately, the differences that do exist between the two are mainly in the variable loops, with tPA containing a longer and more positive 37-loop, a 97-loop that protrudes less from domain scaffold, and a much shorter 186-loop than that of uPA. However, the fluorescence data (**Fig. 4.8**) reveal distinct differences in the Michaelis complexes of PAI-1, with tPA-SPD* resting on the front of the serpin near the proximal hinge, employing exosite contacts with N-terminal P9-P6 RCL residues, while uPA-SPD* leans on the distal hinge of the RCL, engaging in exosite contacts with s1C (P4-P8'). Specifically, the PAI-1-tPA Michaelis complex (**Fig. 4.12 B**), modeled based on the fluorescence data, show interactions between s1C (P4')-s2C, s3C, and P12 or P11-P8 of PAI-1 with the 37-, 60-, and 97-loops of tPA, respectively (**Table 4.2**). In contrast, s1B, P4' in s1C, and P5-P3 interact with the 37-, 60-, and 97-loops, respectively, in the 14-1B-PAI-1-uPA Michaelis complex. Furthermore, more contacts

are present in the tPA than the uPA complex with PAI-1 (**Table 4.2**), and the EPR data (**Fig. 4.10**) reveal that, unlike tPA-SPD*, binding of uPA-SPD* at the distal hinge significantly restricts the mobility of the RCL.

As previously mentioned, native PAI-1 inhibits tc-tPA faster than uPA, and uPA faster than sc-tPA, but RCL insertion (k_{lim}) is faster in the presence of uPA, and the affinity (K_m) greater in the presence of tc-tPA (c.f. Table 1.1). These findings provide an explanation for these noted differences. In terms of k_{lim} , binding of uPA at the distal hinge immobilizes the N-terminal RCL, which can restrict its motion for facile sA incorporation, resulting to its faster insertion. In terms of K_m , sc-tPA participates in more interactions in the Michaelis complex than uPA, which may be similar for tc-tPA, contributing to its greater affinity for PAI-1. It can further be hypothesized that tc-tPA binds the proximal hinge similar to sc-tPA in the Michaelis complex, but induces greater restrictions on RCL mobility than the latter, but less than that of uPA, leading to its faster rate of inhibition than its single-chain form. Such knowledge of the binding and association of these components in the Michaelis complex will be useful in the development of more efficient PAI-1-PA inhibitors.

4.4.c. Why inhibit tPA versus uPA interaction with PAI-1?

PAI-1-tPA signaling via LRP-1 [12] and PAI-1-uPA-uPAR signaling [199] can lead to the increased expression of MMP-9, and plasmin activated from plasminogen by PAs can consequently activate MMP-9. While these processes are important in tissue remodeling after injury under normal conditions, they can be harmful in pathological settings, e.g. cancers, strokes. In the latter case, it may be desirable to inhibit PAI-1-PA interactions, without interfering with other serpin-serine-protease interactions. The

differences in PAI-1-PA interactions revealed here can be used in the development of more specific inhibitors for each, which generally leads to increased efficacy and decreased undesirable side effects of drugs. In addition, difficulties can arise from using tPA as a thrombolytic [12, 213, 214] in acute ischemic stroke, including its fast hepatic clearance [42, 179], rendering it ineffective, or prolonged presence, leading blood-brain barrier (BBB) permeability and oxidative stress [197, 214]. The latter neurotoxicity of tPA can be countered by the neuroprotection provided by uPA [215] shown to alleviate the effects of oxidative stress, but not if the latter is targeted. Also, the risk of neurotoxicity is greater if endogenous PAI-1 levels are high (e.g. due to 4G/4G polymorphism). In this case, the specific inhibition of tPA, and not uPA, may be beneficial.

4.4.d. How does interaction with VN affect PAI-1 interaction with PAs?

Binding of VN alters the specificity of PAI-1 [167], possibly via binding at its secondary site on hE, and affects its interaction with the PAs. Specifically, VN lowers the k_{lim} of PAI-1 with the PAs and K_m with sc-tPA, but not the K_m with tc-tPA and uPA (c.f. Table 1.1). VN also does not affect the SI ratio of PAI-1 with the PAs [86, 92], and thus the partition between the inhibitory and substrate branches. Thus, the effect of VN on the interaction of PAI-1 with the PAs probably involves the formation of the noncovalent Michaelis complex. Interestingly, tPA binding to PAI-1 (**Fig. 4.8 A**) elicits greater changes in solvent accessibility of the same residues, P9-P6, as VN (c.f. Fig. 3.8) and those that do not show an initial decrease during the latency process (c.f. Fig. 2.22 A). Also, VN binding considerably affects the s1C conformation. These results suggest that VN induces changes in RCL conformation to one less favored by the PAs.

4.5. Conclusion

Steady-state fluorescence and EPR investigation demonstrate that uPA binding to the C-terminal RCL in the Michaelis complex restricts its motion, resulting in faster rates of RCL insertion (k_{im}), while sc-tPA binding at the N-terminal RCL engages in more exosite interactions, yet leaves RCL relatively mobile. The Michaelis complex for tc-tPA is likely similar to that of sc-tPA, except with greater restriction of RCL mobility. Thereby, PAI-1 inhibits tc-tPA more rapidly than uPA, and the latter two more quickly than sc-tPA.

Future Directions

Characterizing the loop to strand conformation and dynamics of the PAI-1 RCL by computational and spectroscopic methods reveals important information about the latency transition and interactions with its ligands, including VN and PAs. These studies reveal that the few conformations that are accessible to the RCL may contribute to its meta-stability and facilitate the conversion of PAI-1 to its global free-energy minimum latent state. The new information gathered here on the latency process, specifically the early s1C detachment during the transition and VN delaying full insertion by eliciting a solvent-exposed conformation of the N-terminal RCL, can be used for the development of more effective inhibitors against PAI-1 in its pathophysiological states. The finding that sc-tPA participates in many exosite interactions with the N-terminal RCL, contributing to its higher K_m , and uPA engages with the C-terminal RCL in its exosite that significantly restricts loop mobility, resulting in its faster k_{lim} , can likewise be used for the specific targeting of PAI-1. However, many questions for future work remain to be answered. For instance, is the initial decrease observed by steady-state investigation of the latency transition sufficiently explained by s1C detachment? Does RCL passage through the gate or hF displacement limit the rate of this transition? Does VN affect s1C detachment or other processes during the latency process? How does the IDD affect the RCL conformation in the absence of the SMB domain? How does VN affect the Michaelis complex with PAs?

Due to the success of the combined approach using fluorescence and EPR of RCL-labeled mutants to elucidate structural information, further experiments can be performed to answer these questions. To verify that s1C detachment explains the early

decreases in fluorescence, single-cysteine RCL mutants of the stable 14-1B PAI-1 mutant can be engineered and labeled as presented in this work. These mutants can subsequently be tested by steady-state fluorescence to detect the presence of the initial decrease, which may be longer due to the enhanced stability of the latter in comparison to native PAI-1. Also, PAI-1_R, in which the P14 position mutation to Arg prevents its insertion, can be used to investigate if s1C detachment is a prerequisite for RCL insertion or if these events are mutually exclusive. Furthermore, the latency transition in the presence of VN can be observed to determine if the latter affects any step of the latency transition, including s1C detachment or hF displacement.

Producing VN with the appropriate post-translational modifications and correct disulfide pairing in the SMB by recombinant methods (e.g. *E. coli*, baculovirus) is challenging due to low yields, although initial success with expression in *Drosophila melanogaster* S2 insect cells has been met (data not shown). An additional challenge in purifying intrinsically disordered proteins, which characteristically possess a low hydrophobicity and high density of charge, is the propensity to aggregate and its susceptibility to proteolysis. The latter can be circumvented by thermal/chemical denaturation [216], boiling lysis followed by ion-exchange [217], the use of solubility-promoting buffers [218], or via use of a fusion protein [219]. Upon its purification, the contribution of the IDD alone on the conformation of the RCL can be examined by fluorescence, as the EPR data of full length VN did not show significant changes in RCL dynamics in its presence.

To assess the effect of VN on the interaction of PAI-1 and PAs, the fluorescence and EPR measurements of the RCL-labeled PAI-1 in the presence of active site-

blocked PAs, VN, and/or its truncations can be performed. Also, since the results here pertain to its single chain form, the effect of tc-tPA on the structure of the RCL can be investigated to explain its faster k_{inhib} than uPA and sc-tPA with PAI-1. (tc-tPA can be formed from sc-tPA via plasmin cleavage). Moreover, since VN affects the specificity of PAI-1, the RCL-labeled PAI-1 can be examined by these methods in the presence of active site-blocked thrombin, and differences from PAs compared to obtain information on serpin specificity requirements.

In EPR experiments, though the changes in signal intensity may be explained by changes in the Q factor, and DTNB assays and MALDI analysis indicate the absence of free sulfhydryls and dimerized PAI-1, respectively, the reduction of the MTSL-probe conjugated to PAI-1 could not be excluded because free MTSL retains its paramagnetism and results in sharper line-widths, as observed in the increase in signal intensity in some cases (c.f. Figs. 2.23, 3.11, & 4.10). Reducing agents, such as ascorbate [131, 220] or DTT, can be used to test the latter. Accordingly, if the probe is already reduced, a signal change should not occur. Also, the MTSL spectra contain information in addition to dynamics. Residue-by-residue orientation information can be obtained from simulations of the high-field peak in these spectra to provide greater structural resolution. Moreover, for an additional comparison of PAI-1 RCL dynamics, low-T EPR measurements (liquid nitrogen, ~77 Kelvin) can be performed to collect data on the immobilized RCL. Research into these questions will further the understanding of the nature of PAI-1.

References

1. Kraut, J., *Serine Proteases: Structure and Mechanism of Catalysis*. Annu Rev Biochem, 1977. **46**: p. 331-58.
2. Silverman, G.A., J.C. Whisstock, S.P. Bottomley, J.A. Huntington, D. Kaiserman, C.J. Luke, S.C. Pak, J.M. Reichhart, and P.I. Bird, *Serpins Flex Their Muscle: I. Putting the Clamps on Proteolysis in Diverse Biological Systems*. J Biol Chem, 2010. **285**(32): p. 24299-305.
3. Whisstock, J.C., G.A. Silverman, P.I. Bird, S.P. Bottomley, D. Kaiserman, C.J. Luke, S.C. Pak, J.M. Reichhart, and J.A. Huntington, *Serpins Flex Their Muscle: II. Structural Insights into Target Peptidase Recognition, Polymerization, and Transport Functions*. J Biol Chem, 2010. **285**(32): p. 24307-12.
4. Dupont, D.M., J.B. Madsen, T. Kristensen, J.S. Bodker, G.E. Blouse, T. Wind, and P.A. Andreasen, *Biochemical Properties of Plasminogen Activator Inhibitor-1*. Frontiers in Bioscience, 2009. **14**: p. 1337-1361.
5. Minor, K.H. and C.B. Peterson, *Plasminogen Activator Inhibitor Type 1 Promotes the Self-Association of Vitronectin into Complexes Exhibiting Altered Incorporation into the Extracellular Matrix*. Journal of Biological Chemistry, 2002. **277**(12): p. 10337-10345.
6. Garg, N., N. Goyal, T.L. Strawn, J. Wu, K.M. Mann, D.A. Lawrence, and W.P. Fay, *Plasminogen Activator Inhibitor-1 and Vitronectin Expression Level and Stoichiometry Regulate Vascular Smooth Muscle Cell Migration through Physiological Collagen Matrices*. J Thromb Haemost, 2010. **8**: p. 1847-54.
7. Park, Y.J., G. Liu, E.F. Lorne, X. Zhao, J. Wang, Y. Tsuruta, J. Zmijewski, and E. Abraham, *Pai-1 Inhibits Neutrophil Efferocytosis*. Proceedings of the National Academy of Sciences, 2008. **105**(33): p. 11784-11789.
8. Loskutoff, D.J., *A Slice of Pai*. J Clin Invest, 1993. **92**: p. 2563.
9. Vaughan, D.E., *Pai-1 Antagonists: The Promise and the Peril*. Trans Am Clin Climatol Assoc, 2011. **122**: p. 312-25.
10. Lawrence, D.A., S. Palaniappan, S. Stefansson, S.T. Olson, A.M. Francis-Chmura, J.D. Shore, and D.S. Ginsberg, *Characterization of the Binding of Different Conformational Forms of Plasminogen Activator Inhibitor-1 to Vitronectin: Implications for the Regulation of Pericellular Proteolysis*. Journal of Biological Chemistry, 1997. **272**(12): p. 7676-7680.
11. Keijer, J., M. Linders, A.J. van Zooneveld, H.J. Ehrlich, J.P. de Boer, and H. Pannekoek, *The Interaction of Plasminogen Activator Inhibitor 1 with Plasminogen Activators (Tissue-Type and Urokinase-Type) and Fibrin: Localization of Interaction Sites and Physiologic Relevance*. Blood, 1991. **78**(401-409).

12. Adibhatla, R.M. and J.F. Hatcher, *Tissue Plasminogen Activator (Tpa) and Matrix Metalloproteinases in the Pathogenesis of Stroke: Therapeutic Strategies*. CNS Neurol Disord Drug Targets, 2008. **7**(3): p. 243-53.
13. Usher, P.A., O.F. Thomsen, P. Iversen, M. Johnsen, N. Brünner, G. Høyer-Hansen, P.A. Andreasen, K. Danø, and B.S. Nielsen, *Expression of Urokinase Plasminogen Activator, Its Receptor and Type-1 Inhibitor in Malignant and Benign Prostate Tissue*. International Journal of Cancer, 2005. **113**(6): p. 870-880.
14. Choong, P.F. and A.P. Nadesapillai, *Urokinase Plasminogen Activator System: A Multifunctional Role in Tumor Progression and Metastasis*. Clin Orthop Relat Res, 2003. **415 Suppl**: p. S46-58.
15. Chen, Q., J. Fei, L. Wu, Z. Jiang, Y. Wu, Y. Zheng, and G. Lu, *Detection of Cathepsin B, Cathepsin L, Cystatin C, Urokinase Plasminogen Activator and Urokinase Plasminogen Activator Receptor in the Sera of Lung Cancer Patients*. Oncol Lett, 2011. **2**(4): p. 693-99.
16. Naina, H.V., M.M. Patnaik, U.A. Ali, D. Chen, and A.A. Ashrani, *Systemic Fibrinolysis Caused by Tissue Plasminogen Activator-Producing Metastatic Breast Cancer*. J Clin Oncol, 2010. **28**(11): p. e167-8.
17. Zhang, W., D. Ling, J. Tan, J. Zhang, and L. Li, *Expression of Urokinase Plasminogen Activator and Plasminogen Activator Inhibitor Type-1 in Ovarian Cancer and Its Clinical Significance*. Oncol Rep, 2013. **29**(2): p. 637-45.
18. Tang, L. and X. Han, *The Urokinase Plasminogen Activator System in Breast Cancer Invasion and Metastasis*. Biomed Pharmacother, 2013. **67**(2): p. 179-82.
19. Köller, A., J. Kirchheimer, H. Pflüger, and B.R. Binder, *Tissue Plasminogen Activator Activity in Prostatic Cancer*. Eur Urol, 1984. **10**(6): p. 389-94.
20. Binder, B.R. and J. Mihaly, *The Plasminogen Activator Inhibitor "Paradox" in Cancer*. Immunology Letters, 2008. **118**(2): p. 116-124.
21. Diebold, I., D. Kraicun, S. Bonello, and A. Görlach, *The 'Pai-1 Paradox' in Vascular Remodelling*. Thrombosis and Haemostasis, 2008.
22. Sobel, B.E., *Increased Plasminogen Activator Inhibitor-1 and Vasculopathy : A Reconcilable Paradox*. Circulation, 1999. **99**(19): p. 2496-2498.
23. Vaughan, D.E., *Pai-1 and Cellular Migration: Dabbling in a Paradox*. Arteriosclerosis, Thrombosis, and Vascular Biology, 2002. **22**(10): p. 1522-1523.
24. De Taeye, B., L.H. Smith, and D.E. Vaughan, *Plasminogen Activator Inhibitor-1: A Common Denominator in Obesity, Diabetes and Cardiovascular Disease*. Curr Opin Pharmacol, 2005. **5**(2): p. 149-54.

25. Lyon, C.J. and W.A. Hsueh, *Effect of Plasminogen Activator Inhibitor-1 in Diabetes Mellitus and Cardiovascular Disease*. Am J Med, 2003. **115 Suppl 8A**: p. 62S-68S.
26. Nordt, T.K., K. Peter, J. Ruef, W. Kubler, and C. Bode, *Plasminogen Activator Inhibitor Type-1 (Pai-1) and Its Role in Cardiovascular Disease*. Thromb Haemost, 1999. **82 Suppl 1**: p. 14-8.
27. Ploplis, V.A., *Effects of Altered Plasminogen Activator Inhibitor-1 Expression on Cardiovascular Disease*. Curr Drug Targets, 2011. **12**(12): p. 1782-9.
28. Vaughan, D.E., *Plasminogen Activator Inhibitor-1: A Common Denominator in Cardiovascular Disease*. J Investig Med, 1998. **46**(8): p. 370-6.
29. Ouyang, L., Y. Peng, G. Wu, X. Xu, and Z. He, *[Effect of Plasminogen Activator Inhibitor-1 and Endothelin-1 on the Atherosclerosis in the Maintenance Hemodialysis Patients]*. Zhong Nan Da Xue Xue Bao Yi Xue Ban, 2013. **38**(5): p. 458-67.
30. Binder, B.R., G. Christ, F. Gruber, N. Grubic, P. Hufnagl, M. Krebs, J. Mihaly, and G.W. Prager, *Plasminogen Activator Inhibitor 1: Physiological and Pathophysiological Roles*. News Physiological Science, 2002. **17**: p. 56-61.
31. Schneiderman, J., M.S. Sawdey, M.R. Keeton, G.M. Bordin, E.F. Bernstein, R.B. Dilley, and D.J. Loskutoff, *Increased Type 1 Plasminogen Activator Inhibitor Gene Expression in Atherosclerotic Human Arteries*. Proc Natl Acad Sci U S A, 1992. **89**(15): p. 6998-7002.
32. Munoz-Valle, J.F., S.L. Ruiz-Quezada, E. Oregon-Romero, R.E. Navarro-Hernandez, E. Castaneda-Saucedo, U. De la Cruz-Mosso, B. Illades-Aguiar, M.A. Leyva-Vazquez, N. Castro-Alarcon, and I. Parra-Rojas, *Pai-1 Mrna Expression and Plasma Level in Rheumatoid Arthritis: Relationship with 4g/5g Pai-1 Polymorphism*. Rheumatol Int, 2012. **32**(12): p. 3951-6.
33. Chorostowska-Wynimko, J., R. Swiercz, E. Skrzypczak-Jankun, A. Wojtowicz, S.H. Selman, and J. Jankun, *A Novel Form of the Plasminogen Activator Inhibitor Created by Cysteine Mutations Extends Its Half-Life: Relevance to Cancer and Angiogenesis*. Molecular Cancer Therapeutics, 2009. **2**: p. 19-28.
34. Chazaud, B., R. Ricoux, C. Christov, A. Plonquet, R.K. Gherardi, and G. Barlovatz-Meimon, *Promigratory Effect of Plasminogen Activator Inhibitor-1 on Invasive Breast Cancer Cell Populations*. American Journal of Pathology, 2002. **160**(1): p. 237-246.
35. Alessi, M.C. and I. Juhan-Vague, *Pai-1 and the Metabolic Syndrome: Links, Causes, and Consequences*. Arteriosclerosis, Thrombosis, and Vascular Biology, 2006. **26**(10): p. 2200-2207.

36. Coffey, C.S., F.W. Asselbergs, P.R. Hebert, H.L. Hillege, Q. Li, J.H. Moore, and W.H. van Gilst, *The Association of the Metabolic Syndrome with Pai-1 and T-Pa Levels*. Cardiology Research and Practice, 2011. **2011**: p. 1-8.
37. Juhan-Vague, I., M.C. Alessi, A. Mavri, and P.E. Morange, *Plasminogen Activator Inhibitor-1, Inflammation, Obesity, Insulin Resistance and Vascular Risk*. J Thromb Haemost, 2003. **1**(7): p. 1575-9.
38. Mou, X., C.B. Peterson, and R.A. Prosser, *Tissue-Type Plasminogen Activator-Plasmin-Bdnf Modulate Glutamate-Induced Phase-Shifts of the Mouse Suprachiasmatic Circadian Clock in Vitro*. Molecular and Developmental Neuroscience, 2009. **30**: p. 1451-1460.
39. Eren, M., L.A. Gleaves, J.B. Atkinson, L.E. King, P.J. Declerck, and D.E. Vaughan, *Reactive Site-Dependent Phenotypic Alterations in Plasminogen Activator Inhibitor-1 Transgenic Mice*. J Thromb Haemost, 2007. **5**(7): p. 1500-8.
40. Bernadete Trovo de Marqui, A., *Genetic Polymorphisms and Endometriosis: Contribution of Genes That Regulate Vascular Function and Tissue Remodeling*. Rev Assoc Med Bras, 2012. **58**(5): p. 620-632.
41. Riby, D.M. and M.A. Porter, *Williams Syndrome*. Adv Child Dev Behav, 2010. **39**: p. 163-209.
42. Chandler, W.L., M.C. Alessi, M.F. Aillaud, P. Henderson, P. Vague, and I. Juhan-Vague, *Clearance of Tissue Plasminogen Activator (Tpa) and Tpa/Plasminogen Activator Inhibitor Type 1 (Pai-1) Complex*. Circulation, 1997. **96**: p. 761-768.
43. Samad, F., M. Pandey, P.A. Bell, and D.J. Loskutoff, *Insulin Continues to Induce Plasminogen Activator Inhibitor-1 Gene Expression in Insulin-Resistant Mice and Adipocytes*. Mol Med, 2000. **6**(8): p. 680-92.
44. Chen, Y.Q., M. Su, R.R. Walia, Q. Hao, J.W. Covington, and D.E. Vaughan, *Sp1 Sites Mediate Activation of the Plasminogen Activator Inhibitor-1 Promoter by Glucose in Vascular Smooth Muscle Cells*. J Biol Chem, 1998. **273**(14): p. 8225-31.
45. Juhan-Vague, I., M.C. Alessi, and P.E. Morange, *Hypofibrinolysis and Increased Pai-1 Are Linked to Atherothrombosis Via Insulin Resistance and Obesity*. Ann Med, 2000. **32 Suppl 1**: p. 78-84.
46. Bouchie, J.L., H.C. Chen, R. Carney, J.C. Bagot, P.A. Wilden, and E.P. Feener, *P2y Receptor Regulation of Pai-1 Expression in Vascular Smooth Muscle Cells*. Arterioscler Thromb Vasc Biol, 2000. **20**(3): p. 866-73.
47. Fogo, A.B., *The Role of Angiotensin Ii and Plasminogen Activator Inhibitor-1 in Progressive Glomerulosclerosis*. Am J Kidney Dis, 2000. **35**(2): p. 179-88.

48. Ma, L.J. and A.B. Fogo, *Angiotensin as Inducer of Plasminogen Activator Inhibitor-1 and Fibrosis*. *Contrib Nephrol*, 2001(135): p. 161-70.
49. Braun, O.O., D. Lu, N. Aroonsakool, and P.A. Insel, *Uridine Triphosphate (Utp) Induces Profibrotic Responses in Cardiac Fibroblasts by Activation of P2y2 Receptors*. *J Mol Cell Cardiol*, 2010. **49**(3): p. 362-9.
50. Keeton, M.R., S.A. Curriden, A.J. van Zonneveld, and D.J. Loskutoff, *Identification of Regulatory Sequences in the Type 1 Plasminogen Activator Inhibitor Gene Responsive to Transforming Growth Factor Beta*. *J Biol Chem*, 1991. **266**(34): p. 23048-52.
51. Dennler, S., S. Itoh, D. Vivien, P. ten Dijke, S. Huet, and J.M. Gauthier, *Direct Binding of Smad3 and Smad4 to Critical Tgf Beta-Inducible Elements in the Promoter of Human Plasminogen Activator Inhibitor-Type 1 Gene*. *EMBO J*, 1998. **17**(11): p. 3091-100.
52. Gruber, F., P. Hufnagl, R. Hofer-Warbinek, J.A. Schmid, J.M. Breuss, R. Huber-Beckmann, M. Lucerna, N. Papac, H. Harant, I. Lindley, R. de Martin, and B.R. Binder, *Direct Binding of Nur77/Nak-1 to the Plasminogen Activator Inhibitor 1 (Pai-1) Promoter Regulates Tnf Alpha -Induced Pai-1 Expression*. *Blood*, 2003. **101**(8): p. 3042-8.
53. Wyrzykowska, P. and A. Kasza, *[Regulation of Pai-1 Expression]*. *Postepy Biochem*, 2009. **55**(1): p. 46-53.
54. Narasaki, R., Z. Xu, Z. Liang, L.C. Fung, D. Donahue, F.J. Castellino, and V.A. Ploplis, *The Vitronectin-Binding Domain of Plasminogen Activator Inhibitor-1 Plays an Important Functional Role in Lipopolysaccharide-Induced Lethality in Mice*. *J Thromb Haemost*, 2012. **10**(12): p. 2618-21.
55. Choudhary, A. and R.T. Raines, *An Evaluation of Peptide-Bond Isosteres*. *Chembiochem*, 2011. **12**(12): p. 1801-7.
56. Antalis, T. and D.A. Lawrence, *Serpin Mutagenesis*. *Methods*, 2004. **32**(2): p. 130-140.
57. Blouse, G.E., M.J. Perron, J.H. Thompson, D.E. Day, C.A. Link, and J.D. Shore, *A Concerted Structural Transition in the Plasminogen Activator Inhibitor-1 Mechanism of Inhibition*. *Biochemistry*, 2002. **41**: p. 11997-12009.
58. Hagglof, P., F. Bergstrom, M. Wilczynska, L.B. Johansson, and N. Tor, *The Reactive-Center Loop of Active Pai-1 Is Folded Close to the Protein Core and Can Be Partially Inserted*. *J Mol Biol*, 2004. **335**: p. 823-832.
59. Jensen, J.K., L.C. Thompson, J.C. Bucci, P. Nissen, P.G.W. Gettins, C.B. Peterson, P.A. Andreasen, and J.P. Morth, *Crystal Structure of Plasminogen*

- Activator Inhibitor-1 in an Active Conformation with Normal Thermodynamic Stability*. Journal of Biological Chemistry, 2011. **286**(34): p. 29709-29717.
60. Lawrence, D.A., S.T. Olson, S. Palaniappan, and D. Ginsburg, *Serpin Reactive Center Loop Mobility Is Required for Inhibitor Function but Not for Enzyme Recognition*. Journal of Biological Chemistry, 1994. **269**(44): p. 27657-27662.
 61. Sherman, W.A., G.E. Blouse, M.J. Perron, T. Tran, J.D. Shore, and A. Gafni, *Enthalpy Measurement Using Calorimetry Shows a Significant Difference in Potential Energy between the Active and Latent Conformations of Pai-1*. Biological Chemistry, 2005. **386**(2).
 62. Thompson, L.C., S. Goswami, D.S. Ginsberg, D.E. Day, I.M. Verhamme, and C.B. Peterson, *Metals Affect the Structure and Activity of Human Plasminogen Activator Inhibitor-1. I. Modulation of Stability and Protease Inhibition*. Protein Science, 2011. **20**(2): p. 353-365.
 63. Wind, T., M. Hansen, J.K. Jensen, and P.A. Andreasen, *The Molecular Basis for Anti-Proteolytic and Non-Proteolytic Functions of Plasminogen Activator Inhibitor Type-1: Roles of the Reactive Centre Loop, the Shutter Region, the Flexible Joint Region and the Small Serpin Fragment*. Biological Chemistry, 2002. **383**: p. 21-36.
 64. Boudier, C., A. Gils, P.I.J. Declerck, and J.G. Bieth, *The Conversion of Active to Latent Plasminogen Activator Inhibitor-1 Is an Energetically Silent Event*. Biophysical Journal, 2005. **88**(4): p. 2848-2854.
 65. Verhamme, I.M., J. Kvassman, D.E. Day, S. Debrock, N. Vleugels, P.J. Declerck, and J.D. Shore, *Accelerated Conversion of Human Plasminogen Activator Inhibitor-1 to Its Latent Form by Antibody Binding*. Journal of Biological Chemistry, 1999. **274**(25): p. 17511-17517.
 66. Tucker, H.M., J. Mottonen, E.J. Goldsmith, and R.D. Gerard, *Engineering of Plasminogen Activator Inhibitor-1 to Reduce the Rate of Latency Transition*. Nature Structural Biology, 1995. **2**(6): p. 442-445.
 67. Komissarov, A.A., P.J. Declerck, and J.D. Shore, *Mechanisms of Conversion of Plasminogen Activator Inhibitor 1 from a Suicide Inhibitor to a Substrate by Monoclonal Antibodies*. Journal of Biological Chemistry, 2002. **277**(46): p. 43858-43865.
 68. Komissarov, A.A., A. Zhou, and P.J. Declerck, *Modulation of Serpin Reaction through Stabilization of Transient Intermediate by Ligands Bound to a-Helix F*. Journal of Biological Chemistry, 2007. **282**(36): p. 26306-26315.
 69. Gettins, P.G.W., *The F-Helix of Serpins Plays an Essential, Active Role in the Proteinase Inhibition Mechanism*. FEBS Journal, 2002. **523**: p. 2-6.

70. Berkenpas, M.B., D.A. Lawrence, and D.S. Ginsberg, *Molecular Evolution of Plasminogen Activator Inhibitor-1 Functional Stability*. EMBO Journal, 1995. **14**(13): p. 2969-2977.
71. Stoop, A.A., E. Eldering, T.R. Dafforn, R.J. Read, and H. Pannekoek, *Different Structural Requirements for Plasminogen Activator Inhibitor 1 (Pai-1) During Latency Transition and Proteinase Inhibition as Evidenced by Phage- Displayed Hypermutated Pai-1 Libraries*. J Mol Biol, 2001. **305**: p. 773-783.
72. Wind, T., J.K. Jensen, D.M. Dupont, P. Kulig, and P.A. Andreasen, *Mutational Analysis of Plasminogen Activator Inhibitor-1. Interactions of A-Helix F and Its Neighbouring Structural Elements Regulates the Activity and the Rate of Latency Transition*. European Journal of Biochemistry, 2003. **270**(8): p. 1680-1688.
73. Kjoller, L., P.M. Martensen, L. Sottrup-Jensen, J. Justesen, K.W. Rodenburg, and P.A. Andreasen, *Conformational Changes of the Reactive-Centre Loop and B-Strand 5a Accompany Temperature-Dependent Inhibitor-Substrate Transition of Plasminogen-Activator Inhibitor 1*. European Journal of Biochemistry, 1996. **241**: p. 38-46.
74. Kvassman, J., D.A. Lawrence, and J.D. Shore, *The Acid Stabilization of Plasminogen Activator Inhibitor-1 Depends on Protonation of a Single Group That Affects Loop Insertion into B-Sheet A*. Journal of Biological Chemistry, 1995. **270**(46): p. 27942-27947.
75. Sui, G., H. Mangs, and B. Wiman, *The Role of His143 for the Ph-Dependent Stability of Plasminogen Activator Inhibitor-1*. Biochimica et Biophysica Acta, 1999. **1434**: p. 58-63.
76. Mangs, H., G. Sui, and B. Wiman, *Pai-1 Stability: The Role of Histidine Residues*. FEBS Letters, 2000. **475**: p. 192-196.
77. Andreasen, P.A., R. Egelund, S. Jensen, and K.W. Rodenburg, *Solvent Effects on the Activity and Conformation of Plasminogen Activator Inhibitor-1*. Thromb Haemost, 1999. **81**(3): p. 407-14.
78. Lawrence, D.A., S.T. Olson, S. Muhammad, D.E. Day, J. Kvassman, D.S. Ginsberg, and J.D. Shore, *Partitioning of Serpin-Proteinase Reactions between Stable Inhibition and Substrate Cleavage Is Regulated by the Rate of Serpin Reactive Center Loop Insertion into B-Sheet A*. Journal of Biological Chemistry, 2000. **275**(8): p. 5839-5844.
79. Gils, A. and P.J. Declerck, *Structure-Function Relationships in Serpins: Current Concepts and Controversies*. Thromb Haemost, 1998. **80**: p. 531-41.
80. Blouse, G.E., D.M. Dupont, C.R. Schar, J.K. Jensen, K.H. Minor, J.Y. Anagli, H. Gårdsvoll, M. Ploug, C.B. Peterson, and P.A. Andreasen, *Interactions of Plasminogen Activator Inhibitor-1 with Vitronectin Involve an Extensive Binding*

- Surface and Induce Mutual Conformational Rearrangements*. *Biochemistry*, 2009. **48**: p. 1723-1735.
81. Lin, Z., L. Jiang, C. Yuan, J.K. Jensen, X. Zhang, Z. Luo, B.C. Furie, B. Furie, P.A. Andreasen, and M. Huang, *Structural Basis for Recognition of Urokinase-Type Plasminogen Activator by Plasminogen Activator Inhibitor-1*. *Journal of Biological Chemistry*, 2011. **286**(9): p. 7027-7032.
 82. Hekman, C.M. and D.J. Loskutoff, *Kinetic Analysis of the Interactions between Plasminogen Activator Inhibitor 1 and Both Urokinase and Tissue Plasminogen Activator*. *Archives of Biochemistry and Biophysics*, 1988. **262**(1): p. 199-210.
 83. York, J.D., P. Li, and S. Gardell, *Combinatorial Mutagenesis of the Reactive Site Region in Plasminogen Activator Inhibitor 1*. *Journal of Biological Chemistry*, 1991. **266**(13): p. 8495-8500.
 84. Lawrence, D.A., L. Strandberg, J. Ericson, and T. Ny, *Structure-Function Studies of the Serpin Plasminogen Activator Inhibitor Type 1: Analysis of Chimeric Strained Loop Mutants*. *Journal of Biological Chemistry*, 1990. **265**(33).
 85. Ibarra, C.A., G.E. Blouse, T.D. Christian, and J.D. Shore, *The Contribution of the Exosite Residues of Plasminogen Activator Inhibitor-1 to Proteinase Inhibition*. *Journal of Biological Chemistry*, 2003. **279**(5): p. 3643-3650.
 86. Komissarov, A.A., P.A. Andreasen, J.S. Bodker, P.J. Declerck, J.Y. Anagli, and J.D. Shore, *Additivity in Effects of Vitronectin and Monoclonal Antibodies against -Helix F of Plasminogen Activator Inhibitor-1 on Its Reactions with Target Proteinases*. *Journal of Biological Chemistry*, 2005. **280**(2): p. 1482-1489.
 87. Blouse, G.E., M.J. Perron, J. Kvassman, S. Yunus, J.H. Thompson, R.L. Betts, L.C. Lutter, and J.D. Shore, *Mutation of the Highly Conserved Tryptophan in the Serpin Breach Region Alters the Inhibitory Mechanism of Plasminogen Activator Inhibitor-1*. *Biochemistry*, 2003. **42**: p. 12260-12272.
 88. Whisstock, J.C. and S.P. Bottomley, *Molecular Gymnastics: Serpin Structure, Folding and Misfolding*. *Curr Opin Struct Biol*, 2006. **16**(6): p. 761-8.
 89. Egelund, R., S.L. Schousboe, L. Sottrup-Jensen, K.W. Rodenburg, and P.A. Andreasen, *Type-1 Plasminogen Activator Inhibitor: Conformational Differences between Latent, Active, Reactive-Centre-Cleaved and Plasminogen-Activator-Complexed Forms, as Probed by Proteolytic Susceptibility*. *European Journal of Biochemistry*, 1997. **248**: p. 775-785.
 90. Nukuna, B.N., M.S. Penn, V.E. Anderson, and S.L. Hazen, *Latency and Substrate Binding Globally Reduce Solvent Accessibility of Plasminogen Activator Inhibitor Type 1 (Pai-1): An Adaptation of Pai-1 Conformer Crystal Structures by Hydrogen-Deuterium Exchange*. *Journal of Biological Chemistry*, 2004. **279**(48): p. 50132-50141.

91. Trelle, M.B., D. Hirschberg, A. Jansson, M. Ploug, P. Roepstorff, P.A. Andreasen, and T.J. Jorgensen, *Hydrogen/Deuterium Exchange Mass Spectrometry Reveals Specific Changes in the Local Flexibility of Plasminogen Activator Inhibitor 1 Upon Binding to the Somatomedin B Domain of Vitronectin*. *Biochemistry*, 2012. **51**(41): p. 8256-66.
92. Li, S.H., N.V. Gorlatova, D.A. Lawrence, and B.S. Schwartz, *Structural Differences between Active Forms of Plasminogen Activator Inhibitor Type 1 Revealed by Conformationally Sensitive Ligands*. *Journal of Biological Chemistry*, 2008. **283**(26): p. 18147-18157.
93. Britt Van De Craen, B., I. Scroyen, C. Vranckx, G. Compennolle, H.R. Lijnen, P.J. Declerck, and A. Gils, *Maximal Pai-1 Inhibition in Vivo Requires Neutralizing Antibodies That Recognize and Inhibit Glycosylated Pai-1*. *Thrombosis Research*, 2012. **129**: p. e126-e133.
94. Dupont, D.M., G.E. Blouse, M. Hansen, L. Mathiasen, S. Kjellaard, J.K. Jensen, A. Christensen, A. Gils, P.J. Declerck, P.A. Andreasen, and T. Wind, *Evidence for a Pre-Latent Form of the Serpin Plasminogen Activator Inhibitor-1 with a Detached Beta-Strand 1c*. *Journal of Biological Chemistry*, 2006. **281**(47): p. 36071-36081.
95. Smolarczyk, K., A. Gils, J. Boncela, P.J. Declerck, and C. Cierniewski, *Function-Stabilizing Mechanism of Plasminogen Activator Inhibitor Type 1 Induced Upon Binding to Alpha1-Acid Glycoprotein*. *Biochemistry*, 2005. **44**: p. 12384-12390.
96. Bjorquist, P., J. Ehnebo, and J. Deinum, *Protein Movement During Complex-Formation between Tissue Plasminogen Activator and Plasminogen Activator Inhibitor-1*. *Biochim Biophys Acta*, 1999. **1431**(1): p. 24-9.
97. Schousboe, S.L., R. Egelund, T. Kirkegaard, K.T. Preissner, K.W. Rodenburg, and P.A. Andreasen, *Vitronectin and Substitution of a Beta-Strand 5a Lysine Residue Potentiate Activity-Neutralization of Pa Inhibitor-1 by Monoclonal Antibodies against Alpha-Helix F*. *Thromb Haemost*, 2000. **83**(5): p. 742-51.
98. Verheyden, S., A. Sillen, A. Gils, P.J. Declerck, and Y. Engelborghs, *Tryptophan Properties in Fluorescence and Functional Stability of Plasminogen Activator Inhibitor 1*. *Biophysical Journal*, 2003. **85**: p. 501-510.
99. Fa, M., F. Bergstrom, J. Karolin, L.B.A. Johansson, and T. Ny, *Conformational Studies of Plasminogen Activator Inhibitor Type 1 by Fluorescence Spectroscopy Analysis of the Reactive Centre of Inhibitory and Substrate Forms, and of Their Respective Reactive-Centre Cleaved Forms*. *European Journal of Biochemistry*, 2000. **267**: p. 3729-3734.
100. Fa, M., J. Karolin, S. Aleshkov, L. Strandberg, L.B.A. Johansson, and T. Ny, *Time-Resolved Polarized Fluorescence Spectroscopy Studies of Plasminogen Activator Inhibitor Type 1: Conformational Changes of the Reactive Center Upon*

- Interactions with Target Proteases, Vitronectin and Heparin*. Biochemistry, 1995. **34**(42): p. 13833-13840.
101. Ko, C.W., Z. Wei, R.J. Marsh, D.A. Armoogum, N. Nicolaou, A.J. Bain, A. Zhou, and L. Ying, *Probing Nanosecond Motions of Plasminogen Activator Inhibitor-1 by Time-Resolved Fluorescence Anisotropy*. Molecular BioSystems, 2009. **5**(9): p. 1025.
 102. Backovic, M., E. Stratikos, D.A. Lawrence, and P.G.W. Gettins, *Structural Similarity of the Covalent Complexes Formed between the Serpin Plasminogen Activator Inhibitor-1 and the Arginine-Specific Proteinases Trypsin, Lmw U-Pa, Hmw U-Pa, and T-Pa: Use of Site-Specific Fluorescent Probes of Local Environment*. Protein Science, 2002. **11**: p. 1182-1191.
 103. Egelund, R., A.J. Einholm, K.E. Pedersen, R.W. Nielsen, A. Christensen, J. Deinum, and P.A. Andreasen, *A Regulatory Hydrophobic Area in the Flexible Joint Region of Plasminogen Activator Inhibitor-1, Defined with Fluorescent Activity-Neutralizing Ligands. Ligand-Induced Serpin Polymerization*. Journal of Biological Chemistry, 2001. **276**(16): p. 13077-13086.
 104. Gibson, A., K. Baburaj, D.E. Day, I.M. Verhamme, J.D. Shore, and C.B. Peterson, *The Use of Fluorescent Probes to Characterize Conformation Changes in the Interaction between Vitronectin and Plasminogen Activator Inhibitor-1*. Journal of Biological Chemistry, 1997. **272**(8): p. 5112-5121.
 105. Shore, J.D., D.E. Day, A.M. Francis-Chmura, I.M. Verhamme, J. Kvassman, D.A. Lawrence, and D.S. Ginsberg, *A Fluorescent Probe Study of Plasminogen Activator Inhibitor-1: Evidence for Reactive Center Loop Insertion and Its Role in the Inhibitory Mechanism*. Journal of Biological Chemistry, 1995. **270**(10): p. 5395-5398.
 106. Mast, A.E., J.J. Enghild, and G. Salvesen, *Conformation of the Reactive Site Loop of Alpha1-Proteinase Inhibitor Probed by Limited Proteolysis*. Biochemistry, 1992. **31**: p. 2720-2728.
 107. Kirkegaard, T., S. Jensen, S.L. Schousboe, H.H. Peterson, R. Egelund, P.A. Andreasen, and K.W. Rodenburg, *Engineering of Conformations of Plasminogen Activator Inhibitor-1: A Crucial Role of B-Strand 5a Residues in the Transition of Active Form to Latent and Substrate Forms*. European Journal of Biochemistry, 1999. **263**: p. 577-586.
 108. Hansen, M., M.N. Busse, and P.A. Andreasen, *Importance of the Amino-Acid Composition of the Shutter Region of Plasminogen Activator Inhibitor-1 for Its Transitions to Latent and Substrate Forms*. European Journal of Biochemistry, 2001. **268**: p. 6274-6283.

109. Yi, J. and H. Im, *Structural Factors Affecting the Choice between Latency Transition and Polymerization in Inhibitory Serpins*. Protein Science, 2007. **16**(5): p. 833-841.
110. Gils, A., J. Lu, K. Aertgeerts, I. Knockaert, and P.J. Declerck, *Identification of Positively Charged Residues Contributing to the Stability of Plasminogen Activator Inhibitor 1*. FEBS Letters, 1997. **415**(2): p. 192-195.
111. Gettins, P.G.W., *The F-Helix of Serpins Plays an Essential, Active Role in the Proteinase Inhibition Mechanism*. FEBS Letters, 2002. **523**: p. 2-6.
112. Mottonen, J., A. Strand, J. Symersky, R.M. Sweet, D.E. Danley, K.F. Geoghegan, R.D. Gerard, and E.J. Goldsmith, *Structural Basis of Latency in Plasminogen Activator Inhibitor-1*. Nature Structural Biology, 1992. **355**: p. 270-273.
113. Schar, C.R., J.K. Jensen, A. Christensen, G.E. Blouse, P.A. Andreasen, and C.B. Peterson, *Characterization of a Site on Pai-1 That Binds to Vitronectin Outside of the Somatomedin B Domain*. Journal of Biological Chemistry, 2008. **283**(42): p. 28487-28496.
114. Xue, Y., P. Björquist, T. Inghardt, M. Linschoten, D. Musil, L. Sjölin, and J. Deinum, *Interfering with the Inhibitory Mechanism of Serpins: Crystal Structure of a Complex Formed between Cleaved Plasminogen Activator Inhibitor Type 1 and a Reactive-Centre Loop Peptide*. Structure, 1998. **6**: p. 627-636.
115. Huntington, J.A., R.J. Read, and R.W. Carrell, *Structure of a Serpin-Protease Complex Shows Inhibition by Deformation*. Nature 2000. **407**: p. 923-926.
116. Na, Y. and H. Im, *Specific Interactions of Serpins in Their Native Forms Attenuate Their Conformational Transitions*. Protein Science, 2007. **16**(8): p. 1659-1666.
117. Olson, S.T., R. Swanson, D.E. Day, I.M. Verhamme, J. Kvassman, and J.D. Shore, *Resolution of Michaelis Complex, Acylation, and Conformational Change Steps in the Reactions of the Serpin, Plasminogen Activator Inhibitor-1, with Tissue Plasminogen Activator and Trypsin*. Biochemistry, 2001. **40**(11742-11756).
118. Peterson, F.C., N.C. Gordon, and P.G.W. Gettins, *Formation of a Noncovalent Serpin-Proteinase Complex Involves No Conformational Change in the Serpin. Use of 1h-15n Hsqc Nmr as a Sensitive Nonperturbing Monitor of Conformation*. Biochemistry, 2000. **39**: p. 11884-11892.
119. Audenaert, A., I. Knockaert, D. Collen, and P.J. Declerck, *Conversion of Plasminogen Activator Inhibitor-1 from Inhibitor to Substrate by Point Mutations in the Reactive-Site Loop*. Journal of Biological Chemistry, 1994. **269**(30): p. 19559-19564.

120. Gils, A., I. Knockaert, and P.J. Declerck, *Substrate Behavior of Plasminogen Activator Inhibitor-1 Is Not Associated with a Lack of Insertion of the Reactive Site Loop*. *Biochemistry*, 1996. **35**(23): p. 7474-7481.
121. Gils, A. and P.J. Declerck, *Proteinase Specificity and Functional Diversity in Point Mutants of Plasminogen Activator Inhibitor 1*. *Journal of Biological Chemistry*, 1997. **272**(19): p. 12662-12666.
122. Sherman, P.M., D.A. Lawrence, A.Y. Yang, E.T. Vandenberg, D. Paielli, S.T. Olson, J.D. Shore, and D.S. Ginsberg, *Saturation Mutagenesis of the Plasminogen Activator Inhibitor -1 Reactive Center*. *Journal of Biological Chemistry*, 1992. **267**(11): p. 7588-7595.
123. Zhou, A., R.W. Carrell, and J.A. Huntington, *The Serpin Inhibitory Mechanism Is Critically Dependent on the Length of the Reactive Center Loop*. *Journal of Biological Chemistry*, 2001. **276**(29): p. 27541-27547.
124. Na, Y. and H. Im, *The Length of the Reactive Center Loop Modulates the Latency Transition of Plasminogen Activator Inhibitor-1*. *Protein Science*, 2004. **14**(1): p. 55-63.
125. Zhou, A., J.A. Huntington, N.S. Pannu, R.W. Carrell, and R.J. Read, *How Vitronectin Binds Pai-1 to Modulate Fibrinolysis and Cell Migration*. *Nature Structural Biology*, 2003. **10**(7): p. 541-544.
126. Schar, C.R., G.E. Blouse, K.H. Minor, and C.B. Peterson, *A Deletion Mutant of Vitronectin Lacking the Somatomedin B Domain Exhibits Residual Plasminogen Activator Inhibitor-1-Binding Activity*. *Journal of Biological Chemistry*, 2008. **283**(16): p. 10297-10309.
127. Thompson, L.C., S. Goswami, and C.B. Peterson, *Metals Affect the Structure and Activity of Human Plasminogen Activator Inhibitor-1. II. Binding Affinity and Conformational Changes*. *Protein Science*, 2011. **20**(2): p. 366-378.
128. Gettins, P.G.W. and S.T. Olson, *Exosite Determinants of Serpin Specificity*. *Journal of Biological Chemistry*, 2009. **284**(31): p. 20441-20445.
129. Madison, E.L., E.J. Goldsmith, R.D. Gerard, M.H. Gething, J.F. Sambrook, and R.S. Bassel-Duby, *Amino Acid Residues That Affect Interaction of Tissue-Type Plasminogen Activator with Plasminogen Activator Inhibitor 1*. *Proceedings of the National Academy of Sciences*, 1990. **87**: p. 3530-3533.
130. Williams, R.T. and J.W. Bridges, *Fluorescence of Solutions: A Review*. *J Clin Pathol*, 1964. **17**(4): p. 371-94.
131. Jeschke, G., *Conformational Dynamics and Distribution of Nitroxide Spin Labels*. *Prog Nucl Magn Reson Spectrosc*, 2013. **72**(42-60).

132. Yang, Y., T. Ramelot, S. Ni, R. McCarrick, and M. Kennedy, *Measurement of Rate Constants for Homodimer Subunit Exchange Using Double Electron–Electron Resonance and Paramagnetic Relaxation Enhancements*. Journal of Biomolecular NMR, 2013. **55**(1): p. 47-58.
133. Crane, J.M., C. Mao, A.A. Lilly, V.F. Smith, Y. Suo, W.L. Hubbell, and L.L. Randall, *Mapping of the Docking of Seca onto the Chaperone Secb by Aite-Directed Spin Labeling: Insight into the Mechanism of Ligand Transfer During Protein Export*. J Mol Biol, 2005. **353**(2): p. 295-307.
134. Czogalla, A., A. Pieciul, A. Jezierski, and A.F. Sikorski, *Attaching a Spin to a Protein -- Site-Directed Spin Labeling in Structural Biology*. Acta Biochim Pol, 2007. **54**(2): p. 235-44.
135. Klug, C.S. and J.B. Feix, *Methods and Applications of Site-Directed Spin Labeling Epr Spectroscopy*, in *Methods in Cell Biology*, J.C. Dr. John and Dr. H. William Detrich, III, Editors. 2008, Academic Press. p. 617-658.
136. Weber, R.T., J. Jiang, and D.P. Barr, *Bruker Emx User's Manual*, 1998, Software Version 2.3: Billerica, MA.
137. Molecular Innovations, I., *Method for Making Purified Plasminogen Activator Inhibitor Type-1 (Pai-1) and Purified Pai-1 Made Therefrom* March 21, 2006.
138. Schuck, P., *Size Distribution Analysis of Macromolecules by Sedimentation Velocity Ultracentrifugation and Lamm Equation Modeling*. Biophysical Journal, 2000. **78**: p. 1606-19.
139. Onuchic, J.N., H. Nymeyer, A.E. Garcia, J. Chahine, and N.D. Socci, *The Energy Landscape Theory of Protein Folding: Insights into Folding Mechanisms and Scenarios*. Adv Protein Chem, 2000. **57**: p. 87-152.
140. Onuchic, J.N. and P.G. Wolynes, *Theory of Protein Folding*. Curr Opin Struct Biol, 2004. **14**(1): p. 70-5.
141. Stout, T.J., H. Graham, D.I. Buckley, and D.J. Matthews, *Structures of Active and Latent Pai-1: A Possible Stabilizing Role for Chloride Ions*. Biochemistry, 2000. **39**: p. 8460-8469.
142. Sharp, A.M., P.E. Stein, N.S. Pannu, R.W. Carrell, M.B. Berkenpas, D.S. Ginsberg, D.A. Lawrence, and R.J. Read, *The Active Conformation of Plasminogen Activator Inhibitor 1, a Target for Drugs to Control Fibrinolysis and Cell Adhesion*. Structure, 1999. **7**(2): p. 111-118.
143. Horvath, A.J., B.G. Lu, R.N. Pike, and S.P. Bottomley, *Methods to Measure the Kinetics of Protease Inhibition by Serpins*. Methods Enzymol, 2011. **501**: p. 223-35.

144. Stefansson, S., M. Yepes, N. Gorlatova, D.E. Day, E.G. Moore, A. Zabaleta, G.A. McMahon, and D.A. Lawrence, *Mutants of Plasminogen Activator Inhibitor-1 Designed to Inhibit Neutrophil Elastase and Cathepsin G Are More Effective in Vivo Than Their Endogenous Inhibitors*. Journal of Biological Chemistry, 2004. **279**(29): p. 29981-29987.
145. Wun, T.C., M.O. Palmier, N.R. Siegel, and C.E. Smith, *Affinity Purification of Active Plasminogen Activator Inhibitor-1 (Pai-1) Using Immobilized Anhydrourokinase. Demonstration of the Binding, Stabilization, and Activation of Pai-1 by Vitronectin*. Journal of Biological Chemistry, 1989. **264**(14): p. 7862-7868.
146. Jr., L.D.J., T.M. Reilly, and L.W.H. Jr., *Stabilization of Active Plasminogen Activator Inhibitor-1 Us 5290764 A*. The Dupont Merck Pharmaceutical Company, Jan 14, 1992.
147. De Taeye, B., G. Compennolle, M. Dewilde, W. Biesemans, and P.J. Declerck, *Immobilization of the Distal Hinge in the Labile Serpin Plasminogen Activator Inhibitor 1: Identification of a Transition State with Distinct Conformational and Functional Properties*. Journal of Biological Chemistry, 2003. **278**(26): p. 23899-23905.
148. D'Amico, S., J.A. Martial, and I. Struman, *A Peptide Mimicking the C-Terminal Part of the Reactive Center Loop Induces the Transition to the Latent Form of Plasminogen Activator Inhibitor Type-1*. FEBS Letters, 2012. **586**(6): p. 686-692.
149. Lynn, G.W., W.T. Heller, A. Mayasundari, K.H. Minor, and C.B. Peterson, *A Model for the Three-Dimensional Structure of Human Plasma Vitronectin from Small-Angle Scattering Measurements*. Biochemistry, 2005. **44**(2): p. 565-74.
150. Kjaergaard, M., H. Gårdsvoll, D. Hirschberg, S. Nielbo, A. Mayasundari, C.B. Peterson, A. Jansson, T.J.D. Jørgensen, F.M. Poulsen, and M. Ploug, *Solution Structure of Recombinant Somatomedin B Domain from Vitronectin Produced in Pichia Pastoris*. Protein Science, 2007. **16**(9): p. 1934-1945.
151. Kamikubo, Y., R. De Guzman, G. Kroon, S. Curriden, J.G. Neels, M.J. Churchill, P. Dawson, S. Ołdziej, A. Jagielska, H.A. Scheraga, D.J. Loskutoff, and H.J. Dyson, *Disulfide Bonding Arrangements in Active Forms of the Somatomedin B Domain of Human Vitronectin*. Biochemistry, 2004. **43**(21): p. 6519-6534.
152. Horn, N.A., G.B. Hurst, A. Mayasundari, N.A. Whittemore, E.H. Serpersu, and C.B. Peterson, *Assignment of the Four Disulfides in the N-Terminal Somatomedin B Domain of Native Vitronectin Isolated from Human Plasma*. Journal of Biological Chemistry, 2004. **279**(34): p. 35867-78.
153. Xu, D., K. Baburaj, C.B. Peterson, and Y. Xu, *Model for the Three-Dimensional Structure of Vitronectin: Predictions for the Multi-Domain Protein from Threading and Docking*. Proteins, 2001. **44**(3): p. 312-20.

154. Dunker, A.K., J.D. Lawson, C.J. Brown, R.M. Williams, P. Romero, J.S. Oh, C.J. Oldfield, A.M. Campen, C.M. Ratliff, K.W. Hipps, J. Ausio, M.S. Nissen, R. Reeves, C. Kang, C.R. Kissinger, R.W. Bailey, M.D. Griswold, W. Chiu, E.C. Garner, and Z. Obradovic, *Intrinsically Disordered Protein*. Journal of Molecular Graphics and Modelling, 2001. **19**(1): p. 26-59.
155. Fong, J.H., B.A. Shoemaker, S.O. Garbuzynskiy, M.Y. Lobanov, O.V. Galzitskaya, and A.R. Panchenko, *Intrinsic Disorder in Protein Interactions: Insights from a Comprehensive Structural Analysis*. PLoS Comput Biol, 2009. **5**(3): p. e1000316.
156. Tompa, P., *Intrinsically Unstructured Proteins*. Trends in biochemical sciences, 2002. **27**(10): p. 527-533.
157. Sano, K., K. Asanuma-Date, F. Arisaka, S. Hattori, and H. Ogawa, *Changes in Glycosylation of Vitronectin Modulate Multimerization and Collagen Binding During Liver Regeneration*. Glycobiology, 2007. **17**(7): p. 784-94.
158. Jenne, D., A. Hille, K.K. Stanley, and W.B. Huttner, *Sulfation of Two Tyrosine-Residues in Human Complement S-Protein (Vitronectin)*. Eur J Biochem, 1989. **185**(2): p. 391-5.
159. Schwartz, I., D. Seger, and S. Shaltiel, *Vitronectin*. Int J Biochem Cell Biol, 1999. **31**(5): p. 539-44.
160. Schroeck, F., N. Arroyo de Prada, S. Sperl, M. Schmitt, and V. Magdolen, *Interaction of Plasminogen Activator Inhibitor Type-1 (Pai-1) with Vitronectin (Vn): Mapping the Binding Sites on Pai-1 and Vn*. Biological Chemistry, 2002. **383**: p. 1143-1149.
161. Tomasini, B.R. and D.F. Mosher, *Vitronectin*. Prog Hemost Thromb, 1991. **10**(269-305).
162. Shaffer, M.C., T.P. Foley, and D.W. Barnes, *Quantitation of Spreading Factor in Human Biologic Fluids*. J Lab Clin Med, 1984. **103**(5): p. 783-91.
163. Zhuang, P., H. Li, J.G. Williams, N.V. Wagner, D. Seiffert, and C.B. Peterson, *Characterization of the Denaturation and Renaturation of Human Plasma Vitronectin: II. Investigation into the Mechanism of Formation of Multimers*. Journal of Biological Chemistry, 1996. **271**(24): p. 14333-14343.
164. Minor, K.H., C.R. Schar, G.E. Blouse, J.D. Shore, D.A. Lawrence, P. Schuck, and C.B. Peterson, *A Mechanism for Assembly of Complexes of Vitronectin and Plasminogen Activator Inhibitor-1 from Sedimentation Velocity Analysis*. Journal of Biological Chemistry, 2005. **280**(31): p. 28711-28720.

165. Podor, T.J., S.G. Shaughnessy, M.N. Blackburn, and C.B. Peterson, *New Insights into the Size and Stoichiometry of the Plasminogen Activator Inhibitor Type-1 Vitronectin Complex*. J Biol Chem, 2000. **275**(33): p. 25402-10.
166. Arroyo De Prada, N., F. Schroeck, E. Sinner, B. Muehlenweg, J. Twellmeyer, S. Sperl, O.G. Wilhelm, M. Schmitt, and V. Magdolen, *Interaction of Plasminogen Activator Inhibitor Type-1 (Pai-1) with Vitronectin: Characterization of Different Pai-1 Mutants*. European Journal of Biochemistry, 2002. **269**: p. 184-192.
167. Keijer, J., M. Linders, J.J. Wegman, H.J. Ehrlich, K. Mertens, and H. Pannekoek, *On the Target Specificity of Plasminogen Activator Inhibitor 1: The Role of Heparin, Vitronectin, and the Reactive Site*. Blood, 1991. **78**: p. 1254-1261.
168. van Meijer, M., A. Smilde, M.E. Nesheim, H. Pannekoek, and A.J. Horrevoets, *The Suicide Substrate Reaction between Plasminogen Activator Inhibitor 1 and Thrombin Is Regulated by the Cofactors Vitronectin and Heparin*. Blood, 1997. **90**(5): p. 1874-82.
169. Ehrlich, H.J., R.K. Gebbink, J. Keijer, and H. Pannekoek, *Elucidation of Structural Requirements on Plasminogen Activator Inhibitor 1 for Binding to Heparin*. Journal of Biological Chemistry, 1992. **267**(16): p. 11806-11611.
170. Li, X., G. Zou, W. Yuan, and W. Lu, *Defining the Native Disulfide Topology in the Somatomedin B Domain of Human Vitronectin*. Journal of Biological Chemistry, 2007. **282**(8): p. 5318-5326.
171. Tomasini, B.R. and D.F. Mosher, *Vitronectin*. Prog Hemost Thromb, 1991. **10**: p. 269-305.
172. Spraggon, G., C. Phillips, U.K. Nowak, C.P. Ponting, D. Saunders, C.M. Dobson, D.I. Stuart, and E.Y. Jones, *The Crystal Structure of the Catalytic Domain of Human Urokinase-Type Plasminogen Activator*. Structure, 1995. **3**(7): p. 681-91.
173. Gorelick, F.S. and T. Otani, *Mechanisms of Intracellular Zymogen Activation*. Baillieres Best Pract Res Clin Gastroenterol, 1999. **13**(2): p. 227-40.
174. Jiang, L., K.A. Botkjaer, L.M. Andersen, C. Yuan, P.A. Andreasen, and M. Huang, *Rezymogenation of Active Urokinase Induced by an Inhibitory Antibody*. Biochemical Journal, 2013. **449**(1): p. 161-166.
175. Berg, J.M., J.L. Tymoczko, and L. Stryer, *Biochemistry*. 5th ed. Many Enzymes Are Activated by Specific Proteolytic Cleavage. Vol. Section 10.5. 2002, New York: W. H. Freeman.
176. Neurath, H. and K.A. Walsh, *Role of Proteolytic Enzymes in Biological Regulation: A Review (Limited Proteolysis/Zymogen Activation/Control Mechanisms)*. Proc. Natl. Acad. Sci, 1976. **73**(11): p. 3825-32.

177. Manjabacas, M.C., E. Valero, M. Moreno-Conesa, M. García-Moreno, M. Molina-Alarcón, and R. Varón, *Linear Mixed Irreversible Inhibition of the Autocatalytic Activation of Zymogens: Kinetic Analysis Checked by Simulated Progress Curves*. The International Journal of Biochemistry & Cell Biology, 2002. **34**(4): p. 358-369.
178. Wang, W., X. Pan, and Z. Wang, *Kinetic Analysis of Zymogen Autoactivation in the Presence of a Reversible Inhibitor*. European Journal of Biochemistry, 2004. **271**(23-24): p. 4638-4645.
179. Flemmig, M. and M.F. Melzig, *Serine-Proteases as Plasminogen Activators in Terms of Fibrinolysis*. J Pharm Pharmacol, 2012. **64**(8): p. 1025-39.
180. Downing, A.K., P.C. Driscoll, T.S. Harvey, T.J. Dudgeon, B.O. Smith, M. Baron, and I.D. Campbell, *Solution Structure of the Fibrin Binding Finger Domain of Tissue-Type Plasminogen Activator Determined by 1h Nuclear Magnetic Resonance*. Journal of Molecular Biology, 1992. **225**(3): p. 821-833.
181. Rao, Z., P. Handford, M. Mayhew, V. Knott, G.G. Brownlee, and D. StuartZ, *The Structure of a Ca²⁺-Binding Epidermal Growth Factor-Like Domain: Its Role in Protein-Protein Interactions*. Cell, 1995. **82**(1): p. 131-141.
182. Byeon, I.-J.L. and M. Llinás, *Solution Structure of the Tissue-Type Plasminogen Activator Kringle 2 Domain Complexed to 6-Aminohexanoic Acid an Antifibrinolytic Drug*. Journal of Molecular Biology, 1991. **222**(4): p. 1035-1051.
183. Rénatus, M., R.A. Engh, M.T. Stubbs, R. Huber, S. Fischer, U. Kohnert, and W. Bode, *Lysine 156 Promotes the Anomalous Proenzyme Activity of Tpa: X-Ray Crystal Structure of Single-Chain Human Tpa*. EMBO J, 1997. **16**(16): p. 4797-4805.
184. Collen, D. and H.R. Lijnen, *The Tissue-Type Plasminogen Activator Story*. Arteriosclerosis, Thrombosis, and Vascular Biology, 2009. **29**(8): p. 1151-1155.
185. Prager, G.W., J.M. Breuss, S. Steurer, J. Mihaly, and B.R. Binder, *Vascular Endothelial Growth Factor (Vegf) Induces Rapid Prourokinase (Pro-Upa) Activation on the Surface of Endothelial Cells*. Blood, 2004. **103**(3): p. 955-62.
186. Swedberg, J.E. and J.M. Harris, *Natural and Engineered Plasmin Inhibitors: Applications and Design Strategies*. Chem Biochem, 2012. **13**(3): p. 336-48.
187. Sakharov, D.V., M. Barrett-Bergshoeff, R.T. Hekkenberg, and D.C. Rijken, *Fibrin-Specificity of a Plasminogen Activator Affects the Efficiency of Fibrinolysis and Responsiveness to Ultrasound: Comparison of Nine Plasminogen Activators in Vitro*. Thrombosis and Haemostasis, 1999. **81**(4): p. 605-12.
188. Wilkins-Port, C.E., S.P. Higgins, C.E. Higgins, I. Kobori-Hotchkiss, and P.J. Higgins, *Complex Regulation of the Pericellular Proteolytic Microenvironment During Tumor Progression and Wound Repair: Functional Interactions between*

- the Serine Protease and Matrix Metalloproteinase Cascades*. Biochemistry Research International, 2012. **2012**: p. 1-8.
189. Preissner, K.T. and D. Seiffert, *Role of Vitronectin and Its Receptors in Haemostasis and Vascular Remodeling*. Thrombosis Research, 1998. **89**(1): p. 1-21.
 190. Roomi, M.W., T. Kalinovsky, M. Rath, and A. Niedzwiecki, *Down-Regulation of Urokinase Plasminogen Activator and Matrix Metalloproteinases and up-Regulation of Their Inhibitors by a Novel Nutrient Mixture in Human Prostate Cancer Cell Lines Pc-3 and Du-145*. Oncology Reports, 2011. **26**(6): p. 1407-1414.
 191. Xie, C., X.H. Jiang, J.T. Zhang, T.T. Sun, J.D. Dong, A.J. Sanders, R.Y. Diao, Y. Wang, K.L. Fok, L.L. Tsang, M.K. Yu, X.H. Zhang, Y.W. Chung, L. Ye, M.Y. Zhao, J.H. Guo, Z.J. Xiao, H.Y. Lan, C.F. Ng, K.M. Lau, Z.M. Cai, W.G. Jiang, and H.C. Chan, *Cftr Suppresses Tumor Progression through Mir-193b Targeting Urokinase Plasminogen Activator (Upa) in Prostate Cancer*. Oncogene, 2012.
 192. Dickerman, H.W., H.L. Martinez, J.I. Seeger, and S.A. Kumar, *Estrogen Regulation of Human Breast Cancer Cell Line Mcf-7 Tissue Plasminogen Activator*. Endocrinology, 1989. **125**(1): p. 492-500.
 193. Hurtado, M., J.J. Lozano, E. Castellanos, L.A. López-Fernández, K. Harshman, A.C. Martínez, A.R. Ortiz, T.M. Thomson, and R. Paciucci, *Activation of the Epidermal Growth Factor Signalling Pathway by Tissue Plasminogen Activator in Pancreas Cancer Cells*. Gut, 2007. **56**(9): p. 1266-74.
 194. Ortiz-Zapater, E., S. Peiró, O. Roda, J.M. Corominas, S. Aguilar, C. Ampurdanés, F.X. Real, and P. Navarro, *Tissue Plasminogen Activator Induces Pancreatic Cancer Cell Proliferation by a Non-Catalytic Mechanism That Requires Extracellular Signal-Regulated Kinase 1/2 Activation through Epidermal Growth Factor Receptor and Annexin A2*. Am J Pathol, 2007. **170**(5): p. 1573-84.
 195. Hu, K., J. Yang, S. Tanaka, S.L. Gonias, W.M. Mars, and Y. Liu, *Tissue-Type Plasminogen Activator Acts as a Cytokine That Triggers Intracellular Signal Transduction and Induces Matrix Metalloproteinase-9 Gene Expression*. Journal of Biological Chemistry, 2006. **281**(4): p. 2120-2127.
 196. Narita, T., K. Muromachi, N. Kamio, S. Nakao, K. Matsushima, and H. Hashizume, *Tumor Necrosis Factor A Stimulates Expression and Secretion of Urokinase Plasminogen Activator in Human Dental Pulp Cells*. Journal of Oral Science, 2012. **54**(4): p. 329-336.
 197. Harston, G.W.J., B.A. Sutherland, J. Kennedy, and A.M. Buchan, *The Contribution of L-Arginine to the Neurotoxicity of Recombinant Tissue Plasminogen Activator Following Cerebral Ischemia: A Review of Rtpa Neurotoxicity*. J Cereb Blood Flow Metab, 2010. **30**(11): p. 1804-1816.

198. Wong, B.S.T., K.K.W. Lam, C. Lee, V.H.H. Wong, M.P.Y. Lam, I.K. Chu, W.S.B. Yeung, and P.C.N. Chiu, *Adrenomedullin Enhances Invasion of Human Extravillous Cytotrophoblast-Derived Cell Lines by Regulation of Urokinase Plasminogen Activator Expression and S-Nitrosylation*. *Biology of Reproduction*, 2013. **88**(2): p. 34, 1-11.
199. Schuler, P.J., M. Bendszus, S. Kuehnel, S. Wagner, T.K. Hoffmann, R. Goldbrunner, and G.H. Vince, *Urokinase Plasminogen Activator, Upar, Mmp-2, and Mmp-9 in the C6-Glioblastoma Rat Model*. *In Vivo*, 2012. **26**(4): p. 571-6.
200. Resnati, M., M. Guttinger, S. Valcamonica, S. Sidenius, F. Blasi, and F. Fazioli, *Proteolytic Cleavage of the Urokinase Receptor Substitutes for the Agonist-Induced Chemotactic Effect*. *EMBO J*, 1996. **15**(7): p. 1572-82.
201. Jullienne, A., A. Montagne, C. Orset, F. Lesept, D. Jane, D. Monaghan, E. Maubert, D. Vivien, and C. Ali, *Selective Inhibition of Glun2d-Containing N-Methyl-D-Aspartate Receptors Prevents Tissue Plasminogen Activator-Promoted Neurotoxicity Both in Vitro and in Vivo*. *Molecular Neurodegeneration*, 2011. **6**(1): p. 68.
202. Collen, D. and H. Lijnen, *Basic and Clinical Aspects of Fibrinolysis and Thrombolysis*. *Blood*, 1991. **78**: p. 3114 - 3124.
203. Hacke, W., M. Kaste, E. Bluhmki, M. Brozman, A. Davalos, D. Guidetti, V. Larrue, K. Lees, Z. Medeghri, T. Machnig, D. Schneider, R. von Kummer, N. Wahlgren, D. Toni, and E. Investigators, *Thrombolysis with Alteplase 3 to 4.5 Hours after Acute Ischemic Stroke*. *N Engl J Med*, 2008. **359**: p. 1317 - 1329.
204. Macrez, R., P. Obiang, M. Gauberti, B. Roussel, A. Baron, J. Parcq, F. Casse, Y. Hommet, C. Orset, V. Agin, L. Bezin, T. Berrocoso, K. Petersen, J. Montaner, E. Maubert, D. Vivien, and C. Ali, *Antibodies Preventing the Interaction of Tissue-Type Plasminogen Activator with N-Methyl-D-Aspartate Receptors Reduce Stroke Damages and Extend the Therapeutic Window of Thrombolysis*. *Stroke*, 2011. **42**: p. 2315 - 22.
205. Yepes, M., B. Roussel, C. Ali, and D. Vivien, *Tissue-Type Plasminogen Activator in the Ischemic Brain: More Than a Thrombolytic*. *Trends Neurosci*, 2009. **32**: p. 48 - 55.
206. Zhang, R., Z. Zhang, and M. Chopp, *Thrombolysis with Tissue Plasminogen Activator Alters Adhesion Molecule Expression in the Ischemic Rat Brain*. *Stroke*, 1999. **30**: p. 624 - 629.
207. Wu, F., J. Wu, A.D. Nicholson, R. Echeverry, W.B. Haile, M. Catano, J. An, A.K. Lee, D. Duong, E.B. Dammer, N.T. Seyfried, F.C. Tong, J.R. Votaw, R.L. Medcalf, and M. Yepes, *Tissue-Type Plasminogen Activator Regulates the Neuronal Uptake of Glucose in the Ischemic Brain*. *The Journal of Neuroscience*, 2012. **32**(29): p. 9848-9858.

208. Warshawsky, I., G. Bu, and A.L. Schwartz, *Lrp and the Receptor-Mediated Endocytosis of Plasminogen Activators*. Annals of the New York Academy of Sciences, 1994. **737**(1): p. 70-87.
209. Pierce, B.G., Y. Hourai, and Z. Weng, *Accelerating Protein Docking in Zdock Using an Advanced 3d Convolution Library*. PLoS ONE, 2011. **6**(9): p. e24657.
210. Kvassman, J., I.M. Verhamme, and J.D. Shore, *Inhibitory Mechanism of Serpins: Loop Insertion Forces Acylation of Plasminogen Activator by Plasminogen Activator Inhibitor-1* Biochemistry, 1998. **37**: p. 15491-15502.
211. Gettins, P.G.W., *Serpin Structure, Mechanism, and Function*. Chem. Rev., 2002. **102**: p. 4751-4803.
212. Fortenberry, Y.M., H.C. Whinna, S.T. Cooper, T. Myles, L.L.K. Leung, and F.C. Church, *Essential Thrombin Residues for Inhibition by Protein C Inhibitor with the Cofactors Heparin and Thrombomodulin*. Journal of Thrombosis and Haemostasis, 2007. **5**: p. 1486-92.
213. Aulicky, P., A. Rabinstein, R.C. Seet, J. Neumann, and R. Mikulik, *Dosing of Tissue Plasminogen Activator Often Differs from 0.9 Mg/Kg, but Does Not Affect the Outcome*. J Stroke Cerebrovasc Dis, 2012.
214. Parcq, J., T. Bertrand, A.F. Baron, Y. Hommet, E. Anglès-Cano, and D. Vivien, *Molecular Requirements for Safer Generation of Thrombolytics by Bioengineering the Tissue-Type Plasminogen Activator a Chain*. J Thromb Haemost, 2013. **11**(3): p. 539-46.
215. Cho, E., K. Lee, J. Seo, C.J. Byun, S. Chung, D.C. Suh, P. Carmeliet, J. Koh, J.S. Kim, and J. Lee, *Neuroprotection by Urokinase Plasminogen Activator in the Hippocampus*. Neurobiology of Disease, 2012. **46**(1): p. 215-224.
216. Paz, A., T. Zeev-Ben-Mordehai, J.L. Sussman, and I. Silman, *Purification of Intrinsically Disordered Proteins*, in *Instrumental Analysis of Intrinsically Disordered Proteins*. 2010, John Wiley & Sons, Inc. p. 695-704.
217. Livernois, A.M., D.J. Hnatchuk, E.E. Findlater, and S.P. Graether, *Obtaining Highly Purified Intrinsically Disordered Protein by Boiling Lysis and Single Step Ion Exchange*. Anal Biochem, 2009. **392**(1): p. 70-6.
218. Churion, K.A. and S.E. Bondos, *Identifying Solubility-Promoting Buffers for Intrinsically Disordered Proteins Prior to Purification*. Methods Mol Biol, 2012. **896**: p. 415-27.
219. Hwang, P.M., J.S. Pan, and B.D. Sykes, *A Pagp Fusion Protein System for the Expression of Intrinsically Disordered Proteins in Escherichia Coli*. Protein Expression and Purification, 2012. **85**(1): p. 148-151.

220. Bobko, A.A., I.A. Kirilyuk, I.A. Grigor'ev, J.L. Zweier, and V.V. Khrantsov, *Reversible Reduction of Nitroxides to Hydroxylamines: The Roles for Ascorbate and Glutathione*. *Free Radic Biol Med.*, 2007. **42**(3): p. 404-412.

Vita

Tihami Qureshi was born the fourth daughter to Bengali emigrant parents in Nashville, TN, on Friday, the 18th night of March 1983, the 77th day of the year. As a youth, Qureshi enjoyed a public school education, from attending Westmeade Elementary School for primary school as a wee little one, and then on to Head (“Penitentiary”) Middle School (off Jo Johnson Ave) for 5-6th grades. Thenceforth, Qureshi went to Bellevue Middle School for 7th grade, following which she was briefly home-schooled for disciplinary reasons (note to readers: teenage rebellion has its consequences). Rehabilitated, Qureshi subsequently entered J. T. Moore Middle School for the remainder of middle school. After a brief two-year stint at Hillwood High School, Qureshi entered Hillsboro High School, from which she graduated in 2001. Upon graduating, the wide-eyed Qureshi was accepted to the University of Tennessee, where, after studying abroad in Italy in 2003 and China in 2004, she graduated *cum laude* in the spring of '05 with a bachelors of science degree in microbiology. Subsequently, Qureshi moved back to Nashville, where she worked two jobs, at a doctor’s office and environmental lab, making obvious use of her degree, until realizing the rewards a post-baccalaureate education could afford. Qureshi returned to UTK, and in Fall 2007, entered the Ph. D program in biochemistry, cellular, & molecular biology. And a whole new world of opportunity opened.

“I may not have gone where I intended to go, but I think I have ended up where I needed to be.” ~ Douglas Adams

“All life is an experiment. The more experiments you make, the better.” ~ Ralph Waldo Emerson